Influence of Electrostatic and Intermolecular Interactions on the Solution Behavior and Electrospinning of Functional Nanofibers

Matthew T. Hunley

Dissertation submitted to the faculty of the Virginia Polytechnic Institute and State University in partial fulfillment of the requirements for the degree of

Doctor of Philosophy
In
Macromolecular Science and Engineering

Timothy E. Long, Chair
Donald G. Baird, Member
Richey M. Davis, Member
S. Richard Turner, Member
Garth L. Wilkes, Member

August 27th, 2010
Blacksburg, VA

Keywords: Polyelectrolytes, Surfactants, Carbon Nanotubes, Solution Rheology, Electrospinning

Influence of Electrostatic and Intermolecular Interactions on the Solution Behavior and Electrospinning of Functional Nanofibers

Matthew T. Hunley

ABSTRACT

The solution rheological and electrospinning behavior of a series of charge-containing polymers, surface-active agents, and carbon nanotube composites was studied to investigate the effect of intermolecular interactions, including electrostatic interactions, hydrogen bonding, surface activity, and surface functionalization of carbon nanotubes. The synthesis of novel polyelectrolytes with varied topologies, charge content, and counterions tailored the charged macromolecules to elucidate structure-rheology and structure-processing relationships. In addition, the use of additives for electrospinning, including surfactants and nanofillers, allows us to tailor the functionality of electrospun nanofibers for high-performance applications.

Novel polyelectrolytes based on poly(2-(*N*,*N*-dimethyl)aminoethyl methacrylate) (DMAEMA) were synthesized with the counteranions Cl^-, NO_3^-, $(CN)_2N^-$, BF_4^-, PF_6^-, triflate (TfO^-), and bis(trifluoromethanesulfonyl)imide (Tf_2N^-). The counteranion selection controlled the thermal transitions and degradation; the larger and more charge-delocalized anions typically resulted in lower T_g and higher decomposition temperature. The polyelectrolyte behavior in solution was nearly independent of anion choice, though solution conductivity depended on the electrophoretic mobility of the counterion. Charge containing copolymers of DMAEMA and di(ethylene glycol) methyl ether methacrylate (MEO_2MA) were synthesized and demonstrated that polyelectrolyte behavior in solution was also nearly independent of charge content. Low ionic contents resulted in extended solution conformations and high conductivities. Controlled atom-transfer radical polymerization allowed the synthesis of star-shaped polyelectrolytes with

varying arm numbers and lengths. The solution behavior of the stars deviated slightly from the linear polyelectrolytes due to significant counterion condensation within the star core and constrained polymer conformations.

The linear and star-shaped polyelectrolytes were electrospun to understand the interplay between polyelectrolyte structure and electrospinnability. Similar to other strong polyelectrolytes described in the literature, PDMAEMA-based polyelectrolytes with polar anions (e.g. Cl^-) experienced significant instabilities during electrospinning, requiring high concentrations and viscosities to stabilize the electrospinning jet. The use of large, more hydrophobic anions (BF_4^-, TfO^-) led to increased electrospinnability. Unlike neutral branched polymers, which electrospin nearly identically to linear polymers of similar molecular weight, the star-shaped PDMAEMA-based polyelectrolytes required even higher viscosities than linear polyelectrolytes for stable electrospinning. The correlations between electrospinnability and solution rheological analysis are detailed.

The use of surfactants facilitates the electrospinning of neutral polymers at lower concentrations. However, we have demonstrated that specific cylindrical aggregates of surfactants (wormlike micelles) can be electrospun into microfibers under the proper conditions. Ammonium and phospholipids surfactants as well as organogelators were studied using solution rheology and DLS to determine the effects of micellar structure and solution viscosity on the electrospinnability of low molar mass surfactants. In addition, the effects of charged and uncharged surfactants on the electrospinning behavior of poly(methyl methacrylate) were determined. Added surfactant facilitated uniform fiber formation at lower PMMA concentrations. XPS analysis demonstrated the formation of core-shell fibrous structures resulting from the self-migration of surfactants to the fiber surface.

Hydrogen bonding also influences fiber formation through electrospinning. Star-shaped poly(D,L-lactide)s (PDLLAs) were end-functionalized with adenine (A) or thymine (T) units. The complementary hydrogen bonding between the adenine and thymine lead to thermoresponsive rheological behavior for mixtures of PDLLA-A and PDLLA-T. The mixtures could be electrospun above the hydrogen bond dissociation temperature and resulted in thicker fibers compared to unfunctionalized PDLLA stars. The hydrogen bonding allows the preparation of polymers with a combination desirable solid-state properties and very low processing viscosities.

The effects of carbon nanotube incorporation on electrospinning behavior and fiber morphology were also investigated. Nonfuntionalized and carboxylic-acid functionalized carbon nanotubes were electrospun into polyurethane nanofibers. The nonfunctionalized nanotubes required high-shear melt mixing to disperse within the polyurethane, but remained well dispersed through electrospinning. The surface functionalization with acid groups produced nanotubes which dispersed more readily into the polyurethane solutions. TEM analysis revealed that nanotube dispersion and alignment within the nanofibers was similar for both nonfunctionalized and acid-functionalized nanotubes.

ACKNOWLEDGEMENTS

I would like to extend my thanks firstly to my advisor, Prof. Tim Long, for his constant support and his faith. From the beginning, he fully supported my pursuit of a multidisciplinary degree and my desire to pursue an international internship. His patience probably wore thin as I slowly transitioned from a clumsy chemical engineer to a polymer engineer semi-literate in organic chemistry. His guidance through not only research but the other facets of graduate school, especially proposal writing, will probably serve me equally as much as the scientific background I gained. I also thank the rest of my committee: Dr. Don Baird, Dr. Richey Davis, Dr. Richard Turner, and Dr. Garth Wilkes. Their assistance and support throughout my time at Virginia Tech was equally as important. I am equally indebted to the faculty involved through fellowships and grants: Prof. Ralph Colby at Penn State, Prof. Karen Winey at University of Pennsylvania, Prof. Yosseff Elabd at Drexel University, Prof. Hiroyuki Nishide at Waseda University, and Prof. Axel Müller at Universität Bayreuth. Their input and support was also vital to my success.

No one can accomplish such a feat without the help of many people. With that, I would like to heartily thank those many people who helped along the way, especially Laurie Good, Millie Ryan, Tammy Jo Hiner, Mary Jane Smith, and Valerie Owens, for putting up with the constant barrage of questions and requests. Without their help with paperwork, schedule meetings, ordering, and (most importantly) making sure the stipend kept coming smoothly, I would almost certainly still be trying to figure out how to get the copier to sort and staple. And especially for putting up with the almost daily, “Is Tim in his office yet?” phone calls.

I thank many contributors and funding agencies for providing financial assistance to support my graduate career at Virginia Tech. The Army Research Office for the MAP and

ILEAD MURIs, the NSF for both the EAPSI and DDEP fellowships, as well as MS&IE IGERT which funded my first year. Additionally, Bayer, Eastman, Kraton, and Kimberly-Clark all provided financial assistance or materials throughout the years.

Additionally, the research could not have been accomplished without the support of those in the group I worked closely with, the graduate students, post-docs, and undergrads. The Davidson Crew: Matthew, Andy, John, Becca, Ann, Erika, Shauntrece, Julie, and Matt McKee all worked together for some fun times and indispensible help. The Sub Station II trips were a lifesaver. I want to especially thank Masami Shoji at Waseda University for his tireless translation of Japanese during my stay their (without which I almost definitely would have starved) and his securing baseball tickets for some great games. At the Universität Bayreuth, I have to thank the students and scientists Joe, Felix, Stefan, Alex, Alex, Thomas, Sandrine, Susanne, Christopher, Jiayin, Michael, Hülya, and Weian. The rest of the graduate students, Sharlene, Tomonori, Serkan, Brian, Emily, Gozde, Kalpana, Afia, Tianyu, Mana, Shijing, Steve, Renlong, Eva, Matt Green, Mike, Nancy, Sean, Jenny, and David, all helped make the times here bearable and productive. Postdocs came and postdocs went, and most left a great impression and a lot of knowledge with me. I'd like to especially thank Kevin Miller, Gene Joseph, Dr. Park (though those three were visiting scientists), Sean, Takeo, Bill Heath, Philippe, Erin, and Chris for their help throughout my years. Equally well, I have to thank the undergraduates I worked with who helped further many of the projects we were able to complete: Alex Nichols, Adam Harber, Mike Allen, Kyle Barras, and Bailee Roach.

Lastly, I have to thank my family and friends for their love and support throughout graduate school, especially my parents Sam and Linda Hunley and Karen Kowalski, and especially the siblings Michael, Josh, and Betty. I have to thank all the grandparents, uncles,

aunts, cousins, and every other family member for their support. And especially the other great friends in Blacksburg, Dr. Matt ‘Grandpa’ Clark, Mary Etna, Richard, Jake. And of course, I have to thank Shuo for the love and support throughout the years of graduate school. Without her support and listening to me vent, I most certainly could not have made it through.

ATTRIBUTION

Prof. Timothy E. Long
Professor of Chemistry, Virginia Tech

Dr. Matthew G. McKee
Former graduate student in the Long Research Group, my mentor as an undergraduate and collaborator on several research projects involving electrospun surfactants, polyelectrolytes, and PDLLA

Jenneffer P. England
Master's student in Prof. Turner's group, previously in the Long Research Group, helped synthesizing and electrospinning polyelectrolytes

Prof. Axel H.E. Müller
Professor at Universität Bayreuth, collaborated with the synthesis of star-shaped PDMAEMA

Alex Nichols
Undergraduate student from Austin College, synthesized and characterized the gelators

Adam Harber
Undergraduate from Virginia Tech Chemical Engineering, electrospun and characterized PMMA fibers with surface-migrating additives

Dr. Josh Orlicki
Research scientist at Army Research Laboratories, collaborated on the electrospun PMMA with surface-migrating additives

Dr. Adam Rawlett
Research scientist at Army Research Laboratories, collaborated on the electrospun PMMA with surface-migrating additives

Dr. Afia Karikari
Former graduate student in the Long Research Group, synthesized star-shaped PDLLAs

Dr. Brian Mather
Former graduate student in the Long Research Group, collaborated on electrospun star PDLLAs

Dr. John Layman
Former graduate student in the Long Research Group, collaborated on many projects and discussions including polyelectrolytes and surfactants

Dr. Ann Fornof

Former graduate student in the Long Research Group, collaborated on melt electrospun PDLLAs

Dr. Petra Pötschke

Research scientist at the Institut der Polymerforschung in Dresden, collaborated and provided materials for electrospun nonfunctionalized MWCNTs in TPU

Emily Anderson

Former graduate student in the Long Research Group, synthesized the polyurethane used to electrospin acid-functionalized MWCNTs

Bailee Roach

Undergraduate student of chemical engineering at Virginia Tech, electrospun polyurethane with carbon nanotubes

Dr. Sean Ramirez

Former postdoctoral assistant in the Long Research Group, synthesized functionalized MWCNTs

Dr. Eugene Joseph

Research scientist in the Long Group and Chemical Engineering, collaborated with the electrospinning of PU/MWCNT composites

Table of Contents

List of Figures

List of Tables

List of Schemes

Chapter 1: Introduction

1.1 Dissertation Overview

The central theme of this dissertation encompasses the harnessing of specific intermolecular interactions, including hydrogen bonds and electrostatic interactions, to create functional nanoscale fibers via electrospinning. The effect of these intermolecular associations on polymer solution behavior, such as solution rheology, conductivity, and fiber forming ability, was of paramount interest. The first three chapters following this one provide insight into the electrospinning technique and recent progress electrospinning functional polymers. The second chapter reviews the current state of understanding the behavior of charged polymers during electrospinning. The third and fourth chapters are published perspective articles highlighting the electrospinning of functional membranes for high-performance applications and phospholipid membranes, respectively.

The fifth chapter focuses on the influence of counteranion on thermal, solution, and electrospinning behaviors of polyelectrolytes. Poly(2-(*N*,*N*-dimethylamino)ethyl methacrylate) (PDMAEMA)-based polyelectrolytes were synthesized with a variety of anions ranging from polar halide anion to the hydrophobic bis(trifluoromethanesulfonyl)imide anion ($(CF_3SO_2)_2N^-$). The anion controlled the thermal degradation behavior and thermal transitions, and all aqueous-soluble polymers exhibited polyelectrolyte behavior in solution. The electrospinning behavior deviated significantly from that expected for neutral polymers and was highly dependent on counteranion. The sixth chapter describes the solution rheology and conductivity of copolymers of DMAEMA-HCl and diethylene glycol methyl ether methacrylate. Thermal analysis suggested these copolymers exhibited phase-mixed behaviors. Solution conductivity and rheology revealed

polyelectrolyte behavior at low ionic contents, and high conductivities were achieved at even 50% ionic content. The seventh chapter details the investigation of topological effects on polyelectrolyte solution behavior and electrospinning. Star-shaped PDMAEMA polymers were synthesized using atom-transfer radical polymerization and compared to linear PDMAEMA-based polyelectrolytes. The stars showed lower solution conductivities due to increased counteranion condensation within the cores. Unlike branched neutral polymers, which electrospin similar to neutral linear polymers, the star-shaped polyelectrolytes required significantly higher viscosities (> 1500 cP) and solution concentrations to form fibers through electrospinning.

Chapter Eight describes the solution rheology and electrospinning of wormlike micelles of low molar mass surfactants. Cylindrical micelles of surfactants (self-assembled through electrostatic interactions) can be electrospun into microfibers due to sufficient solution elasticity. Different surfactants including phospholipids and quaternary ammoniums were studied through rheology and electrospinning to understand the structure-electrospinnability effects. The ninth chapter focuses on electrospinning the presence of an oligomeric surface-active additive. The additive facilitates the electrospinning of uniform poly(methyl methacrylate) fibers at low concentrations. XPS analysis revealed that the fibers consisted of core-shell geometry with the surface-active additive forming the outside shell. The tenth chapter describes harnessing intermolecular hydrogen bonding to facilitate electrospinning of polylactide. The star-shaped polylactides terminally-functionalized with adenine and thymine complementary hydrogen bonding groups. These groups led to significantly increased viscosities above the dissociation temperature, and facilitated melt electrospinning of the low molecular weight stars. These

associative properties can be harnessed to develop materials with very low processing viscosities but very high solid-state mechanical properties.

The eleventh and twelfth chapters focus on polyurethane nanofibers electrospun in the presence of multiwall carbon nanotubes. The eleventh chapter describes the dispersion of unfunctionalized nanotubes through a high-shear melt mixing technique and the alignment of nanotubes in the electrospun fibers. Similarly, the twelfth chapter describes acid-functionalized carbon nanotubes dispersed into polyurethane solutions by ultrasonication. Both techniques led to highly aligned nanotubes in the resulting polyurethane nanofibers. The thirteenth chapter summarizes the accomplishments of the dissertation and the fourteenth chapter describes potential future projects stemming from the research presented in this dissertation.

Chapter 2: Electrospinning of Polyelectrolytes: Charging Forward

2.1 Abstract

Despite the overwhelming acceptance of electrospinning as a simple and versatile fiber formation process, relatively little fundamental understanding exists concerning the electrospinning of charged macromolecules. Polyelectrolyte membranes offer significant functional improvements for applications including gas sensing, ion capture and exchange, and cellular adhesion. Many reports on electrospinning of charge-containing polymers indicate that significantly higher viscosities are required for stable electrospinning, much higher than expected for neutral polymers. This review focuses on the electrospinning behavior of polyelectrolytes and their processing differences compared to neutral polymers. The electrospinning behavior of a wide variety of strong and weak polyelectrolytes is described with emphasis on the correlations between solution rheological behavior and electrospinnability. In addition, the advantages of functional polyelectrolyte nanofibers for high-performance applications are detailed.

2.2 List of Polymer Abbreviations Used

PAA – Poly(acrylic acid)
PAANa – Polyacrylate sodium salt
PAMPS – Poly(2-acrylamido-2-methyl-1-propane sulfonic acid)
PVOH –poly(vinyl alcohol)
PEO – poly(ethylene oxide)
PCL - polycaprolactone
PLLA – polylactide
PMMA – poly(methyl methacrylate)
PAH – poly(allylamine hydrochloride)
PVP – poly(vinyl pyridine)
PSSNa – poly(styrene sulfonate sodium salt)
PSS –poly(styrene sulfonate)
PDMAEMA –poly(2-(*N*,*N*-dimethyl)aminoethyl methacrylate)
Poly(MEBIm-BF_4) – poly(1-[2-methacryloyloxy)ethyl]-3-butylimidazolium tetrafluoroborate)
PVIM – poly(1-vinylimidazole)
PEVIMBr - poly(1-ethyl-3-vinylimidazolium bromide)

PBVIMBr – poly(1-butyl-3-vinylimidazolium bromide)
POVIMBr – poly(1-octyl-3-vinylimidazolium bromide)
SIS – poly(styrene-isoprene-styrene) block copolymer
SEBS – poly(styrene-(ethylene-*ran*-butylene)-styrene) block copolymer
PPy - polypyrrolidone
S-SEBS - poly(styrene sulfonate-(ethylene-*ran*-butylene)-styrene sulfonate) block copolymer

2.3 Recent Surge in Electrospinning

Electrospinning has evolved in recent years from a limited research interest to an industrially-feasible membrane fabrication technique.[1,2] The simplicity and versatility of the electrospinning technique has led to exponential growth in research publications in the field. Polymers and other materials forming electrospun fibers include polyolefins,[3,4] acrylics,[5-7] polyesters,[8,9] polyamides,[10,11] polyethers,[12-14] polysulfones,[15] biopolymers (such as cellulose, chitosan, silk, and even DNA),[16-19] phospholipids and surfactants,[20-22] carbon nanotube composites,[23-25] carbon fibers,[26] silanes,[27,28] and metal oxides and ceramics.[29-31] The wide range of materials suitable for electrospinning makes such membranes highly suited for a variety of applications including tissue engineering,[32] high performance filtration,[33] ultrafast and sensitive gas/liquid sensing,[34] ion-exchange,[35,36] and conductive membranes for electroactive devices.[28,37,38] The Donaldson Company, Inc. currently commercially produces electrospun membranes with a production line manufacturing tens of thousands of square meters of polyamide membranes each day.[39]

Electrospinning utilizes a high electric potential to draw a droplet of polymer solution or melt through the air towards a grounded or oppositely charged target. Figure 2.1 illustrates a typical electrospinning process. The repulsive forces between surface charges on the electrospinning jet lead to significant drawing of the fibers before deposition on the target.[1] Typically, electrospinning jets experience a bending instability which causes the jet to spiral in loops of increasing diameter before deposition, as depicted in Figure 2.1b.[1] During solution

electrospinning, the rapid evaporation of the solvent from the jet also leads to significant reduction of jet diameter. Electrospun nanofibers often have diameters on the order of 10 to 100 nm. The geometry of the collecting target can be controlled to tailor the nanofibrous membrane structures. Recent reports describe the collection of mats of randomly oriented fibers, mats of aligned fibers,[40] and even three-dimensional scaffolds of randomly oriented or aligned fibers.[41,42]

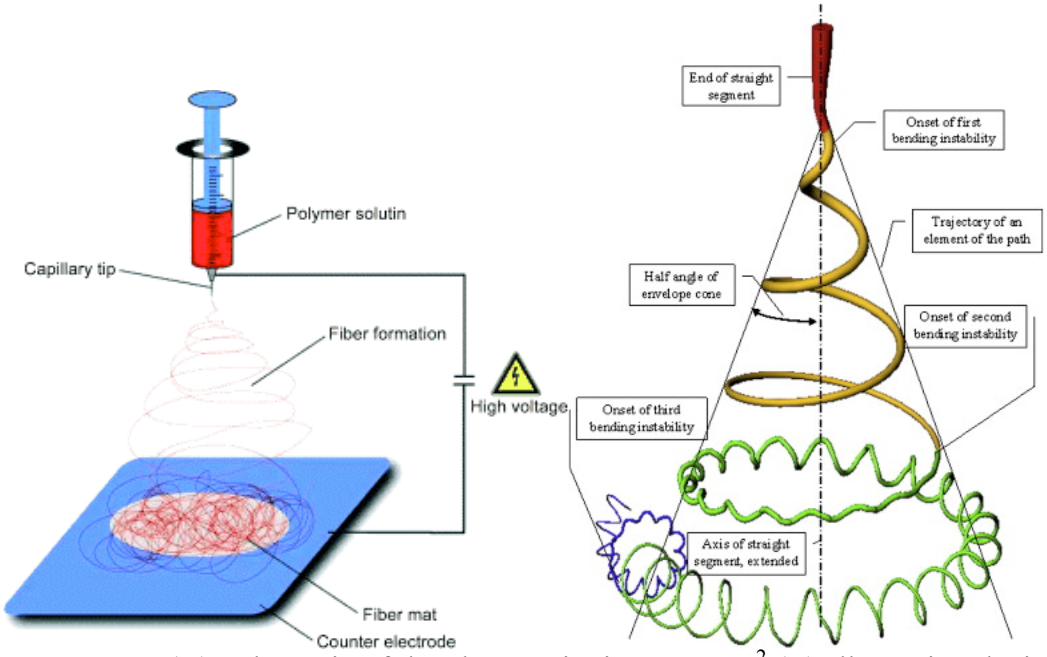

Figure 2.1. (A) Schematic of the electrospinning process.[2] (B) Illustration depicting the looping and bending of the electrospinning jet after the bending instability.[1]

2.4 Understanding the Electrospinning Behavior of Neutral Polymers

2.4.1 Requirement of Solution Elasticity

Capillary breakup represents the most common instability affecting solution electrospinning.[1] Surface tension pulls the electrospinning jet into droplets, preventing electrospinning at low polymer concentrations. Wnek et al.[43] proposed a dimensionless electrospinning number, $Vq/\gamma R^2$, to describe the balance of electrical and surface forces on the electrospinning jet, where Vq is the electrical energy and γR^2 is the surface free energy of the

Taylor cone. When the electrospinning number exceeds one, a jet of liquid will be ejected from the Taylor cone. An electrospinning number less than one indicates droplets of polymer solution ejecting from the Taylor cone. Higher voltages and lower surface tensions increase the electrospinning number, and both are known to aid in the formation of uniform fibers. The electrospinning number acts as a general rule of thumb, helping to explain certain phenomena observed when electrospinning parameters are changed.

Our research group first developed a semi-empirical correlation relating electrospun fiber morphology and fiber diameter to solution rheological transitions.[9] For a series of linear and branched polyesters of varying molecular weights, beaded fibers first formed above the critical concentration for entanglements (c_e) and uniform fibers formed above $2c_e$. These transitions corresponded to zero-shear viscosities (η_0) of 10 and 100 cP, respectively. When fiber diameter was plotted versus normalized concentration (c/c_e), the fiber diameter relationships all collapsed to a single curve independent of topology and molecular weight. Figure 2.2 shows fiber diameter versus normalized concentration for the series of polyesters as well as the semi-empirical fiber diameter relationship. In this review, the term "electrospinnability" will refer to a given polymer's tendency to form fibers at a specific solution concentration and viscosity. Polymers that form fibers at lower viscosities are referred to as more electrospinnable.

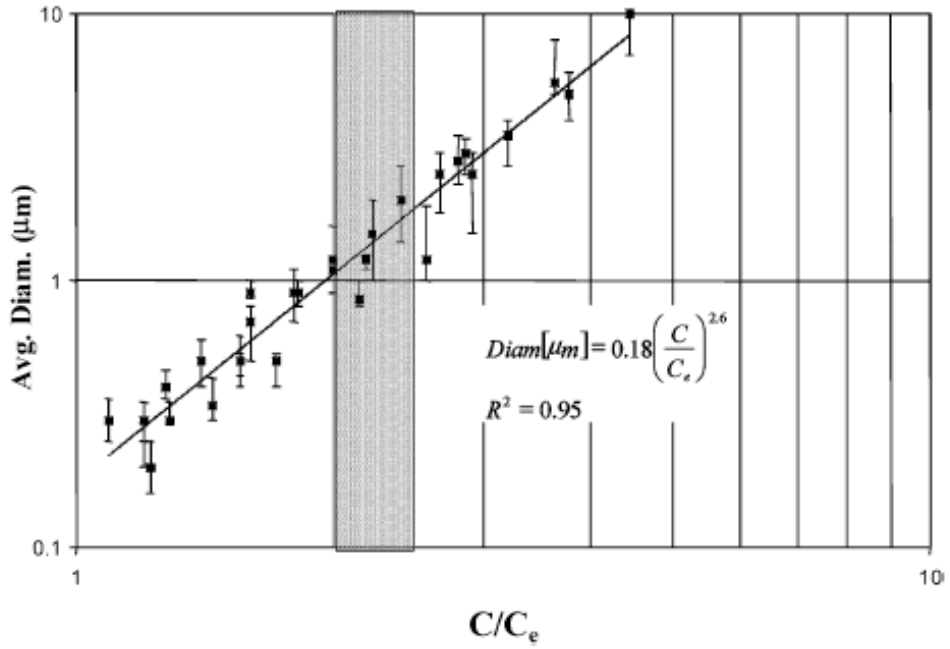

Figure 2.2. Fiber diameter plotted versus normalized concentration for a series of linear and branched polyesters. The solid line represents a least-squares regression best fit to the data.[9]

Wnek and coworkers[43] analyzed the electrospinning transitions based on the solution entanglement number ($(n_e)_{soln}$) and predicted fiber formation at greater than two entanglements per chain ($(n_e)_{soln} > 2$) and uniform fibers at $(n_e)_{soln} > 3.5$. The entanglement number can be calculated from the equation

$$(n_e)_{sol'n} = \frac{\phi_p M_w}{M_e},$$

where ϕ_p is the polymer volume fraction, M_w is the polymer weight-average molecular weight, and M_e is the polymer's critical molecular weight for entanglements. Figure 2.3 demonstrates the different electrospinning regimes for polystyrene of various molecular weights. The predicted solution entanglement numbers for electrospinning agreed well with experimental results and with the predictions based on c_e. Wilkes et al.[44] monitored fiber evolution in relation to the overlap concentration c^*. They observed only droplets in the dilute regime ($c/c^* < 1$) and

droplets with some beaded fibers in semi-dilute unentangled regime ($c/c^* > 1$). In the semi-dilute entangled regime ($c/c^* > 3$), they observed beaded and uniform fibers. Above $6c/c^*$ (corresponding to $c > 2c_e$), only uniform fibers formed. Recent reports from our research group[20,21] describing electrospun surfactants and from Rutledge et al.[45] detailing electrospun Boger fluids implied that the primary requirement for electrospinning is sufficient solution elasticity to stabilize the electrospinning jet over the short processing time, not necessarily polymer entanglements. This agrees with other results demonstrating that very high molecular weight polymers form stable fibers at concentrations below c_e.[43]

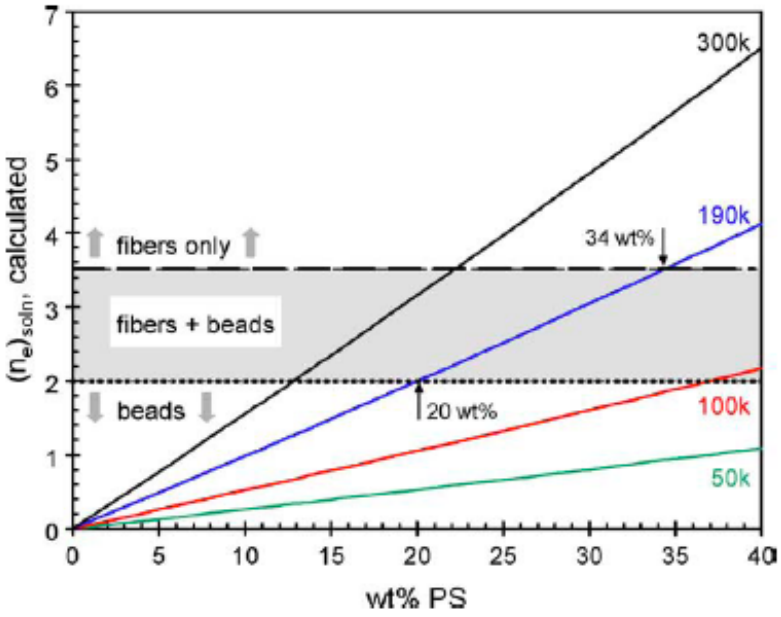

Figure 2.3. Calculated solution entanglement numbers versus polystyrene concentration for polymers with different molecular weights. The horizontal lines represent the different electrospinning regimes.[43]

2.4.2 Influence of Low Molar Mass Electrolyte

The addition of low molar mass electrolyte to neutral polymer solutions facilitates the formation of nanometer-diameter fibers. In terms of Wnek's electrospinning number, the added

salt increases the electrical energy of the Taylor cone, promoting fiber formation. Supaphol et al.[46] reported the electrospinning of poly(ethylene oxide) (PEO) with various amounts of inorganic salt. At low concentrations of salt (0.1% w/v), the salt resulted in a reduction of fiber diameter. However, at higher salt concentrations, the increased electrical energy of the Taylor cone led to a higher mass throughput and thicker fibers. Kim et al.[47] confirmed the increased throughput by measuring increasing mass rate of fiber deposition as a function of electrolyte concentration. Gupta et al.[48] studied the electrospinning of polycaprolactone (PCL) with added pyridine, a fugative weak salt. The addition of pyridine suppressed bead formation at lower polymer concentrations. However, fiber diameter increased exponentially as the concentration of pyridine increased. Other studies reported that the addition of electrolyte led to a decrease in fiber diameter.[47,49] Kim et al.[47] electrospun PAMPS in the presence of NaCl and $CaCl_2$. They found that the added salt decreased the average fiber diameter and decreased the number of beads due to more drawing during fiber formation. However, the mass throughput during electrospinning increased significantly due to increased electrical energy on the jet, and the thickness of the electrospun mat grew much faster. Figure 2.4 plots the fiber deposition rate and average fiber diameter of the PAMPS fibers as a function of NaCl or $CaCl_2$ concentration.

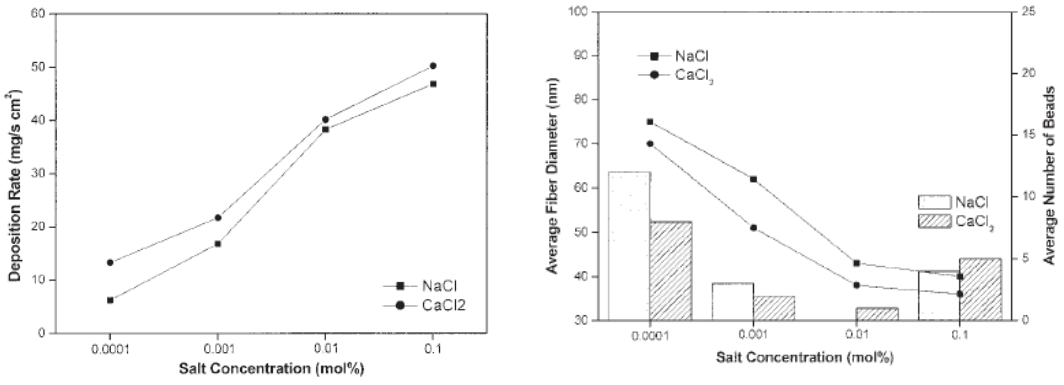

Figure 2.4. Influence of inorganic salt concentration on the (a) fiber deposition rate and (b) fiber diameter and number of beads for electrospun PAMPS.[47]

Surfactants affect the electrospinning process in two ways: increasing the conductivity (electrical energy) and decreasing surface tension (surface free energy) of the electrospinning solution. Both effects increase the electrospinning number, aiding in the electrospinning process. Often the addition of small amounts (< 5 wt%) of surfactant to electrospinning solutions results in uniform fibers at significantly lower polymer concentrations. Supaphol et al.[46] electrospun PEO in the presence of sodium dodecyl sulfonate (SDS) surfactant and found 3% w/v SDS was sufficient to decrease bead formation during electrospinning of a 4% PEO solution. Increasing levels of SDS also led to increased fiber diameters similar to increasing inorganic salt concentrations. The suppression of beads is demonstrated in the SEM micrographs in Figure 2.5. Lin et al.[50] found that the addition of cationic surfactant to polystyrene solutions suppressed the bead formation and led to decreases in fiber diameter. The fiber diameter reduction was greater for charged surfactants than for non-surface-active salts and uncharged surfactants. Our laboratories recently reported that oligomeric perfluorinated surface-active additives suppressed bead formation in poly(methyl methacrylate) fibers with no significant change in fiber diameter.[6] Surface analysis of the fibers also indicated the additive selectively migrated to the fiber surface, creating core-shell fibers with PMMA core and perfluorinated surface.

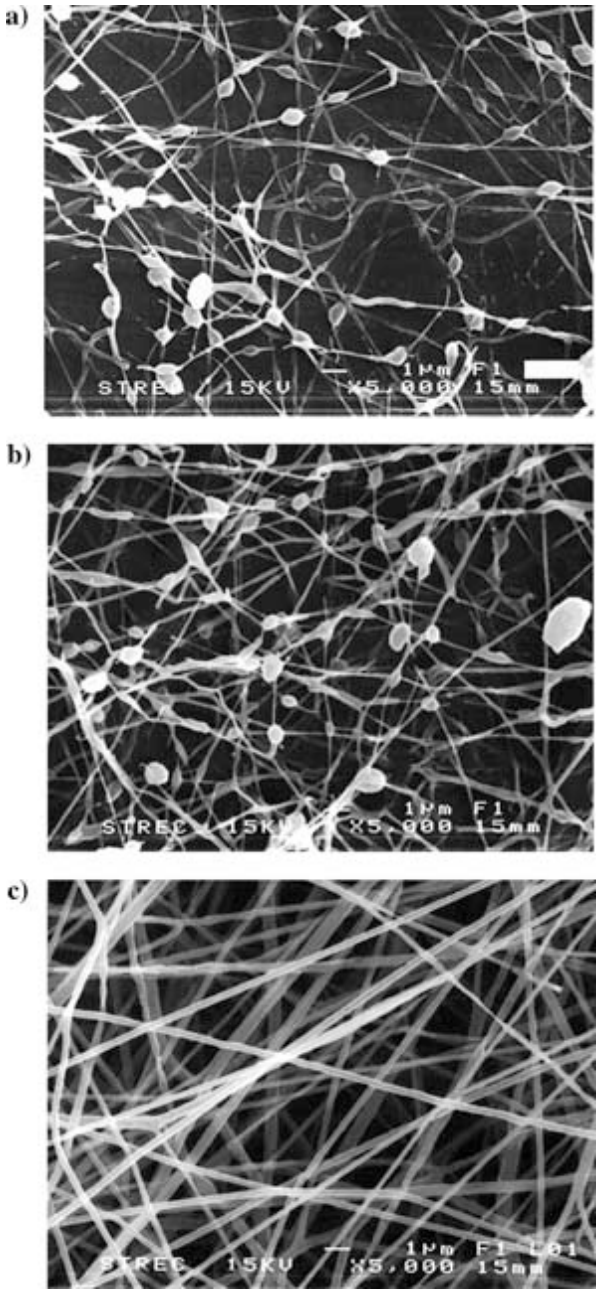

Figure 2.5. The effect of added SDS on the beaded fiber formation of PEO from solutions of 4% PEO. From top to bottom: 0.5, 1.0, and 6.0 wt% SDS.[46]

Surfactants also facilitate the electrospinning of biopolymers which are otherwise difficult if not impossible to electrospin, such as alginate,[51] chitosan,[52] and DNA.[18] Our research group recently demonstrated wormlike micelles of surfactants can be electrospun to form surfactant nanofibers.[20,21,53]

2.5 Electrospinning of Polyelectrolytes

Over the past few years, reports of electrospun polyelectrolytes and ionomers have increased in frequency. However, the charged macromolecules often present processing difficulties and their electrospinning behavior deviates significantly from that of neutral polymers. Literature reports of electrospun polyelectrolytes are often seemingly contradictory and confusing. Many studies describe extremely high viscosities required for fiber formation; other charged polymers display electrospinning behavior very similar to neutral polymers. Few reports dedicate more than a couple cursory sentences to explain the instabilities experienced by polyelectrolytes. Table 2.1 lists a wide variety of the polyelectrolytes, ionomers, and polyelectrolyte blends reported in the literature, as well as the viscosity at the onset of electrospinning when available.

Table 2.1. Electrospun Polyelectrolytes and Their Electrospinning Transitions

Polymer	Onset of Electrospinning		Ref.
	Viscosity	Entanglement Number	
poly(2-acrylamido-3-methyl-1-propane sulfonic acid)	< 90 cP		105
Poly(acrylic acid)	32 cP (H2O) 131 cP (DMF)		106
Poly(acrylic acid)/poly(allylamine hydrochloride) blend			76
Poly(acrylic acid)/poly(vinyl alcohol) blend			83
Chitosan			17,61
Chitosan/PEO blend			52
Quaternized chitosan/poly(vinyl pyrrolidone)			59
Poly(dimethylaminoethyl methacrylate hydrochloride)	1000 cP	$8c_e$	7
Poly(dimethylaminoethyl methacrylate triflic acid)	30 cP	$1.2c_e$	67
Sulfonated poly(ether ether ketone ketone)	90 cP		68
Poly(1-[2-(Methacryloyloxy)ethyl]-3-butylimidazolium BF_4)	~10 (specific) 4.6 cP (?)	$1.25c_e$	72
Nafion			37
Nafion/poly(acrylic acid) blend			5
PPV Precursor			107
Poly(styrene sulfonate) sodium salt			69,70

2.5.1 Weak Polyelectrolytes

Weak polyelectrolytes do not necessarily fully dissociate in solution. They often contain protonatable groups such as amines (chitosan, for example) or acid groups (poly(acrylic acid) (PAA), for example), the dissociation of which can be controlled by solution conditions. The ability of these functional groups to protonate and deprotonate depending on solution conditions means these polyelectrolytes do not retain a permanent charge. As such, these polyelectrolytes

often electrospin at lower viscosities with fewer instabilities. As a result, PAA was one of the first polyelectrolytes electrospun.[54-56] Scheme 2.1 shows the chemical structure of PAA and its deprotonation to form a charged polymer. Shi et al.[57] found the onset of fiber formation for PAA of 240,000 g/mol around 15 wt%. Solvent conditions dramatically affected fiber formation. Ding et al.[58] found the addition of ethanol to water reduced bead formation and led to thicker fibers due to increased viscosity at constant polymer concentration. However, no thorough reports fully correlate the solution rheology of PAA to electrospinning behavior.

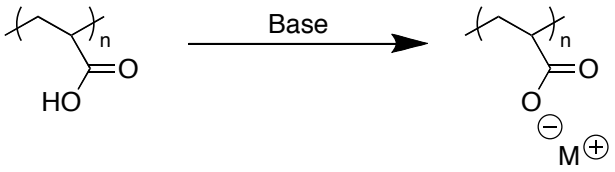

Scheme 2.1. Structure and deprotonation of PAA.

Chitin and its soluble deacetylated form chitosan (Scheme 2.2) represent one of the most abundant biopolymers, and many studies have investigated the electrospinning behavior of this biopolymer.[16,17,52,59-62] After some reported unsuccessful attempts to electrospun pure chitosan,[63] Ohkawa et al.[17,61] reported the successful electrospinning of chitosan from very viscous solutions in trifluoroacetic acid (TFA). In this acidic solvent, chitosan becomes highly protonated and charged, hindering electrospinning. Unlike poly(acrylic acid), chitosan required very high viscosities to electrospin. Ohkawa and coworkers found that beaded fibers formed between 200 and 800 cP and uniform fibers formed between 800 and 1000 cP. Above 1000 cP, the solution viscosity hindered electrospinning. The electrospinnability of chitosan with varying molecular weights is shown in Figure 2.6.[17] Fiber diameters versus polymer concentration fit a single linear relationship regardless of chitosan molecular weight. The authors, however, presented no discussion why such high viscosities were required for electrospinning.

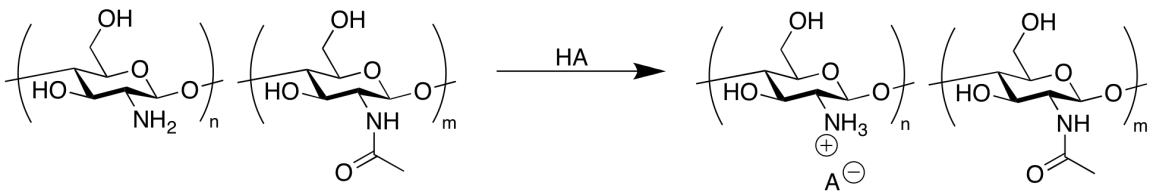

Scheme 2.2. Chemical structure of chitosan and its protonation in acidic solvent. The degree of deacetylation (DA = $n/(n+m)*100\%$) varies depending on the preparation.

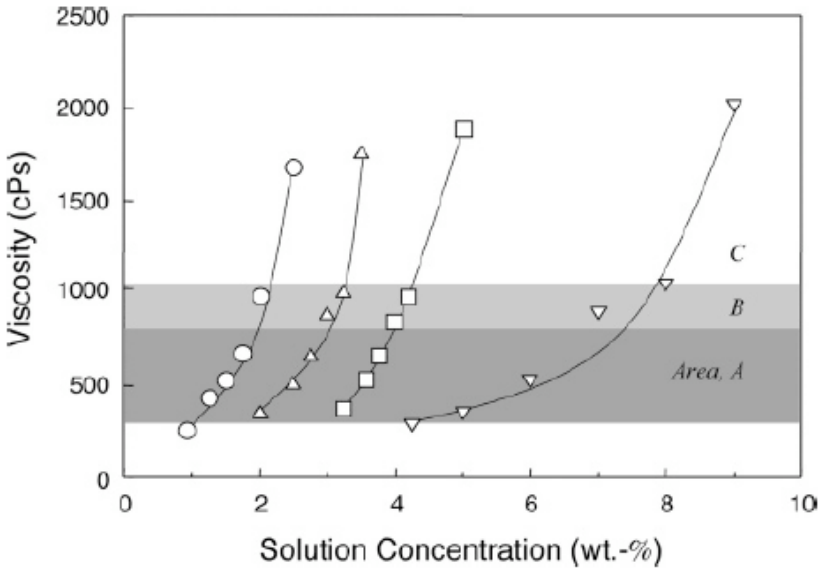

Figure 2.6. Electrospinnability of four chitosan samples of different molecular weights. The shaded areas represent different electrospinning regimes: A – beaded fibers; B – uniform fibers; C – no fiber formation due to high viscosity. The viscosity-average molecular weights investigated were 1.80×10^6 (circles), 1.58×10^6 (triangles), 1.31×10^6 (squares), and 2.1×10^5 (inverted triangles) g/mol.[17]

The degree of deacetylation of chitosan also plays a large role in its electrospinnability. Higher levels of deacetylation lead to higher charge densities along the polymer chain and more polyelectrolyte behavior. The polymers electrospun by Ohkawa et al.[17,61] had deacetylations between 70 - 80%. Jang et al.[64] electrospun 54% deacetylated chitosan and observed uniform fiber formation below 500 cP for several molecular weights when electrospun from 90% aqueous

acetic acid. These authors found chitosan of intermediate molecular weight (106,000 g/mol) electrospun better than higher or lower molecular weight samples. However, Krause et al.[65] were unable to electrospin chitosan of 85% deacetylation, even at concentrations exceeding 4500 cP solution viscosity (5 wt% chitosan in 90% aqueous acetic acid, roughly $2.5c_e$). Westbroek et al.[66] found that chitosan (190,000 – 310,000 g/mol) of 75-85% deacetylation electrospun at 3 wt% in the same 90% aqueous acetic acid solvent.

2.5.2 Strong Polyelectrolytes

Our research laboratories were the first to investigate the electrospinning of a strong polyelectrolyte, poly(2-dimethylaminoethyl methacrylate hydrochloride) (PDMAEMA-HCl).[7] The chemical structure of PDMAEMA-HCl is shown in Scheme 2.3. We related the solution rheology of PDMAEMA-HCl to the electrospinning behavior and found that this strong polyelectrolyte electrospun at viscosities greater than 1000 cP and normalized concentrations of at least $8c_e$. The addition of NaCl salt to the PDMAEMA-HCl solutions led to contraction of the extended polyelectrolyte conformation and rheological behavior similar to neutral polymers. The added salt also influenced electrospinning, and fibers formed at significantly lower viscosities and entanglement numbers. At 50 wt% added NaCl, the onset of fiber formation occurred at $1.7c_e$ and 100 cP, much closer to the predicted behavior for neutral polymers. Figure 2.7 shows the electrospun fiber diameter versus normalized concentration for PDMAEMA-HCl with various concentrations of added salt. The differences between polyelectrolyte electrospinning behavior and neutral polymer behavior were attributed to instabilities in the electrospinning jet caused by strong charge repulsions under the electric field. In the presence of salt, charge screening reduced the instabilities during electrospinning, making fiber formation at lower concentrations and viscosities possible. However, fiber diameters remained at least one

order of magnitude lower than those expected for neutral polymers at the same normalized concentrations and viscosities due to the high conductivities.

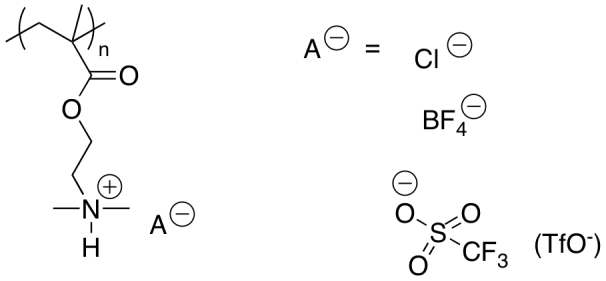

Scheme 2.3. Structure of PDMAEMA-based polyelectrolytes with various counteranions.

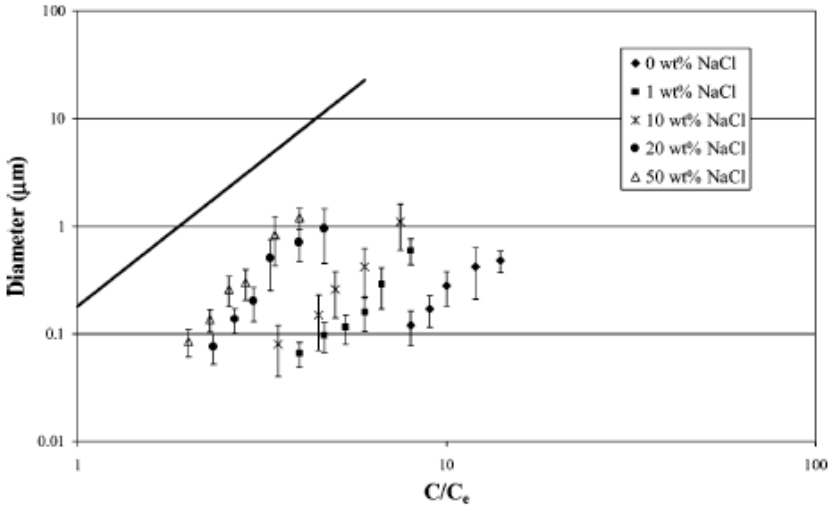

Figure 2.7. Diameter plotted versus normalized concentration for PDMAEMA-HCl fibers electrospun from 80/20 H_2O/methanol with increasing levels of added NaCl. The solid line represents the semi-empirical fiber diameter correlation previously developed for neutral, non-associating polymers.[7]

We further investigated the effect of counteranion on polyelectrolyte electrospinning behavior and synthesized polyelectrolytes PDMAEMA-HBF_4 and PDMAEMA-HOTf (Scheme 2.3).[67] Independent of the counteranion, all polyelectrolytes exhibited polyelectrolyte behavior in solution as indicated by solution rheology. The polyelectrolytes with larger, more hydrophobic anions electrospun at lower viscosities and solution entanglement numbers.

PDMAEMA-HBF_4 and PDMAEMA-HOTf both electrospun at viscosities of 30 cP, which corresponded with normalized solution concentrations of $1.8c_e$ and $1.2c_e$, respectively. All polyelectrolyte fibers had nanometer diameters, significantly lower than the fiber diameters expect for neutral polymers at the same viscosities.

Recently, other reports have described the electrospinning of strong anionic polyelectrolytes including sulfonated poly(ether ether ketone ketone) (SPEEKK),[68] poly(styrene sulfonate).[69,70] The onset of fiber formation for the SPEEKK was reported between 10 and 12.5 wt% in solution, corresponding to viscosity around 50 cP. Shaw et al.[70] found the onset of fiber formation for aqueous PSSH solutions at $2c_e$ and uniform fiber formation at $3.5c_e$, which corresponded to solution viscosities of 210 cP and 2990 cP, respectively. Scheme 2.4 shows the ion-exchange of PSSNa to form PSSH, indicating the structural differences between the two polymers. The onset of fiber formation corresponded to a transition in the storage modulus scaling behavior of the solutions, as depicted in Figure 2.8. The uptick in solution elasticity occurred at 15 wt%, but the measured c_e occurred at about 7 wt%. The authors proposed that the elasticity required to stabilize the jet did not form until well above the critical concentration for entanglements.

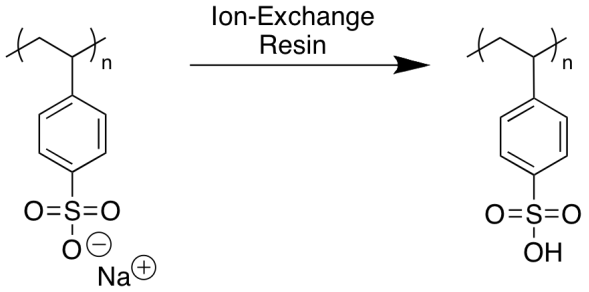

Scheme 2.4. Ion-exchange of PSSNa to form PSSH.

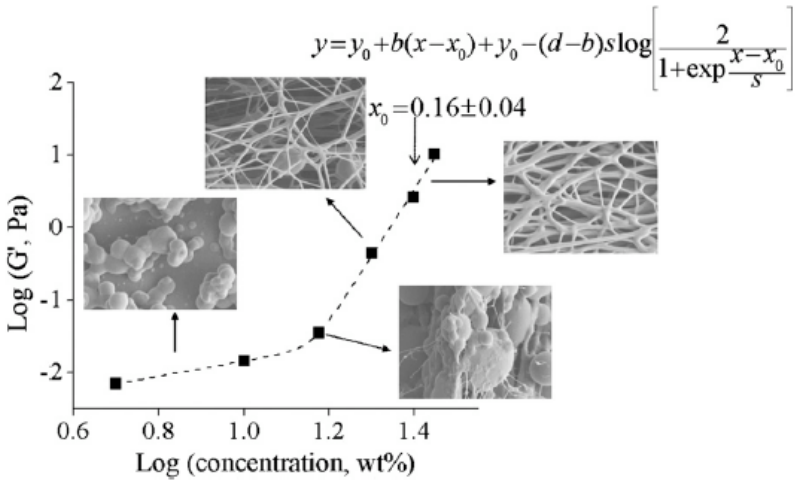

Figure 2.8. Plot of G' versus PSSH concentration with SEM images illustrating the fiber morphology at various concentrations. The dashed line represents a continuous kink equation fit to the data.[70]

Han and coworkers[71] reported the electrospinning of sodium alginate (Scheme 2.5). This anionic biopolymer did not electrospin from water due to strong intermolecular interactions. However, upon introduction of glycerol to the solvent system, the alginate assumes a more flexible conformation in solution. The addition of glycerol breaks up intramolecular hydrogen bonding of the sodium alginate, allowing it to assume a more expanded and flexible conformation in solution. Figure 2.9 schematically illustrates the influence of glycerol on the solution conformation of sodium alginate. The different conformation was confirmed by significant increases in solution viscosity upon the addition of glycerol. Uniform electrospun fibers were readily formed from concentrated solutions in mixtures of water and glycerol. However, the electrospinning of uniform alginate fibers from the water/glycerol solvent still required extremely high viscosities in excess of 100,000 cP.

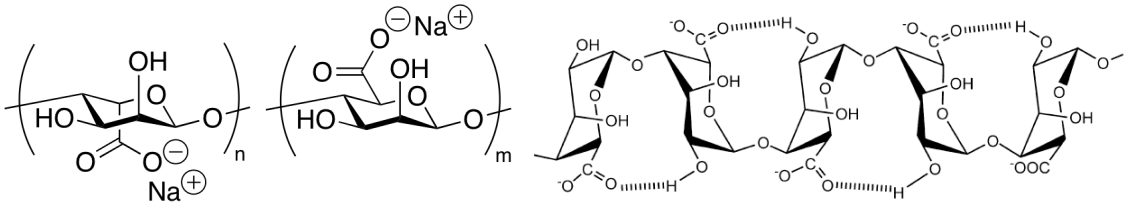

Scheme 2.5. (A) Chemical structure of sodium alginate. (B) Intramolecular hydrogen-bonding of the guluronate blocks in sodium alginate.[71]

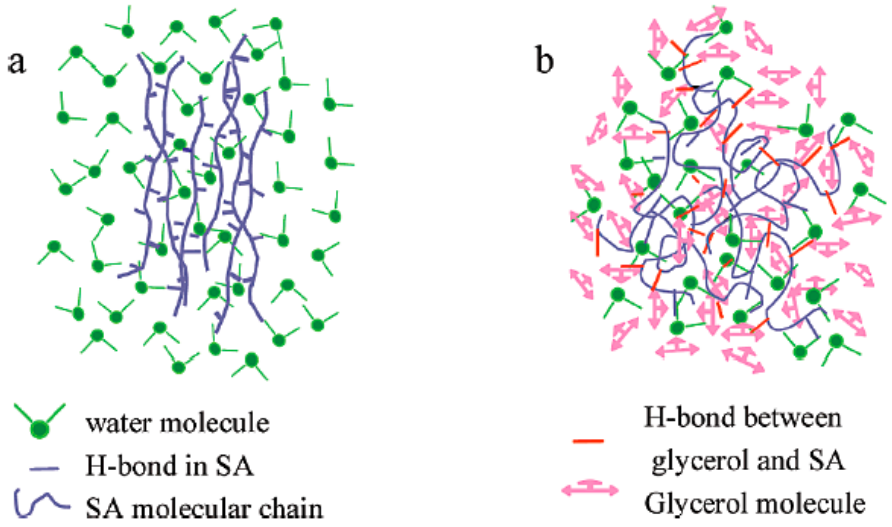

Figure 2.9. Schematic depiction of solution conformation of sodium alginate in (a) water and (b) water/glycol solvent systems. The addition of glycerol disrupts hydrogen-bonding between alginate, leading to a more expanded conformation and dramatically increased viscosities.[71]

Chen and Elabd[72] synthesized a polyelectrolyte from the ionic liquid monomer 1-[2-(methacryloyloxy)ethyl]-3-butylimidazolium tetrafluoroborate (Scheme 2.6) and electrospun this polymerized ionic liquid from a cosolvent of 3/1 acetonitrile/DMF. Solution rheology indicated that the polymer exhibited polyelectrolyte behavior, however, the onset of fiber formation in electrospinning occurred at $1.25c_e$ and uniform fibers formed at $2c_e$. The fiber diameters were almost one order of magnitude smaller than those expected for neutral polymers due to the high conductivities of the polyelectrolyte solutions. As observed by our laboratories for PDMAEMA-

based polyelectrolytes,[67] the use of a charge-delocalized counteranion (BF_4^- in this case) resulted in the onset of fiber formation at low entanglement numbers.

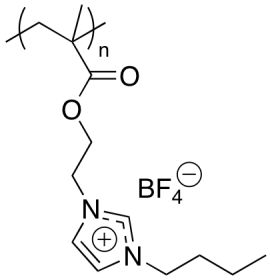

Scheme 2.6. Structure of poly(1-[2-(methacryloyloxy)ethyl]-3-butylimidazolium tetrafluoroborate) polymerized ionic liquid.

To better understand the behavior of charge-containing polymers during electrospinning, our research group has recently investigated the electrospinning of alkylated poly(1-vinyl imidazolium)s, the structures of which are shown in Scheme 2.7. Poly(1-vinylimidazole) (PVIM) exhibited rheological behavior expected for a neutral polymer, while the alkylated polyelectrolytes all showed polyelectrolyte-type scaling in solution rheology. Table 2.2 lists the onsets of fiber formation for all imidazolium-based polyelectrolytes investigated. PVIM electrospun from a water/methanol solvent mixture only at very high viscosities of 340 cP or $3.3c_e$. The discrepancy between PVIM behavior and the behavior expected for neutral polymers could arise from electrochemically-induced oxidation and charging of the imidazole ring during electrospinning. The charged polyimidazoliums also electrospun successfully. PEVIMBr required very high viscosities to form fibers, almost twice the viscosity of PVIM. However, PBVIMBr and POVIMBr, electrospun at much lower normalized concentrations and viscosities. The occurrence of instabilities during electrospinning decreased as the alkyl chain length and hydrophobicity of the polycation increased.

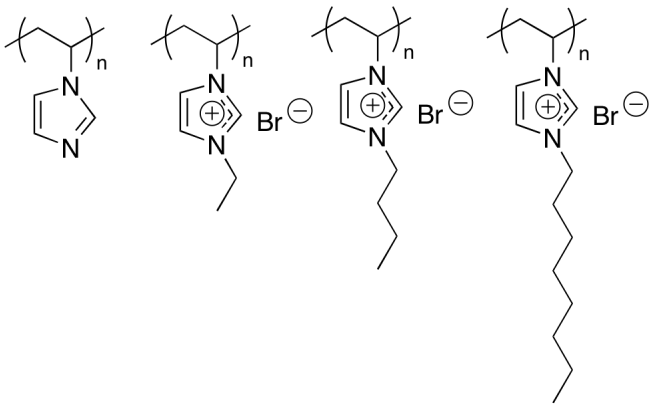

Scheme 2.7. Structures of alkylated poly(vinyl imidazoliums). From left to right: poly(1-vinyl imidazole), poly(1-ethyl-3-vinyl imidazolium bromide), poly(1-butyl-3-vinyl imidazolium bromide), and poly(1-octyl-3-vinyl imidazolium bromide).

Table 2.2. Onset of Fiber Formation for Poly(1-alkyl-3-vinyl imidazolium bromide)s.

Polymer	Onset of Fiber Formation	
	c/c_e	η_0 (cP)
PVIM	3.3	340
PEVIMBr	3.7	780
PBVIMBr	1.9	40
POVIMBr	1.3	30

2.5.3 Trends in the Electrospinnability of Polyelectrolytes

Unlike neutral polymer electrospinning, the electrospinning behavior of polyelectrolytes cannot be completely explained using solution elasticity. The solution viscosity required for fiber formation varies over orders of magnitude for different polyelectrolytes, and the $(n_e)_{soln}$ also varies dramatically. The onset of fiber formation (in terms of normalized concentration and solution viscosity) appears to depend heavily on chemical structure and the presence of salt to screen electrostatic interactions. Several studies indicated that the hydrophilicity of the specific ions strongly affects the instabilities experienced during electrospinning. The PDMAEMA-based polyelectrolytes with large, hydrophobic, charge-delocalized counteranions (BF_4^- and TfO^-

) electrospun at comparatively very low concentrations and viscosities. Similarly, the more hydrophobic poly(1-alkyl-3-vinyl imidazolium bromide)s with longer alkyl functionalities electrospun at c/c_e and viscosities similar to neutral polymers. The strong polyelectrolyte poly(MEBIM-BF_4) synthesized by Chen and Elabd behaved similarly, forming beaded fibers at concentrations as low as $1.25c_e$.

The other polyelectrolytes discussed demonstrated similar correlations. The electrospinnability of weak polyelectrolytes can be increased by decreasing the amount of charge on the polyelectrolyte. PAA electrospun more readily under acidic conditions or in less polar solvents when the carboxylic acid group remained protonated. Chitosan with lower degrees of deacetylation successfully electrospun at lower viscosities and concentrations than the more highly-charged chitosan. In most reports, chitosan was electrospun under very acidic conditions, when the counteranion was either acetate or trifluoroacetate. In addition, most electrospun anionic polyelectrolytes had small, polar countercations (primarily sodium cations). Exchanging these cations for larger, hydrophobic organic cations (such as tetraalkylammonium ions) could lead to increased electrospinnability at lower concentrations and viscosities.

2.5.4 Polyelectrolytes as a Processing Aid

The addition of low levels of polyelectrolyte to neutral polymer electrospinning solutions aids fiber formation in the same ways as adding low molar mass electrolyte and surfactant. Park et al.[73] added PAA-Na or PAH to solutions of PEO at concentrations less than 5 wt% and measured decreases in surface tension and dramatic increases in solution conductivity. At a constant PEO concentration, the added polyelectrolyte led to a reduction in fiber diameter and a suppression of beaded fiber formation. Similarly, Rashkov et al.[59] found that increasing the ratio of quaternized chitosan to PVP in composite electrospun fibers led to a decrease in fiber

diameter and decrease in the standard deviation of fiber diameters. The researchers extended the electrospinning of polyelectrolytes in the presence of neutral polymers to form fibers containing chitosan, PAMPS, and poly(PAMPS-*co*-PAA) copolymers, all electrospun in the presence of PVOH or polyacrylamide.[74] In all cases, increasing levels of polyelectrolyte led to decreased fiber diameters. Conversely, Li and Hsieh[75] electrospun PAA with PVOH and observed an increase in fiber diameter as PAA content increased.

PAA has also been used to facilitate the electrospinning of other ionomers and polyelectrolytes. Chunder and coworkers[76] electrospun blends of PAA and poly(allylamine hydrochloride) (PAH) at low pH when the ratio of PAA to PAH was above 2. Elabd et al.[5] reported that the addition of PAA to Nafion® allowed the formation of polyelectrolyte nanofibers. PAA provided sufficient entanglements to electrospin the Nafion; without the PAA, Nafion® did not form electrospun fibers.

2.5.5 Layer-by-Layer Fiber Assembly

Layer-by-layer (LbL) assembly involves the sequential assembly of oppositely charged polyelectrolytes to form a repeating bilayer structure. Applying this technique to the surface of electrospun nanofibers yields nanofibrous polyelectrolyte membranes. In addition, the LbL technique can use readily-electrospun uncharged polymer fibers. The technique is schematically depicted in Figure 2.10. Ge et al.[77] developed hollow multilayered polyelectrolyte tubes by first electrospinning polystyrene microfibers, alternatively coating with PAH and PSSNa, followed by selective dissolution of the PS core. To prevent buckling or collapse of the hollow structures, further experiments demonstrated that the thickness of the hollow fibers needed to be at least 0.17 times the diameter of the tube.[78] Figure 2.11 shows SEM micrographs of the hollow polyelectrolyte multilayered tubes.

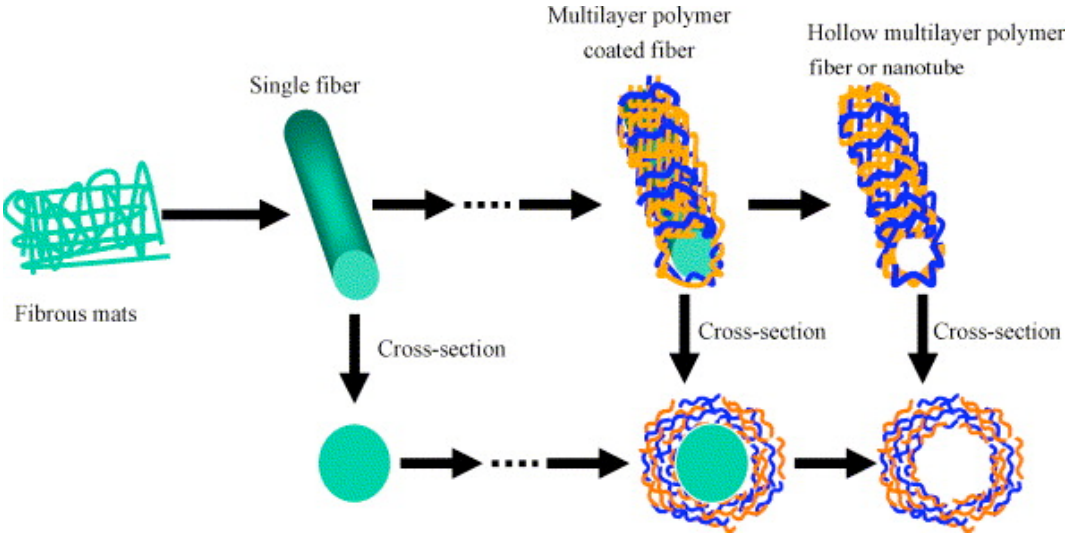

Figure 2.10. Schematic of layer-by-layer self assembly of polyelectrolyte multilayers onto an electrospun fiber surface.[77]

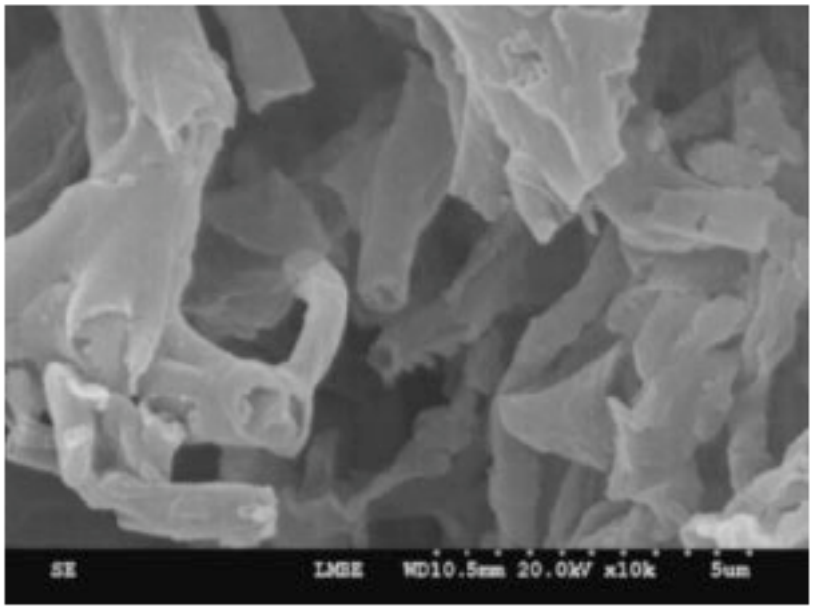

Figure 2.11. Hollow PAH/PSSNa multilayered tubes.[78]

The LbL technique also allows the formation of multifunctional nanofibrous membranes of oppositely-charged polyelectrolytes which would otherwise precipitate from solution, thereby preventing traditional electrospinning. Polycationic chitosan and polyanionic sodium alginate

are both derived from biopolymers and both promote cellular growth. However, in solution together they form insoluble polyelectrolyte complexes. However, these two polymers have been deposited by LbL techniques on the surface of either cellulose[79] or polyamide[80] electrospun fibers. These composite membranes promoted the growth of human bronchial epithelial cells or beagle cartilage cells, respectively. However, the deposition of more than ten polyelectrolyte bilayers on the polyamide fibers led to a loss of the fibrous morphology and film formation, resulting in a dramatic loss in cell attachment and proliferation. The LbL technique allows the formations of fiber surface chemistries not possible by tradition electrospinning techniques.

2.5.6 Polyelectrolyte Complexes

Similar to the LbL technique, the electrospinning of polyelectrolyte complexes (PECs) will generate nanofibers comprised of oppositely-charged polyelectrolytes. However, the strong electrostatic interactions between PECs leads to rapid coagulation and precipitation, so electrospinning conditions must be properly designed. Ohkawa et al.[81] discovered that a side-by-side electrospinning approach, with one solution of chitosan and one solution of PAA, led to PEC formation during electrospinning as the solutions mixed. By electrospinning side-by-side in a continuous fashion, the PECs that formed during electrospinning formed solid continuous fibers. The resulting PEC composite fibers did not dissolve in water and exhibited promising toughness, with extensibilities approaching 30%. Rashkov et al.[62] simplified this technique by electrospinning from a homogenous solution of oppositely charged polyelectrolytes. Below pH 3, PAA remains protonated and cannot form a PEC with chitosan. By electrospinning from a concentration aqueous formic acid solution, the two polymers remained in solution. During electrospinning, as the water and formic acid evaporated and the PAA began to deprotonate, the

PEC formed. Novel insoluble composite fibers of chitosan/PAA and chitosan/PAMPS were prepared through this technique.

2.6 Applications for Polyelectrolyte Fibers

2.6.1 Ultrafast Sensors

Nanofibrous electrospun membranes outperform many conventional sensing membranes due to their high surface area and high porosity.[34] Sensing mechanisms include acoustic wave measuruments (i.e via a quartz-crystal microbalance), resistive measurements, and even optical/photoluminescent measurements. Many reports have demonstrated PAA-based electrospun membranes as high efficiency and ultrafast sensors for humidity[82,83] and ammonia.[58] Ding et al.[83] electrospun composite membranes of PAA and PVOH onto QCM crystals to measure humidity. They found that the frequency shift response was highly dependent on humidity level and the sensor morphology. Nanofibers with higher surface area demonstrated the largest and fastest response, as shown in Figure 2.12. The response times decreased approximately 50% for the nanofibrous sensors compared to film sensors of the same composition. For example, upon increasing the relative humidity from 70% to 80%, the characteristic response times decreased from 151 s for the film sensor to 95 s and 84 s for the PAA-PVOH and pure PAA electrospun membranes. The frequency shifts were stable over a period of one month at high humidity. Similar membranes have shown ultrasensitive responses to ammonia gas concentrations on the order of 100 ppb.[58]

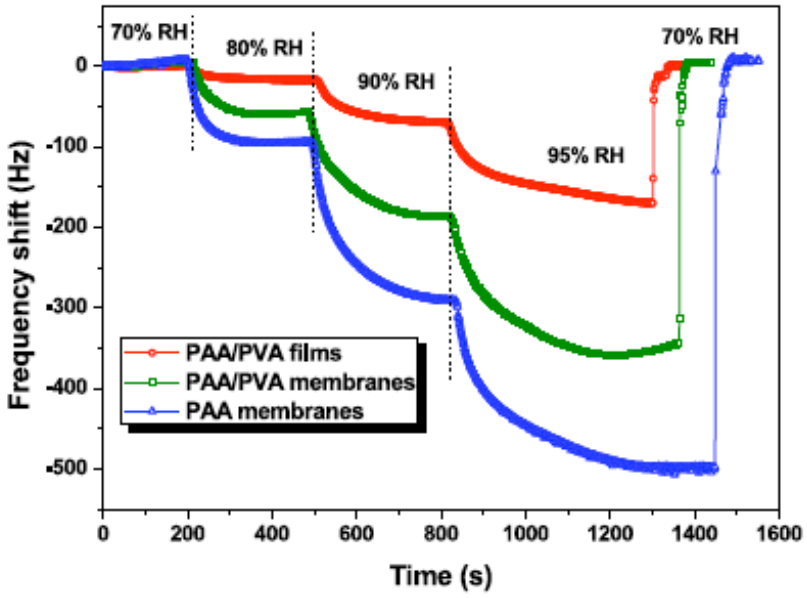

Figure 2.12. Frequency shift response for QCM sensors coated in PAA-PVOH composite film or fibers upon increases in ambient humidity.[83]

Optoelectronic sensors rely on increased or quenched emissions as a response to specific solutes. Samuelson et al.[54,84] developed fluorophore-containing sensors for optical sensing. PAA conjugated with pyrene methanol formed electrospun nanofibers which exhibited dramatic fluorescence quenching in the presence of electron-deficient metal ions (i.e. Fe^{3+} and Hg^{2+}) as well as nitro-aromatic compounds such as DNT and TNT.[54] The emission quenching of the electrospun fibers was about 2 to 3 orders of magnitude greater than films of the same conjugated polymer. Similarly, the researchers created a core-shell fibrous sensor by electrostatically coating cellulose acetate fibers with hydrolyzed poly[2-(3-thienyl)ethanol butoxy carbonyl-methyl urethane] (in the sodium salt form).[84] These fibers showed rapid, strong fluorescence quenching in response to low concentrations (10^{-7} M) of cytochrome *c* and methyl viologen. Chen et al.[85] found similar results for electrospun fibers of PMMA and poly{[9,9-di(3,30-N,N0-trimethylammonium) propylfluorenyl-2,7-diyl]-alt-(9,9-dioctylfluorenyl-2,7-diyl)} diiodide salt (PF^{+}). The aligned nanofibers formed phase-separated structures with periodic PF^{+}

domains (Figure 2.13a). The cationic nanofibers showed significant fluorescence quenching in the presence of negatively charged plasmid DNA. Figure 2.13b shows the emission spectra of the fibers upon exposure to varying concentrations of plasmid DNA.

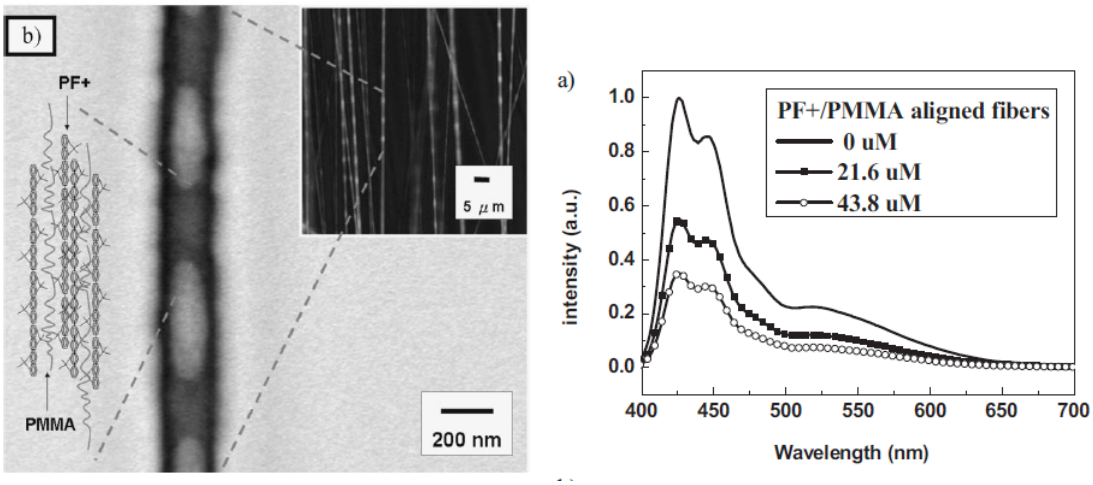

Figure 2.13. Electrospun PMMA/PF+ Nanofibers and their luminescence response to plasmid DNA.[85]

2.6.2 Filtration and Water Purification

Due to their high porosity and small pore size, electrospun nanofibrous membranes are ideally suited for filtration applications.[33] The Donaldson Company, Inc., commercially produces electrospun membranes for air filtration applications.[39] The use of polyelectrolytes enhances the performance of electrospun filters by introducing specific surface chemistries to further purify liquid and air media. Polystyrene nanofibers have been sulfonated for use as an ion-exchanger with controllable ion-exchange capacities based on sulfonation time.[35] Similar membranes based on sulfonated composites of polystyrene and poly(styrene-isoprene-styrene) were able to remove Cu^{2+} ions from solution.[36] Shi et al.[57] electrospun and crosslinked PAA-PVOH membranes and found the membranes remained dimensionally stable in water upon long immersions. The PAA membranes quickly removed Cu^{2+} ions from solution with efficiencies up

to 91% copper removal in less than 30 min. The nanofibers showed strong specificity, with no absorption of calcium, and strong copper complexations in the presence of 50 pp Ca^{2+} ions, as shown in Figure 2.14. Chitosan composite membranes showed similar rapid ion uptake from aqueous solutions. These nanofibers were shown to uptake Cu^{2+}, Pb^{2+}, and Cr^{6+} from aqueous solutions.[86,87] Equilibrium copper adsorption for the nanofibers was 6 and 11 times higher than equilibrium copper adsorption for chitosan nanoparticles and films, indicating the increased surface area of the nanofibers significantly enhanced separation performance.[87] The chitosan nanofibrous membrane also showed significant promise for water and aerosol filtration by efficiently separating polystyrene beads, exhibiting antibacterial activity against *E. coli*, and even exhibiting 70% aerosol filtration efficiency.[86]

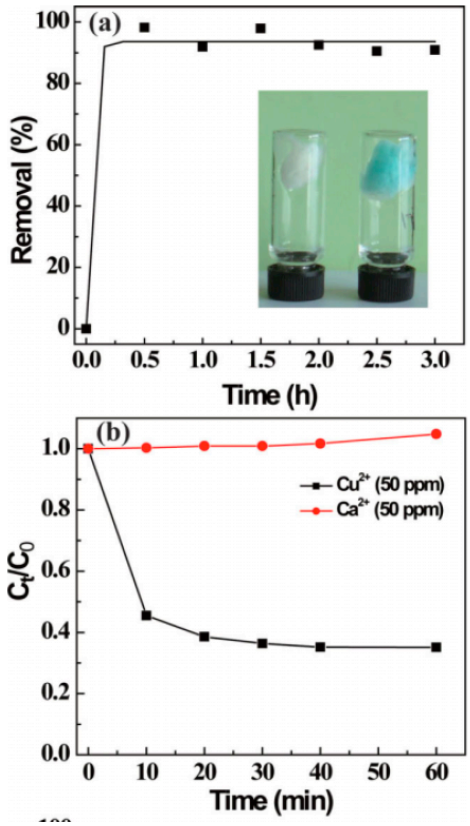

Figure 2.14. Removal of Cu^{2+} ions from solution by PAA-PVOH crosslinked mats. (A) Removal of Cu^{2+} ions over time with inset showing fibrous membrane before and after exposure to Cu^{2+}.[57]

2.6.3 Tissue Engineering

In terms of the number of publications, tissue engineering represents the most popular use of electrospun membranes. Electrospun scaffolds can direct the growth and differentiation of a wide variety of cells and organs, and many recent reviews cover the application of nanofibers for tissue engineering.[32,88-91] Electrospun fibers mimic the natural extracellular matrix, making them ideal for this application.[92] Figure 2.15 shows cross-sectional SEM micrographs of extracellular matrix and an electrospun biomimic comprising cellulose acetate. Most reports of electrospun tissue engineering scaffolds focus on the use of biocompatible (e.g. PLLA, PLGA, PCL) or bioderived (e.g. collagen, fibroin, chitosan) polymers to improve cellular compatibility. Due to

the large number of reviews written on the subject in recent years, this section will only concentrate on the added benefits of charge-containing polymers on electrospun tissue engineering scaffolds.

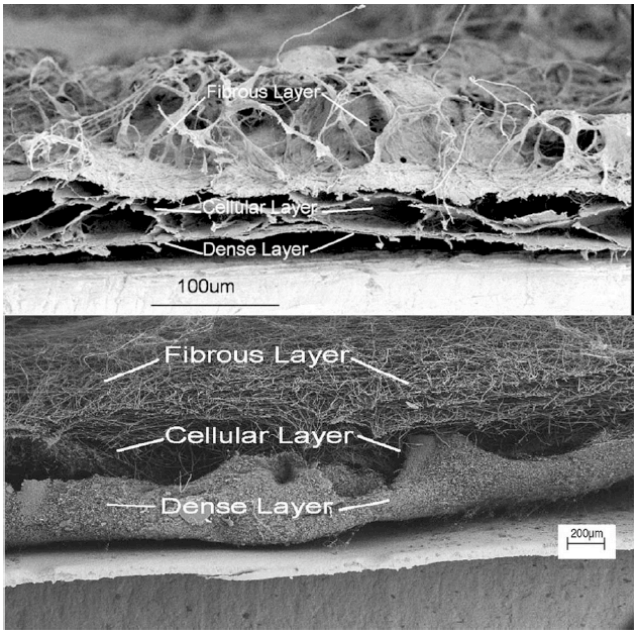

Figure 2.15. (a) SEM image of porcine urinary bladder matrix. (b) SEM image of ECM-mimicking electrospun membrane.[92]

Cationic polymers (i.e. chitosan) aid in cellular adhesion through electrostatic interactions with cells. Chitosan was electrospun at varying ratios with PCL, and fluorescence microscopy revealed that increasing levels of chitosan lead to increased adhesion of MC3T3-E1 cells, as shown in Figure 2.16.[93] The chitosan also directed the attached cells to deposit calcium and express ALP, vital in the formation of bone-like tissue. The ALP expression and calcium deposition increased dramatically as the chitosan content of the scaffold increased. The cationic nature of the chitosan-containing scaffolds electrostatically interacted with the GAGs and growth factors, promoting cellular differentiation. Gu and Ding et al.[94,95] similarly showed that galactosylated chitosan membranes showed improved affinity for hepatocyte adhesion. The use

of galactosylated chitosan membranes in a liver-mimicking bioreactor led to increased hepatocyte adhesion (by a factor of 1.59), as well as 1.73-fold and 2.86-fold increase in the protein and urea synthesis of the bioreactor, respectively.[95] Cationic electrospun membranes of linear PEI showed similarly high affinities for human fibroblast cells.[96]

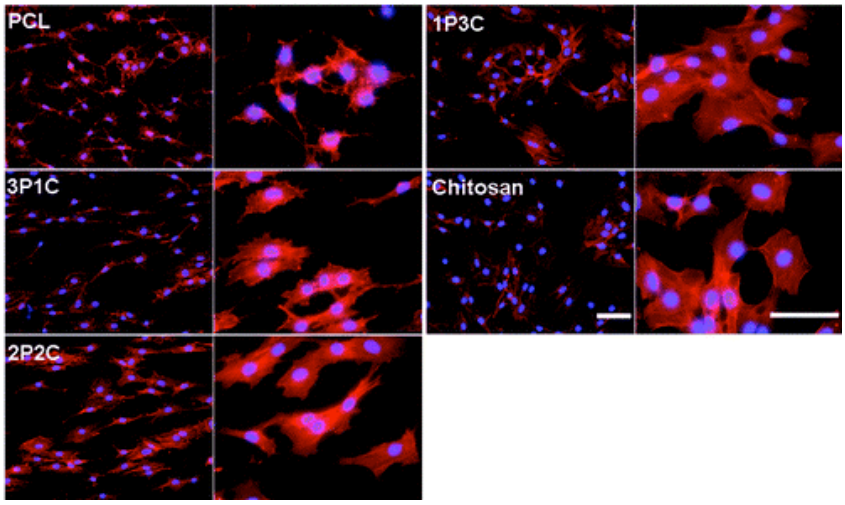

Figure 2.16. Fluorescent microscopy micrographs of MC3T3-E1 cells cultured on electrospun mats of PCL, chitosan, and composite mats of varying PCL and chitosan levels.[93]

The incorporation of gelatin into nanofibrous membranes provides similar enhancements in cellular proliferation and differentiation. Since gelatin alone possesses very little mechanical properties, the incorporation of a second biocompatible fiber allows to formation of more mechanically stable nanofibrous membranes. Electrospun PLCL/gelatin composite nanofibers showed successful adhesion of human mesenchymal stem cells.[97] Increased gelatin content resulted in increased osteogenic differentiation and increased mineralization for bone engineering scaffolds. Polycaprolactone/gelatin (70/30 ratio) nanofibers also showed affinity for neonatal mouse cerebellum C17.2 stem cells.[98] The alignment of the fibers significantly impacted neurite extension and cellular morphology, but neurite extension was significantly more pronounced for PCL/gelatin scaffolds than pure PCL scaffolds. Figure 2.17 shows the proliferation and extension of the neural cells on the random and aligned electrospun

membranes. They observed more than 50% increase in cell viability with gelatin in the fibers. NIH3T3 fibroblast cells were observed to proliferate on composite gelatin/polyurethane membranes, but the cells adhered almost exclusively to the gelatin.[99] Cellular proliferation decreased dramatically as the ratio of polyurethane in the fibers increased.

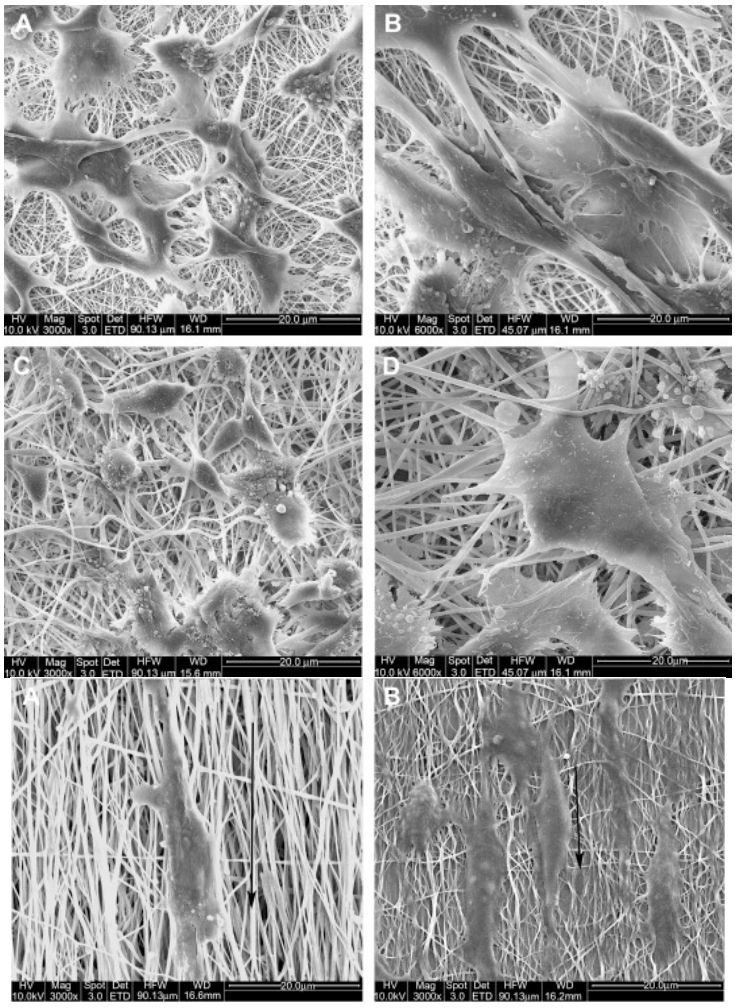

Figure 2.17. SEM images of neural cell proliferation on random and aligned electrospun mats of PCL and PCL/gelatin.[98]

2.6.4 Other Applications

The high surface area and porous nature of electrospun membranes make them applicable for a variety of electrochemical and electromechanical applications. Lee et al.[100] electrospun composite polypyrrole/ SEBS membranes and measured their electrochemical properties. They

investigated membranes with both sulfonated and unsulfonated SEBS. After doping with lithium ions, the membranes exhibited electrolyte-electrode interfacial resistances of 18 and 14, respectively, compared to 33 for a film of polypyrrole/SEBS. The increased surface area of the electrospun fibers significantly decreased this interfacial resistance. For battery applications, the electrospun PPy/SEBS electrospun membrane showed about 30% increase in specific discharge capacity compared to the cast film (60 mAh/g versus 45 mAh/g, respectively). The PPy/sulfonated SEBS electrospun membrane, however, exhibited 80 mAh/g specific discharge capacity, indicating the importance of charged macromolecules for this application. Leo et al.[37,101] generated similar membranes from Nafion® doped with ionic liquid for electromechanical actuators. Compared to a doped film of similar thickness, the electrospun Nafion® mat had a conductivity three times as high (0.92 mS/cm vs 0.30 mS/cm). Strain response analysis of the electromechanical actuators revealed that the actuator comprising electrospun fibers exhibited a strain rate of 1.34%/s, while the actuator made from the film had a strain rate of 0.88%/s, a 52% increase for the nanofiber actuator. Similar results have been observed for paper actuators of cellulose nanofibers.[38]

Electrospun membranes also excel as proton-conducting fuel-cell membranes. The proton exchange membranes rely on charged or acidic sites within the polymer for proton conductivity to drive the fuel cells. Nafion® nanofibrous membranes were compared to Nafion® films for proton exchange membrane performance.[102] The fibrous membranes showed lower ultimate proton conductivity than solid films, but proton conductivity followed a linear trend with Nafion® volume fraction. The use of nanofibrous sulfonated polysulfone/sulfonated POSS composites aided proton conductivity.[103] The voids in these fibrous membranes were filled with polyurethane to form a gas impermeable membrane,

and the proton conductivity remained higher than solid Nafion® films. These composite nanofibrous membranes offer tremendous advantage over current PEMs. Zhu et al.[104] extended the nanofibrous fuel cells one step further to create a single nanowire-based micro fuel cell (Figure 2.18). Using micro- and nanometer scale fibers composed on Nafion and PVP, the researchers observed proton conductivities significantly higher than Nafion films. The proton conductivity increased exponentially as fiber diameter decreased, as seen in Figure 2.19. The authors hypothesized this resulted from orientation of the microphase-separated channels within Nafion during electrospinning. The micro fuel cell with a fiber of diameter 2.1 μm exhibited a maximum current-density of 1.21 μA/μm^2, which is 10^4 times greater than values reported for conventional fuel cells.

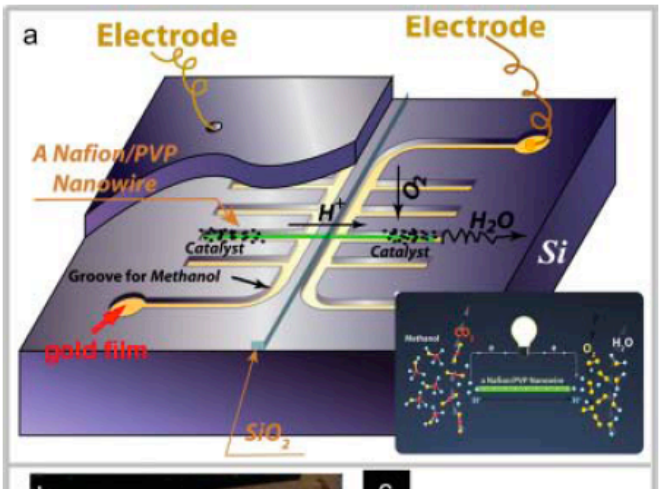

Figure 2.18. Schematic depiction of a micro fuel cell utilizing a Nafion/PVP composite nanowire.[104]

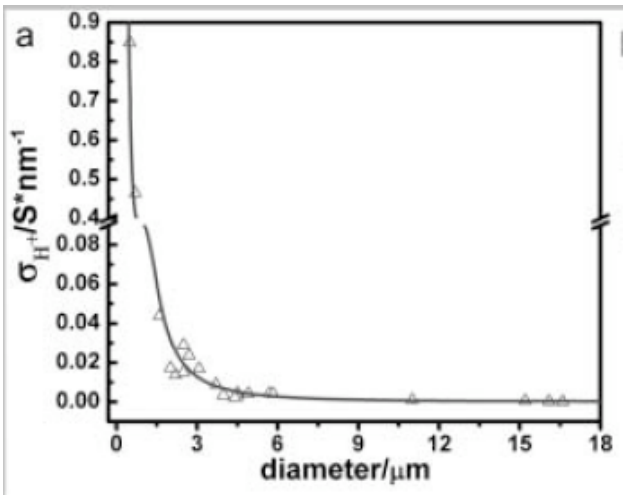

Figure 2.19. Proton conductivity as a function of Nafion/PVP composite microfiber diameter for micro fuel cells.[104]

2.7 Conclusions and Outlook

The electrospinning of charged macromolecules enables new classes of nanoporous membranes for emerging technologies including tissue engineering scaffolds, electroactive devices, and gas sensors. Although preliminary reports indicated inconsistent electrospinning behavior of polyelectrolytes, recent studies have provided a more complete picture of the structural parameters affecting electrospinning. Strong polyelectrolytes or weak polyelectrolytes under highly-charged conditions often experience instabilities and require very high viscosities and solution entanglement numbers before fiber formation. Incorporating charge-delocalized counterions or hydrophobic ions along the polymer chain allowed researchers to control the onset of fiber formation at lower viscosities and solution entanglement numbers. The exponential research growth in electrospinning polyelectrolytes is indicative of their extreme potential in nanofibrous membranes.

However, a multitude of unanswered questions about polyelectrolyte electrospinning behavior remains, which comes as no surprise considering the difficulty electrospinning such polymers. The fundamental research correlating solution rheology and polyelectrolyte structure to electrospinnability lacks any ability to predict fiber formation regimes. In-depth investigations into the phase-separated morphologies of electrospun ionomers are required to confirm if the high-shear processing disrupts these morphologies. In addition, harnessing the specific behavior of polyelectrolytes could lead to novel electrospun fibrous morphologies. Can block copolymers containing only one charged block be used to create specific fibrous structures including core-shell and janus-type nanofibers? Similarly, the microphase separation behavior of neutral block copolymers (i.e. styrene-butadiene-styrene triblock copolymers) during electrospinning is well understood, but thorough investigations are required to understand how the presence of polyelectrolyte blocks can influence this self-assembly. The application of recently developed electrospinning techniques and trends will help to realize novel functional scaffolds in this emerging field.

2.8 References

1. Reneker, D. H.; Yarin, A. L. *Polymer* **2008,** *49*, 2387-2425.
2. Greiner, A.; Wendorff, J. H. *Angew. Chem., Int. Ed. Engl.* **2007,** *46*, 5670-5703.
3. Givens, S. R.; Gardner, K. H.; Rabolt, J. F.; Chase, D. B. *Macromolecules* **2007,** *40*, 8013-8018.
4. van Reenen, A. J.; Keulder, L. *Macromol. Mater. Eng.* **2010,** *295*, 666-670.
5. Chen, H.; Snyder, J. D.; Elabd, Y. A. *Macromolecules* **2008,** *41*, 128-135.
6. Hunley, M. T.; Harber, A.; Orlicki, J. A.; Rawlett, A. M.; Long, T. E. *Langmuir* **2008,** *24*, 654-657.
7. McKee, M. G.; Hunley, M. T.; Layman, J. M.; Long, T. E. *Macromolecules* **2006,** *39*, 575-583.
8. Pham, Q. P.; Sharma, U.; Mikos, A. G. *Biomacromolecules* **2006,** *7*, 2796-2805.
9. McKee, M. G.; Wilkes, G. L.; Colby, R. H.; Long, T. E. *Macromolecules* **2004,** *37*, 1760-1767.
10. Bellan, L. M.; Craighead, H. G. *Polymer* **2008,** *49*, 3125-3129.
11. Stephens, J. S.; Chase, D. B.; Rabolt, J. F. *Macromolecules* **2004,** *37*, 877-881.

12. Ajao, J. A.; Abiona, A. A.; Chigome, S.; Fasasi, A. Y.; Osinkolu, G. A.; Maaza, M. *Journal of Materials Science* **2010,** *45*, 2324-2329.
13. Nie, H.; He, A.; Wu, W.; Zheng, J.; Xu, S.; Li, J.; Han, C. C. *Polymer* **2009,** *50*, 4926-4934.
14. Tripatanasuwan, S.; Reneker, D. H. *Polymer* **2009,** *50*, 1835-1837.
15. Tang, Z.; Qiu, C.; McCutcheon, J. R.; Yoon, K.; Ma, H.; Fang, D.; Lee, E.; Kopp, C.; Hsiao, B. S.; Chu, B. *J. Polym. Sci., Part B: Polym. Phys.* **2009,** *47*, 2288-2300.
16. Park, W. H.; Jeong, L.; Yoo, D. I.; Hudson, S. *Polymer* **2004,** *45*, 7151-7157.
17. Ohkawa, K.; Minato, K.-I.; Kumagai, G.; Hayashi, S.; Yamamoto, H. *Biomacromolecules* **2006,** *7*, 3291-3294.
18. Ner, Y.; Grote, J. G.; Stuart, J. A.; Sotzing, G. A. *Soft Matter* **2008,** *4*, 1448-1453.
19. Frey, M. W. *Polym. Rev.* **2008,** *48*, 378-391.
20. McKee, M. G.; Layman, J. M.; Cashion, M. P.; Long, T. E. *Science (Washington, DC, U. S.)* **2006,** *311*, 353-355.
21. Cashion, M. P.; Li, X.; Geng, Y.; Hunley, M. T.; Long, T. E. *Langmuir* **2010,** *26*, 678-683.
22. Hunley, M. T.; Karikari, A. S.; McKee, M. G.; Mather, B. D.; Layman, J. M.; Fornof, A. R.; Long, T. E. *Macromolecular Symposia* **2008,** *270*, 1-7.
23. Hunley, M. T.; Poetschke, P.; Long, T. E. *Macromolecular Rapid Communications* **2009,** *30*, 2102-2106.
24. Xie, J.; MacEwan, M. R.; Schwartz, A. G.; Xia, Y. *Nanoscale* **2010,** *2*, 35-44.
25. Sahoo, N. G.; Rana, S.; Cho, J. W.; Li, L.; Chan, S. H. *Prog. Polym. Sci.* **2010,** *35*, 837-867.
26. Ruiz-Rosas, R.; Bedia, J.; Lallave, M.; Loscertales, I. G.; Barrero, A.; Rodriquez-Mirasol, J.; Cordero, T. *Carbon* **2010,** *48*, 696-705.
27. Lim, H. S.; Baek, J. H.; Park, K.; Shin, H. S.; Kim, J.; Cho, J. H. *Advanced Materials* **2010,** *22*, 2138-2141.
28. McDowell, J. J.; Zacharia, N. S.; Puzzo, D.; Manners, I.; Ozin, G. A. *J. Am. Chem. Soc.* **2010,** *132*, 3236-3237.
29. Zhang, H.; Li, Z.; Wang, W.; Wang, C.; Liu, L. *Journal of the American Ceramic Society* **2010,** *93*, 142-146.
30. Lotus, A. F.; Bender, E. T.; Evans, E. A.; Ramsier, R. D.; Reneker, D. H.; Chase, G. G. *Journal of Applied Physics* **2008,** *103*, 024910/1-024910/6.
31. Remant, B. K. C.; Kim, C. K.; Khil, M. S.; Kim, H. Y.; Kim, I. S. *Materials Science and Engineering, C: Biomimetic and Supramolecular Systems* **2008,** *28*, 70-74.
32. Agarwal, S.; Wendorff, J. H.; Greiner, A. *Advanced Materials* **2009,** *21*, 3343-3351.
33. Ramakrishna, S.; Jose, R.; Archana, P. S.; Nair, A. S.; Balamurugan, R.; Venugopal, J.; Teo, W. E. *Journal of Materials Science* **2010,** *In press*.
34. Ding, B.; Wang, M.; Yu, J.; Sun, G. *Sensors* **2009,** *9*, 1609-1624.
35. An, H.; Shin, C.; Chase, G. G. *Journal of Membrane Science* **2006,** *283*, 84-87.
36. Feng, S.; Shen, X. *e-Polymers* **2010**.
37. Nah, C.; Kwak, S. K.; Kim, N.; Lyu, M.-Y.; Hwang, B. S.; Akle, B.; Leo, D. J. *Key Eng. Mater.* **2007,** *334-335*, 1001.
38. Lee, E.-H.; Kim, H.-M.; Lim, S.-K.; Kim, K.-S.; Chin, I.-J. *Molecular Crystals and Liquid Crystals* **2009,** *499*, 581-589.
39. Donaldson Company, Inc. - Americas Region - English. http://www.donaldson.com/en/index.html (July 28th, 2010),
40. Teo, W. E.; Ramakrishna, S. *Nanotechnology* **2006,** *17*, R89-R106.

41. Moroni, L.; De Wijn, J. R.; Van Blitterswijk, C. A. *Journal of Biomaterials Science, Polymer Edition* **2008,** *19*, 543-572.
42. Kim, G. H.; Son, J. G.; Park, S. A.; Kim, W. D. *Macromol. Rapid Commun.* **2008,** *29*, 1577-1581.
43. Shenoy, S. L.; Bates, W. D.; Frisch, H. L.; Wnek, G. E. *Polymer* **2005,** *46*, 3372-3384.
44. Gupta, P.; Elkins, C.; Long, T. E.; Wilkes, G. L. *Polymer* **2005,** *46*, 4799-4810.
45. Yu, J. H.; Fridrikh, S. V.; Rutledge, G. C. *Polymer* **2006,** *47*, 4789-4797.
46. Arayanarakul, K.; Choktaweesap, N.; Aht-ong, D.; Meechaisue, C.; Supaphol, P. *Macromol. Mater. Eng.* **2006,** *291*, 581-591.
47. Kim, S. J.; Lee, C. K.; Kim, S. I. *J. Appl. Polym. Sci.* **2005,** *96*, 1388-1393.
48. Moghe, A. K.; Hufenus, R.; Hudson, S. M.; Gupta, B. S. *Polymer* **2009,** *50*, 3311-3318.
49. Seo, J. M.; Arumugam, G. K.; Khan, S.; Heiden, P. A. *Macromol. Mater. Eng.* **2009,** *294*, 35-44.
50. Lin, T.; Wang, H.; Wang, H.; Wang, X. *Nanotechnology* **2004,** *15*, 1375-1381.
51. Kim, G.; Park, K.-e. *Polym. Eng. Sci.* **2009,** *49*, 2242-2248.
52. Kriegel, C.; Kit, K. M.; McClements, D. J.; Weiss, J. *Polymer* **2009,** *50*, 189-200.
53. Hunley, M. T.; McKee, M. G.; Long, T. E. *Journal of Materials Chemistry* **2007,** *17*, 605-608.
54. Wang, X.; Drew, C.; Lee, S.-H.; Senecal, K. J.; Kumar, J.; Samuelson, L. A. *Nano Lett.* **2002,** *2*, 1273-1275.
55. Theron, S. A.; Zussman, E.; Yarin, A. L. *Polymer* **2004,** *45*, 2017-2030.
56. Kim, B.; Park, H.; Lee, S.-H.; Sigmund, W. M. *Mater. Lett.* **2005,** *59*, 829-832.
57. Xiao, S.; Shen, M.; Ma, H.; Guo, R.; Zhu, M.; Wang, S.; Shi, X. *J. Appl. Polym. Sci.* **2010,** *116*, 2409-2417.
58. Ding, B.; Yamazaki, M.; Shiratori, S. *Sens. Actuators, B* **2005,** *B106*, 477-483.
59. Ignatova, M.; Manolova, N.; Rashkov, I. *Eur. Polym. J.* **2007,** *43*, 1112-1122.
60. Jayakumar, R.; Prabaharan, M.; Nair, S. V.; Tamura, H. *Biotechnology Advances* **2010,** *28*, 142-140.
61. Ohkawa, K.; Cha, D.; Kim, H.; Nishida, A.; Yamamoto, H. *Macromol. Rapid Commun.* **2004,** *25*, 1600-1605.
62. Penchev, H.; Paneva, D.; Manolova, N.; Rashkov, I. *Macromol. Rapid Commun.* **2008,** *29*, 677-681.
63. Min, B.-M.; Lee, S. W.; Lim, J. N.; You, Y.; Lee, T. S.; Kang, P. H.; Park, W. H. *Polymer* **2004,** *45*, 7137-7142.
64. Geng, X.; Kwon, O.-H.; Jang, J. *Biomaterials* **2005,** *26*, 5427-5432.
65. Klossner, R. R.; Queen, H. A.; Coughlin, A. J.; Krause, W. E. *Biomacromolecules* **2008,** *9*, 2947-2953.
66. De Vrieze, S.; Westbroek, P.; Van Camp, T.; Van Langenhove, L. *Journal of Materials Science* **2007,** *42*, 8029-8034.
67. Hunley, M. T.; England, J. P.; Long, T. E. **2010**.
68. Li, X.; Hao, X.; Xu, D.; Zhang, G.; Zhong, S.; Na, H.; Wang, D. *J. Membr. Sci.* **2006,** *281*, 1-6.
69. McCann, J. T.; Lim, B.; Ostermann, R.; Rycenga, M.; Marquez, M.; Xia, Y. *Nano Lett.* **2007,** *7*, 2470-2474.
70. Subramanian, C.; Weiss, R. A.; Shaw, M. T. *Polymer* **2010,** *51*, 1983-1989.

71. Nie, H.; He, A.; Zheng, J.; Xu, S.; Li, J.; Han, C. C. *Biomacromolecules* **2008,** *9*, 1362-1365.
72. Chen, H.; Elabd, Y. A. *Macromolecules* **2009,** *42*, 3368-3373.
73. Son, W. K.; Youk, J. H.; Lee, T. S.; Park, W. H. *Polymer* **2004,** *45*, 2959-2966.
74. Mincheva, R.; Manolova, N.; Paneva, D.; Rashkov, I. *J. Bioact. Compat. Polym.* **2005,** *20*, 419-435.
75. Li, L.; Hsieh, Y.-L. *Nanotechnology* **2005,** *16*, 2852-2860.
76. Chunder, A.; Sarkar, S.; Yu, Y.; Zhai, L. *Colloids Surf., B* **2007,** *58*, 172-179.
77. Ge, L.; Pan, C.; Chen, H.; Wang, X.; Wang, C.; Gu, Z. *Colloids and Surfaces A: Phsicochemical and Engineering Aspects* **2007,** *293*, 272-277.
78. Ge, L.; Wang, X.; Tu, Z.; Pan, C.; Wang, C.; Gu, Z. *Japanese Journal of Applied Physics* **2007,** *46*, 6790-6795.
79. Deng, H.; Zhou, X.; Wang, X.; Zhang, C.; Ding, B.; Zhang, Q.; Du, Y. *Carbohydrate Polymers* **2009,** *80*, 474-479.
80. Park, J. H.; Kim, B. S.; Tae, H. J.; Kim, I. S.; Kim, H. Y.; Khil, M. S. *Fibers and Polymers* **2009,** *10*, 419-424.
81. Ohkawa, K.; Ando, M.; Shirakabe, Y.; Takahashi, Y.; Yamada, M.; Shirai, H.; Yamamoto, H. *Textile Research Journal* **2002,** *72*, 120-124.
82. Li, P.; Li, Y.; Ying, B.; Yang, M. *Sens. Actuators, B* **2009,** *B141*, 390-395.
83. Wang, X.; Ding, B.; Yu, J.; Wang, M.; Pan, F. *Nanotechnology* **2010,** *21*, 055502/1-055502/6.
84. Wang, X.; Kim, Y.-G.; Drew, C.; Ku, B.-C.; Kumar, J.; Samuelson, L. A. *Nano Lett.* **2004,** *4*, 331-334.
85. Kuo, C.-C.; Wang, C.-T.; Chen, W.-C. *Macromol. Mater. Eng.* **2008,** *293*, 999-1008.
86. Desai, K.; Kit, K.; Li, J.; Davidson, P. M.; Zivanovic, S.; Meyer, H. *Polymer* **2009,** *50*, 3661-3669.
87. Haider, S.; Park, S.-Y. *Journal of Membrane Science* **2008,** *328*, 90-96.
88. Agarwal, S.; Wendorff, J. H.; Greiner, A. *Polymer* **2008,** *49*, 5603-5621.
89. Barnes, C. P.; Sell, S. A.; Boland, E. D.; Simpson, D. G.; Bowlin, G. L. *Advanced Drug Delivery Reviews* **2007,** *59*, 1413-1433.
90. Dong, Y.; Liao, S.; Ngiam, M.; Chan, C. K.; Ramakrishna, S. *Tissue Engineering, Part B: Reviews* **2009,** *15*, 333-351.
91. Lee, K. Y.; Jeong, L.; Kang, Y. O.; Lee, S. J.; Park, W. H. *Advanced Drug Delivery Reviews* **2009,** *61*, 1020-1032.
92. Han, D.; Gouma, P.-I. *Nanomedicine: Nanotechnology, Biology, and Medicine* **2006,** *2*, 37-41.
93. Yang, X.; Chen, X.; Wang, H. *Biomacromolecules* **2009,** *10*, 2772-2778.
94. Feng, Z.-Q.; Chu, X.; Huang, N.-P.; Wang, T.; Wang, Y.; Shi, X.; Ding, Y.; Gu, Z.-Z. *Biomaterials* **2009,** *30*, 2753-2763.
95. Chu, X.-H.; Shi, X.-L.; Feng, Z.-Q.; Gu, J.-Y.; Xu, H.-Y.; Zhang, Y.; Gu, Z.-Z.; Ding, Y.-T. *Biomaterials* **2009,** *30*, 4533-4538.
96. Khanam, N.; Mikoryak, C.; Draper, R. K.; Balkus, K. J., Jr. *Acta Biomaterialia* **2007,** *3*, 1050-1059.
97. Rim, N. G.; Lee, J. H.; Jeong, S. I.; Lee, B. K.; Kim, C. H.; Shin, H. *Macromolecular Bioscience* **2009,** *9*, 795-804.

98. Ghasemi-Mobarakeh, L.; Prabhakaran, M. P.; Morshed, M.; Nasr-Esfahani, M.-H.; Ramakrishna, S. *Biomaterials* **2008,** *29*, 4532-4539.
99. Kim, S. E.; Heo, D. N.; Lee, J. B.; Kim, J. R.; Park, S. H.; Jeon, S. H.; Kwon, I. K. *Biomedical Materials* **2009,** *4*, 044106/1-044105/11.
100. Ju, Y.-W.; Park, J.-H.; Jung, H.-R.; Lee, W.-J. *Electrochim. Acta* **2007,** *52*, 4841-4847.
101. Akle, B. J.; Leo, D. J.; Nah, C.; Kader, A. M. *Materials Research Society Symposium Proceedings* **2005,** *889*.
102. Lee, K. M.; Choi, J.; Wycisk, R.; Pintauro, P. N.; Mather, P. T. *ECS Transactions* **2009,** *25*, 1451-1458.
103. Choi, J.; Lee, K. M.; Wycisk, R.; Pintauro, P. N.; Mather, P. T. *Journal of the Electrochemical Society* **2010,** *157*, B914-B919.
104. Pan, C.; Wu, H.; Wang, C.; Wang, B.; Zhang, L.; Cheng, Z.; Hu, P.; Pan, W.; Zhou, Z.; Yang, X.; Zhu, J. *Advanced Materials* **2008,** *20*, 1644-1648.
105. Kim, S. J.; Lim, J. Y.; Kim, I. Y.; Lee, S. H.; Lee, T. S.; Kim, S. I. *Smart Mater. Struct.* **2005,** *14*, N16-N20.
106. Li, L.; Hsieh, Y.-L. *Polymer* **2005,** *46*, 5133-5139.
107. Xin, Y.; Huang, Z.; Yang, P.; Jiang, Z.; Wang, C.; Shao, C. *J. Appl. Polym. Sci.* **2009,** *114*, 1864-1869.

Chapter 3: Electrospinning Functional Nanoscale Fibers: A Perspective for the Future

(From: Hunley, M.T. and Long, T.E. *Polymer International* **2008**, *57*, 385-389.)

3.1 Abstract

Over the past decade, electrospinning has grown from a small niche process to a widely used fiber formation technique. Applying a strong electric potential on a polymer solution or melt produces nanoscale fibers. These nanofibers form non-woven textile mats, oriented fibrous bundles and even three-dimensional structured scaffolds, all with large surface areas and high porosity. Major applications of electrospun membranes include tissue engineering, controlled drug delivery, sensing, separations, filtration, catalysis and nanowires. This perspective article highlights many recent advances in electrospun fibers for functional applications, with an emphasis on the advantages and proposed technologies for these non-woven fibrous scaffolds.

3.2 Introduction

Electrospinning of submicrometer polymer fibers has seen a tremendous increase in research and commercial attention over the past decade. A quick literature search on the term 'electrospinning' reveals an apparent exponential trend in research activities over the past ten years, as shown in Fig. 3.1. The large majority of research manuscripts and patents reiterate that electrospun fibers are easy to fabricate, cost-effective and easily scalable from laboratory to commercial production. However, only a limited number of companies have commercially implemented electrospun fibers, and an apparent focus remains on biomedical technologies. This commercial lag begs the question, do electrospun fibers possess any competitive advantage over current, commercially produced melt- and solution-spun fibers? In this perspective article, we highlight recent efforts in the formation of functional fibers on the nanoscale using melt and

solution electrospinning, and provide our perspective on the applicability and advantages of electrospun membranes.

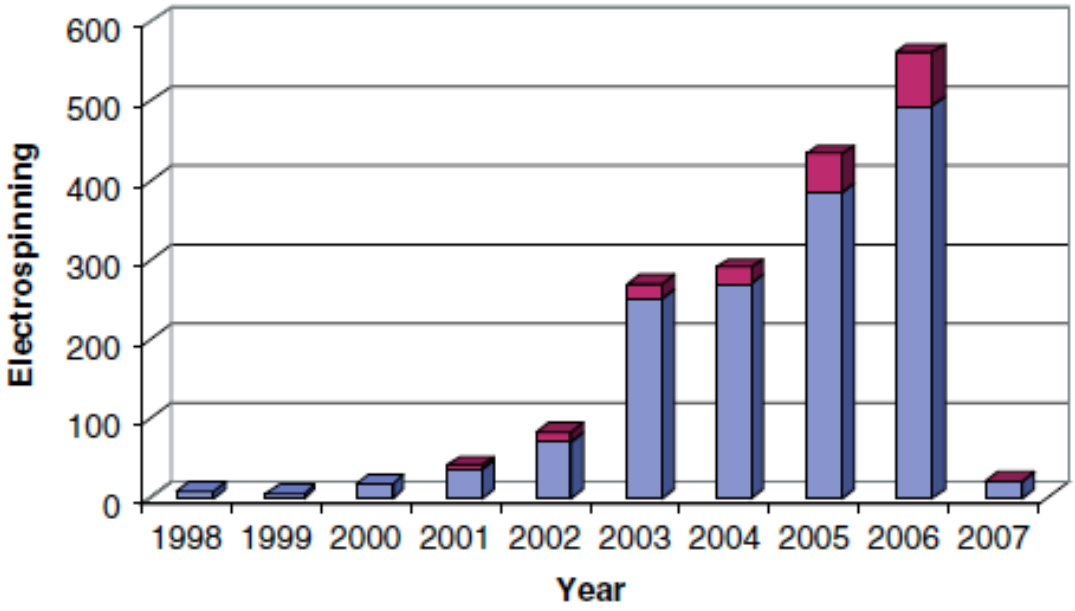

Figure 3.1. Publications involving 'electrospinning' during the past decade. Darker-colored caps on each column indicate patent applications. Search performed on the SciFinder search engine on 20 November 2006, using keyword 'electrospinning,' and analyzed by publication year.

3.3 The Electrospinning Process

Typical electrospinning is a solution-based process, and most manuscripts implement a solution operation. Our research group has focused on the utility of semi-empirical models to correlate solution structure with electrospinnability.[1] Polymer solutions of sufficient viscosity are metered through a capillary and placed under high electric potential (typically 10–30 kV). The large potential causes a droplet of solution to accelerate towards a grounded or oppositely charged collector. During chaotic flight, solvent evaporates quickly from the polymer 'jet', reducing the jet diameter and increasing the charge density on the surface. The increased surface

charges lead to a 'bending instability', resulting in chaotic whipping and stretching of the polymer jet before ultimate deposition on the grounded target.[2] Fig. 3.2 shows schematically a typical electrospinning apparatus with a UV irradiation attachment.[3] In this example, the fibers form under UV light, which initiates a photoreaction in the high-surface-area fibers. Typical electrospun mats comprise a randomly oriented, nonwoven fibrous mesh. Many groups have investigated using rotating take-up mandrels or differing counter electrode geometries in an effort to create oriented fiber mats and three-dimensional fibrous structures, such as tubular scaffolds.[4] Electrospinning from the melt has demonstrated the possibility of eliminating solvent requirements for many different polymers.[5] In fact, our current efforts implement supramolecular structure for the formation of biodegradable scaffolds.

3.4 Electrospun Fibers as Biological Scaffolds

Perhaps the most important feature relating to biological applicability of electrospun fibers is their ability to mimic the extracellular matrix (ECM). The ECM comprises the macro environment surrounding and communicating with growing cells.[6] Composed mostly of polysaccharides and fibrous proteins, this matrix differs in chemical and physical structure from tissue to tissue. For example, the ECM of tendons is composed of aligned fibrils, while the ECM of skin is more randomly oriented and mesh-like.[6] The portability of the electrospinning process complements the wide range of ECM structures and compositions.

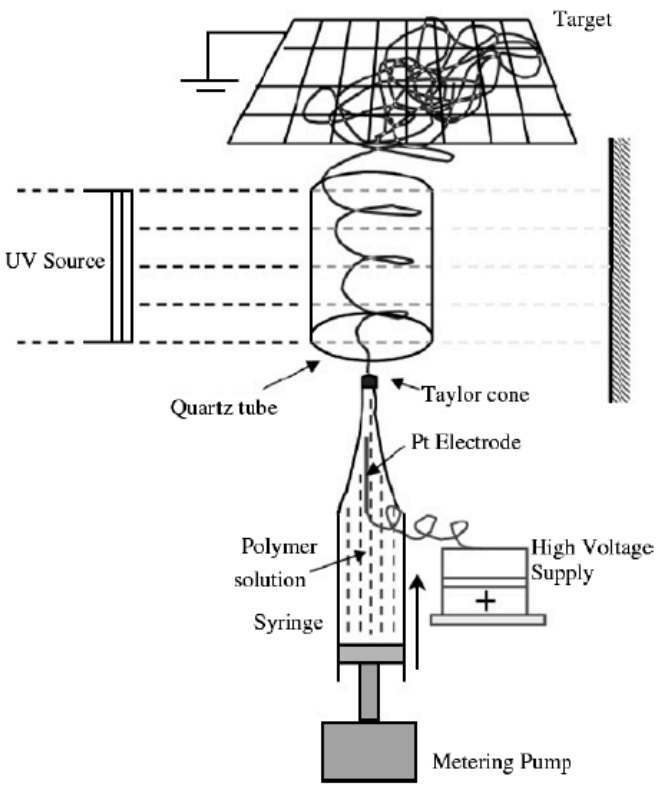

Figure 3.2. Reactive electrospinning as illustrated with the formation of electrospun fibers with *in situ* UV irradiation. Reprinted from Ref. 3.

Many researchers have shown that cells impregnated into electrospun membranes proliferate well.[6,7] Some researchers have particularly demonstrated the successful adhesion, differentiation and outgrowth of nerve cells on nanofibrous scaffolds of poly(lactide-coglycolide).[7] These successful in vitro and in vivo studies suggest possible neural regeneration, and implants in rats showed good incorporation into existing tissue.

Several researchers are currently investigating the degradation properties of cell scaffolds composed of polylactide, polyglycolide and collagen, among other polymers.[6,8] These biopolymer nanofibers have shown promising biodegradation and bioresorption properties, as well as excellent cell adhesion and proliferation. Our research group has also demonstrated the

electrospinning of low molar mass phospholipids, which are proposed to offer significant biosorption properties and biocompatibility.[9] Engineered scaffolds with controllable in vivo degradation should significantly reduce tissue degradation while allowing cells to grow into self-supporting tissues. The process of seeding electrospun scaffolds with live cells provides added challenges, particularly in distributing cells uniformly throughout the scaffolds. Townsend-Nicholson and Jayasinghe have overcome this problem by electrospinning live cells.[10] Using a coaxial electrospinning set-up with a cell suspension in the inner capillary and polydimethylsiloxane (PDMS) through the outer needle, they observed homogeneous cell seeding throughout the entire scaffold with no evidence of cellular damage. Coaxial electrospinning requires a modified spinneret to independently meter two fluids in a core/shell arrangement.[11] Fig. 3.3 illustrates a typical coaxial apparatus, which closely resembles the traditional electrospinning apparatus. For the case of electrospinning a cellular suspension within a PDMS shell, the shell acts as a supporting scaffold for the growing cells after electrospinning, resulting in highly uniform cell distribution within the PDMS fibers. Such electrospun tissue engineering scaffolds promise to greatly enhance the opportunities for organ and tissue (even nerve tissue) regeneration.

In addition to tissue engineering scaffolds, electrospun fibers afford simple and effective drug delivery membranes. Traditional drug delivery systems rely on the release of adequate drug levels throughout the entire body, which can lead to possibly toxic levels and side effects.[12] Impregnated electrospun scaffolds allow site-specific targeting, reducing both the amount of medicine required and the concentration in other areas of the body.[13] The wide range of solvents and polymers applicable for electrospinning also permits the incorporation of hydrophobic and hydrophilic drugs, proteins and even plasmid DNA within electrospun scaffolds.

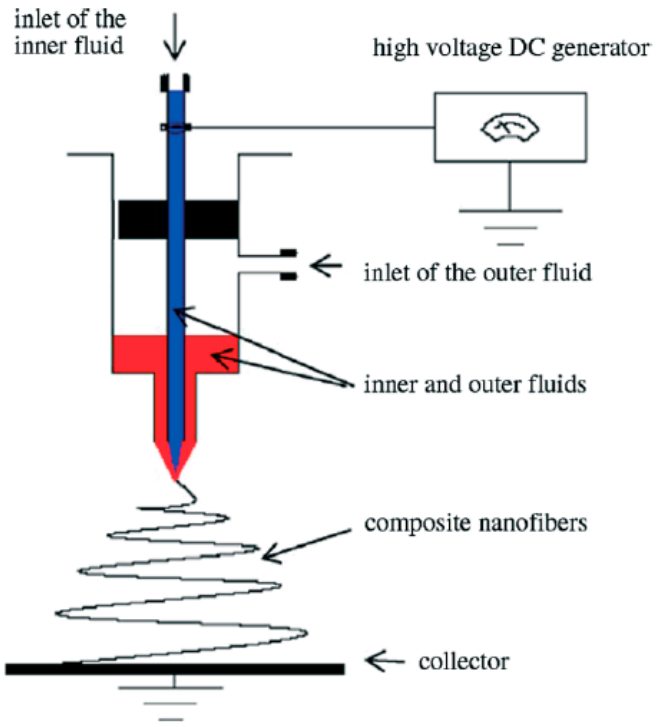

Figure 3.3. Typical coaxial electrospinning apparatus, illustrating the incorporation of one fluid within a shell of another polymeric fluid. Reprinted from Ref. 11.

The simplest electrospun drug delivery membranes contain physically encapsulated drugs. Due to the high surface area and porosity of such membranes, a significant drug burst release is observed. This burst yields initial delivery rates far exceeding those of long-time delivery. Several methods have emerged to prevent this burst release. For example, Casper et al.[14] have functionalized poly(ethylene glycol) (PEG) with low molecular weight heparin (LMWH), a glycosaminoglycan known to bind growth factors. The PEG–LMWH polymer was electrospun and release of the heparin slowed from 24 h to a minimum of 14 days. This retention significantly improved binding of growth factors to the electrospun scaffold. In addition, Zeng et al.[15] demonstrated that a coating of poly(p-xylylene) on poly(vinyl alcohol) retarded the release of bovine serum albumin (BSA). For uncoated fibers, BSA from the fibers saturated a water

solution at 37 ◦C faster thanmeasurements were possible. After coating with poly(p-xylylene), the fibers showed more controlled release of BSA, without a loss of enzymatic functionality for greater than 20 days.

A more common technique for controlling burst release of drugs and proteins from electrospun fibers used coaxial electrospinning. The coaxial technique approached this problem in a similar fashion to the coating technique of Zeng et al. The shell of the fiber acted as a barrier to drug diffusion from the fiber core. This barrier slowed drug release to a controlled rate, and the kinetics approached zeroth order. The protein BSA as well as antioxidant reservatrol and antibiotic getamycin sulfate have been incorporated within coaxially electrospun fibers and studied extensively.[13] The controlled release of these therapeutics lengthened to several weeks through encapsulation within the core.

Electrospun scaffolds provide excellent multifunctional platforms for biological applications. As previously explained, their resemblance to the ECM promotes cell growth and differentiation for healthy tissue engineering; in addition, incorporated drugs and proteins show controlled release over weeks or even months. The readily adaptable electrospinning process also combines these benefits, yielding ECM-analogous tissue engineering scaffolds with proteins to promote healthy cell growth and proliferation. Although they do not posses the strength and durability of typical melt- or solution-drawn polymeric fibers, these membranes are readily biodegradable and bioresorbable,[16] allowing a growing tissue or organ to simply engulf its scaffold. Electrospun scaffolds allow tailored tissue engineering opportunities on a small and adaptable scale.

3.5 Ultrafast and Sensitive Electrospun Sensors

Most sensing methods rely on some interaction (e.g. physical adsorption, chemical reaction and light absorbance) of analyte molecules with the sensor.[17,18] Electrospun membranes offer high surface area, highly porous membranes that are applicable for fast and sensitive sensing. Such functional scaffolds have shown improved sensitivities over conventional materials for applications including gas (and humidity) sensing[19,20] and glucose detection,[17,20] among others.

For gas sensing, the high porosity of electrospun membranes allows the gas to permeate quickly through the entire mat, while the high specific surface area provides plentiful contact for contaminant sensing. Resistance-based sensors have shown response times of the order of seconds for concentrations of less than 1 ppm NO2 in air, and estimated sensitivity limits of 1 ppbNO2 for titanium oxide/poly(vinyl acetate) mats.[19] Aussawasathien et al.[20] have developed humidity sensors and demonstrated low response times with significantly enhanced sensitivity compared to thin films.

Biosensing using electrospun nanofibers is possible through the immobilization of biologically relevant molecules.[17,18] Ren et al.[17] immobilized glucose oxidase in electrospun poly(vinyl alcohol) fibers. Glucose concentrations as low as 1 mmol L−1 were detected through ampoteric changes, with response times of approximately 1 s using the fibrous mat as an electrode. Sawicka et al.[18] immobilized urease enzyme within a poly(vinyl pyrrolidone) membrane for urea sensing. Instead of directly testing for urea the urease selectively decomposed the urea, with NH_3 as a byproduct. Potentiometrically detected ammonia levels allowed determination of urea concentrations less than 1 mmol L−1.

3.6 Fibers Capable of Molecular Recognition

Incorporating functional molecules within electrospun membranes allows molecular imprinting of the polymeric fibers. Such imprinting follows either of two strategies: inclusion of a sacrificial template molecule[21] or incorporation of an appropriate binding molecule.[22,23] In the sacrificial template method, a target molecule is included within the electrospinning solution and subsequently removed after fiber formation. Chronakis et al.[21] included the drug 2,4-dichlorophenoxyacetic acid (DCA) in poly(ethylene terephthalate) (PET)–poly(allyl amine) blend fibers. The PET added strength and solvent resistance to the fibers, while the functional groups of poly(allyl amine) interacted with and conformed to the structure of DCA. After electrospinning, DCA easily rinsed away to leave fibers with molecularly imprinted pores. Radioligand binding analysis indicated that DCA interacted strongly with the imprinted fibers, which suggested a viable means to separate or purify the drug.

Molecular recognition was incorporated within electrospun fibers through the inclusion of functional molecules. Analogous to the enzymes used in sensors as described above, functional fibers associate with target molecules for effective separation. Yang et al.[22] electrospun polyacrylonitrile functionalized with pendant sugar groups. The sugar pendants interacted selectively with the protein BSA rather than concanavalin A (Con-A). For certain sugar compositions, the fibers achieved essentially 100% separation of protein mixtures. In addition, our group has functionalized poly(alkyl methacrylates) with self-complementary multiple hydrogen bonding pendant groups (Fig. 3.4).[23] The resulting fibers showed enriched surface concentrations of the hydrogen bonding groups, which led to molecular-dependent adhesive and recognition properties. Molecular imprinting and molecular recognition sites enable tailored high-surface-area electrospun membranes that dramatically simplify complex separation operations, even for difficult-to-separate protein mixtures.

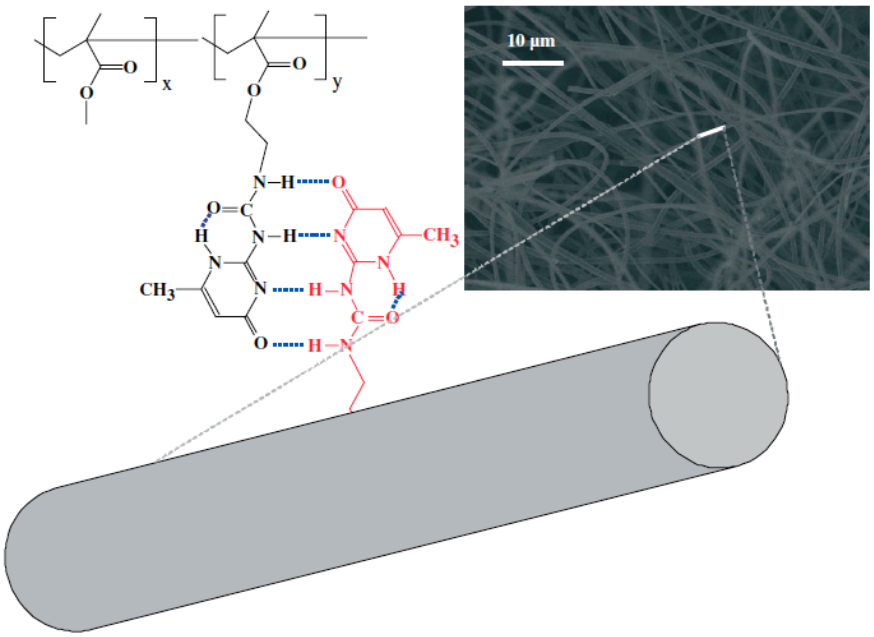

Figure 3.4. Schematic representation of surface enrichment and self-complementary hydrogen bonding of functionalized methacrylate polymers.

3.7 Other Applications

As highlighted above, electrospun fibers are highly applicable for separation operations. These membranes also function well in traditional filtration applications, primarily due to their high porosity and tunable pore sizes. Although they lack mechanical strength and durability, several research groups have reported that the inclusion of electrospun membranes as a layer within filters improves overall filtration efficiency without a significant change in pressure drop.[24] Another study expanded on the layered filter method, demonstrating that layers of thin fibers promote high flux and efficient filtration, while layers of thicker fibers are stronger and support the filter.25 Schreuder-Gibson et al.,[26,27] studied many such electrospun filters. In one study, the residual positive and negative charges on the electrospun fibers significantly improved aerosol filtration.[26] Fiber diameter also contributed to aerosol penetration levels. In addition, electrospun deformable elastomeric membranes demonstrated highly effective filtration

properties.[27] The relative processing ease of electrospun membranes also contributes to their attractiveness as efficient filters.

The large surface area of electrospun fibers also appeals to the field of heterogeneous catalysis. It has previously been shown that ceramic sol–gel precursors can be electrospun and subsequently annealed to create porous, fibrous ceramic membranes. Zhan et al.[28] have shown that such ceramics apply to heterogeneous catalysis. These authors created hollow TiO2 fibers with hexagonally packed surface pores through coaxial electrospinning. The TiO2 fibers served as a catalyst in the photodegradation of methylene blue and formaldehyde. In comparison to similar nanoparticles and mesoporous powders, the electrospun fibers showed significant increased degradation rates for both compounds. Similarly, Bruno et al.[29] used polyacrylonitrile and poly(styrene sulfonate) membranes that were functionalized with PEG–hematin to catalyze the polymerization of polypyrrole and polyethylenedioxythiophene. As expected, the large surface area of the nanofibers contributed to increased heterogeneous catalytic activity.

An emerging application for nanofibers with a high aspect ratio is nanowires. Conductive wires on the sub-500nm scale are proposed to aid in the miniaturization of electronics. Significant research has demonstrated that electrospun fibers can form conductive nanowires. The incorporation of oriented carbon nanotubes within fibrous membranes has led to anisotropic properties, such as electrical and thermal conductivity.[30] In addition, the pyrolysis of polyacrylonitrile fibers into carbon nanofibers yields wholly conductive carbon fibers and have received significant attention.[31] Although the conductivity and electrical properties of these fibers are well documented, only a few patents have demonstrated their use in actual applications, ranging from fuel cells to electrodes.[32] The carbon nanofibers showed comparable behavior to conventional conductive wires in all applications.

3.8 Summary and Outlook

During the rebirth of polymer electrospinning over the past decade, the applicability of electrospun fibers has become apparent across many fields. This highly adaptable process allows the formation of functional fibrous membranes for applications such as tissue engineering, controlled drug delivery, sensing, molecular recognition, separations and catalysis. Although their mechanical properties lag behind other textiles and membranes, electrospun scaffolds offer an unprecedented flexibility and modularity in design. Improvements in strength and durability, and their incorporation in composite membranes, will allow these scaffolds to compete with existing membrane technology. Moreover, their improvements over existing technology in such areas as tissue engineering and molecular recognition will provide ample opportunities for emerging technologies. Currently, the research field of electrospinning is ripe with functional materials (from bioresorbable cell scaffolds to ceramic solid-phase catalysts) and continued research interest is expected to improve most areas of life, from medicine to fuel cells.

3.9 Acknowledgements

The material presented is based upon work supportedby, or in part by, the US Army Research Laboratory and the US Army Research Office under grant number DAAD19-02-1-0275 Macromolecular Architecture for Performance (MAP) MURI.

3.10 References

1 McKee MG, Wilkes GL, Colby RH and Long TE, Macromolecules 37:1760 (2004).
2 Shin YM, Hohman MM, Brenner MP and Rutledge GC, Appl Phys Lett 78:1149 (2001).
3 Gupta P, Trenor SR, Long TE and Wilkes GL, Macromolecules 37:9211 (2004).
4 Teo WE and Ramakrishna S, Nanotechnology 17:R89–R106 (2006).
5 Lyons J and Ko F, Polym News 30:170 (2005).
6 Teo W-E, He Wand Ramakrishna S, Biotechnol J 1:918 (2006).
7 Bini TB, Gao S, Wang S and Ramakrishna S, J Mater Sci 41:6453 (2006).
8 Boland ED, Pawlowski KJ, Barnes CP, Simpson DG,Wnek GE and Bowlin GL, ACS Symp Ser 918:188 (2006).

9 McKee MG, Layman JM, Cashion MP and Long TE, Science (Washington, DC) 311:353 (2006).
10 Townsend-Nicholson A and Jayasinghe SN, Biomacromolecules 7:3364 (2006).
11 Song T, Zhang YZ and Zhou TJ, J Magn Magn Mater 303:e286–e289 (2006).
12 Langer R and Peppas NA, AIChE J 49:2990 (2003).
13 Vaseashta A, Erdem A and Stamatin I, Mater Res Soc Symp Proc 920:143 (2006).
14 Casper CL, Yamaguchi N, Kiick KL and Rabolt JF, Biomacromolecules 6:1998 (2005).
15 Zeng J, Aigner A, Czubayko F, Kissel T, Wendorff JH and Greiner A, Biomacromolecules 6:1484 (2005).
16 Katti DS, Robinson KW, Ko FK and Laurencin CT, J Biomed Mater Res B 70B:286 (2004).
17 Ren G, Xu X, Liu Q,Cheng J,Yuan X, Wu L, et al, React Funct Polym 66:1559 (2006).
18 Sawicka K, Gouma P and Simon S, Sens Actuators B 108:585 (2005).
19 Kim I-D, Rothschild A, Lee BH, Kim DY, Jo SM and Tuller HL, Nano Lett 6:2009 (2006).
20 Aussawasathien D, Dong JH and Dai L, Synth Met 154:37 (2005).
21 Chronakis IS, Milosevic B, Frenot A and Ye L, Macromolecules 39:357 (2006).
22 Yang Q, Wu J, Li J-J, Hu M-X and Xu Z-K, Macromol Rapid Commun 27:1942 (2006).
23 McKee MG, Elkins CL and Long TE, Polymer 45:8705 (2004).
24 Chase GG and Reneker DH, Fluid/Particle Separation J 16:105 (2004).
25 Shutov AA, Tech Phys Lett 31:1026 (2005).
26 Schreuder-Gibson HL, Gibson P, Tsai P, Gupta P and Wilkes G, Int Nonwovens J 13:39 (2004).
27 Schreuder-Gibson H, Gibson P, Wadsworth L, Hemphill S and Vontorcik J, Adv Filtrat Separat Technol 15:525 (2002).
28 Zhan S, Chen D, Jiao X and Tao C, J Phys Chem B 110:11199 (2006).
29 Bruno FF, Drew C, Nagarajan R, Wang X, Kumar J and Samuelson LA, PMSE Prepr 90:234 (2004).
30 Xie X-L, Mai Y-W and Zhou X-P, Mater Sci Eng R49:89 (2005).
31 Sutasinpromprae J, Jitjaicham S, Nithitanakul M, Meechaisue C and Supaphol P, Polym Int 55:825 (2006).
32 Kim C, Preparation method of nanocomposite carbon fiber material by electrospinning, preparation method of electrode catalyst for polymer electrolyte fuel cell or dmfc, and electrode catalyst prepared by the method. KR Patent Application (2005).

Chapter 4: Submicron Functional Fibrous Scaffolds Based on Electrospun Phospholipids

(From: Hunley, M.T.; McKee, M.G.; Long, T.E. *J. Mater. Chem.* **2007**, *17*, 605-608.)

4.1 Abstract

Wormlike micelles of phospholipids were recently electrospun into ultraporous, high surface area fibrous membranes. These biologically-derived materials offer many potential applications, such as cell growth scaffolds, purification membranes, and drug-delivery platforms. Future work in tailoring the electrospinning process and phospholipid properties is expected to create new durable, biofunctional materials. These initial efforts have introduced the concept of low molar mass amphiphiles as precursors of biocompatible fibers through solution electrospinning.

4.2 Introduction

Phospholipid membranes have received significant attention recently, due to their suitability as drug-delivery platforms,[1,2] biosensors,[3–6] and biocompatible scaffolds. [3,7–9] In nature, the cell membrane consists of a phospholipid bilayer containing various proteins and lipids. This complex membrane controls all communication and exchange between intra- and extracellular matter. The high degree of selectivity of these biological membranes suggests that such phospholipid-based materials will offer great value in therapeutic and biological applications. Currently, lipids are popularly used as vesicles and bilayer membranes, self-assembled monolayers, or in a liquid crystalline phase as self-assembled suprastructures.[3,5–12]

Membranes are commonly investigated in the form of supported lipid membranes. These bilayers are typically formed by either sequential Langmuir–Blodgett (LB) deposition[6,13] or vesicle adsorption.[14,15] Langmuir–Blodgett films have the advantage of being reliably fabricated with precise control over thickness on a variety of substrates. However, this technique

is time intensive and requires precise experimental techniques and conditions. Vesicle adsorption involves the adsorption and subsequent collapse of a vesicle onto a substrate. After collapse, the lipids remain as an adsorbed bilayer membrane. This method proves easier to implement in the laboratory compared to LB techniques, although defects are often introduced upon spontaneous vesicle collapse. In addition, vesicles provide three-dimensional structures for the investigation of lipid membranes.[16] Liquid crystalline self-assemblies of functionalized phospholipids have also received intense attention. These structures were shown to form complex three-dimensional structures and undergo polymerization with full retention of the superstructures. The polymerized self-assemblies were subsequently used as templates for ceramic and inorganic materials, as well as applications in therapeutics and molecular recognition.[10,11] Such polymerizable phospholipids also have applications as durable vesicles and biocompatible polymers.[17,18]

Electrospinning provides a means of creating another three-dimensional phospholipid structure, which is composed of a fibrous scaffold. After its invention in 1934 as an extension of electrospraying,[19] electrospinning remained relatively dormant until a revival by Reneker and Chun in 1996.[20] Since then, this process has received tremendous attention. Most recently, our group has shown that fibers can be successfully formed from entangled wormlike micelles of phospholipids, and semi-empirical models were generated relating solution rheology and dynamics to fiber size and appearance.[21–23]

Unlike traditional solution spinning, which relies on mechanical contact to form fibers, electrospinning utilizes a very large electric potential (typically of the order of 10–30 kV) to draw a fiber from solution. Fig. 4.1 illustrates a typical electrospinning process. The solution is metered from a syringe at a controlled flow rate and connected to the positive lead of a high-

voltage power supply. A stainless steel target is grounded approximately 10–20 cm away. As a droplet forms at the tip of the syringe, the high electric potential elongates the droplet into a conical shape, termed a ‘‘Taylor cone.’’ In the electrospraying process (commonly used for paint applications), the Taylor cone breaks up into droplets which accelerate towards the target. However, in the presence of significant entanglements in solution, the tip of the Taylor cone will stabilize and accelerate towards the grounded target as a continuous jet. During the flight, solvent evaporates rapidly, leading to a decrease in jet diameter and an increase in surface charge density. The increased surface repulsion leads to a bending instability, and the jet subsequently whips and bends chaotically in an ever-increasing conical shape. The tremendous repulsive forces in the jet lead to significant drawing, which results in fibers with submicron diameters. The fiber jet finally deposits on the target in a random pattern to create a non-woven fibrous membrane.

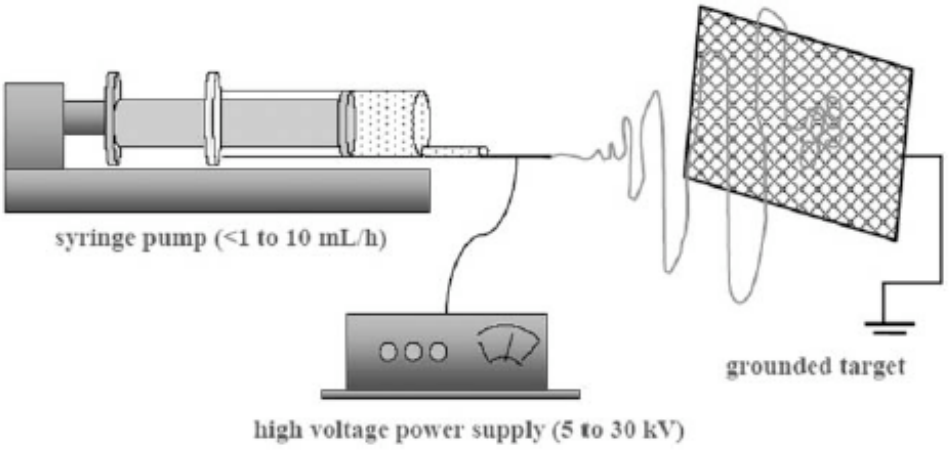

Figure 4.1. Conventional solution electrospinning setup.

This highlight focuses on the current state of research for electrospinning selfassembling phospholipids. Areas that are deemed vital for further research in the applicability of electrospun phospholipids are proposed and discussed.

4.3 Electrospinning of Phospholipid Assemblies

Our research group has recently shown that aggregations of lecithin, which is a phospholipid mixture derived from soybean, are suitable for electrospinning from a solvent mixture of 70:30 wt% chloroform:*N*,*N'*-dimethylformamide (DMF). At low solution concentrations, the lecithin forms spherical micelles. However, as the concentration increases, the spherical micelles undergo onedimensional growth into wormlike micelles (WLMs).[24] The WLMs exist in solution as equilibrated aggregations. In a similar fashion to polymers, which undergo scission and recombination in a random fashion, WLMs also undergo chain scission upon introduction of stress or shear.[25–28] However, at higher concentrations, WLMs will entangle and behave like semi-dilute polymer chains. In the presence of these entanglements and with solutions of sufficient viscosity, electrospinning becomes possible.[22,29–31]

Solution rheology of lecithin solutions was similar to semi-dilute polymer solutions. An entanglement concentration was identified at 35 wt% solids. Specific viscosity scaled with concentration to the 2.4 and 8.4 powers below and above this transition, respectively. These dependencies are much stronger than observed for neutral solutions (scaling exponents of 1.25 and 3.75, respectively), and originate from intermolecular interactions. Cappelaere, et al., also noticed similar deviations for the surfactant cetyltrimethylammoniumbromide, where the viscosity scaled with concentration to the power of 12.[32]

Similar to neutral polymer behavior, electrospinning lecithin is possible at concentrations above the critical concentration for entanglements, c_e. Fig. 4.2 shows field-emission scanning electron microscope (FESEM) images of lecithin fibers. At concentrations below c_e (35 wt%), only droplets formed. However, the presence of fibers between droplets is evident above c_e, and uniform fibers form at concentrations above 43 wt%. Average fiber diameters followed a power-law relationship with solution concentration, as illustrated in Fig. 4.3. For illustrative purposes,

the empirical fiber diameter relationship for neutral, non-associating polymers is also shown.[22] The large deviation between phospholipid fiber diameter and neutral polymer behavior stems from intermolecular associations. Similar deviations were observed in poly(alkyl methacrylates) copolymerized with self-complementary hydrogen-bonding groups.[33]

4.4 Future Work in Electrospinning Phospholipids

This work is the first report of electrospun fiber formation from small molecules. However, as observed with phospholipid bilayer membranes,[9,34] electrospun phospholipid scaffolds lack the durability required for rigorous applications such as tissue engineering and biosensing. A primary concern is the facile hydration and breakdown of the phospholipid fibers in the presence of moisture. Earlier work was conducted to investigate the influence of added polymers on stable surfactant micelles from electrospinning.[35,36] However, this mechanical improvement was relatively minor, as covalent bonds did not attach the surfactants to the fibers. Direct polymerization of the wormlike micelles could theoretically create more durable phospholipid fibers. Recent research and reviews by O'Brien et al.[11] and others[10,37] indicate that phospholipids and amphiphiles containing polymerizable moieties can retain their self-assembled structure upon reaction. Future work in phospholipid fibers involves the synthesis of designer lipids and surfactants with polymerizable groups to introduce crosslinks and mechanical durability to the fibrous scaffolds.

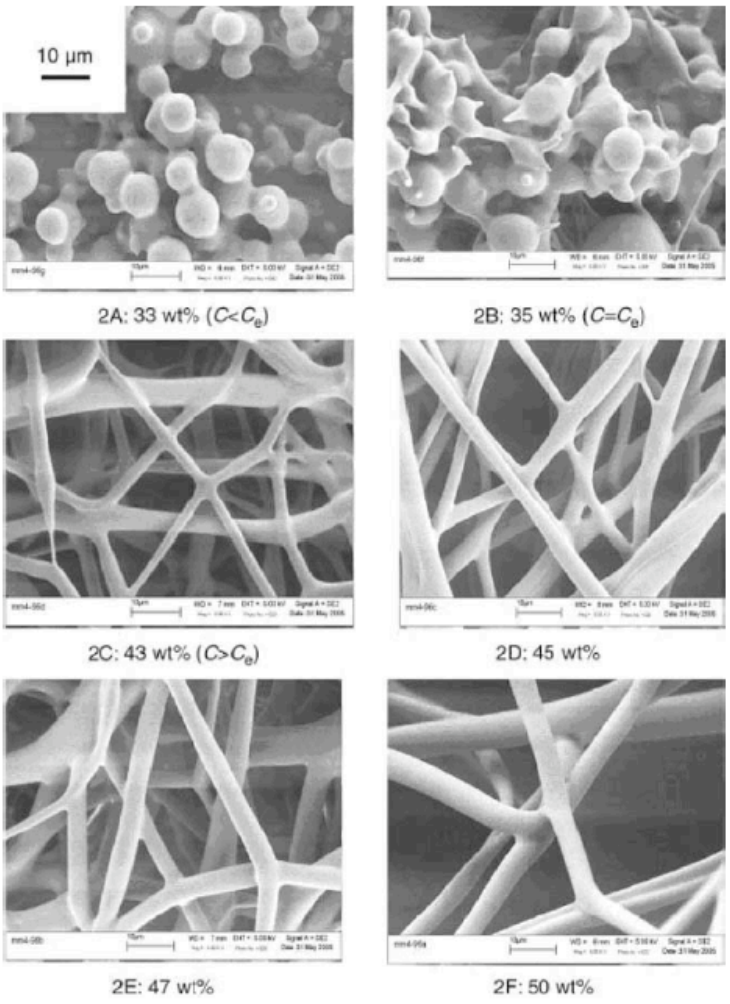

Figure 4.2. FESEM images of the lecithin fibers as a function of solution concentration (reprinted with permission from ref. 21).

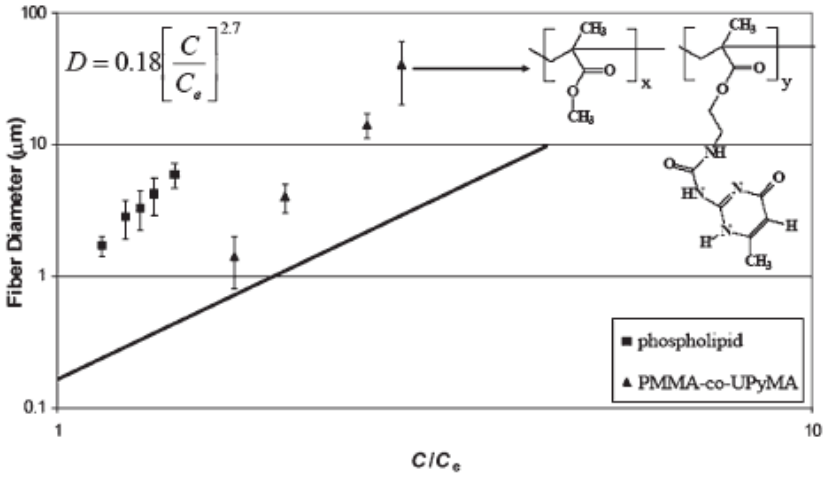

Figure 4.3. Fiber diameter correlation for electrospun lecithin (squares). Behavior for neutral, non-associating polymers (line) and hydrogen-bonding polymers (triangles) are also shown for comparison.

The electrospun phospholipids lend themselves to a wide range of applications. Nakai and coworkers have shown that phospholipid-functionalized alkyl methacrylates suppress platelet adhesion.[38] Similar work demonstrated that phospholipids are valid candidates for blood purification membranes and artificial organs.[39,40] Also, due to their biological origin, phospholipid fibers are suitable scaffolds for cell growth. However, their use in biological applications will require biocompatibility studies to verify that electrospun (and polymerized) phospholipid fibers remain cytocompatible and platelet suppressing. Electrospun polymeric fibers were reported earlier as cell growth scaffolds,[41–43] and phospholipid scaffolds are expected to mimic the extracellular matrix, creating applications in tissue growth and engineering.[41,44,45] Additionally, phospholipid membranes and vesicles successfully performed as gene- and drug-delivery platforms.[1,2] By incorporating a specific gene or drug in the electrospinning process, controlled-release therapeutic scaffolds could be fabricated.[46,47] Among those mentioned, countless other applications are possible for electrospun phospholipid scaffolds. This emerging

field presents many avenues of future research, and suggests new, biologically-compatible materials.

4.5 References

1 V. Saroglou, S. Hatziantoniou, M. Smyrniotakis, I. Kyrikou , T. Mavromoustakos, A. Zompra, V. Magata, P. Cordopatis and C. Demetzos, J. Pept. Sci., 2005, 12, 43–50.
2 T. Sebti and K. Amighi, Eur. J. Pharm. Biopharm., 2006, 63, 51–58.
3 E. Sackmann, Science, 1996, 271, 43–48.
4 B. A. Cornell, V. L. B. Braach-Maksvytis, L. G. King, P. D. J. Osman, B. Raguse, L. Wieczorek and R. J. Pace, Nature, 1997, 387, 580–583.
5 C. Ziegler and W. Go¨ pel, Curr. Opin. Chem. Biol., 1998, 2, 585–591.
6 M. Stelzle, G. Weissmu¨ ller and E. Sackmann, J. Phys. Chem., 1993, 97, 2974–2981.
7 G. Elender, M. Ku¨hner and E. Sackmann, Biosens. Bioelectron., 1996, 11, 565–577.
8 T. Cha, A. Guo and X.-Y. Zhu, Biophys. J., 2006, 90, 1270–1274.
9 E. Reimhult, F. Ho¨o¨k and B. Kasemo, Langmuir, 2003, 19, 1681–1691.
10 S. A. Miller, J. H. Ding and D. L. Gin, Curr. Opin. Colloid Interface Sci., 1999, 4, 338–347.
11 D. F. O'Brien, B. Armitage, A. Benedicto, D. E. Bennett, H. G. Lamparski, Y.-S. Lee, W. Srisiri and T. M. Sisson, Acc. Chem. Res., 1998, 31, 861–868.
12 J. T. Groves and S. G. Boxer, Acc. Chem. Res., 2002, 35, 149–157.
13 J. Lahiri, G. D. Fate, S. B. Ungashe and J. T. Groves, J. Am. Chem. Soc., 1996, 118, 2347–2358.
14 J. T. Groves, N. Ulman, P. S. Cremer and S. G. Boxer, Langmuir, 1998, 14, 3347–3350.
15 H. Mueller, H.-J. Butt and E. Bamberg, J. Phys. Chem. B, 2000, 104, 4552–4559.
16 A. R. Curran, R. H. Templer and P. J. Booth, Biochemistry, 1999, 38, 9328–9336.
17 H. H. Hub, B. Hupfer, H. Koch and H. Ringsdorf, Angew. Chem., Int. Ed. Engl., 1980, 19, 938–940.
18 T. Nakaya and Y. J. Li, Des. Monomers Polym., 2003, 6, 309–351.
19 A. Formhals, U.S. Pat. 1975504, 1934.
20 D. H. Reneke r and I . Chun, Nanotechnology, 1996, 7, 216–223.
21 M. G. McKee , J . M. Layman, M. P. Cashion and T. E. Long, Science, 2006, 311, 353–355.
22 M. G. McKee, G. L. Wilkes, R. H. Colby and T. E. Long, Macromolecules, 2004, 37, 1760–1767.
23 M. G. McKee, M. T. Hunley, J. M. Layman and T. E. Long, Macromolecules, 2006, 39, 575–583.
24 Y. A. Shchipunov and H. Hoffmann, Rheol. Acta, 2000, 39, 542–553.
25 L. J. Magid, J. Phys. Chem. B, 1998, 102, 4064–4074.
26 B. O'Shaughnessy and J. Yu, Phys. Rev. Lett., 1995, 74, 4329–4332.
27 T. Shikata and H. Hirata, Langmuir, 1987, 3, 1081–1086.
28 W. Siriwatwechakul , T. LaFleur, R. K. Prud'homme and P. Sullivan, Langmuir, 2004, 20, 8970–8974.
29 J. H. Yu, S. V. Fridrikh and G. C. Rutledge, Polymer, 2006, 47, 4789–4797.
30 S. L. Shenoy, W. D. Bates and G. Wnek, Polymer, 2005, 46, 8990–9004.
31 J. M. Deitzel, J. Kleinmeyer, D. Harris and N. C. B. Tan, Polymer, 2001, 42, 261–272.

32 E. Cappelaere, R. Cressely and J. P. Decruppe, Coll. Surf., A, 1995, 104, 353–374.
33 C. L. Elkins, T. Park, M. G. McKee and T. E. Long, J. Polym. Sci., Part A: Polym. Chem., 2005, 43, 4618–4631.
34 E. Reimhult, F. Ho¨o¨k and B. Kasemo, J. Chem. Phys., 2002, 117, 7401–7404.
35 T. Lin, H. Wang, H. Wang and X. Wang, Nanotechnology, 2004, 15, 1375–1381.
36 T. E. Herricks, S.-H. Kim, J. Kim, D. Li, J. H. Kwak, J. W. Grate, S. H. Kim and Y. Xia, J. Mater. Chem., 2005, 15, 3241–3245.
37 B. A. Pindzola, B. P. Hoag and D. L. Gin, J. Am. Chem. Soc., 2001, 123, 4617–4618.
38 S. Nakai, T. Nakaya and M. Imoto, Macromol. Chem. Phys., 1978, 79, 2349–2353.
39 A. Korematsu, Y. Takemoto, T. Nakaya and H. Inoue, Biomaterials, 2002, 23, 263–271.
40 N. Morimoto, Y. Iwasaki, N. Nakabayashi and K. Ishihara, Biomaterials, 2002, 23, 4881–4887.
41 L. A. Smith and P. X. Ma, Colloids Surf., B, 2004, 39, 125–131.
42 M. R. Williamson, R. Black and C. Kielty, Biomaterials, 2006, 27, 3608–3616.
43 W. Patcharaporn, N. Sanchavanakit, P. Pavasant and P. Supaphol, J. Nanosci. Nanotechnol., 2006, 6, 514–522.
44 C. L. Casper, N. Yamaguchi, K. L. Kiick and J. F. Rabolt, Biomacromolecules, 2005, 6, 1998–2007.
45 D. Han and P.-I. Gouma, Nanomedicine, 2006, 2, 37–41.
46 Z.-M. Huang, C.-L. He, A. Yang, Y. Zhang, X.-J. Han, J. Yin and Q. Wu, J. Biomed. Mater. Res., 2006, 77A, 169–179.
47 D. Liang, Y. K. Luu, K. Kim, B. S. Hsiao, M. Hadjiargyrou and B. Chu, Nucleic Acids Res., 2005, 33, e170.

Chapter 5: Influence of Counteranion on the Thermal and Solution Behavior of Poly(2-dimethylaminoethyl methacrylate)-based Polyelectrolytes

(From: Hunley, M.T.; England, J.P.; Long, T.E. *Macromolecules* **2010**, *Submitted*)

5.1 Abstract

Poly(2-dimethylaminoethyl methacrylate) (PDMAEMA) was synthesized and subsequently neutralized with various acids to form PDMAEMA·HCl, PDMAEMA·HBF4, and PDMAEMA·HOTf polyelectrolytes. In addition, ion exchange of the chloride anion provided polyelectrolytes with NO3-, N(CN)2-, PF6-, and Tf2N- anions. The glass transition temperature (T_g) decreased significantly with anion in the order Cl- > PF6- > BF4- > NO3- > TfO- > Tf2N-. The polyelectrolytes with larger, weakly-coordinated anions required less thermal energy to dissociate ionic interactions, leading to tailored thermal behavior. Solution conductivity of the water-soluble polyelectrolytes decreased in the order Cl- > NO3- > BF4- > N(CN)2- > TfO-, which was consistent with counteranion mobility. Solution rheology revealed polyelectrolyte behavior for PDMAEMA·HCl, PDMAEMA·HBF4, and PDMAEMA·HOTf. PDMAEMA·HCl underwent an electrospraying-electrospinning transition at three times the critical concentration for entanglement (Ce), which was consistent with other cationic polyelectrolytes. However, the BF4- and TfO- polyelectrolytes exhibited an onset of fiber formation at 1.4-1.8Ce, much closer to the behavior of neutral, non-associating polymers. Fiber diameters for all polyelectrolytes were 1 – 2 orders of magnitude smaller than those for neutral polymers due to increased conductivities of the electrospinning solutions.

5.2 Introduction

Ionic liquid monomers provide relatively unexplored families of new charged macromolecules.[1-4] Compared to conventional polyelectrolytes, polymerized ionic liquids typically exhibit lower thermal transitions and enhanced ionic conductivities due to the presence of weakly coordinated ions. The ionic conductivities of these polyelectrolytes approach and often exceed those of polymer films simply doped with conventional ionic liquids. These desirable properties have lead to the use of polymerized ionic liquids in many applications including electromechanical actuators,[5,6] photovoltaics,[7] and electrochromic devices.[8]

The physical properties of polymerized ionic liquids depend strongly on the choice of cation and anion. Mercerreyes et al.[9,10] investigated the properties of polycations based on ammonium, imidazolium, and 4-vinylpyridinium cations. They reported that counteranion choice led to significant changes in solubility and thermal stability. The choice of larger, less coordinating anions also led to lower thermal transitions due to increased free volume and weaker ionic interactions. Typically, the larger non–polar anions (such as $CF_3SO_3^-$ and $(CF_3SO_2)_2N^-$, referred to as TfO^- and Tf_2N^-, respectively) resulted in a significantly increased thermal stability due to the lower basicity and nucleophilicity of the anion. Polyelectrolytes with non-polar anions also do not dissolve in water, but are readily soluble in polar organic solvents. The Elabd research group[2,11] investigated random copolymers incorporating an imidazolium-based ionic liquid acrylic monomer with either BF_4^- or Tf_2N^- counteranions. The ratio of anions was varied to control T_g over the range 265 to 345 K. The ionic conductivities (at 373 K) of the copolymers in the solid state increased dramatically as the T_g decreased, primarily due to increased mobility of ions in the low T_g matrix.

The solution rheological behavior of polyelectrolytes differs significantly from neutral polymers.[12,13] Strong coulombic repulsion between charged repeat units leads to extended

conformations in dilute solution. At higher polymer concentrations, the increased ionic strength reduces the Debye screening length, and the polymer chain contracts to smaller dimensions. Unlike neutral polymers, this contraction leads to a decrease in the chain relaxation time of polyelectrolytes with increasing concentration in semi-dilute solutions. Specific viscosity (η_{sp}) describes the polymer contribution to viscosity as

$$\eta_{sp} \equiv \frac{\eta_0 - \eta_s}{\eta_s},$$

where η_0 is the zero-shear viscosity of the polymer solution and η_s is the solvent viscosity. In dilute solutions, specific viscosity increases linearly with concentration until the overlap concentration, c^*. Above c^*, in the semi-dilute unentangled regime, polymer chains begin to experience intermolecular interactions. As concentration increases further, polymer chains become constrained and begin to entangle above the entanglement concentration, c_e. The specific viscosity of polymer solutions scales with concentration in the semi-dilute unentangled and semi-dilute entangled regimes as

$$\begin{aligned} \eta_{sp} &\sim C^{1/3\nu-1} \qquad for\, C^* < C < C_e \\ \eta_{sp} &\sim C^{3/3\nu-1} \qquad for\, C_e < C < C_D \end{aligned},$$

where ν is a geometrical parameter termed the Flory exponent.[13] For neutral polymers in a good solvent, ν equals 0.588, and the scaling exponents for semi-dilute unentangled and entangled regimes become 1.3 and 3.9, respectively. Polyelectrolytes have elongated conformations in solution and ν equals 1, hence the scaling exponents are 0.5 and 1.5, respectively. In addition, due to the extended chains in dilute solution, the overlap concentration occurs at lower concentrations and a larger semi-dilute unentangled regime is observed relative to neutral polymer solutions.

Electrospinning of polymer solutions employs an applied electric field to draw fibers from solution.[14-16] The applied electric potential causes a droplet of solution to form a Taylor cone, and once the applied potential exceeds a critical value, the solution will accelerate towards a grounded or oppositely-charged target. The critical voltage occurs as the electrical energy of the Taylor cone exceeds the surface free energy.[17] During flight, the polymer jet experiences significant elongation due to surface charge repulsion; surface tension acts against this repulsion and pulls the jet into droplets. Neutral polymers form electrospun fibers once the solutions become sufficiently elastic to suppress the Rayleigh instability, which leads to breakup of the jet into droplets.[17,18] Our laboratories first demonstrated that neutral, non-associating polymers exhibit the electrospraying-to-electrospinning transition at concentrations near c_e, and uniform fibers form at higher concentrations near $2c_e$.[18] These transitions corresponded to zero shear viscosities of approximately 10 cP and 30 cP, respectively. Wilkes and coworkers confirmed this finding and demonstrated that polymers with broad molecular weight distributions require even higher degrees of solution entanglement to form uniform fibers.[19] Wnek and coworkers[17] correlated this transition to the number of entanglements per chain in solution, $(n_e)_{soln}$, and predicted fiber formation at $(n_e)_{soln} = 2$ and uniform fiber formation at $(n_e)_{soln} = 3.5$.

The introduction of surfactants can lower surface tension and aid the formation of bead-free electrospun fibers at lower concentrations.[20,21] In addition, increasing the solution conductivity through introduction of low molar mass electrolytes decreases the concentration required to form uniform fibers.[22,23] The increased conductivity leads to greater stretching of the polymer jet and reduces or eliminates bead formation. A significant reduction in fiber diameter due to this additional stretching also occurs. The addition of small amounts of polyelectrolyte to neutral polymer solutions also facilitates bead suppression in the same manner.[24]

Pure polyelectrolyte solutions present difficulties during electrospinning. Poly(acrylic acid) (PAA) has been successfully electrospun from water and DMF.[25] Uniform fibers were obtained from both solvent systems, although the fibers electrospun from water had larger diameters at similar viscosities and conductivities. However, the fraction of PAA repeat units bearing dissociated carboxylate groups depends on the solution pH and pKa of the carboxylic acid and is not necessarily 100%. Other polyelectrolytes or ionomers such as poly(allylamine hydrochloride),[26] chitosan,[27] and Nafion®[26,28,29] have been successfully electrospun in the presence of neutral polymers. Our research group was the first to electrospin a strong polyelectrolyte, poly(2-dimethylaminoethyl methacrylate) hydrogen chloride (PDMAEMA-HCl).[30] The Xia research group[31] electrospun high molecular weight poly(styrene sulfonate) sodium salt at 20 wt% from an 88% formic acid solvent, but provided no discussion of solution properties. Recently, Yamamoto et al.[32,33] reported the electrospinning of chitosan from trifluoroacetic acid solution; they thoroughly correlated the electrospinnability to solution viscosity for various molecular weights. Beaded fibers formed above a zero-shear viscosity of 200 cP, and uniform fibers formed above viscosities of 800 cP for several different molecular weight chitosan samples studied. Solutions more viscous than 1000 cP failed to electrospin due to the extremely high viscosity. These solution viscosities are much higher than those observed by Long et al. for neutral non-associating polymers (beaded fibers above 10 cP, uniform fibers above 30 cP), but an explanation for this discrepancy was not reported.

Our research group recently reported the rheological characterization and successful electrospinning of the cationic polyelectrolyte PDMAEMA·HCl.[30] Fiber formation required surprisingly high solution concentrations above $8c_e$ and solution viscosities greater than 1000 cP. We hypothesized that the large repulsive forces on the polyelectrolyte chain under an electric

field coupled with the relatively low mobility of the polyions led to breakup of the electrospinning jet until sufficient elasticity was present to stabilize the jet. The addition of sodium chloride screened the charges on the polyelectrolyte chain and resulted in lower entanglement numbers and viscosities required for electrospinning.

In the present study, we have synthesized a series of polyelectrolytes based on PDMAEMA, with counteranions of Cl^-, BF_4^-, NO_3^-, $N(CN)_2^-$, PF_6^-, TfO^-, and Tf_2N^-. Thermal degradation temperatures increased 100 °C and the glass transition temperature decreased 130 °C through simple anion exchange. The choice of counteranion also had a significant effect on solution conductivity and electrospinning behavior. We analyzed the electrospinning behavior in terms of previously developed semi-empirical correlations for neutral polymers and observations for polyelectrolytes. PDMAEMA·HCl exhibited typical polyelectrolyte electrospinning behavior, but as the anion was exchanged to BF_4^- and TfO^-, electrospinning behavior resembled neutral polymers in the presence of salt.

5.3 Experimental

5.3.1 Materials

The monomer 2-(*N*,*N*-dimethylamino)ethyl methacrylate (DMAEMA) (98%) was purchased from Sigma Aldrich and passed through a silica column to remove inhibitor prior to use. 2,2'-Azobisisobutyronitrile (AIBN) (Sigma Aldrich, 98%) was recrystallized from methanol. Sodium dicyanamide (Sigma Aldrich, 96%), sodium nitrate (Sigma Aldrich, 98%), trifluoromethanesulfonic acid (Sigma Aldrich, 98%), potassium hexafluorophosphate (Sigma Aldrich, 98%), lithium bis(trifluoromethane)sulfonimide (Fluka, puriss.), and tetrafluoroboric acid (Sigma Aldrich, 48 wt% solution in water) were used without further purification.

Tetrahydrofuran (THF), hexanes, methanol, hydrochloric acid, and deionized water were obtained from commercial sources and used as received.

5.3.2 Polymerization of DMAEMA

In a sample polymerization, 35.7 mL of DMAEMA (33.3 g, 0.211 mol, 20 wt%) was added to 150 mL of THF in a two-necked, round-bottomed flask equipped with a magnetic stir bar. The flask was attached to a reflux condenser and submerged into an oil bath at 65 °C. After the flask was purged with N_2 for 10 min, 0.0346 g AIBN (0.211 mmol, 0.1 mol% versus DMAEMA) was added and the reaction mixture was purged with N_2 for another 10 min. The polymerization proceeded at 65 °C for 24 h. After 24 h, the reaction mixture was concentrated and precipitated into 4 L of hexanes and stirred for 2 h. The solvent was decanted and the polymer dried *in vacuo* overnight at 65 °C. The typical yield after isolation was 60-70%. ^{1}H NMR (400 MHz, $CDCl_3$, δ): 4.1-3.9 (s, 2H, -OCH_2-), 2.6-2.5 (s, 2H –CH_2N-), 2.3-2.2 (s, 6H, -NCH_3), 2.0-1.7 (s, 2H, -CH_2-), 1.1-0.8 (s, 3H, -CH_3).

5.3.3 Protonation and Anion Exchange of PDMAEMA

PDMAEMA was dissolved at 10 wt% in deionized water and subsequently titrated with HCl, HBF_4, or CF_3SO_3H to pH 5 to form PDMAEMA·HCl, PDMAEMA·HBF_4, or PDMAEMA·HOTf, respectively. After stirring for 8 h, the polyelectrolyte solution was precipitated into acetone, decanted, and dried *in vacuo* overnight at 65 °C. ^{1}H NMR (400 MHz, D_2O, δ): 11.7-11.4 (s, 1H, NH), 4.5-4.2 (s, 2H, -OCH_2-), 3.6-3.3 (s, 2H, -CH_2N), 3.0-2.7 (s, 6H, -NCH_3), 2.2-1.8 (s, 2H, -CH_2-), 1.2-0.7 (s, 3H, -CH_3).

Anion exchanges of PDMAEMA·HCl were performed by either precipitation or dialysis. In a typical precipitation anion exchange, 0.324 g PDMAEMA·HCl (1.7 mmol of repeat unit) was dissolved in 5 mL deionized water. Aqueous $Li(CF_3SO_2)_2N$ (2.40 g (8.4 mmol, 5

equivalents) in 5 mL deionized water) was slowly added dropwise to the polymer solution. A white precipitate quickly formed. The precipitate was stirred for 24 h, decanted, and washed thoroughly with deionized water to remove all residual salt. PDMAEMA·HPF_6 was prepared in a similar manner. In a typical dialysis anion exchange, 0.375 g PDMAEMA·HCl (1.9 mmol of repeat unit) was dissolved in 5 mL deionized water and added to a solution of 0.863 g $NaN(CN)_2$ (9.7 mmol, 5 equivalents) in 5 mL deionized water. The mixed solution was syringed into a SpectraPore dialysis cassette (molecular weight cutoff of 3500 g/mol) and the cassette placed in a beaker of deionized water. After 6 h and 12 h, the deionized water was changed and another 0.863 g $NaN(CN)_2$ added. After another 10 h, the deionized water was changed without salt. This water was changed after an additional 6 h and 12 h. Then, the polymer solution was removed from the dialysis cassette and water removed *in vacuo* to isolate the polymer PDMAEMA·$HN(CN)_2$. PDMAEMA·HNO_3 was prepared in a similar manner. XPS analysis confirmed less than 0.2% chlorine in each anion-exchanged polymer.

5.3.4 Analytical Methods

^{1}H NMR spectra were obtained on a Varian INOVA 400 MHz spectrometer at 23 °C in $CDCl_3$, D_2O, or DMSO-d_6. Thermal analysis was performed on a TA Instruments Q500 thermogravimetric analyzer (TGA) and a TA Instruments Q1000 differential scanning calorimeter (DSC). TGA was conducted from ambient to 600 °C at 10 °C/min, and DSC was conducted from 0 to 200 °C at 10 °C/min, using only the second heating scan for analysis. X-ray photoelectron spectroscopy was conducted on a Perkin-Elmer 5300 with a Mg anode at 13 kV accelerating voltage. Size exclusion chromatography was performed as reported previously.[34] Solution conductivity was measured using an ACORN CON6 probe at 25 °C. The average of three measurements was taken. Field emission scanning electron microscopy (FESEM) of

electrospun fibers was performed using a LEO 1550 FESEM at 5 keV accelerating voltage. Prior to FESEM analysis, fibers were sputter coated with 10 nm of 60/40 gold/platinum to prevent excessive charge buildup in the SEM.

5.3.5 Solution Rheology and Electrospinning

Solutions for rheology and electrospinning were prepared by dissolving the desired amount of polymer in an 80/20 (wt/wt) mixture of deionized water/methanol. The solutions were allowed to stir magnetically for three days to ensure equilibration. Solution rheology was conducted on a TA Instruments AR-G2 strain-controlled rheometer equipped with concentric cylinder geometry. The solutions were allowed to equilibrate at 25 °C for 2 min prior to measurement. Solutions for electrospinning were loaded into a syringe equipped with an 18-gauge needle. The syringe was placed into a syringe pump and the needle connected to a high voltage power supply. The polymer solution was metered at a rate of 3 mL/h and the potential set to 25 kV. Fibers began collecting on a grounded, stainless steel mesh target immediately after the voltage was applied. A ¼" x ¼" section of the target was collected for FESEM analysis.

5.4 Results and Discussion

5.4.1 Synthesis and Ion Exchange

PDMAEMA was synthesized using conventional free radical polymerization in THF with 0.1 mol% AIBN as initiator. After isolation, the polymer was dissolved in deionized water and titrated with either HCl, HBF_4, or CF_3SO_3H to form the corresponding polyelectrolytes, as illustrated in Scheme 5.1. XPS analysis confirmed quantitative formation of the polyelectrolytes. As described in our previous report,[34] an aqueous solvent containing 0.7 M $NaNO_3$, 0.1 M Tris, 200 ppm NaN_3 (pH adjusted to 6.0 with acetic acid) dissolved the polyelectrolytes and prevented

column interactions for molecular weight analysis using size exclusion chromatography. Dynamic light scattering also confirmed that all polyelectrolytes did not aggregate in the SEC solutions. Table 5.1 lists the molecular weights of all polymers investigated. Each polymer was dialyzed against the SEC solvent before analysis to ensure the only ions in solution were from the solvent. Thus, as shown in Table 5.1, one would expect that reported molecular weights are independent of the counteranion and reflect the degree of polymerization, easily comparable for all polymers. Number-average molecular weights ranged from 82 200 g/mol to 113 000 g/mol. To investigate the effect of molecular weight on electrospinning, higher molecular weight PDMAEMA·HCl and PDMAEMA·HBF_4 were synthesized in DI H_2O using 0.5 wt% ammonium persulfate as the initiator. These two polyelectrolytes had number-average molecular weights of 184 000 g/mol and 191 000 g/mol, respectively.

Scheme 5.1. Synthesis of PDMAEMA and neutralization with acid to form the polyelectrolytes PDMAEMA·HCl, PDMAEMA·HBF_4, and PDMAEMA·HOTf.

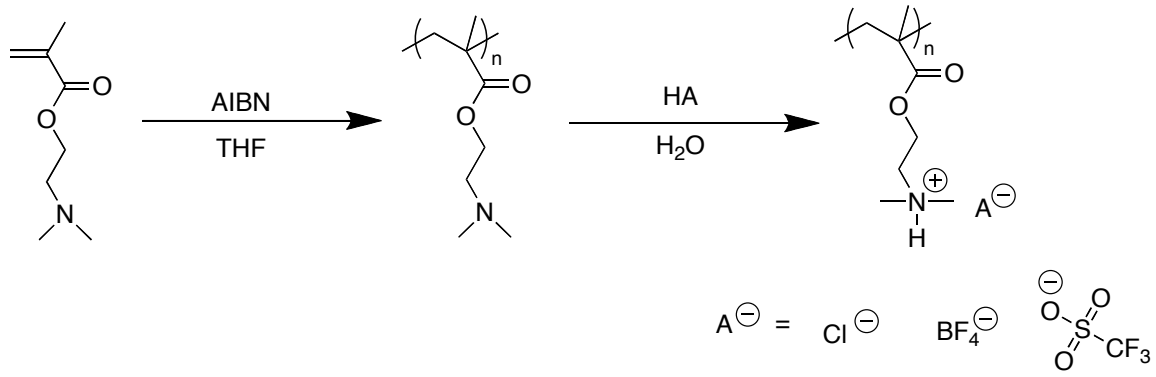

Molecular weight distributions for polyelectrolytes synthesized in THF were lower than expected for conventional free radical polymerizations. However, PDMAEMA·HCl synthesized in water had M_w/M_n of 1.51, which is expected for free radical polymerizations. A sample of

PDMAEMA was polymerized in THF to confirm that the low dispersities of the polymers resulted from isolation procedures and not poor chromatography during SEC analysis. Half of the sample was precipitated in hexanes, consistent with the other polymerizations. The second half of the sample was dialyzed against water and subsequently freeze-dried to remove residual monomer. SEC analysis indicated that the precipitated polymer had M_n = 138 000 g/mol with M_w/M_n = 1.08, and the dialyzed polymer had M_n = 81 100 g/mol with M_w/M_n = 1.30. The precipitation removed much of the lower molecular weight fraction, resulting in an M_n 70% higher and a significantly narrower polydispersity. This analysis confirmed that fractionation during precipitation led to narrow molecular weight distributions observed during SEC analysis.

Anion exchange of the Cl^- anion yielded four new polyelectrolytes with the anions NO_3^-, $N(CN)_2^-$, PF_6^-, and Tf_2N^-, as illustrated in Scheme 5.2. XPS analysis after anion exchange confirmed complete disappearance of chlorine from all samples. Because these four new polyelectrolytes were prepared from the same PDMAEMA·HCl precursor, the degree of polymerization matched the precursor, and SEC indicated nearly identical molecular weights. All polymers except PDMAEMA·HPF_6 and PDMAEMA·$HNTf_2$ dissolved in water, but only PDMAEMA·HCl, PDMAEMA·HNO_3, and PDMAMA·$HN(CN)_2$ dissolved in 0.1 M salt solutions. DMSO dissolved all polyelectrolytes regardless of counteranion. Table 5.2 presents the solubilities of each polyelectrolyte in several common polar solvents to form visually clear solutions.

Table 5.1. SEC Molecular Weights and Thermal Properties of PDMAEMA-based Polyelectrolytes

Polymer	M_n (g/mol)[a]	M_w/M_n[a]	T_g (°C)[b]	$T_{d,5\%}$ (°C)[c]
PDMAEMA	113 000	1.21	19	295
PDMAEMA-HCl (THF)	96 200	1.15	164	230
PDMAEMA-HCl (H_2O)	184 000	1.51	160	230
PDMAEMA-HBF_4	191 000	1.21	131	286
PDMAEMA-HNO_3	96 200	1.15	130	243
PDMAEMA-$HN(CN)_2$	96 200	1.15	n.d.[d]	244
PDMAEMA-HPF_6	96 200	1.15	164	242
PDMAEMA-HOTf	82 200	1.01	70	310
PDMAEMA-$HNTf_2$	96 200	1.15	38	320

[a]Molecular weights and distributions determined by SEC for polymers dialyzed against SEC solvent.

[b]Glass transition temperatures measured by DSC.

[c]Temperature at 5% weight loss as determined by TGA.

[d]No glass transition observed by DSC.

Scheme 5.2. Anion exchange of PDMAEMA·HCl to form PDMAEMA·HNO_3, PDMAEMA·$HN(CN)_2$, PDMAEMA·HPF_6, and PDMAEMA·$HNTf_2$.

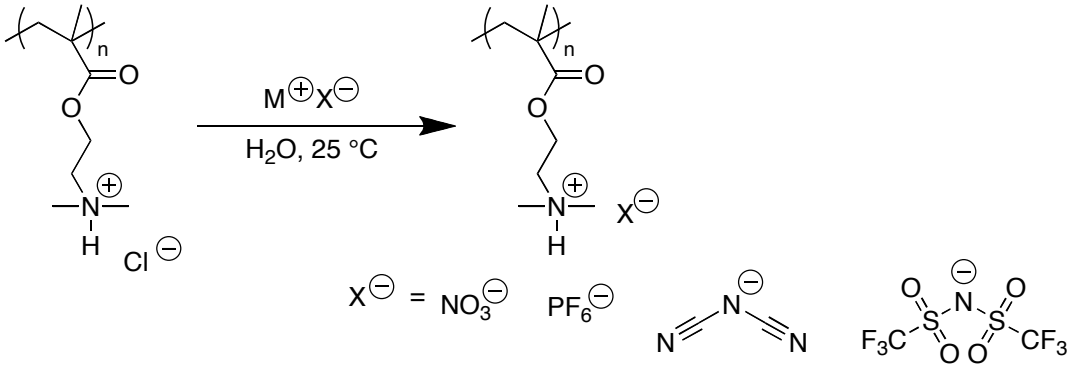

Table 5.2. Solubility of PDMAEMA-Based Polyelectrolytes in Aqueous and Polar Organic Solvents.[a]

Polymer	H_2O	0.1M [NaX][b]	Acetone	DMSO
PDMAEMA	+	-	+	+
PDMAEMA-HCl	+	+	-	+
PDMAEMA-HBF_4	+	-	-	+
PDMAEMA-HNO_3	+	+	-	+
PDMAEMA-$HN(CN)_2$	+	+	-	+
PDMAEMA-HPF_6	-	-	+	+
PDMAEMA-HOTf	+	-	+	+
PDMAEMA-$HNTf_2$	-	-	+	+

[a]Solubility indicated by '+' for soluble and '-' for insoluble or only sparingly soluble.
[b][NaX] represents the sodium (or lithium) salt bearing the same anion as the polyelectrolyte. For example, NaCl for PDMAEMA-HCl or $NaBF_4$ for PDMAEMA-HBF_4. NaCl was used for PDMAEMA.

The change of counteranion also affected the resonances of specific protons in the ^{1}H NMR spectra, most notably the ammonium proton. In DMSO-d_6, this proton appeared at 11.4 ppm for PDMAEMA·HCl, but shifted upfield to 10.0 ppm for PDMAEMA·HNO_3, 9.6 ppm for PDMAEMA·HPF_6, and 9.5 ppm for PDMAEMA·HOTf and PDMAEMA·$HNTf_2$. Similar trends, though smaller in magnitude, were observed for the methyl and methylene protons near the ammonium. Shifts in ^{1}H NMR resonances in imidazolium salts upon ion exchange correlate to the interactions between cation and anion.[35,36] Lungwitz et al.[36] determined the Kamlet-Taft hydrogen-bonding ability of a series of anions with 1-butyl-3-methylimidazolium. They observed a linear relationship between the chemical shift of the proton attached to the 2-position of the imidazolium ring and the hydrogen-bond basicity (β) and acidity (α) of the anion. The upfield shift in the ammonium proton observed in this study also correlated with the α- and β-values for the different anions determined by Lungwitz et al.

5.4.2 Thermal Analysis of PDMAEMA Polyelectrolytes

Thermogravimetric analysis (TGA) indicated the counteranion dictates thermal degradation behavior. Figure 5.1 shows the TGA thermograms for PDMAEMA and two

polyelectrolytes. Neutral PDMAEMA lost approximately 50% of the initial sample mass at 300 °C and the remainder at 400 °C. For PDMAEMA·HCl, degradation began slightly above 230 °C, with approximately 60% weight loss occurring in the first step. The remainder of the mass degraded completely around 400 °C. The initial weight loss corresponded to the loss of the anion and ammonium group through the Hofmann elimination mechanism. The second weight loss step involves further degradation of the polymer backbone. The Hofmann elimination reaction depends strongly on the basicity of the anion,[37] and polyelectrolytes with less basic counteranions (such as PDMAEMA·HOTf) did not begin degrading until greater than 300 °C. The onset of degradation is tabulated in Table 5.1 for all polyelectrolytes.

Anion choice also significantly impacted the polyelectrolyte T_g. Neutral PDMAEMA exhibited a glass transition at 19 °C. The polyelectrolyte PDMAEMA·HCl, however, had a T_g of 164 °C due to the introduction of ionic aggregation. Upon anion exchange to the larger anions, weaker interactions between cation and anion led to reductions in T_g. Polyelectrolyte T_g decreased according to the series $Cl^- > PF_6^- > BF_4^- > NO_3^- > TfO^- > Tf_2N^-$. PDMAEMA·$HPF_6$ exhibited a relatively high T_g of 164 °C, which was presumably due to hydrogen bonding interactions between the anion and cation. All thermal transitions are listed in Table 5.1 with the onset of thermal degradation.

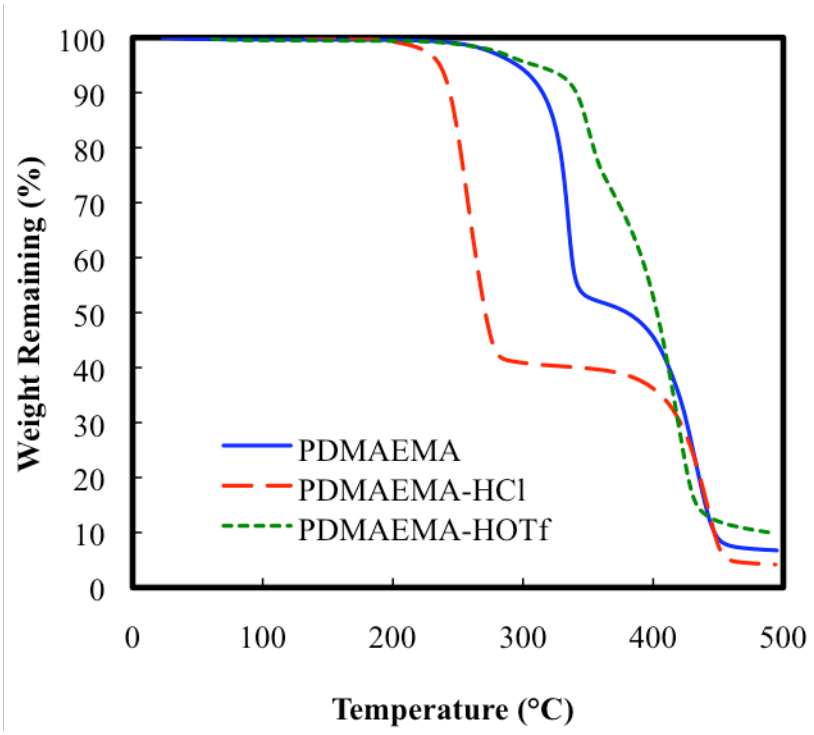

Figure 5.1. Thermogravimetric analysis of PDMAEMA (solid blue line), PDMAEMA·HCl (dashed red line), and PDMAEMA·HOTf (dotted green line).

5.4.3 Solution Conductivity

Solution conductivity of the water-soluble polyelectrolytes exhibited a strong dependence on the counterion. In aqueous solution, the Cl^- anion dissociated to a large degree from the polymer and led to a high conductivity. The solution conductivity of the polyelectrolytes at constant molar concentration decreased in the order of counterions $Cl^- > NO_3^- > BF_4^- > N(CN)_2^- > TfO^-$, as tabulated in Table 5.3. The decrease in solution conductivity correlated closely to a decrease in the ionic mobility of the counteranions, as reported in the literature.[38,39] Counterion mobility dominated the conductivity in dilute solutions due to the relatively low mobility of the large polycation.

Table 5.3. Solution Conductivity of PDMAEMA-Based Polyelectrolytes

Anion	Conductivity (10^6 S cm^{-1})[a]	Ionic Mobility (10^{-8} m^2 s^{-1} V^{-1})
[Cl^-]	1705 ± 18	7.91[b]
[NO_3^-]	1670 ± 16	7.40[b]
[BF_4^-]	1559 ± 8	7.77[c]
[$N(CN)_2^-$]	1322 ± 2	5.07[c]
[TfO^-]	1216 ± 7	3.80[c]

[a]Solution conductivity measured in DI H_2O at 298 K at a polymer concentration of 0.15 mol repeat unit/L.
[b]At 298 K, from Ref. [X][38]
[c]At 303 K, estimated from Ref. [Y][39] using $u = \Lambda/zF$.

As expected, polymer concentration also had a large effect on the conductivity of the polyelectrolytes, as shown in Figure 5.2 for PDMAEMA, PDMAEMA·HCl, PDMAEMA·HBF_4, and PDMAEMA·HOTf. These conductivity measurements were performed with a cosolvent of 80/20 (wt/wt) H_2O/methanol, the same solvent used for subsequent electrospinning. PDMAEMA conductivities ranged from 35 – 175 μS/cm at the selected concentrations, and the data fit a power law relationship with an exponent of 0.84. The polyelectrolytes had conductivities two orders of magnitude greater than the neutral polyelectrolyte. The conductivities increased with each counteranion in the same order observed previously in Table 5.3. Again, the conductivity of each polyelectrolyte fit a power-law relationship, as observed in previous reports for polyelectrolyte solutions in the semi-dilute regimes.[40,41]

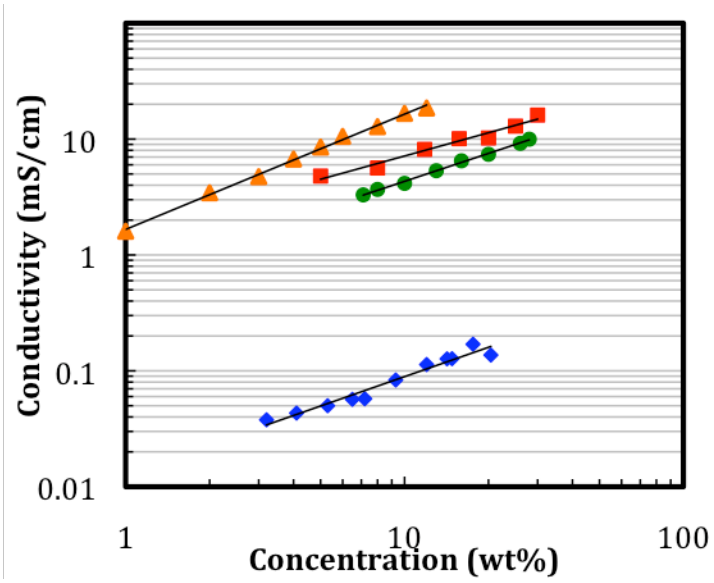

Figure 5.2. Solution conductivity versus polyelectrolyte concentration for PDMAEMA (diamonds), PDMAEMA·HCl (184 kDa) (triangles), PDMAEMA·HBF_4 (squares), and PDMAEMA·HOTf (circles) in 80/20 H_2O/methanol. The solid lines are power-law fits to the data.

5.4.4 Solution Rheology

Steady-shear rheological experiments were performed on the polyelectrolyte solutions over the semi-dilute unentangled and entangled regimes. Figure 5.3 shows the specific viscosity versus concentration for PDMAEMA and the Cl^-, BF_4^-, and TfO^- polyelectrolytes. As expected, viscosity scaling relationships indicated that PDMAEMA behaved as a neutral polymer in water, with scaling factors of 1.2 and 4.4 in the semi-dilute unentangled and entangled regimes, respectively. The critical concentration for entanglements occurred near 10 wt% based on the transition between these two regimes. The polyelectrolytes exhibited weaker viscosity scaling relationships; the scaling factors above and below entanglement and the estimated c_e values are tabulated in Table 5.4. The large differences in entanglement concentration resulted from the differences in polyelectrolyte molecular weight. However, the viscosity scaling relationships confirmed that PDMAEMA·HCl, PDMAEMA·HBF_4, and PDMAEMA·HOTf all behaved as strong polyelectrolytes in solution.

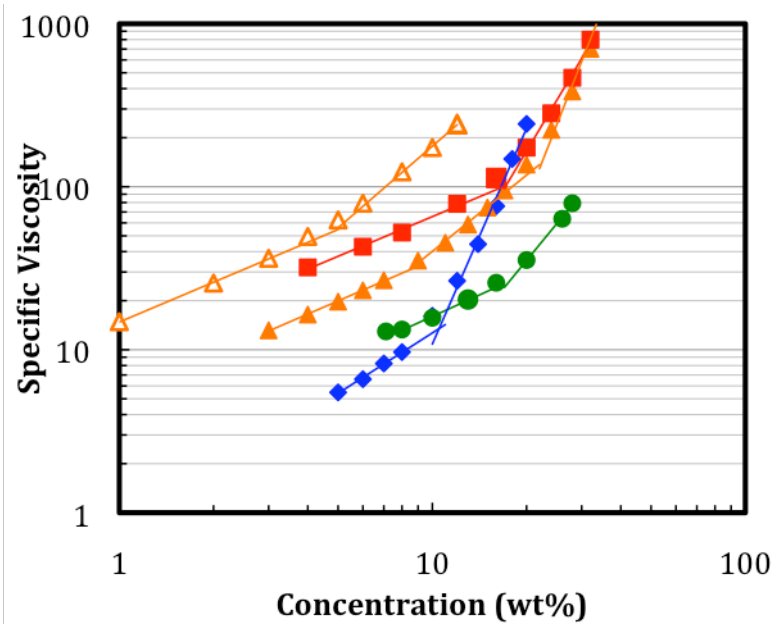

Figure 5.3. Concentration dependence of specific viscosity for PDMAEMA-based polyelectrolytes in 80/20 H_2O/methanol: PDMAEMA (diamonds), PDMAEMA·HCl (96 kDa) (filled triangles), PDMAEMA·HCl (184 kDa) (open triangles), PDMAEMA·HBF_4 (squares), and PDMAEMA·HOTf (circles). The break in the power-law lines represents the c_e of each polymer.

Table 5.4. Rheological Scaling Relationships for PDMAEMA Polymers

Anion	c_e (wt%)	Scaling Factor	
		$c^* < c < c_e$	$c_e < c < c_D$
Neutral	10	1.2	4.4
Cl^- (96 kDa)	9	0.8	1.7
Cl^- (184 kDa)	5	0.8	1.7
BF_4^-	11	0.7	1.5
TfO^-	17	0.8	2.3

5.4.5 Electrospinning

Neutral PDMAEMA and the Cl^-, BF_4^-, and TfO^- polyelectrolytes were electrospun from solutions in the semi-dilute unentangled and semi-dilute entangled regimes to investigate the effect of polyelectrolyte structure on both the onset of fiber formation and fiber diameter relationships. All polymers were electrospun at constant conditions (25 kV, 3 mL/h, 20 cm working distance) from an 80/20 (wt/wt) H_2O/methanol solvent mixture to ensure changes in

electrospinning behavior resulted from solution behavior and not processing parameters. Figure 5.4 shows FESEM images of electrospun PDMAEMA fibers. The neutral polymer fibers formed a uniform mat on the target at concentrations above c_e. Beaded fiber formation first occurred at a concentration of 12.5 wt% (~1.2c_e) and uniform fibers formed at 15 wt% and above (>1.5c_e). The onset of fiber formation agreed with our previous results for neutral polymers (beaded fiber formation above c_e and at a viscosity of approximately 10 cP).[18] However, uniform fibers formed at lower concentrations than expected (1.5c_e instead of 2c_e). This discrepancy in uniform fiber formation was presumed to result from the low T_g of PDMAEMA, resulting in fiber stretching even after solvent evaporation.

Figure 5.5 shows the FESEM micrographs of electrospun polyelectrolyte nanofibers. The polyelectrolyte fibers also collected as a uniform mat. Both high and low molecular weight PDMAEMA·HCl exhibited an onset of fiber formation just above 3c_e and viscosities just above 300 cP. This higher onset of fiber formation was similar to the previous reports on electrospun cationic PDMAEMA·HCl[30] and chitosan,[32,33] where significantly higher entanglements and viscosities were required to stabilize the electrospinning jet compared to neutral polymers.

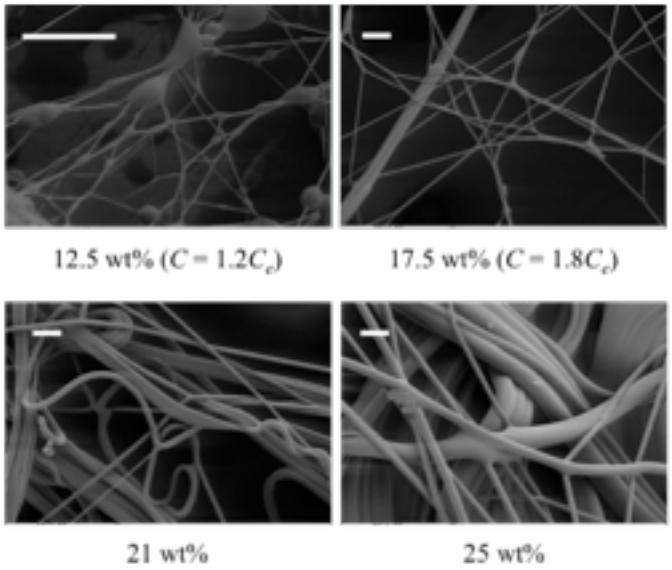

Figure 5.4. FESEM micrographs depicting electrospun PDMAEMA fibers. The scale bars represent 20 μm.

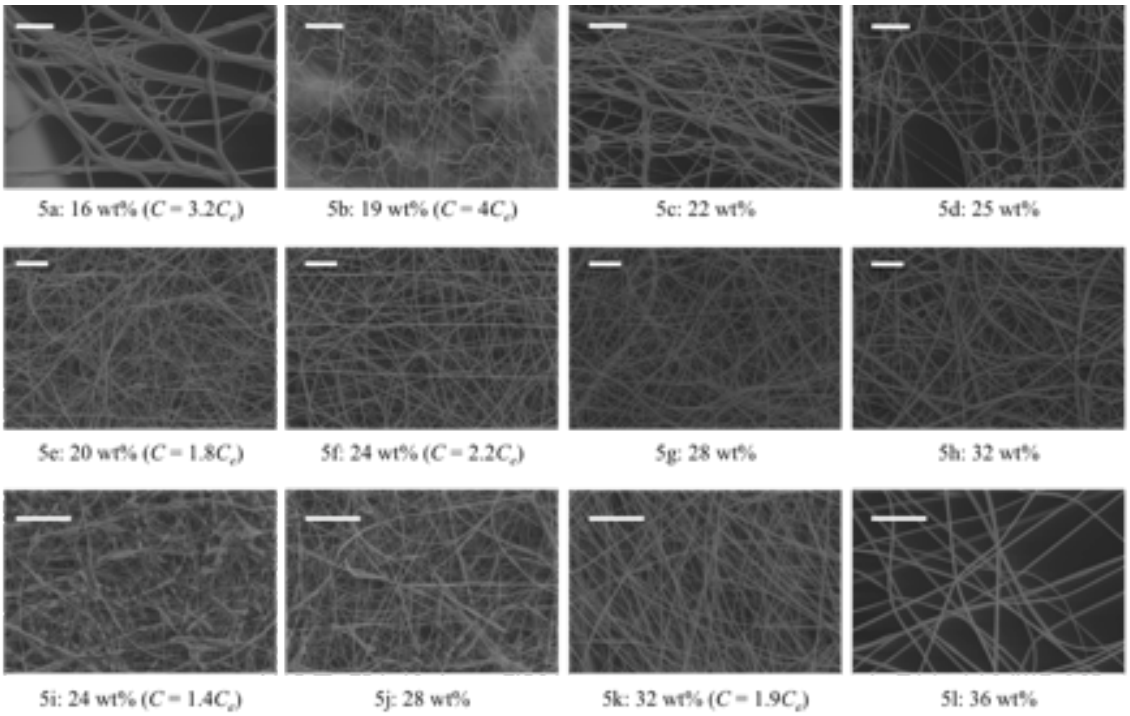

Figure 5.5. FESEM micrographs depicting electrospun PDMAEMA-based polyelectrolyte fibers: (a) - (d) PDMAEMA·HCl, (e) – (h) PDMAEMA·HBF_4, (i) – (l) PDMAEMA·HOTf. The scale bars represent 10 μm.

Table 5.5 lists the normalized concentrations (c/c_e) and zero-shear viscosities at the onset of electrospinning for PDMAEMA and the electrospun polyelectrolytes. The entanglement number required for fiber formation decreased with anion as $Cl^- > BF_4^- > TfO^-$. The BF_4^- and TfO^- polyelectrolytes also required only 30 cP solution viscosity to form fibers, one order of magnitude lower than PDMAEMA·HCl. Previously, the breakup of the electrospinning jet for polyelectrolytes was attributed to the inter- and intramolecular repulsions of the highly-charged polymer chain.[30] The results from this study, as well as those of Chen and Elabd,[11] indicated that polycations with large, hydrophobic anions exhibit electrospinning behavior similar to neutral polymers doped with salt.

Table 5.5. Onset of Fiber Formation versus Polymer Counteranion and Molecular Weight.

Anion	Onset of Fiber Formation	
	c/c_e	η_0 (cP)
Neutral	1.2	13
[Cl^-] (96 kDa)	3.1	330
[Cl^-] (184 kDa)	3.2	320
[BF_4^-]	1.8	30
[TfO^-]	1.2	30

Figure 5.6 compares fiber diameter versus normalized concentration relationship of the electrospun polyelectrolytes with our previously developed semi-empirical relationship.[18] PDMAEMA exhibited typical electrospinning behavior of a neutral polymer, however fiber diameters deviated from the non-associating correlation due to intermolecular associations. The amino group in the PDMAEMA repeat unit exhibited associative interactions, leading to slightly higher fiber diameter scaling relationships. Solution rheology probes these intermolecular associations, and Figure 5.7 shows the fiber diameter versus zero-shear viscosity. The analysis

based on solution flow behavior indicated that PDMAEMA exhibited neutral polymer behavior during electrospinning.

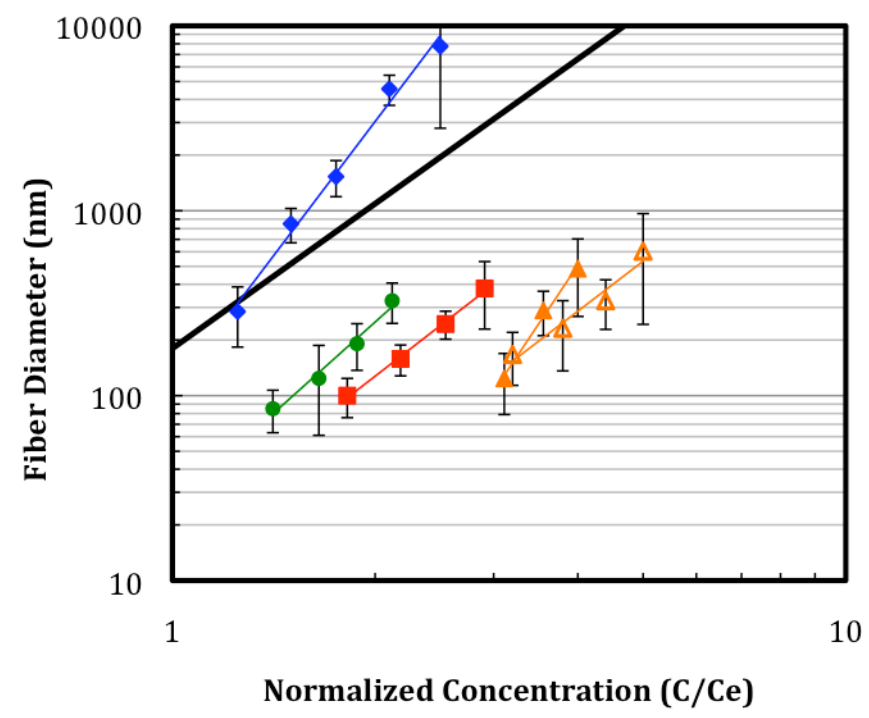

Figure 5.6. Fiber diameters versus normalized concentration for electrospun PDMAEMA and polyelectrolytes. (PDMAEMA (diamonds), PDMAEMA·HCl (96 kDa) (filled triangles), PDMAEMA·HCl (184 kDa) (open triangles), PDMAEMA·HBF_4 (squares), and PDMAEMA·HOTf (circles)) The solid line represents a semi-empirical correlation for neutral, non-associating polymers.[18]

The polyelectrolyte fibers had significantly reduced fiber diameters compared to the neutral polymer fibers (Figure 5.6). Increased solution conductivity led to increased electrostatic repulsions and stretching of the electrospinning jet, resulting in thinner fibers. Regardless of anion, all polyelectrolytes formed fibers with similar diameters (80-400 nm). Although the counteranion had insignificant effect on the fiber diameters, the more hydrophobic BF_4^- and TfO^- anions decreased the minimum number of entanglements required for stable electrospinning. This also correlated with a reduction in the required zero-shear viscosity at the onset of fiber formation (Figure 5.7). The decrease in onset of electrospinning correlates with decreasing polarizability of the counteranion.[42] Lungwitz et al. studied to effect of anion on the Kamlet-Taft

parameters of 1-butyl-3-methylimidazolium ionic liquids and found that polarizability (π^*) of the ionic liquids decreased from 1.13 for Cl^- to 0.96 for BF_4^- to 0.90 for TfO^-. Higher values of π^* also correlate with increased ion pairing. Under the large electric potential during electrospinning, the large polarizability of the Cl^- anion may lead to the instabilities inhibiting electrospinning. However, more experiments are needed to confirm this relationship.

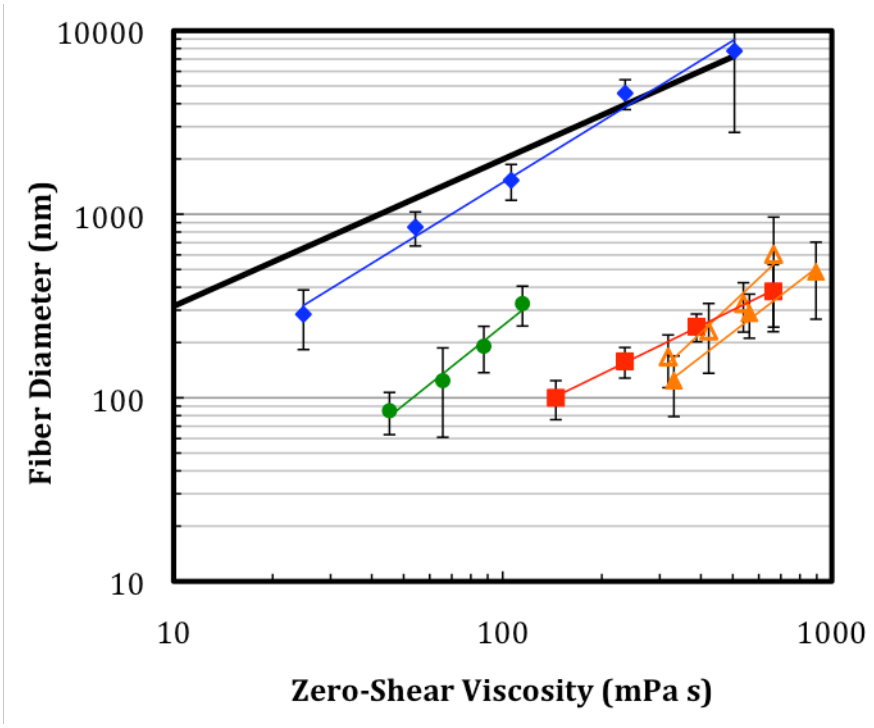

Figure 5.7. Fiber diameters versus zero shear viscosity for PDMAEMA and polyelectrolytes. (PDMAEMA (diamonds), PDMAEMA·HCl (96 kDa) (filled triangles), PDMAEMA·HCl (184 kDa) (open triangles), PDMAEMA·HBF_4 (squares), and PDMAEMA·HOTf (circles)) The solid line represents a semi-empirical correlation for neutral, non-associating polymers.[18]

5.5 Conclusions

The thermal, solution, and electrospinning properties of a series of polyelectrolytes with varying anions were investigated. Ion exchange from a halide counteranion to larger, ionic-liquid type anions led to significant reductions in glass transition temperature due to weaker ionic interactions. Three polyelectrolytes were investigated in the solution state: PDMAEMA·HCl,

PDMAEMA·HBF_4, and PDMAEMA·HOTf. Slight differences in solution conductivity were attributed to differences in counterion mobility and the rheological behavior of all three polymers indicated polyelectrolyte behavior. For the first time, the electrospinning behavior of polyelectrolytes was correlated with polymer chemical structure. The electrospinning behavior showed significant dependence on counteranion. PDMAEMA·HCl required large entanglement numbers (>3c_e) to form fibers, while PDMAEMA·HBF_4 and PDMAEMA·HOTf formed beaded fibers at much lower solution entanglement numbers (~1-1.5c_e), similar to neutral polymer behavior. All three polyelectrolytes formed fibers much thinner than predicted for neutral polymers due to the increased ionic conductivity of the electrospinning solutions. The larger, delocalized counteranions enabled fiber formation at lower solution viscosities and solution entanglement numbers, suggesting electrospinning of polyelectrolytes which had previously been difficult to electrospin. This observation allows us to expand the classes of polymers capable of electrospinning to generate high surface area membranes applicable for electromechanical devices.

5.6 Acknowledgements

This material is based upon work supported by the U.S. Army Research Laboratory and the U.S. Army Research Office under contract/grant number W911NF-07-1-0452 Ionic Liquids in Electro-Active Devices Multidisciplinary University Research Initiative (ILEAD MURI).

5.7 References

1. Green, M. D.; Long, T. E. *Polym. Rev.* **2009,** *49*, 291 - 314.
2. Chen, H.; Choi, J.-H.; Salas-de la Cruz, D.; Winey, K. I.; Elabd, Y. A. *Macromolecules* **2009,** *42*, 4809-4816.
3. Matsumi, N.; Sugai, K.; Miyake, M.; Ohno, H. *Macromolecules* **2006,** *39*, 6924-6927.
4. Yoshizawa, M.; Ohno, H. *Electrochim. Acta* **2001,** *46*, 1723-1728.
5. Duncan, A. J.; et al. *Smart Mater. Struct.* **2009,** *18*, 104005.
6. Duncan, A. J.; Layman, J. M.; Cashion, M. P.; Leo, D. J.; Long, T. E. *Polym. Int.* **2010,** *59*, 25-35.

7. Taranekar, P.; Qiao, Q.; Jiang, H.; Ghiviriga, I.; Schanze, K. S.; Reynolds, J. R. *J. Am. Chem. Soc.* **2007,** *129*, 8958-8959.
8. Jain, V.; Khiterer, M.; Montazami, R.; Yochum, H. M.; Shea, K. J.; Heflin, J. R. *Appl. Mater. Interface* **2009,** *1*, 83-89.
9. Marcilla, R.; Blazquez, J. A.; Fernandez, R.; Grande, H.; Pomposo, J. A.; Mecerreyes, D. *Macromol. Chem. Phys.* **2005,** *206*, 299-304.
10. Marcilla, R.; Blazquez, J. A.; Rodriquez, J.; Pomposo, J. A.; Mecerreyes, D. *J. Polym. Sci., Part A: Polym. Chem.* **2004,** *42*, 208-212.
11. Chen, H.; Elabd, Y. A. *Macromolecules* **2009,** *42*, 3368-3373.
12. Dobrynin, A. V.; Rubinstein, M. *Prog. Polym. Sci.* **2005,** *30*, 1049-1118.
13. Colby, R. H. *Rheol. Acta* **2010,** *49*, 425-442.
14. Greiner, A.; Wendorff, J. H. *Angew. Chem., Int. Ed. Engl.* **2007,** *46*, 5670-5703.
15. Reneker, D. H.; Yarin, A. L. *Polymer* **2008,** *49*, 2387-2425.
16. Thavasi, V.; Singh, G.; Ramakrishna, S. *Energy Environ. Sci.* **2008,** *1*, 205-221.
17. Shenoy, S. L.; Bates, W. D.; Frisch, H. L.; Wnek, G. E. *Polymer* **2005,** *46*, 3372-3384.
18. McKee, M. G.; Wilkes, G. L.; Colby, R. H.; Long, T. E. *Macromolecules* **2004,** *37*, 1760-1767.
19. Gupta, P.; Elkins, C.; Long, T. E.; Wilkes, G. L. *Polymer* **2005,** *46*, 4799-4810.
20. Hunley, M. T.; Harber, A.; Orlicki, J. A.; Rawlett, A. M.; Long, T. E. *Langmuir* **2008,** *24*, 654-657.
21. Wang, S.-Q.; He, J.-H.; Xu, L. *Polym. Int.* **2008,** *57*, 1079-1082.
22. Lin, T.; et al. *Nanotechnology* **2004,** *15*, 1375.
23. Arayanarakul, K.; Choktaweesap, N.; Aht-ong, D.; Meechaisue, C.; Supaphol, P. *Macromol. Mater. Eng.* **2006,** *291*, 581-591.
24. Jacobs, V.; Anandjiwala, R. D.; Maaza, M. *J. Appl. Polym. Sci.* **2010,** *115*, 3130-3136.
25. Li, L.; Hsieh, Y.-L. *Polymer* **2005,** *46*, 5133-5139.
26. Chunder, A.; Sarkar, S.; Yu, Y.; Zhai, L. *Colloids Surf., B* **2007,** *58*, 172-179.
27. Park, W. H.; Jeong, L.; Yoo, D. I.; Hudson, S. *Polymer* **2004,** *45*, 7151-7157.
28. Laforgue, A.; Robitaille, L.; Mokrini, A.; Ajji, A. *Macromol. Mater. Eng.* **2007,** *292*, 1229-1236.
29. Nah, C.; Kwak, S. K.; Kim, N.; Lyu, M.-Y.; Hwang, B. S.; Akle, B.; Leo, D. J. *Key Eng. Mater.* **2007,** *334-335*, 1001.
30. McKee, M. G.; Hunley, M. T.; Layman, J. M.; Long, T. E. *Macromolecules* **2006,** *39*, 575-583.
31. McCann, J. T.; Lim, B.; Ostermann, R.; Rycenga, M.; Marquez, M.; Xia, Y. *Nano Lett.* **2007,** *7*, 2470-2474.
32. Ohkawa, K.; Cha, D.; Kim, H.; Nishida, A.; Yamamoto, H. *Macromol. Rapid Commun.* **2004,** *25*, 1600-1605.
33. Ohkawa, K.; Minato, K.-I.; Kumagai, G.; Hayashi, S.; Yamamoto, H. *Biomacromolecules* **2006,** *7*, 3291-3294.
34. Layman, J. M.; Ramirez, S. M.; Green, M. D.; Long, T. E. *Biomacromolecules* **2009,** *10*, 1244-1252.
35. Lin, S.-T.; Ding, M.-F.; Chang, C.-W.; Lue, S.-S. *Tetrahedron* **2004,** *60*, 9441-9446.
36. Lungwitz, R.; Friedrich, M.; Linert, W.; Spange, S. *New J. Chem.* **2008,** *32*, 1493-1499.
37. March, J., *Advanced Organic Chemistry: Reactions, Mechanims, and Structure*. 3rd ed.; Wiley: New York, 1985.

38. Atkins, P.; de Paula, J., *Physical Chemistry*. 7 ed.; W. H. Freeman: New York, 2001.
39. Wong, C.-L.; Soriano, A. N.; Li, M.-H. *Fluid Phase Equilibr.* **2008,** *271*, 43-52.
40. Bordi, F.; Colby, R. H.; Cametti, C.; De Lorenzo, L.; Gili, T. *J. Phys. Chem., B* **2002,** *106*, 6887-6893.
41. Truzzolillo, D.; Bordi, F.; Cametti, C.; Sennato, S. *Phys. Rev. E* **2009,** *79*, 011804-1 - 011804-3.
42. Lungwitz, R.; Strehmel, V.; Spange, S. *New J. Chem.* **2010**.

Chapter 6: Effect of Di(ethylene glycol) Methacrylate Comonomer on Rheological Behavior and Conductivity of Poly(dimethylaminoethyl methacrylate)-based Polyelectrolytes

6.1 Abstract

Copolymers of (*N*,*N*-dimethylamino)ethyl methacrylate (DMAEMA) and di(ethylene glycol) methyl ether methacrylate (MEO_2MA) were prepared with DMAEMA mole fractions from 0 to 100 mol%. Differential scanning calorimetry revealed one glass transition temperature, confirming the absence of micro-phase separation in the random copolymers. After neutralization with hydrochloric acid or tetrafluoroboric acid, the copolymers also exhibited a single glass transition temperature. The T_g's of the ionomers were higher than predicated using the Fox equation, suggesting restricted polymer mobility due to intramolecular interactions between repeating units. Solution rheological analysis of poly(DMAEMA·HCl-*co*-MEO_2MA) copolymers revealed that low levels of ionic content led to polyelectrolyte behavior and extended conformations in solution. Solution conductivity analysis determined the fraction of free ions in solution. At low ionic contents, almost all ion pairs were dissociated; however, at higher ionic contents, a significant portion of ions did not dissociate in solution. The homopolymer PDMAEMA·HCl exhibited approximately 57% free ions in solution.

6.2 Introduction

Electroactive devices such as electromechanical actuators and fuel cells require highly conductive polymer-electrolyte membranes (PEMs) for effective performance.[1] The PEMs rely on rapid ion movement for fast response or actuation times. Nafion® has emerged as the benchmark ionomer for PEM applications due to its high modulus and high ionic conductivity.[1,2] Current morphological models cite the presence of interconnected ionic clusters as a network for

fast ion conduction.[2,3] Novel ionomers often underperform Nafion® in terms of ionic conductivity due to the lack of an interconnected conduction pathway. Many polyelectrolytes also exhibit high glass transition temperatures, which severely restrict ion mobility. Various methods have emerged to overcome the low conductivities, including swelling the polymer with a conductive diluent (such as ionic liquid);[4,5] utilizing 'ionic liquid-type' counterions (such as the imidazolium cation or bis(trifluoromethanesulfonyl)imide anion) to reduce ionic coordination;[6] and adding flexble spacers between the polymer backbone and charged unit to increase ionic mobility.[7]

Poly(di(ethylene glycol) methyl ether methacrylate) ($PMEO_2MA$) exhibits a cloud point in water at 26 °C, and many reports detail the thermoresponsive behavior of $PMEO_2MA$ homopolymers as well as random and block copolymers.[8-11] $PMEO_2MA$ also exhibited a very low glass transition temperature at -40 °C[8] and demonstrated no micro-phase separation when polymerized with charge-containing monomers.[12] Selvaraj et al.[13] studied the ionic conductivity of $PMEO_2MA$ after addition of $LiClO_4$. The polymer-salt complexes showed good ionic conductivity at ambient temperatures, indicating that the di(ethylene glycol) unit successfully complexed ionic salts to promote conduction. In contrast, Liu et al.[10] investigated the ionic conductivities of similar homopolymers with hexadecyl groups replacing the methyl ether. These polymers were semi-crystalline and showed modest conductivities without a major reduction in crystallinity upon doping with $LiClO_4$. However, limited further work on the conductivity and solution behavior of homopolymers or copolymers of MEO_2MA exists in the literature.

In this manuscript, we report the copolymerization of 2-(N,N-dimethylamino)ethyl methacrylate (DMAEMA) with MEO_2MA to form a series of copolymers ranging from 0 to

100% DMAEMA. Neutralization of the amine group afforded ionomers with the counteranions Cl^-, BF_4^-, and Tf_2N^-. The thermal, solution rheological, and conductivity behavior of these ionomers and polyelectrolytes were studied to determine the influence of miscible, low-T_g comonomer on the polymer behavior.

6.3 Experimental Section

6.3.1 Materials

2-(*N*,*N*-dimethylamino)ethyl methacrylate (DMAEMA) (97%) and di(ethylene glycol) methyl ether methacrylate (MEO_2MA) (95%) were purchased from Sigma-Aldrich and passed over basic alumina to remove inhibitors before use. Azobisisobutyronitrile (AIBN) was purchased from Sigma-Aldrich and recrystallized from methanol. Hydrochloric acid, tetrafluoroboric acid, and lithium bis(trifluoromethanesulfonyl)imide were purchased from Sigma-Aldrich and used as received. Solvents tetrahydrofuran (THF), hexanes, and deionized water were obtained from commercial sources and used as received.

6.3.2 Polymerization and Polymer Neutralization

In a typical copolymerization, 15.0 mL DMAEMA (89.0 mmol) and 16.4 mL MEO_2MA (89.0 mmol) were added to a 250-mL round-bottomed flask containing 135 mL THF (120 g, 20 wt% monomer in THF), and equipped with a magnetic stir bar and reflux condenser. The reaction mixture was purged with nitrogen to remove oxygen. After 15 min, 146 mg AIBN (0.89 mmol, 0.5 mol% compared to monomer) was added and the reaction flask was placed in an oil bath at 65 °C. After 24 h, the reaction was removed from the oil bath and precipitated into 4 L of hexanes. The solvent was decanted and the precipitated polymer was dissolved in 100 mL of deionized water and freeze-dried for two days to remove all solvent. The monomer ratio was varied to synthesize a series of copolymers ranging from 100 mol% DMAEMA to 100 mol%

MEO_2MA. Typical isolated yield: 60%. The copolymer composition was verified by ^1H NMR. ^1H NMR (400 MHz, $CDCl_3$, δ, for 50/50 copolymer): 4.0-4.2 (br, 4H), 3.6-3.8 (d, 2H), 3.5-3.6 (d, 4H), 3.3 (s, 3H), 2.6 (br, 2H), 2.3 (s, 6H), 1.6-2.0 (br, 4H), 0.6-1.1 (br, 6H).

To form the polyelectrolytes, the dried polymers were dissolved at 10 wt% in deionized water. Each polymer was titrated to pH 5 using either hydrochloric acid or tetrafluoroboric acid. The polymers were then freeze-dried to remove all solvent.

6.3.3 Instrumentation

^1H NMR spectroscopy was performed on a Varian INOVA NMR operating at 400 MHz and 23 °C. Samples for NMR were dissolved in $CDCl_3$, D_2O, or DMSO-d_6, depending on polymer solubility, for one day prior to analysis. Thermogravimetric analyses (TGA) were conducted using a TA Instruments Q500 under a nitrogen atmosphere at a heating rate of 10 °C/min. Differential scanning calorimetry (DSC) was performed on a TA Instruments Q2000 under a nitrogen purge at 10 °C/min. The glass transition temperature was determined using the second heat scan. Solution conductivities were measured using a two-electrode Oakton tester (Acorn series, model CON6) calibrated with 1413 μS and 2764 μS standard solutions obtained from VWR. The average of three measurements is reported with the standard deviation. Solution rheology was conducted on a TA Instruments AR-G2 rheometer equipped with concentric cylinder geometry at 25.0±0.1 °C. Samples were thermally equilibrated for 2 min prior to shearing. Steady state shear measurements were taken from 0.1 to 1000 s^{-1}. The specific viscosity, η_{sp}, was calculated as $\eta_{sp} = (\eta_0 - \eta_s)/\eta_s$, where η_0 is the zero-shear viscosity of each solution and η_s is the viscosity of the solvent.

6.4 Results and Discussion

6.4.1 Copolymerization and Polymer Characterization

Random copolymerizations of MEO_2MA and DMAEMA were performed in THF using 0.5 mol% AIBN as an initiator, as shown in Scheme 6.1. ^1H NMR monitored the composition of the copolymers. Immediately prior to starting the reaction, an aliquot of the reaction mixture was collected to accurately determine the monomer feed ratio using NMR; after 2 h of polymerization, a second aliquot was removed to determine copolymer composition. The short polymerization of 2 h ensured that the copolymer composition reflected the monomer reactivities. After 24 h, the remainder of the polymerization solution was precipitated and isolated. The signals from protons on the terminal methyl group of MEO_2MA (at 3.4 ppm) and the *N*-methyl groups of DMAEMA (at 2.25 ppm) were well-resolved in both the monomer and polymer spectra, and these proton signals allowed comparison of monomer ratios in all samples. The copolymer compositions after 2 h of polymerization closely matched the compositions after 24 h of polymerization, suggesting the polymer composition remained the same throughout the polymerization. Table 6.1 compares the monomer feed ratios and copolymer compositions of the copolymer series. Copolymer compositions agreed very well with monomer feed ratios. Since both monomers have the methacrylate group, good copolymerization was expected.

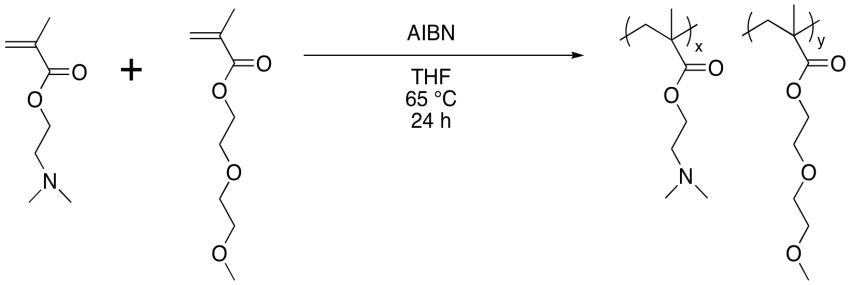

Scheme 6.1. Copolymerization of DMAEMA and MEO_2MA using conventional free radical copolymerization conditions.

Table 6.1. Copolymer Compositions and Thermal Analysis of P(DMAEMA-*co*-MEO_2MA) Copolymers

[DMAEMA]:[MEO_2MA] in feed[a]	[DMAEMA]:[MEO_2MA] in copolymer[b]	T_g (°C)[d]	$T_{d,5\%}$ (°C)[d]
100:0	100:0	19	295
83:17	83:17	10	280
72:28	72:28	0	280
51:49	51:49	-2	275
34:66	34:66	-18	275
17:83	13:87	-34	270
0:100	0:100	-37	270

[a]Determined by ^{1}H NMR.
[b]Determined by ^{1}H NMR after 2 h of polymerization.
[c]Determined by DSC, 10 °C/min, 2nd heating scan.
[d]Determined by TGA, 10 °C/min.

Table 6.1 also lists the glass transition temperatures and onset of thermal degradation of the copolymers. The onset of thermal degradation represents the temperature at which 5% weight loss occurred, measured by TGA under N_2. As the ratio of MEO_2MA in the copolymers increased, the degradation temperatures slightly decreased from 295 °C for PDMAEMA homopolymer to 270 °C for $PMEO_2MA$ homopolymer. However, this decrease falls within the experimental error of the instrument. The glass transition temperature also decreased systematically from 19 °C for PDMAEMA homopolymer to -37 °C for $PMEO_2MA$ homopolymer. The presence of only one glass transition, as well as the linear relationship between copolymer composition and T_g, suggested the copolymers do not micro-phase separate. The increased size and mobility of the di(ethylene glycol) side chains lead to the very low T_g's of the copolymers.

6.4.2 Neutralization and Polyelectrolyte Characterization

Scheme 6.2 illustrates the neutralization of the poly(DMAEMA-*co*-MEO_2MA) copolymers with HCl to form the poly(DMAEMA·HCl-*co*-MEO_2MA) ionomers and polyelectrolytes. Similar neutralizations yielded charged copolymers with BF_4^- counteranion.

XPS analysis confirmed complete titration. The ionomers and polyelectrolytes were prepared at all copolymer compositions. Previous work in our laboratories and others has demonstrated that the counteranion controls the solubility and thermal properties of DMAEMA-based polyelectrolytes.[14-16] Copolymer polyelectrolytes with Cl^- and BF_4^- anions remained water-soluble after protonation, however the charged copolymers no longer dissolved in acetone or chloroform when the ionic content was greater than 30 mol%. Figure 6.1 shows the glass transition temperatures as a function of DMAEMA monomer content for both the neutral and charged copolymers. The glass transition temperatures of each copolymer series increased systematically as DMAEMA content increased.

The Fox equation predicts the glass transition of random copolymers as a function of the glass transitions of the respective homopolymers ($T_{g,A}$ and $T_{g,B}$) and the weight fractions of each monomer unit (w_A and w_B):

$$\frac{1}{T_g} = \frac{w_A}{T_{g,A}} + \frac{w_B}{T_{g,B}}.$$

By convention, the monomers A and B are defined such that $T_{g,A} < T_{g,B}$. The Fox equation assumes no significant interactions between monomer units. This model agreed well with experimental data for the neutral copolymers. However, the Fox equation did not fit the experimentally observed linear relationship between T_g and copolymer composition for the charged copolymers with either Cl^- or BF_4^- anions, indicating strong interactions between monomer units.

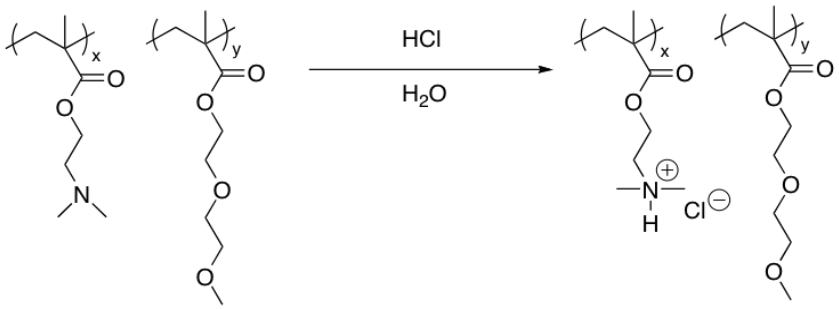

Scheme 6.2. Neutralization of poly(DMAEMA-*co*-MEO_2MA) with HCl to form poly(DMAEMA·HCl-*co*-MEO_2MA) copolymer polyelectrolyte.

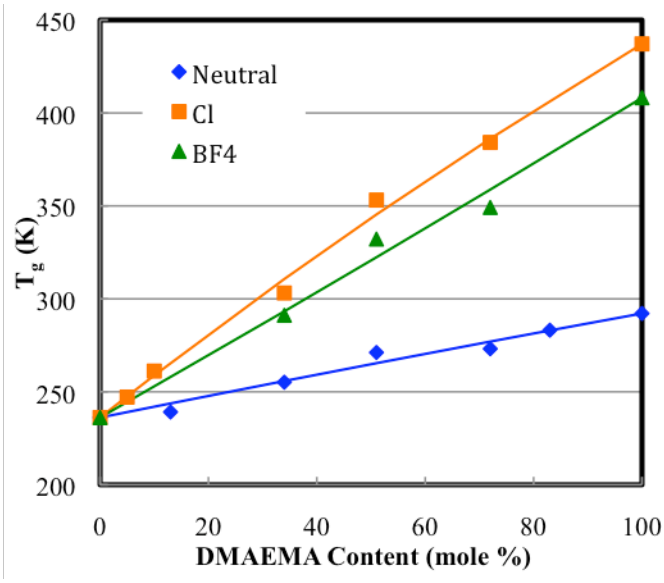

Figure 6.1. Glass transition temperatures as a function of DMAEMA content for the neutral and charged copolymers. The symbols represent experimental data and the solid lines show predictions based on the Gordon-Taylor equation with *K*-values of 0.8 for neutral, 0.9 for [Cl^-], 1.4 for [BF_4^-].

The Gordon-Taylor equation describes the glass transition temperature of a random copolymer as

$$T_g = \frac{T_{g,A} w_A + K T_{g,B} w_B}{w_A + K w_B},$$

where K is a fitting parameter.[17] In the absence of significant interactions between the two monomers, the parameter K can be estimated as $K = (\rho_1/\rho_2)/(\Delta\alpha_2/\Delta\alpha_1)$, where $\Delta\alpha_i = \alpha_{melt} - \alpha_{glass}$. The Fox equation is a special case of the non-interaction limit where the thermal expansivities of each monomer unit are assumed equal and $K \approx T_{g,A}/T_{g,B}$. The Solver feature of Microsoft

Excel fit the Gordon-Taylor equation to the experimental glass transition temperature data, illustrated as solid lines in Figure 6.1. The fittings provided experimental values for the *K*-parameters for each copolymer series. For the neutral copolymers, the calculated *K*-value of 0.80 agreed well with the ratio of glass transition temperatures, $T_{g,A}/T_{g,B} = 0.81$. This agreement with the Fox relationship suggested only minor interactions between monomer units. However, the copolymer polyelectrolytes exhibited estimated *K*-values of 0.89 and 1.4 for the Cl^- and BF_4^- counteranions, respectively (the corresponding T_g ratios for these two copolymers are 0.54 and 0.58, respectively). The large positive deviations indicated strong interactions between repeating units in the charged copolymer. Crown ethers coordinate strongly with cationic species, including alkali metals and ammonium cations, through ion-dipole interactions.[18] In a similar fashion, the MEO_2MA repeating units can interact with the cationic $DMAEMA{\cdot}H^+$ monomer units, severely restricting the copolymer mobility and increasing the glass transition temperature.

6.4.3 Solution Rheology

Rheology provides a highly-sensitive technique to investigate the intermolecular interactions of polyelectrolytes. Theoretical and experimental observations demonstrate that polyelectrolytes exhibit extended conformations in polar solvent due to charge repulsions along the polyelectrolyte backbone.[19,20] This different conformation leads to significant differences in the solution rheology. The overlap concentration, c^*, occurs at lower concentrations compared to uncharged polymers, and the semi-dilute unentangled regime ($c^* < c < c_e$) can extended up to 100 or 1000 times c^*, with higher values expected at higher molecular weights.[21] As a comparison, the critical concentration for entanglements (c_e) for neutral polymers is typically 5 to 10 times c^*. In addition, the viscosity scaling behavior with concentration changes dramatically. Neutral polymers have scaling factors of 1.25 and 3.75 in the semi-dilute

unentangled and semi-dilute entangled regimes, respectively. However, polyelectrolytes have scaling factors of 0.5 and 1.5 above and below c_e, respectively.

The solution rheology of the poly(DMAEMA·HCl-*co*-MEO_2MA) charged copolymer was investigated in DI H_2O. Figure 6.2(a) shows the specific viscosity of the different copolymers versus normalized concentration, c/c^*. The overlap concentration, c^*, was approximated as the concentration where the specific viscosity equals 1. As ionic content in the copolymers increased, the dependence of viscosity on concentration decreased. Colby et al.[22] observed a similar decrease in the specific viscosities of a series of poly(vinyl pyridine)-based ionomers with varying levels of methylation. In addition, the breadth of the semi-dilute unentangled regime ($c^* < c < c_e$) increased significantly for the copolymers as ionic content increased. The semi-dilute unentangled regime and c_e become more apparent in the plot of reduced viscosity ($\eta_{sp}c^*/c$) versus normalized concentration in Figure 6.2(b). The reduced viscosity decreased with concentration in the semi-dilute unentangled regime, but increased with concentration above c_e in the semi-dilute entangled concentration regime. These reduced viscosity trends suggested polyelectrolyte behavior in solution.

Table 6.2 summarizes the specific viscosity scaling factors and rheological transitions of the charged copolymers. At high ionic content, the scaling factors agreed well with theoretical predications for polyelectrolytes. However, at very low ionic contents (5 and 10 mol%), the scaling factors were intermediate between polyelectrolyte and neutral polymer behavior. This intermediate behavior at low ionic contents was previously reported.[22] In addition, as ionic content increased, the rheological transitions decreased dramatically, while the ratio of c_e/c^* simultaneously increased. These significant changes in rheological transitions suggested significant changes in molecular weight of the copolymers. The specific viscosity at a constant

concentration of 4 wt% polymer (in the semi-dilute unentangled regime for each polymer) also increased systematically as ionic content increased. This increase suggested that molecular weights were higher for the copolymers with higher DMAEMA content. Protons neighboring an ether oxygen are relatively labile for chain transfer reactions,[23] increasing the rate of chain transfer to monomer for MEO_2MA. The molecular weight changes indicated by solution rheological analysis presumably occurred due to increased chain transfer to monomer. In addition, solution rheology indicated the onset of polyelectrolyte solution behavior occurs at very low ionic contents of approximately 10 mol%.

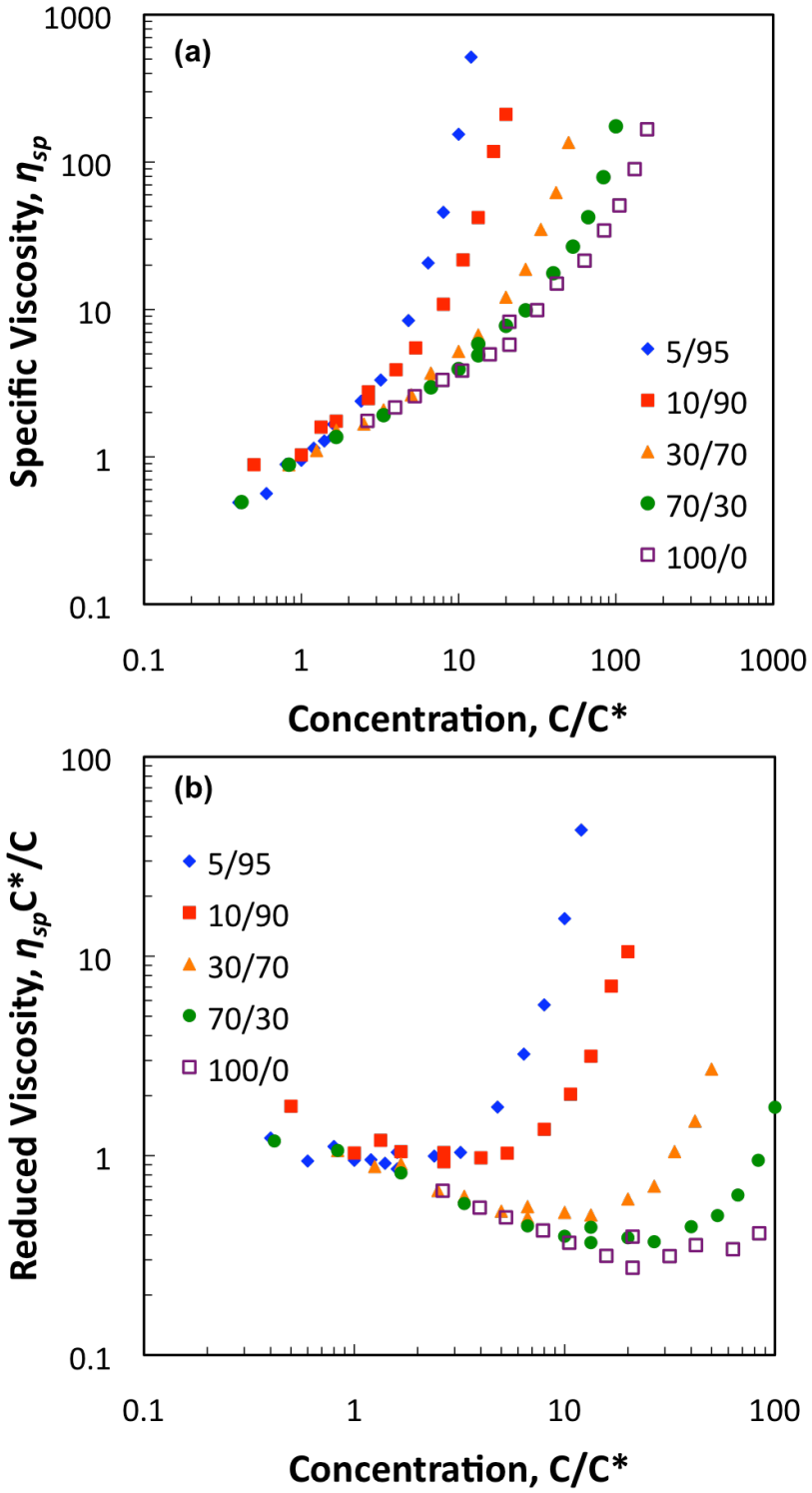

Figure 6.2. (a) Specific viscosities of poly(DMAEMA·HCl-*co*-MEO_2MA) copolymer polyelectrolytes in DI H_2O, plotted versus C/C^*. The overlap concentration, C^*, was estimated as the concentration at a specific viscosity of 1. (b) Reduced viscosities of the same copolymer polyelectrolytes as a function of C/C^*. The legends indicate DMAEMA-HCl/MEO_2MA ratios.

Table 6.2. Viscosity Scaling Factors and Rheological Transitions for P(DMAEMA·HCl-*co*-MEO_2MA) Copolymer Polyelectrolytes

DMAEMA Content (mol%)	Scaling Factor $c^* < c < c_e$	Scaling Factor $c_e < c$	c^* (wt%)	c_e (wt%)	c_e/c^*	η_{sp} at 4 wt%
5	0.8	3.3	2.5	9	4	1.7
10	0.8	3.2	1.5	10	7	2.8
30	0.6	2.3	0.6	8	13	3.7
70	0.6	1.5	0.3	6	20	5.8
100	0.6	1.3	0.2	5	25	8.3

6.4.4 Solution Conductivity

Figure 6.3 shows solution conductivity measured for the charged poly(DMAEMA-HCl-*co*-MEO_2MA) copolymers over the semi-dilute unentangled and semi-dilute entangled concentrations regimes in deionized water. The conductivities of the copolymers all exhibited power law scaling behavior with concentration, as observed in previous reports.[24] The uncharged polymers (not shown) showed almost no change in conductivity with changing copolymer composition. However, increasing the ionic content of the poly(DMAEMA·HCl-*co*-MEO_2MA) copolymers significantly increased the solution conductivity at constant polymer concentration. The charged copolymers also exhibited power law behavior at lower concentrations, but at higher concentrations the dependence weakened, as reported previously for polymer solutions in the semi-dilute entangled regime.[25] In addition, above a 50:50 DMAEMA·HCl:MEO_2MA ratio, the conductivity showed little increase with increasing ionic content.

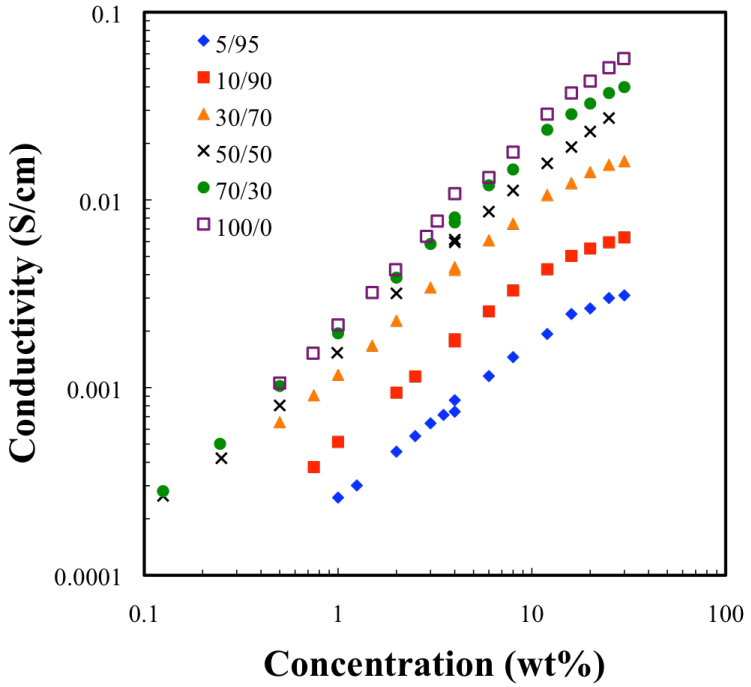

Figure 6.3. Solution conductivities of poly(DMAEMA·HCl-*co*-MEO_2MA) copolymer polyelectrolytes in DI H_2O. The legend indicates the ratio of DMAEMA/MEO_2MA in the copolymers.

Polyelectrolyte counterions do not fully dissociate in solution due to the large coulombic repulsions experienced by the polyelectrolyte backbone.[20,22,25] The molar conductivity, Λ_m, describes the contribution of each repeating unit to the ionic conductivity. Molar conductivity is defined as $\Lambda_m = (\sigma - \sigma_s)/c$, where σ and σ_s are the conductivities of the polymer solution and solvent, respectively, and c is the polymer concentration, usually expressed in terms of moles of monomer units per liter (sometimes expressed with the units monomol/L). Figure 6.4 shows the molar conductivity versus concentration for the poly(DMAEMA·HCl-*co*-MEO_2MA) copolymer series. At low concentrations, the molar conductivities were nearly independent of polymer concentration, but at higher concentrations a strong decrease in molar conductivity was observed. The decrease in molar conductivity in entangled and concentrated solutions corresponds to a significant decrease in electrophoretic

mobility of the counterion due to the high viscosities and decrease in free counterions due to the constricted chain dimensions.[25]

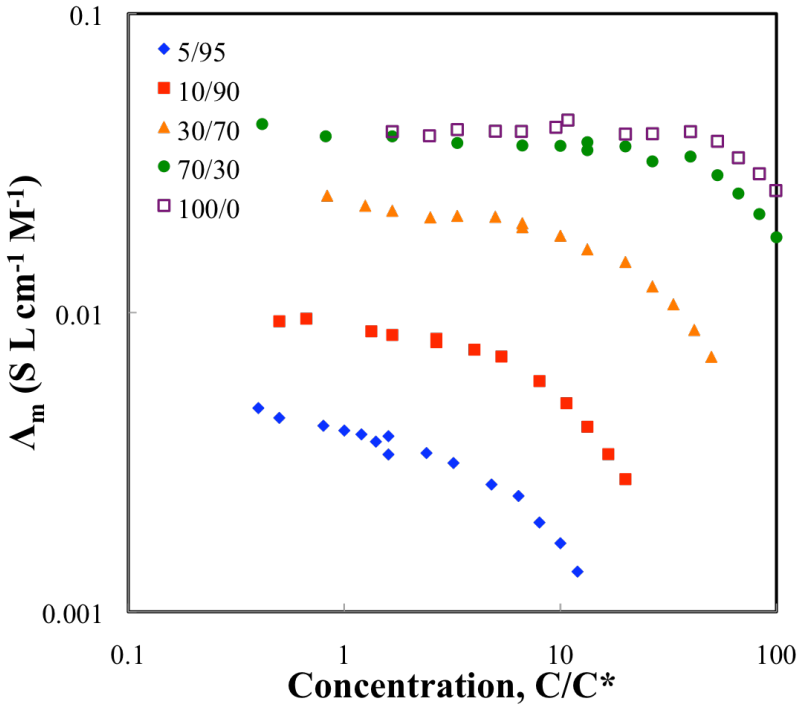

Figure 6.4. Solution molar conductivities of poly(DMAEMA·HCl-*co*-MEO_2MA) copolymer polyelectrolytes in DI H_2O. The legend indicates DMAEMA/MEO_2MA ratio in the copolymers.

Dou and Colby[22] developed a technique to experimentally determine the fraction of free counterions for a series of ionomers in solution. At low ionic content, the counterions were assumed to fully dissociate from the polymer chain. Here, we assume that all counterions of a 5:95 P(DMAEMA·HCl-*co*-MEO_2MA) ionomer dissociate, and therefore the effective charge, f = 0.05 (equal to the mole fraction of charged monomers). The effective charge of the other polymers was determined by fitting curves of Λ/f versus c/c^* to the 5:95 copolymer. Table 6.3 lists the effective charges estimated through this technique. As the ionic content increased in the copolymers, the fraction of condensed counterions also increased due to charge repulsions.

Table 6.3. Effective Charge of P(DMAEMA·HCl-*co*-MEO_2MA) Copolymer Polyelectrolytes

[DMAEMA·HCl]:[MEO_2MA] ratio in polymer	f
5:95	0.05
10:90	0.10
30:70	0.26
50:50	0.39
70:30	0.57
100:0	0.58

6.5 Conclusions

A series of copolymers of DMAEMA and MEO_2MA were prepared and characterized using thermal analysis, solution rheology, and solution conductivity. Both the neutral and charged copolymers with counteranions Cl^- and BF_4^- exhibited a single glass transition temperature, indicating the absence of micro-phase separation within the copolymers. Coordination between the ether oxygen of the MEO_2MA monomer units and the positive ammonium of the charged DMAEMA-HCl monomer units restricted polymer mobility and led to positive deviations of the glass transition temperature from Fox equation predictions. Polyelectrolyte solution dynamics were observed for all ionomers regardless of the ionic content. Conductivity analysis allowed the determination of free ion fractions, and experimental values were significantly lower than the actual ionic content at high DMAEMA-HCl mole fractions. These results indicate that high levels of ionic content are not necessary for high ionic conductivities. The incorporation of low-T_g monomer can significantly improve conductivity by increasing polymer mobility without sacrificing a significant fraction of conducting anions. These miscible ionomers offer tremendous advantages over phase-separated copolymers for electroactive devices.

6.6 Acknowledgements

This material is based upon work supported by the U.S. Army Research Laboratory and the U.S. Army Research Office under contract/grant number W911NF-07-1-0452 Ionic Liquids in Electro-Active Devices Multidisciplinary University Research Initiative (ILEAD MURI).

6.7 References

1. Duncan, A. J.; Leo, D. J.; Long, T. E. *Macromolecules* **2008,** *41*, 7765-7775.
2. Mauritz, K. A.; Moore, R. B. *Chemical Reviews* **2004,** *104*, 4535-4586.
3. Eisenberg, A.; Hird, B.; Moore, R. B. *Macromolecules* **1990,** *23*, 4098-4107.
4. Brown, R. H.; Duncan, A. J.; Choi, J.-H.; Park, J. K.; Wu, T.; Leo, D. J.; Winey, K. I.; Moore, R. B.; Long, T. E. *Macromolecules* **2010,** *43*, 790-796.
5. Duncan, A. J.; et al. *Smart Mater. Struct.* **2009,** *18*, 104005.
6. Chen, H.; Choi, J.-H.; Salas-de la Cruz, D.; Winey, K. I.; Elabd, Y. A. *Macromolecules* **2009,** *42*, 4809-4816.
7. Ohno, H. *Macromolecular Symposia* **2007,** *249-250*, 551-556.
8. Han, S.; Hagiwara, M.; Ishizone, T. *Macromolecules* **2003,** *36*, 8312-8319.
9. Ishizone, T.; Seki, A.; Hagiwara, M.; Han, S. *Macromolecules* **2008,** *41*.
10. Liu, G.; Reinhout, M.; Mainguy, B.; Baker, G. L. *Macromolecules* **2006,** *39*, 4726-4734.
11. Lutz, J.-F.; Hoth, A. *Macromolecules* **2006,** *2006*, 893-896.
12. Munoz-Bonilla, A.; Fernandez-Garcia, M.; Haddleton, D. M. *Soft Matter* **2007,** *3*, 725-731.
13. Selvaraj, I.; Chaklanobis, S.; Chandrasekhar, V. *Journal of Polymer Science, Part A: Polymer Chemistry* **1993,** *31*, 2643-6.
14. Hunley, M. T.; England, J. P.; Long, T. E. **2010**, Submitted.
15. Marcilla, R.; Blazquez, J. A.; Fernandez, R.; Grande, H.; Pomposo, J. A.; Mecerreyes, D. *Macromol. Chem. Phys.* **2005,** *206*, 299-304.
16. Marcilla, R.; Blazquez, J. A.; Rodriquez, J.; Pomposo, J. A.; Mecerreyes, D. *J. Polym. Sci., Part A: Polym. Chem.* **2004,** *42*, 208-212.
17. Penzel, E.; Rieger, J.; Schneider, H. A. *Polymer* **1997,** *38*, 325-337.
18. Buschmann, H.-J.; Mutihac, R.-C.; Schollmeyer, E. *Journal of Solution Chemistry* **2009,** *38*, 209-217.
19. Colby, R. H. *Rheol. Acta* **2010,** *49*, 425-442.
20. Dobrynin, A. V.; Rubinstein, M. *Prog. Polym. Sci.* **2005,** *30*, 1049-1118.
21. Krause, W. E.; Tan, J. S.; Colby, R. H. *J. Polym. Sci., Part B: Polym. Phys.* **1999,** *37*, 3429-3437.
22. Dou, S.; Colby, R. H. *J. Polym. Sci., Part B: Polym. Phys.* **2006,** *44*, 2001-2013.
23. Odian, G., *Principles of Polymerization*. 4th ed.; John Wiley & Sons: Hoboken, New Jersey, 2004.
24. Truzzolillo, D.; Bordi, F.; Cametti, C.; Sennato, S. *Phys. Rev. E* **2009,** *79*, 011804-1 - 011804-3.
25. Bordi, F.; Colby, R. H.; Cametti, C.; De Lorenzo, L.; Gili, T. *J. Phys. Chem., B* **2002,** *106*, 6887-6893.

Chapter 7: Influence of Topology on the Electrospinning Behavior of Cationic Polyelectrolytes

7.1 Abstract

Star-shaped polyelectrolytes based on poly(2-(*N*,*N*-dimethylamino)ethyl methacrylate) were synthesized using five- and eight-armed initiators through atom transfer radical polymerization. The polymerizations were monitored by ^{1}H NMR. SEC analysis confirmed that the star polymers had narrow polydispersities, but the SEC dramatically underestimated the molecular weights of the stars compared to ^{1}H NMR analysis. Thermal analysis revealed that the electrostatic charges and counterion choice controlled thermal transitions, which were nearly independent of the number of arms. However, solution behavior of the polyelectrolytes differed dramatically from the linear polyelectrolytes. The solution conductivities of the star polyelectrolytes were only half those of the linear polyelectrolytes, while rheological scaling factors in the semi-dilute concentration regimes increased slightly for the star polyelectrolytes. The differences in solution behavior resulted from the collapsed conformation of the star polyelectrolytes compared to linear polyelectrolytes, which causes increased counterion condensation along the polymer chain. The solution electrospinning behavior of the star polyelectrolytes also differed significantly from linear polyelectrolytes. Higher solution entanglement numbers and solution viscosities were required to stabilize the electrospinning jet for the star polymers compared to the linear polyelectrolytes.

7.2 Introduction

Polyelectrolytes with nonlinear topologies differ dramatically from their linear analogues in many aspects. Branched and star-shaped polyelectrolytes are constrained to more compact

conformations compared to linear polymers of the same molecular weight. The reduced chain dimensions for the same molecular weight lead to reduced viscosity and more globular conformations in solution. The constrained conformation results in increased gene delivery for branched and star-shaped polyelectrolytes compared to the linear analogues.[1] The non-linear topology allows the polyelectrolytes to strongly compact DNA within the polyplex, leading to improved transfection. Polyelectrolytes with brush- or star-like topologies exhibit different counterion dissociations and conformations in the proximity of the core as compared to the less-spatially-confined arms.

In solution, linear polyelectrolytes adopt an extended conformation.[2] The polymer structure can be described as a linear series of blobs, where the polymer conformation within each blob closely resembles a random walk. The length scale of the electrostatic blobs, ξ_{el}, depends on the ionic strength of the solution and the Kuhn segment length of the polymer, among other factors. Contrary to being fully dissociated, a certain number of counterions condense onto the polymer chain, effecting neutralizing a fraction of the charges.[3,4] The counterion condensation results in less entropy for the ion, but the condensation can become energetically favorable when a decrease in charge density along the polymer chain results in freedom of the polymer chain to adopted a more random conformation in solution.[5] The fraction of free ions, f, for a polyelectrolyte in polar solvents often ranges between 20 to 80%.

The constraint of a central branching point leads to different solution behavior for star-shaped and comb polyelectrolytes compared to linear polyelectrolytes.[5] Due to increased counterion condensation, the osmotic coefficient ϕ (defined as the ratio of measured osmotic pressure to the theoretical value) decreases dramatically compared to linear polyelectrolytes. Müller et al.[6] reported that the osmotic coefficients of poly(acrylic acid) (PAA) stars were

significantly lower than those of linear PAA (all at constant neutralization) throughout the dilute concentration regime, and the osmotic coefficient decreased dramatically as the number of arms in the PAA stars increased. They also reported an increase in the apparent pK_a values of the PAA stars as the number of arms increased with constant arm length. At a constant number of arms and increasing arm length, the apparent pK_a values decreased as the importance of the central core decreased. The pK_a values indicate the level of deprotonation in solution, and higher pK_a indicates more counterion condensation.

Uncharged star polymers in dilute solution are stretched compared to uncharged linear polymers due to crowding around the central branching point.[7] In the semi-dilute regime, the stars consist of stretched cores surrounded by a medium of overlapping or entangled arms. The outer portions of each arm behave similarly to linear polymers in semi-dilute solution. Shusharina and Rubinstein[5] theoretically analyzed the scaling of star polyelectrolyte radii in dilute and semi-dilute solutions. Above the overlap concentration, polyelectrolyte stars decreased in radius without interdigitation until significantly higher concentrations. At much higher concentration in the semi-dilute unentangled and semi-dilute entangled regimes, the arms of the stars behaved as linear polyelectrolytes in semi-dilute solution.

Electrospinning of polymers has recently emerged as a popular processing technique to develop membranes and scaffolds of nanoscale fibers.[8,9] Due to their high specific surface area and high porosity, electrospun scaffolds are ideal for filtration,[10] tissue engineering,[11] ultrafast sensing,[12] and electro-active devices.[13,14] Our research group developed semi-empirical correlations relating the solution rheological behavior to the electrospinning behavior of neutral, non-associating polymers.[15] Above the critical concentration for entanglements, c_e, neutral polymer solutions have enough elasticity to prevent the capillary breakup and form fibers.

Beaded fibers form between c_e and $2c_e$, and uniform fibers form above $2c_e$. When electrospun fiber diameters are plotted versus normalized concentration (c/c_e), the fiber diameters fit a single power law relationship regardless of topology and molecular weight. The correlation was developed for a variety of neutral, non-associating linear and branched polyesters. Other reports have reiterated that sufficient solution elasticity is required to stabilize the electrospinning jet for stable electrospinning.[16,17]

The electrospinning of polyelectrolytes does not follow the same trends as neutral polymer electrospinning. Many reports confirm that strong polyelectrolytes require significantly higher normalized concentrations and viscosities to electrospin compared to neutral polymers.[18-20] Our research group electrospun poly(2-dimethylaminoethyl methacrylate hydrochloride) (PDMAEMA-HCl) from 4:1 water:methanol solvent mixtures and found that normalized concentrations of $8c_e$ and solution viscosities greater than 1000 cP were required before the onset of fiber formation.[18] Similar results were reported for chitosan electrospun from trifluoroacetic acid.[19] The onset of electrospinning was observed above 200 cP regardless of molecular weight, and uniform fiber formation occurred above 800 cP. However, Chen and Elabd[21] electrospun the polyelectrolyte poly(1-[2-methacryloyloxy)ethyl]-3-butylimidazolium tetrafluoroborate) at significantly lower solution concentrations and viscosities, similar to neutral polymers.

To the best of our knowledge, no studies have investigated the effect of macromolecular topology on the electrospinning of polyelectrolytes. Although neutral polymers with highly-branched topologies electrospin at the same normalized concentrations and viscosities, the added counterion condensation of star polyelectrolytes may aid in the electrospinning of these polymers. We synthesized star-shaped PDMAEMA-based polyelectrolytes using 5-arm and 8-

arm star initiators as previously demonstrated.[22] The solution conductivity and rheological behaviors were thoroughly studied, along with the electrospinning behavior.

7.3 Experimental

7.3.1 Materials

2-(N,N-dimethylamino)ethyl methacrylate (DMAEMA) (98%) was purchased from Sigma-Aldrich and passed a silica column to remove inhibitor before use. Ethyl-2-bromo-2-methylpropionate (EBIB) (purum, ≥ 97.0%), 1,1,4,7,10,10-hexamethyltriethylenetetramine (HMTETA) (97%), copper(I) bromide (99.999%), iodomethane (*ReagentPlus*, 99.5%), and anisole (anhydrous, 99.7%) were purchased from Sigma-Aldrich and used as received. The star initiators were synthesized as reported previously.[23] Sodium chloride, de-ionized water, hexanes, methanol, and all other solvents were obtained from commercial sources and used without further purification.

7.3.2 Controlled Polymerization of Star Polymers

Star-shaped PDMAEMA polymers were synthesized using ATRP conditions reported previously.[22] Briefly, DMAEMA (8.0 g, 51 mmol) was added to 50 mL anisole in a sealed flask equipped with a magnetic stir bar. The 5-arm initiator (37.7 mg, 0.0408 mmol, 250:1 M:I ratio) was added to the flask, along with a small amount of trioxane to monitor the reaction by ^{1}H NMR. The solution was degassed for 20 minutes and placed in an oil bath at 60 °C. In a separate flask, CuBr (29.1 mg, 0.202 mmol) and HMTETA (46.8 mg, 0.202 mmol) were mixed with 15 mL anisole. The catalyst/ligand dispersion was degassed for 15 minutes and added to the monomer solution to start the reaction. Aliquots were collected at specific time intervals to monitor the conversion by ^{1}H NMR. After 24 h, the polymer solution was passed over a short column of silica gel to remove the copper, followed by precipitation into 400 mL of hexanes.

The solvent was decanted and the solid polymer dissolved in water and dialyzed against de-ionized water for two days to remove all residual copper and monomer. The purified polymer solution was freeze-dried to collect solid polymer powder (2.75 g isolated, 34%).

7.3.3 Protonation of PDMAEMA Polymers

The star-shaped PDMAEMA was neutralized with either hydrochloric acid or tetrafluoroboric acid to generate polyelectrolytes with the Cl^- and BF_4^- anions, respectively. PDMAEMA was first dissolved at 10 wt% in de-ionized water and subsequently titrated with acid to pH 4. The polyelectrolytes were precipitated in excess acetone and dried *in vacuo* overnight.

7.3.4 Methylation of PDMAEMA Poylmers

Linear and star-shaped PDMAEMA were methylated to form the corresponding quaternary ammonium polyelectrolytes for rheology and electrospinning. PDMAEMA (5.0 g, 32 mmol repeating unit) was dissolved in 45 mL acetone in a 100 mL round bottomed flask equipped with a magnetic stirrer. Methyl iodide (6.8 g, 3.0 mL, 1.5 equivalents per PDMAEMA repeat unit) was added and the reaction was stirred at ambient temperature for 18 h. The solution slowly became cloudy as the polyelectrolyte precipitated. Afterwards, the acetone was evaporated using a rotary evaporatory and the polymer dissolved in water. The solution was dialyzed against de-ionized water for two days to remove all residual methyl iodide.

7.3.5 Analytical Methods

^{1}H NMR analyses were performed using a Varian INOVA NMR operating at 23 °C and 400 MHz. Differential scanning calorimetry was performed using either a Perkin-Elmer Pyris 1 DSC or a TA Instruments Q1000 DSC. Samples were analyzed at 10 °C/min and the T_g on the second heating cycle is reported. Size exclusion chromatography was performed in

dimethylacetamide (DMAc) as reported previously, and reported values are relative to PEO standards. Solution rheology was performed using a TA Instruments AR-G2 rheometer equipped with a cone-and-plate geometry (2° cone, 40 cm diameter, 56 μm truncation) with a Peltier plate at 25.0 ± 0.1 °C. Steady shear experiments were performed from 0.01 to 1000 Hz and the zero-shear viscosity was determined from the Newtonian flow regime. Specific viscosity was calculated as $\eta_{sp} = (\eta_0 - \eta_{solvent})/\eta_{solvent}$. Solution conductivity was performed using an Oakton CON6 two-electrode probe at 25 °C. The average of three measurements are reported.

7.4 Results and Discussion

7.4.1 Synthesis and Characterization

Star-shaped PDMAEMA was synthesized as described in previous reports.[22,24] Scheme 7.1 depicts the synthesis of a five-armed star PDMAEMA in anisole using the catalyst/ligand pair Cu(I)Br/HMTETA. The polymerization was monitored by ^{1}H NMR. Trioxane was added to the polymerization as an inert integration aid for NMR analysis. Figure 7.1 shows the conversion versus time for linear PDMAEMA initiated with EBIB as well as the five-armed star-shaped PDMAEMA. The rate of polymerization of linear PDMAEMA decreased as the monomer to initiator ratio (M:I) increased due to decreased concentrations of active end groups. The five-armed star PDMAEMA showed slower polymerization kinetics than expected for the M:I ratio 250:1. Müller et al.[22] previously reported that the initiation efficiency of the saccharide-based initiators was around 60% for PDMAEMA polymerizations. The slower kinetics of the star-shaped polymerizations also suggested that fewer arms are active in polymerization. Neutralization of the PDMAEMA stars with acid was conducted in water to

generated star-shaped polyelectrolytes with Cl^- and BF_4^- counteranions. The titration was confirmed by ^1H NMR as reported previously for linear PDMAEMA-based polyelectrolytes.[20]

Scheme 7.1. Synthesis and schematic depiction of the five-armed star-shaped PDMAEMA.

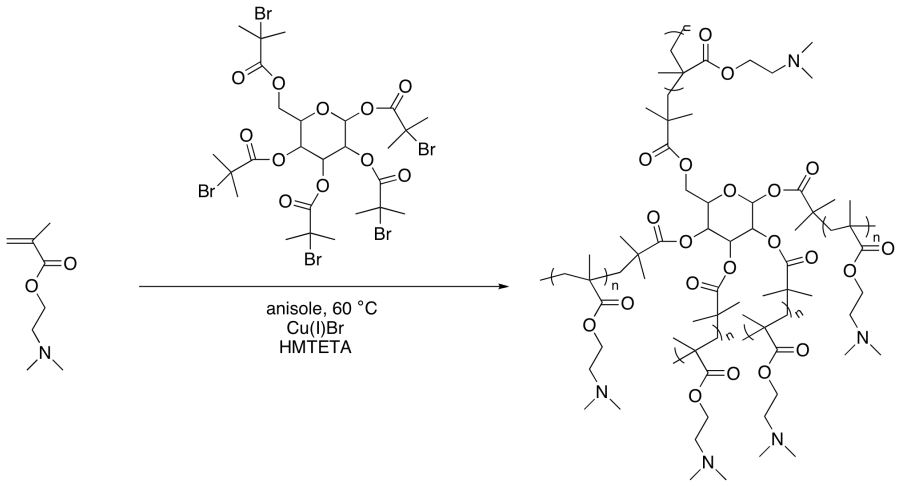

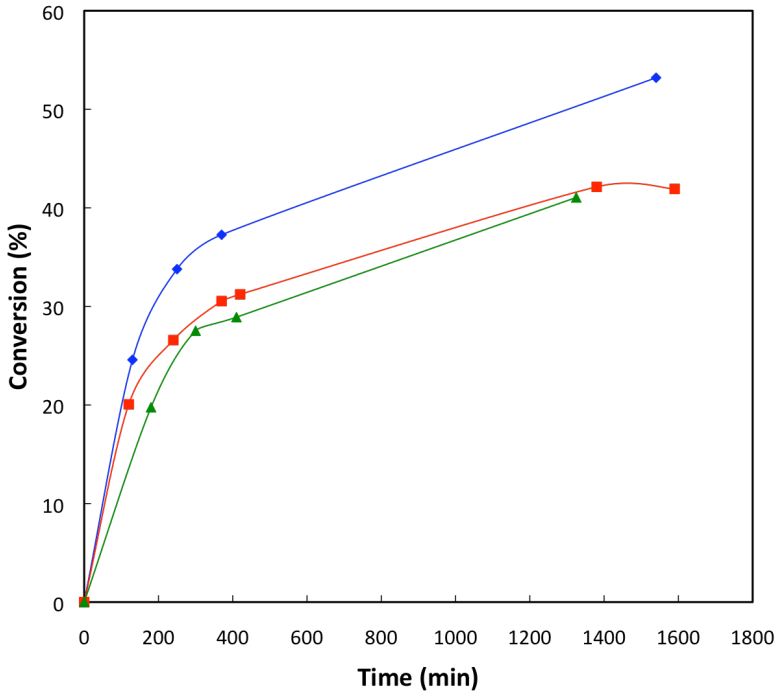

Figure 7.1. Conversion versus time for PDMAEMA polymerizations for linear PDMAEMA at M:I ratios of 300:1 (diamonds) and 500:1 (squares) as well as five-armed star PDMAEMA at M:I ratio of 250:1 (triangles).

SEC analysis in DMAc successfully separated the star-shaped polymers. Table 7.1 lists the molecular weights estimated from ^{1}H NMR and SEC. The M_w/M_n for every polymer was between 1.1 and 1.3, consistent with previous reports on the ATRP of DMAEMA.[22] For the linear polymers, M_n's by SEC were slightly lower than those calculated from NMR analysis. In DMAc, the PDMAEMA polymers form tighter coils, resulting in slightly lower hydrodynamic radii compared to the PEO standards. SEC analysis of the star-shaped polymers indicated significantly lower molecular weights than calculated by NMR, as expected. The hydrodynamic radii of the star-shaped polymers are much lower than those of linear polymers of corresponding molecular weights, and SEC analysis significantly underestimates the molecular weight. However, the SEC analysis confirms a narrow polydispersity for all samples. The eight-armed star-shaped PDMAEMA with $M_{n,SEC}$ of 176 000 g/mol could not be analyzed for molecular weight by NMR since increased viscosity hindered integration of residual monomer peaks.

Table 7.1. Molecular Weight Analysis of Star-Shaped PDMAEMA

# of Arms	M_n[a] (g/mol)	M_n[b] (g/mol)	M_w[b] (g/mol)	M_w/M_n	$M_{n,arm}$[c] (g/mol)
1	33 300	19 100	24 400	1.28	33 300
1	47 000	33 300	42 500	1.28	47 000
5[d]	81 100	23 600	29 400	1.24	16 200
5[d]	133 000	58 900	69 300	1.18	26 600
8[d]	231 000	65 600	77 900	1.19	28 900
8[d]	n.d.	176 000	195 000	1.11	(22 000)[e]

[a]Determined by ^{1}H NMR.
[b]Determined by SEC.
[c]Estimated from ^{1}H NMR molecular weights
[d]Theoretical arm number
[e]Estimated from SEC molecular weights

Thermal analysis of the star-shaped PDMAEMA and polyelectrolytes indicated that the topology did not have significant impact on the solid-state thermal properties. Table 7.2 lists the

measured T_g's for the linear and star-shaped polymers with different counteranions. No significant change was observed upon changing the polyelectrolyte topology.

Table 7.2. Glass Transition Temperatures of Linear and Star-Shaped Polyelectrolytes

# of Arms	$M_{n,SEC}$ (g/mol)	T_g (°C)		
		Neutral	Cl^-	BF_4^-
1	19 100	21	172	135
1	33 300	22	175	140
5	23 600	21	169	139
5	58 900	20	168	142
8	65 600	20	163	127
8	176 000	21	177	141

7.4.2 Solution Rheology and Conductivity

The linear and five-armed PDMAEMA polymers were methylated and dialyzed against NaCl to form the poly(2-(*N*,*N*,*N*-trimethylammonium)ethyl methacrylate chloride) (PTMAEMACl) star-shaped polyelectrolytes. The amine groups were methylated rather than protonated to suppress any pH-dependent ion dissociation. The polyelectrolyte structures were confirmed by ^{1}H NMR analysis. Rheological and conductivity measurements revealed the differences in behavior of linear and star-shaped polyelectrolytes in solution. We previously reported a solvent mixture of 4:1 water:methanol for the successful electrospinning of PDMAEMA-based polyelectrolytes,[18,20] and all solution rheology, conductivity, and electrospinning experiments in this report utilized the same solvent system. Figure 7.2 below shows the specific viscosity as a function of polymer concentration for uncharged PDMAEMA stars of two molecular weights as well as the linear PDMAEMA. The viscosity scaling factors are identical for each star-shaped polymer: 1.8 below c_e and 5.5 above c_e. The c_e increases from 9 wt% to 12 wt% as molecular weight increases. Linear PDMAEMA in the same solvent system exhibited scaling factors of 1.2 and 4.4 below and above c_e.

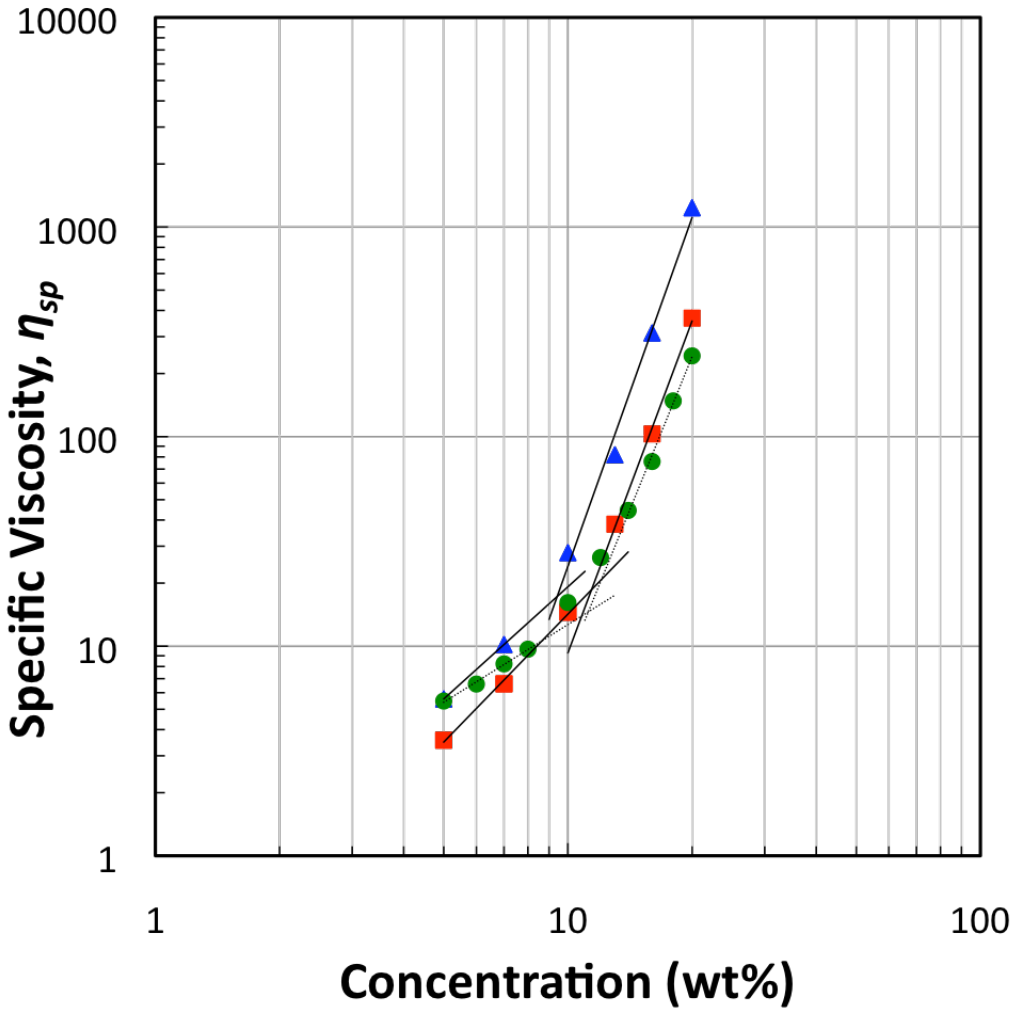

Figure 7.2. Specific viscosity versus polymer concentration for linear PDMAEMA (circles) and five-armed star-shaped PDMAEMA of two different molecular weights (triangles and squares). The lines represent power law fits for each concentration regime.

The specific viscosity versus concentration for the charged PTMAEMACl polymers is shown in Figure 7.3. The scaling factors in the semi-dilute regimes decreased to 0.5 below c_e and 2.1 above c_e. In addition, the c_e's decreased to 8 and 9 wt% for the two star-shaped polyelectrolytes. The scaling factor in the semi-dilute unentangled regime matches that expected for polyelectrolytes, but the scaling factor in the semi-dilute entangled regime is slightly higher than expected for linear polyelectrolytes ($\eta_{sp} \sim C^{1.5}$). Table 7.3 summarizes the specific viscosity scaling factors for the linear and star-shaped polymers. Both the uncharged and charged star-shaped polymers exhibited slight increases in rheological scaling factors compared to the linear

analogues. The increase arises from the more collapsed structure of the star-shaped polyelectrolytes compared to linear polyelectrolytes of the same molecular weight.[5] The transition from semi-dilute unentangled to entangled regimes also appeared more gradual, with significant curving observed in the data around the transition.

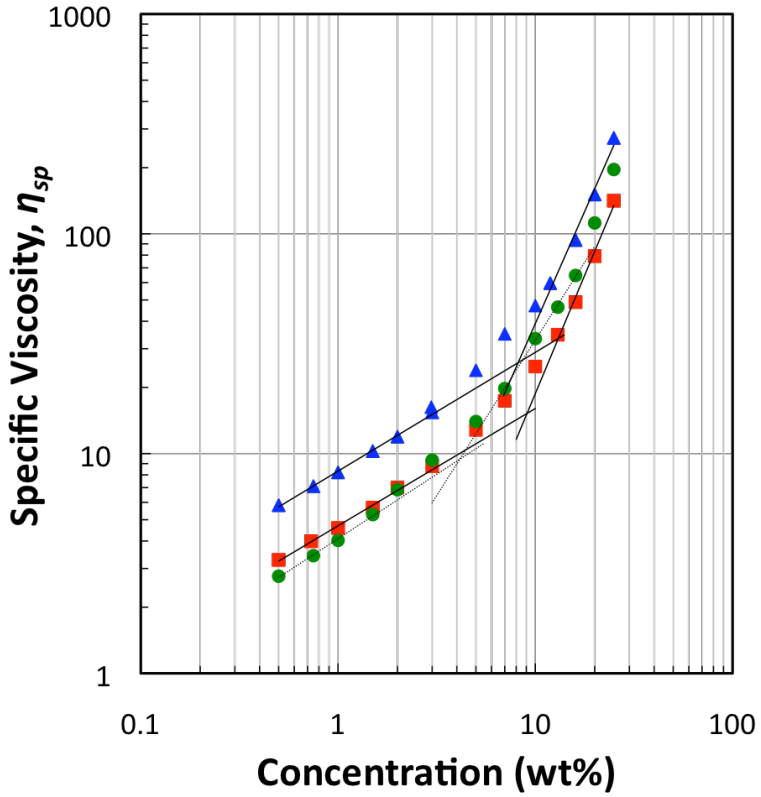

Figure 7.3. Specific viscosity versus polymer concentration for linear PTMAEMACl (circles) and five-armed star-shaped PTMAEMACl of two different molecular weights (triangles and squares). The lines represent power law fits for each concentration regime.

Table 7.3. Solution Rheological Scaling Factors

Polymer	Linear		Five-Armed Star	
	$c^* < c < c_e$	$c_e < c < c_D$	$c^* < c < c_e$	$c_e < c < c_D$
PDMAEMA	1.2	4.4	1.8	5.5
PTMAEMACl	0.8	1.7	0.5	2.1

Solution conductivity also revealed differences between the star-shaped and linear polyelectrolytes. Figure 7.4 shows the solution conductivity versus polymer concentration for linear and star-shaped PTMAEMACl. All polyelectrolytes exhibited power-law conductivity

behavior throughout the semi-dilute unentangled and semi-dilute entangled regimes. The star-shaped polyelectrolytes both exhibited similar solution conductivities independent of molecular weight. However, the conductivities of the linear PTMAEMACl were about twice that of the star polyelectrolytes. The reduced conductivities further suggested the star-shaped polyelectrolytes had high counterion condensation, as described by Rubinstein et al.[5]

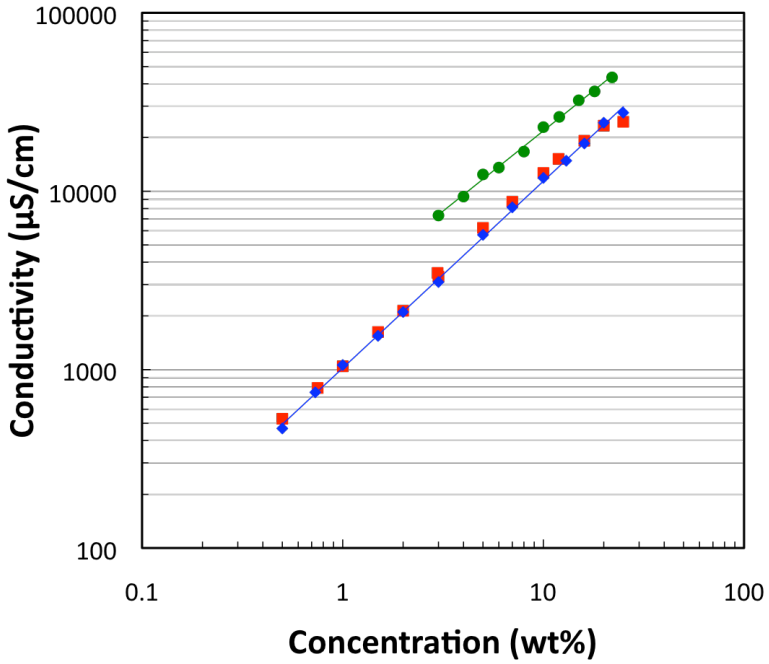

Figure 7.4. Solution conductivity of PTMAEMACl polyelectrolytes with varying topology: linear PTMAEMACl (circles) and five-armed star-shaped PTMAEMACl of two different molecular weights (diamonds and squares). The lines represent power law fits for each concentration regime.

7.4.3 Electrospinning

The uncharged and charged star-shaped polymers were electrospun from the 4:1 water:methanol solvent system. For the uncharged PDMAEMA stars, the onset of fiber formation was observed around c_e, consistent with previous reports on the electrospinning of uncharged branched polyesters.[15] Figure 7.5 shows the FESEM micrographs of the electrospun PDMAEMA fibers. Around the c_e, non-uniform fibers with large beads were observed. At

increasing concentrations, uniform fibers formed with increasing average fiber diameters. Uniform fibers formed at concentrations just below 2ce, consistent with linear PDMAEMA polymers. Presumably, the low T_g allows stretching into uniform fibers after solidification.

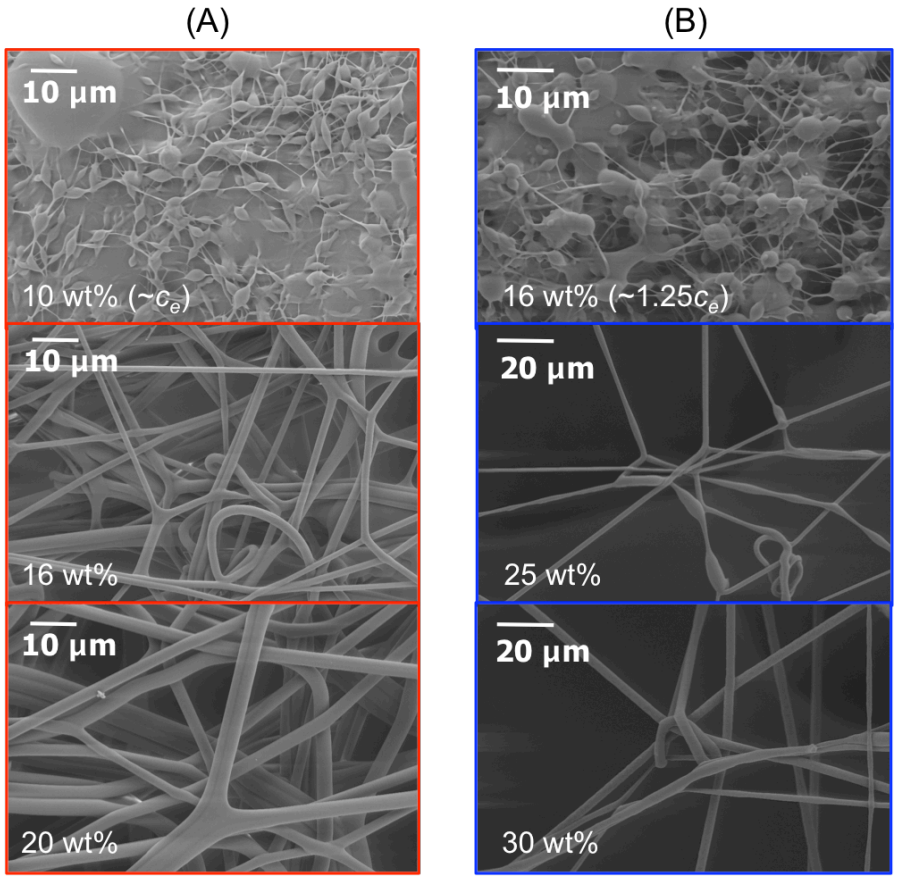

Figure 7.5. FESEM images of electrospun five-armed star-shaped PDMAEMA fibers from different solution concentrations. Images in (A) and (B) represent the higher and lower molecular weight PDMAEMA stars.

The polyelectrolytes exhibited significantly different electrospinning behavior. Fiber formation was not observed until concentrations exceeding 4 or 5 times the c_e. Figure 7.6 shows images of the electrospun linear and star–shaped PTMAEMACl's. The onset of fiber formation occurred below $4c_e$ for the linear PTMAEMACl and at about $4.5c_e$ for both star-shaped polymers. Uniform fiber formation occurred at $4.5c_e$ and $5c_e$ for the linear and star polyelectrolytes, respectively. The onset of fiber formation corresponded to solution viscosity of about 300 cP for the linear PTMAEMACl. For the star-shaped PTMAEMACl, the onset of fiber

formation and uniform fiber formation occurred around 1500 cP and 4500 cP, respectively, much higher than observed for the neutral stars. Our group previously electrospun linear PDMAEMA-HCl and observed fiber formation at $3.3c_e$, corresponding to 330 cP.

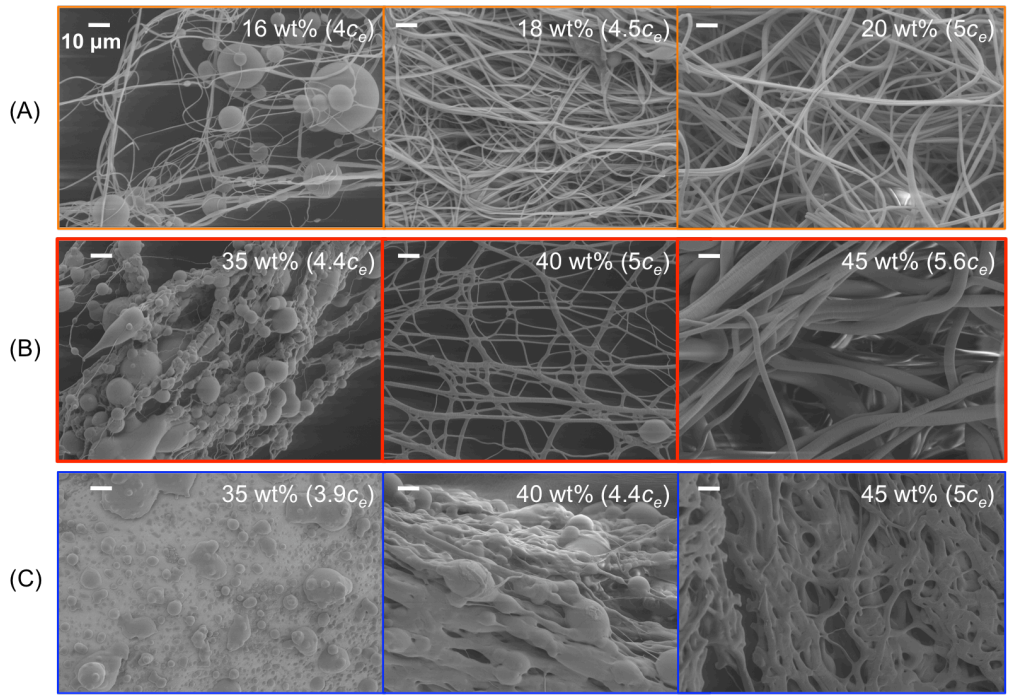

Figure 7.6. FESEM micrographs of electrospun (A) linear PTMAEMACl and (B & C) star PTMAEMACl polyelectrolytes of different molecular weights. The scale bar represents 10 µm.

Table 7.4 lists the onset of fiber formation for the uncharged star PDMAEMAs as well as the linear and star-shaped PTMAEMACl's. As reported often in the literature, the polyelectrolytes required significantly higher viscosities and entanglements to stabilize the electrospinning jet. In addition, the star-shaped polyelectrolytes required significantly higher viscosities for electrospinning than the linear polyelectrolytes. Previous reports have hypothesized that electrostatic repulsions of the charged macromolecules lead to instabilities destabilizing the electrospinning jet. In the case of charged star-shaped polymers, electrospinning required even higher viscosities. The confined nature of the charges within the

core of the star polyelectrolytes could lead to increased electrostatic repulsions under the high electric field.

Table 7.4. Onset of Fiber Formation versus Polymer Topology and Molecular Weight.

Polymer	Onset of Fiber Formation	
	η_0 (cP)	c/c_e
Star PDMAEMA	100	1.4
Star PDMAEMA	76	1.4
Linear PTMAEMACl	300	3.5
Star PTMAEMACl	1650	4.5
Star PTMAEMACl	1470	4.5

Figure 7.7 shows fiber diameter versus concentration compared to the semi-empirical correlations developed previously in our laboratories for neutral, non-associating polymers. The uncharged PDMAEMA stars exhibited fiber diameter scaling behavior very expected for neutral polymers. The slightly increased scaling factors have been observed previously,[20] and stem from inter- and intramolecular associations of the amine group. The polyelectrolytes electrospun at much high normalized concentrations. The polyelectrolyte fibers are also orders of magnitude thinner in diameter than expected for neutral polymers at the same normalized concentrations and viscosities. The reduced fiber diameter results from increased solution conductivity leading to extensive drawing of the polymer jet during electrospinning. The star-shaped polyelectrolytes had significantly larger fibers than the linear polyelectrolytes at similar normalized concentrations.

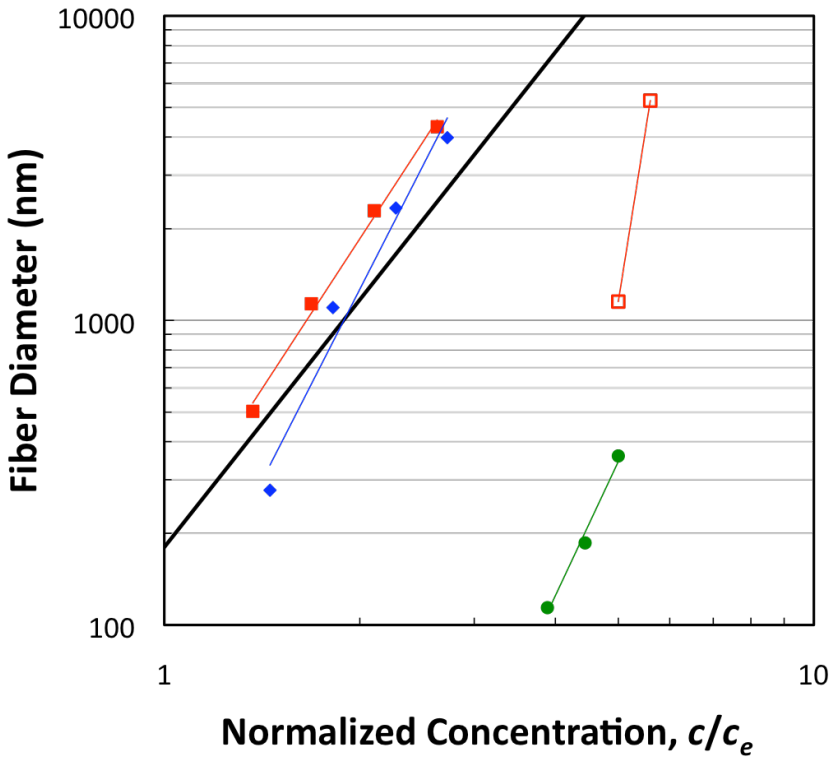

Figure 7.7. Fiber diameter versus normalized concentration for neutral and charged star-shaped PDMAEMA: Neutral five-armed star-shaped PDMAEMA (squares and diamonds), charged five-armed star-shaped PTMAEMACl (open squares), and linear PTMAEMACl (circles).

7.5 Conclusions

Star-shaped uncharged PDMAEMA and charged PTMAEMACl polymers with narrow polydispersities were prepared by ATRP. The thermal transitions of these star polymers matched the linear polymers, suggesting that topology has little effect on the solid state properties of the polyelectrolytes. However, solution behavior differed dramatically for the star-shaped polyelectrolytes. Specific viscosity scaling factors were larger for the star-shaped polymers in the semi-dilute unentangled and semi-dilute entangled regimes, indicative of the smaller hydrodynamic radii for the stars. Solution conductivity also decreased significantly due to increased counterion condensation within the polyelectrolyte stars. The uncharged star-shaped polymers electrospun above c_e, as expected for neutral polymer. The charged linear PTMAEMACl had an onset of fiber formation at $3.5c_e$ and 300 cP, very similar to the transition

observed for other polyelectrolytes. However, star-shaped PTMAEMACl did not electrospin until 4.5c_e and approximately 1500 cP. The compact conformation of the star polyelectrolytes could lead to increased electrostatic repulsions between charges under the electric field, destabilizing the electrospinning jet for star polyelectrolytes.

7.6 Acknowledgements

This material is based upon work supported by the U.S. Army Research Laboratory and the U.S. Army Research Office under contract/grant number W911NF-07-1-0452 Ionic Liquids in Electro-Active Devices Multidisciplinary University Research Initiative (ILEAD MURI) as well as National Science Foundation under Grant No. 0824923 Doctoral Dissertation Enhancement Project (DDEP).

7.7 References

1. Schallon, A.; Jerome, V.; Walther, A.; Synatschke, C. V.; Müller, A. H. E.; Freitag, R. *Reactive & Functional Polymers* **2010,** *70*, 1-10.
2. Colby, R. H. *Rheol. Acta* **2010,** *49*, 425-442.
3. Dobrynin, A. V.; Rubinstein, M. *Prog. Polym. Sci.* **2005,** *30*, 1049-1118.
4. Dou, S.; Colby, R. H. *J. Polym. Sci., Part B: Polym. Phys.* **2006,** *44*, 2001-2013.
5. Shusharina, N. P.; Rubinstein, M. *Macromolecules* **2008,** *41*, 203-217.
6. Plamper, F. A.; Becker, H.; Lanzendörfer, M.; Patel, M.; Wittemann, A.; Ballauff, M.; Müller, A. H. E. *Macromol. Chem. Phys.* **2005,** *206*, 1813-1825.
7. Marques, C. M.; Izzo, D.; Charitat, T.; Mendes, E. *European Physical Journal B* **1998,** *3*, 353-358.
8. Reneker, D. H.; Yarin, A. L. *Polymer* **2008,** *49*, 2387-2425.
9. Greiner, A.; Wendorff, J. H. *Angew. Chem., Int. Ed. Engl.* **2007,** *46*, 5670-5703.
10. Desai, K.; Kit, K.; Li, J.; Davidson, P. M.; Zivanovic, S.; Meyer, H. *Polymer* **2009,** *50*, 3661-3669.
11. Agarwal, S.; Wendorff, J. H.; Greiner, A. *Advanced Materials* **2009,** *21*, 3343-3351.
12. Ding, B.; Wang, M.; Yu, J.; Sun, G. *Sensors* **2009,** *9*, 1609-1624.
13. Lee, E.-H.; Kim, H.-M.; Lim, S.-K.; Kim, K.-S.; Chin, I.-J. *Molecular Crystals and Liquid Crystals* **2009,** *499*, 581-589.
14. Nah, C.; Kwak, S. K.; Kim, N.; Lyu, M.-Y.; Hwang, B. S.; Akle, B.; Leo, D. J. *Key Eng. Mater.* **2007,** *334-335*, 1001.
15. McKee, M. G.; Wilkes, G. L.; Colby, R. H.; Long, T. E. *Macromolecules* **2004,** *37*, 1760-1767.

16. Shenoy, S. L.; Bates, W. D.; Frisch, H. L.; Wnek, G. E. *Polymer* **2005,** *46*, 3372-3384.
17. Yu, J. H.; Fridrikh, S. V.; Rutledge, G. C. *Polymer* **2006,** *47*, 4789-4797.
18. McKee, M. G.; Hunley, M. T.; Layman, J. M.; Long, T. E. *Macromolecules* **2006,** *39*, 575-583.
19. Ohkawa, K.; Minato, K.-I.; Kumagai, G.; Hayashi, S.; Yamamoto, H. *Biomacromolecules* **2006,** *7*, 3291-3294.
20. Hunley, M. T.; England, J. P.; Long, T. E. **2010**, Submitted.
21. Chen, H.; Elabd, Y. A. *Macromolecules* **2009,** *42*, 3368-3373.
22. Plamper, F. A.; Schmalz, A.; Penott-Chang, E.; Drechsler, M.; Jusufi, A.; Ballauff, M.; Müller, A. H. E. *Macromolecules* **2007,** *40*, 5689-5697.
23. Stenzel-Rosenbaum, M. H.; Davis, T. P.; Chen, V.; Fane, A. G. *Macromolecules* **2001,** *34*, 5433-5438.

Chapter 8: Harnessing Low Molar Mass Surfactants for Electrospinning Functional Fibers

8.1 Abstract

Self-assembled aggregates of low molar mass amphiphiles were electrospun to form microfibers. Cetyltrimethylammonium bromide (CTAB) formed wormlike micelles in water and glucose/water solutions. At concentrations above the entanglement of these wormlike micelles, electrospun fibers were formed. The phospholipid mixture asolectin was electrospun in the presence of water (in a stoichiometric ratio to asolectin). The water induced branching and network formation of the wormlike micelles, increasing viscosity scaling relationships. At 3 moles of water per mole asolectin, only beaded fibers formed; at 6 moles of water per mole asolectin, no electrospun fibers formed. Low molar mass organogelators were synthesized, and the gels were electrospun to form films of gelator fibrils. The electrospinning process could not disrupt the gel enough to form fibers. A dispersion of the gelators, however, formed self-supporting fibers with complex surface morphology. The addition of CTAB to poly(methyl methacrylate) (PMMA) solutions facilitated electrospinning at very low concentrations. Without CTAB, the PMMA with a Mw of 571,000 g/mol electrospun above 2 wt% in 4:1 DMF:THF. With the addition of 0.5 and 1.0 mM CTAB, the onset of electrospinning decreased to < 1wt% PMMA. The reduced surface tension and increased solution conductivity facilitated the electrospinning at lower concentrations.

8.2 Introduction

As research interest in electrospinning has increased dramatically over recent years, the development of novel techniques to electrospin functional membranes has also progressed rapidly. Membranes composed of core-shell fiber composites,[1-3] carbon nanotube

nanocomposite fibers,[4,5] polyelectrolyte fibers,[6-8] fibers with molecular recognition,[9,10] and even fibers with the ability to direct cell growth and differentiation have been developed.[11-13] Our laboratories recently demonstrated that supramolecular wormlike micelles of low molar mass surfactants and phospholipids can form electrospun fibers from both solution[14,15] and melt.[16] The use of surfactants and naturally-produced phospholipids allows us to create fibrous membranes that mimic the natural composition of cell membranes.

Electrospinning typically requires entangled polymer solutions to prevent capillary breakup and form uniform fibers.[17,18] The presence of entanglements increases the relaxation time of the polymer solution, stabilizing the electrospinning jet over the short processing time scale. Certain surfactants, depending on chemical structure and functionality, form one-dimensional aggregates in solution called cylindrical micelles or wormlike micelles.[19,20] Phospholipids, double-tailed ammonium surfactants, and ammonium-based gemini surfactants commonly form wormlike micelles in solution. As wormlike micelles grow in length, they coil in solution and can entangle at high concentrations, analogous to flexible polymers.[19] These entangled wormlike micelle solutions exhibit viscoelastic behavior, and the solution elasticity enables electrospinning. To date, our research group has electrospun microfibers of phospholipids[14,16] and ammonium-based gemini surfactants.[15]

In this report, we studied the electrospinnability of several low molar mass amphiphiles. The electrospinning ability of wormlike micelles of CTAB was studied and compared to the electrospinning of phospholipids and gemini surfactants. Correlations to micellar length provided us with insight into the electrospinnability of surfactant solutions. In addition, we added water to the phospholipid wormlike micelles to induce branching, and found that the highly branched and network hindered electrospinning. We also demonstrated for the first time

the electrospinning of an organogelator from dispersion. Moreover, we investigated the onset of electrospinning of poly(methyl methacrylate) with small amounts of added surfactant. The surfactant facilitated the electrospinning at very low polymer concentrations by reducing surface tension and increasing conductivity.

8.3 Experimental

8.3.1 Materials

The surfactants, 1-hexadecyltrimethylammonium bromide and asolectin from soybean, were purchased from Fluka and dried *in vacuo* at ambient temperature before use. D-(+)-Glucose was purchased from Alfa Aesar and dried *in vacuo* before use. 1,6-Diisocyanatohexane (98%), 1-dodecylamine (98%), 1-hexadecylisocyanate (97%), and (1*S*,2*S*)-(+)-1,2-diaminocyclohexane (98%) were purchased from Sigma Aldrich and used as received. Poly(methyl methacrylate) with nominal molecular weights of 360,000 g/mol and 570,000 g/mol were purchased from Sigma-Aldrich and used as received. De-ionized water (DI H_2O), methanol, chloroform ($CHCl_3$), *N*,*N*-dimethylformamide (DMF), tetrahydrofuran (THF), and all other solvents were purchased from commercial sources and used as received.

8.3.2 Electrospinning and Fiber Characterization

All electrospinning experiments were performed in a homemade plexiglass box to prevent air currents from interfering. The solution was placed in a 20-mL plastic syringe equipped with an 18-guage stainless steel needle. The syringe was placed in a syringe pump and solution metered at 5 mL/h. The positive lead of a high voltage power supply was connected to the syringe needle. The electric potential was raised to 25 kV and fibers collected on a stainless steel mesh. Fibers for microscopy were sputter coated with 15 nm of 60/40 gold/palladium and imaged using a LEO 1550 field emission scanning electron microscopy (FESEM). The FESEM

software was used to determine fiber diameter, and the averages and standard deviation of twenty individual measurements are reported.

8.3.3 Synthesis of 1,1'-(hexane-1,6-diyl)bis(3-dodecylurea) (1)

1-Dodecylamine (10 g, 54 mmol) was dissolved in 100 mL of toluene in a round-bottomed flask equipped with a magnetic stir bar. The flask was placed into an oil bath at 100 °C. 1,6-Diisocyanatohexane (9.1 g, 54 mmol) was added dropwise over the course of 1 h, and the reaction was maintained at 100 °C for 24 h. After polymerization, the gelator was recrystallized from *p*-xylene and dried *in vacuo* at 65 °C to yield a white powder in quantitative yield. ^{1}H NMR (400 MHz, $CDCl_3$, δ): 5.4 (s, 4H), 3.0 (s, 8H), 1.4 (s, 8H), 1.3 (br, 40H), 0.9 (t, 6H).

8.3.4 Sythesis of 1,1'-((1*S*,2*S*)-cyclohexane-1,2-diyl)bis(1-hexadecylurea) (2)

1-hexadecylisocyanate (10 g, 37 mmol) was dissolved in 100 mL of toluene in a round-bottomed flask equipped with a magnetic stir bar. The flask was placed into an oil bath at 100 °C. 1,2-Diaminocyclohexane (4.3 g, 37 mmol) was added dropwise over the course of 1 h, and the reaction was maintained at 100 °C for 24 h. After polymerization, the gelator was recrystallized from diethyl ether and dried *in vacuo* at 65 °C to yield a white powder in quantitative yield. ^{1}H NMR (400 MHz, $CDCl_3$, δ): 4.9 (br, 2H), 4.3 (br, 2H), 3.5 (br, 2H), 3.1 (br, 4H), 2.1 (s, 4H), 1.6-1.2 (br, 60H) 0.9 (br, 6H).

8.4 Results and Discussion

8.4.1 Solution Characterization and Electrospinning of CTAB

Scheme 8.1 shows the structure of cetyltrimethylammonium bromide (CTAB) surfactant. CTAB is known to form wormlike micelles in aqueous and saline solutions.[20,21] The micellization of CTAB in de-ionized water (DI H_2O) occurred through DLS, as shown in Figure

8.1. The critical micelle concentration (cmc) was identified around 0.9 mM, and the CTAB micelles had radii about 250 nm, which remained constant with increasing concentration.[22] Recently, Porcar et al.[23] demonstrated that adding glucose to cetylpyridinium L_3 sponge phases increased the viscosity of the brine phase without affecting the surfactant sponge morphology. The "sweetened" solvent allowed them to access similar morphologies over a range of solution viscosities. DLS of the CTAB micelles in a solvent mixture of 1:2 glucose:DI H_2O indicated the cmc remained around 0.9 mM. Micellar sizes measured by DLS for the CTAB micelles in sugar water increased dramatically to around 900 nm. However, this measurement did not take into account the increased solution viscosity. DLS estimates the micellar radius, *r*, based on particle diffusion rates using the Einstein-Stokes equation,

$$r = \frac{kT}{6\pi D\eta},$$

where *k* is the Boltzmann constant, *T* is the temperature, *D* is the diffusion coefficient, and η is the solvent viscosity. The apparent increase in micellar size in the "sweetened" solvent resulted from the much larger solution viscosity of the sugar water, causing the CTAB micelles to diffuse slower. Steady shear rheology revealed that the 1:2 glucose:DI H_2O solvent had a viscosity of 2.7 cP at 30 °C, approximately 3 times that of DI H_2O alone. Factoring in the much larger viscosity into the Einstein-Stokes equation estimated the micellar radius approximately 300 nm, in close agreement to the micellar size in DI H_2O.

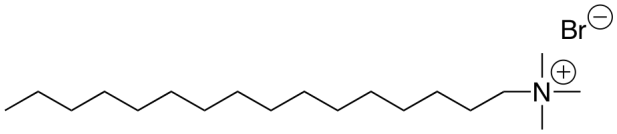

Scheme 8.1. Structure of CTAB.

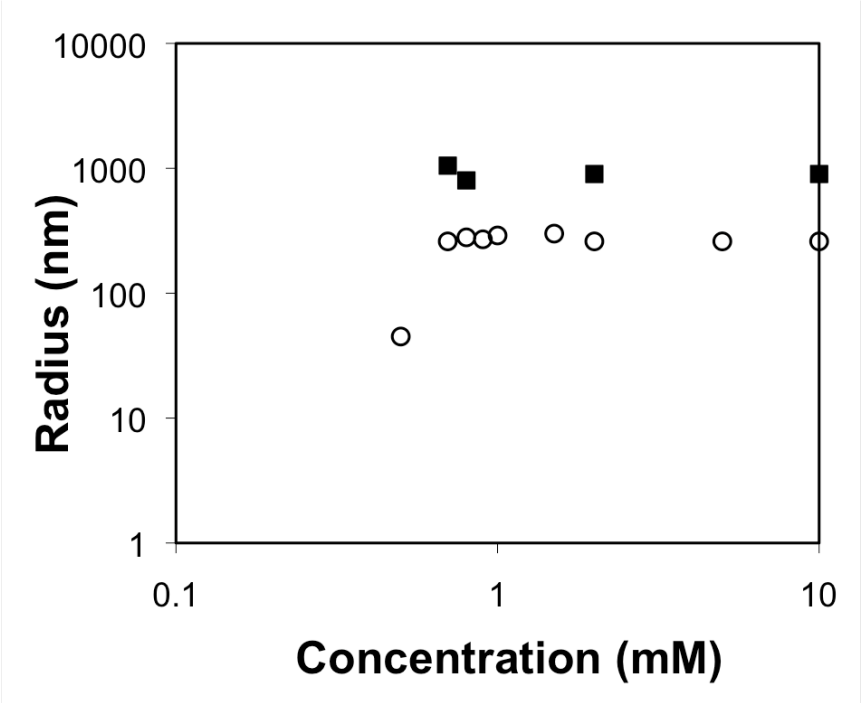

Figure 8.1. CTAB micellar size determined by DLS in DI H_2O (circles) and "sweetened" water (1:2 glucose:H_2O) (squares).

CTAB forms elongated cylindrical micelles at high concentrations in water.[20,21] Solution rheology of CTAB in both water and sugar water revealed the impact of the glucose thickening agent on the flow behavior of CTAB micellar solutions. Figure 8.2 shows the steady shear flow curves of solutions of CTAB at various concentrations in both DI H_2O and "sweetened" water. In water, the CTAB micelles exhibited Newtonian behavior up to 18 wt% solids. Above 18 wt%, strong shear thinning behavior occurred, similar to entangled polymer solutions. Above 22 wt% CTAB, the solutions formed a lyotropic liquid crystalline phase,[21] resulting in different shear thinning behavior observed through rheology. In sugar water, the CTAB solutions exhibited slight shear thinning behavior at all shear rates as the shearing disrupted the hydrogen-bonding of the glucose. Beginning at 18 wt% CTAB, strong shear thinning characteristic of polymer solutions was observed. Again, at CTAB concentrations of 25 wt% and above, lyotropic liquid crystalline phases formed.

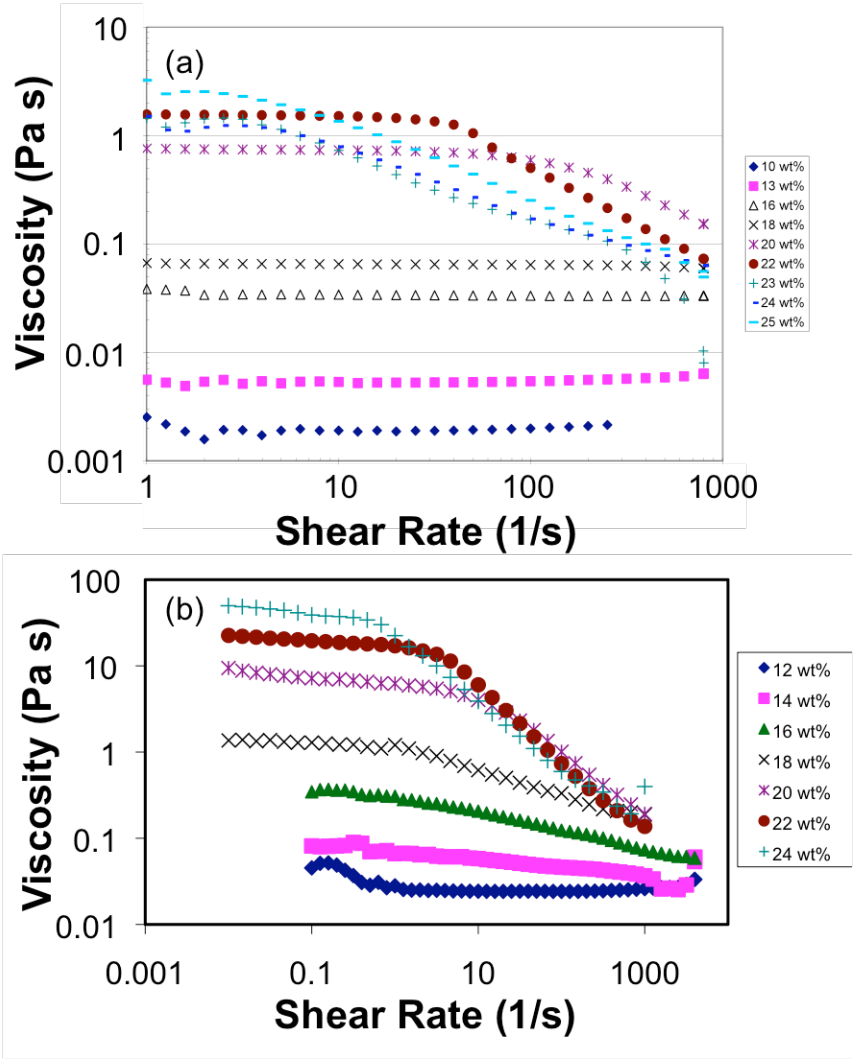

Figure 8.2. Steady shear flow curves of CTAB at 30 °C and varying concentrations in (a) DI H_2O and (b) 1:2 glucose:DI H_2O solvent.

Figure 8.3 shows the zero-shear viscosity as a function of CTAB concentration for solutions in both water and sugar water. The CTAB/DI H_2O solutions demonstrated a critical point in viscosity scaling at about 11 wt%, above which viscosity scaled with CTAB concentration to the power of 10.2. Cressely et al.[21] reported that scaling behavior for CTAB rods in pure water as high as 12, in reasonable agreement with the data observed here. In "sweetened" water, the solution viscosities at constant CTAB concentrations increased by approximately one order of magnitude. The viscosity scaled with concentration in sugar water to

the 10.6 power, very similar to behavior of CTAB in DI H_2O. The similar scaling behavior suggested that the glucose acted only as a thickening agent and did not significantly alter the cylindrical micellar morphology of the CTAB.

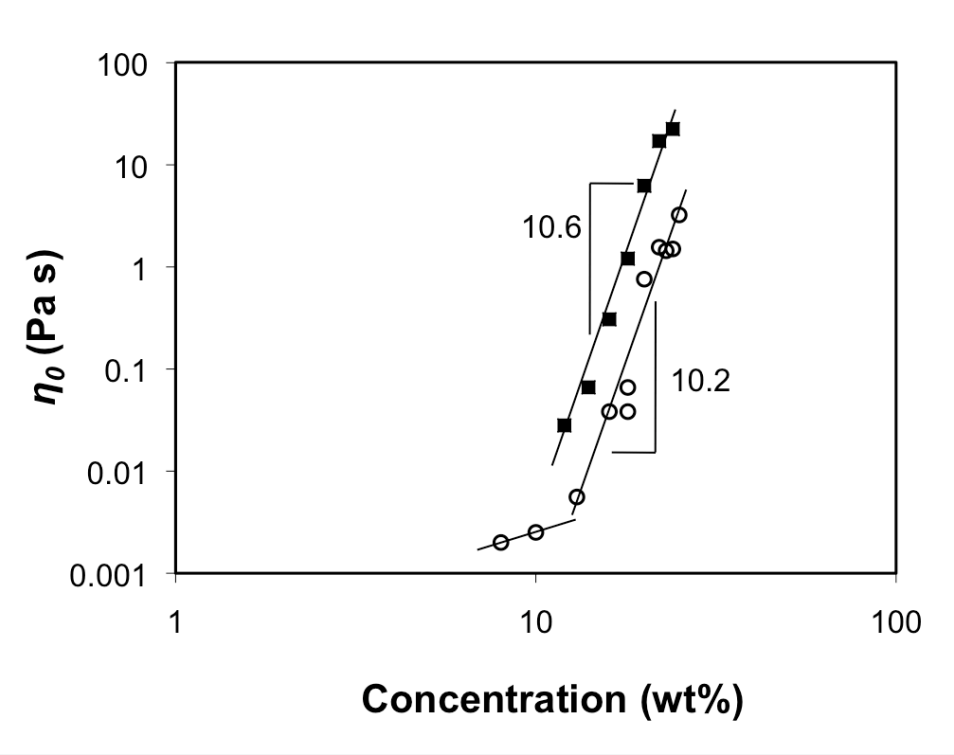

Figure 8.3. Variation of zero-shear viscosity with CTAB concentration in DI H_2O and glucose/DI H_2O solutions at 30 °C.

Our group recently reported that a solvent mixture of 1:1 water:methanol reduced the Krafft temperature of 12-2-12 gemini surfactant, enabling electrospinning of wormlike micelles at room temperature.[15] Akbar et al.[22] also reported that CTAB forms micelles in mixed solvents of water and alcohols. Figure 8.4 shows the zero-shear viscosity as a function of concentration for CTAB in a solvent mixture of 1:1 water:methanol. This solvent mixture reduces the tendency of the wormlike micelles to elongate, resulting in lower viscosities and lower viscosity scaling relationships compared to the CTAB solutions in pure water. A transition was observed at about 18 wt% CTAB, corresponding to the c^*. Above and below this transition, specific

viscosity scaled with concentration to the 1.5 and 2.7 powers, respectively, and no lyotropic liquid crystalline behavior was observed even at concentrations approaching 40 wt% CTAB. The low scaling factors and low viscosities indicated that CTAB did not form wormlike micelles in this solvent.

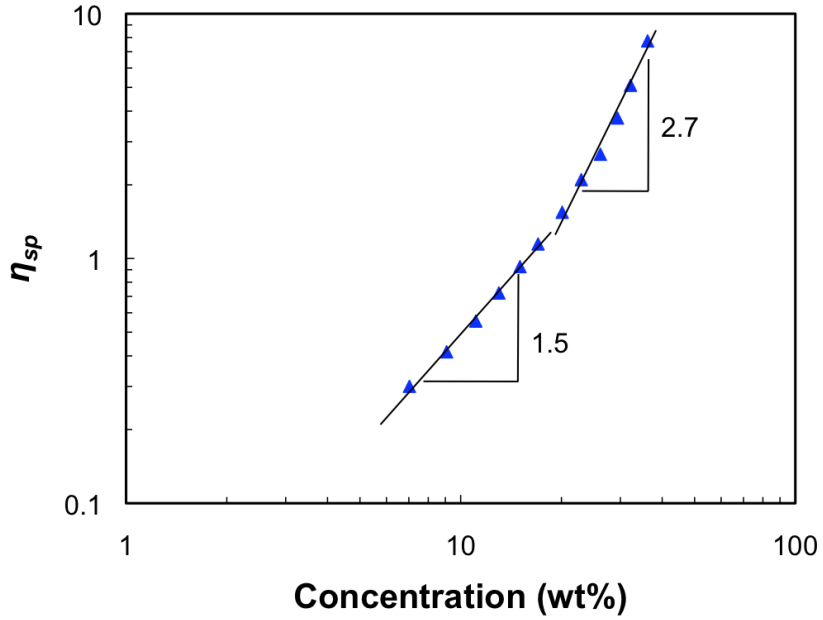

Figure 8.4. Specific viscosity CTAB in 1:1 water:methanol solvent.

Solutions of CTAB in solvent systems of water, glucose water, and water:methanol were electrospun to form surfactant microfibers. Electrospinning successfully produced fibers from the first two solvent systems; no fibers formed from the water:methanol solvent system. Figure 8.5 shows representative FESEM images of the CTAB fibers electrospun from water and sugar water. CTAB electrospun from water at concentrations of 22 and 24 wt%. At 22 wt%, some fibers appeared interspersed among droplets. At 24 wt%, longer fibers with occasional droplets were observed. Above 24 wt%, in the liquid crystalline solutions, no fiber formation occurred. In "sweetened" water, the fibers formed beginning at 18 wt% due to the increased solution viscosity. However, the observed fibers were significantly larger (10 to 100 μm in diameter) and exhibited very non-uniform surfaces. The surface morphology resulted from the presence of

significant amounts of sugar, which did not evaporate during electrospinning. In both cases, the fibers easily disintegrated into a crystalline powder upon rough handling as no polymer entanglements could add mechanical integrity to the fibers. The inability to electrospin fibers from water:methanol solvent likely resulted from the lack of entangled wormlike micelles to stabilize the electrospinning jet. In addition, these solutions had very low viscosities although the CTAB concentration was very high.

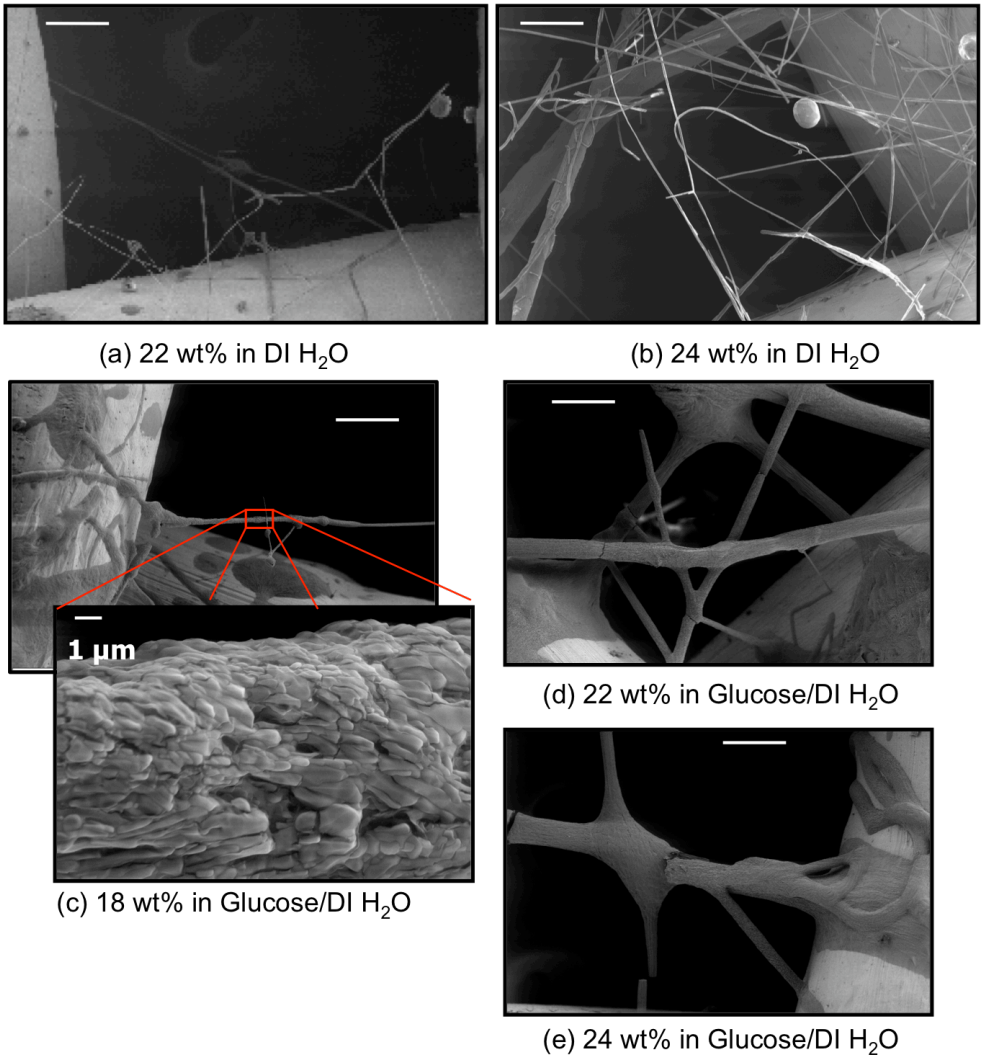

Figure 8.5. FESEM micrographs of CTAB fibers electrospun from (a – b) DI H_2O and (c – e) glucose/DI H_2O solutions. The scale bars represent 100 µm unless noted.

Many reports in the literature describe the formation of wormlike micelles of CTAB.[19-21] However, CTAB micelles did not electrospin as readily as other surfactants previously studied, including phospholipids[14,16] and gemini surfactants.[15] The electrospinnability of polymer solutions depends on the presence of entanglements (or significant intermolecular interactions) to provide elasticity to the solutions.[17,18,24] Flexible wormlike micelles composed of surfactants also entangle in solution, but the rigidity and length of these micelles vary dramatically depending on surfactant nature and the presence of salt.[19,20] Recent advances in solution scattering techniques have allowed in depth interrogations of the length and flexibility of surfactant micelles.[19] Figure 8.6 illustrates the solution conformation of a flexible wormlike micelle (analogous to a flexible polymer coil), highlighting the contour length, L, and persistence length, l_p. Using small angle neutron scattering, the contour length of asolectin wormlike micelles was estimated as 3600 nm with a persistence length of only 16 nm.[25] The short persistence length compared to overall micellar length indicated that the micelles were able to coil in solution, allowing them to entangle at high concentrations, analogous to flexible polymer chains. Similar experiments measured the micellar contour lengths of 12-2-12 ammonium gemini surfactants at 1000 to 2000 nm.[26] However, measurements of CTAB micelles in water indicated a contour length of only 130 to 780 nm and a persistence length of 11 to 36 nm.[19] Compared to the asolectin and 12-2-12 micelles, the CTAB micelles more closely resembled rods than entangled worms. The CTAB micelles were not much longer than their persistence length, suggesting that high degrees of entanglement are not likely. The much longer micelles of asolectin or gemini surfactants are able to form many entanglements to stabilize the electrospinning jet. We hypothesize that the electrospinnability of wormlike micelles depends on the length of the micelles and their ability to entangle.

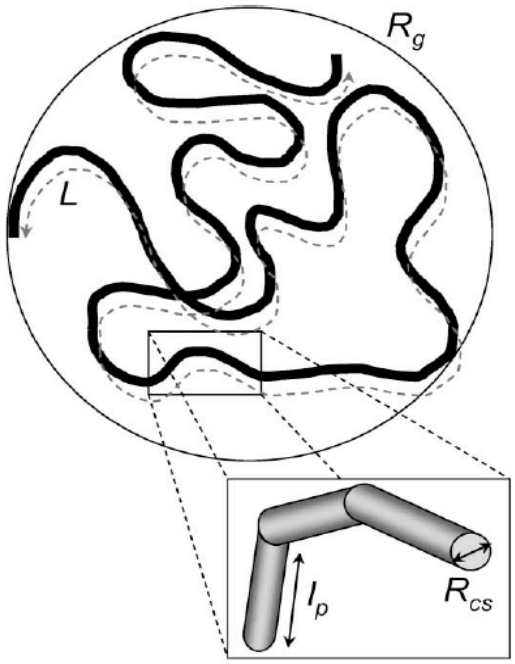

Figure 8.6. Illustration of a flexible wormlike micelle demonstrating the contour length L, radius of gyration R_g, and persistence length l_p.[19]

8.4.2 Effect of Water on Micellization and Electrospinning of Asolectin

Our laboratories recently demonstrated the electrospinning of wormlike micelles of the phospholipid mixture asolectin, both from solution and from the melt.[14,16,27] Scheme 8.2 shows representative structures of the phospholipid components of asolectin. At high concentrations in a $CHCl_3$/DMF solvent mixture, the wormlike micelles entangled sufficiently to stabilize the electrospinning jet and form uniform fibers. Shchipunov and Hoffmann[28] reported that the addition of water to asolectin wormlike micelles in a stoichiometric ratio imparts shear thickening behavior on the wormlike micelle solutions. Low amounts of added water ($n_w < 2$, where n_w is the molar ratio of water to asolectin) lead to extension and slight branching of the micelles. Branching of the wormlike micelles increased dramatically as the molar ratio of water increased. The addition of high amounts of water ($n_w > 5$) led to the formation of an interconnected, highly-branched network of cylindrical micelles. Previous work investigating

electrospun polymers found that increasing the molecular weight allowed the formation of thinner fibers at lower concentrations, and branching played no significant role in fiber formation. To determine if micellar length could be modified to control the electrospinning behavior, we investigated solutions of asolectin with n_w = 0, 3, and 6 through rheology and electrospinning.

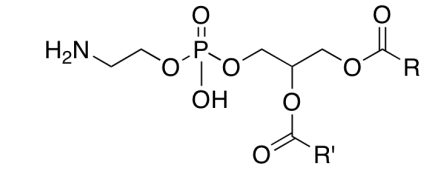

Phosphatidylethanol-amine ~35 mol%

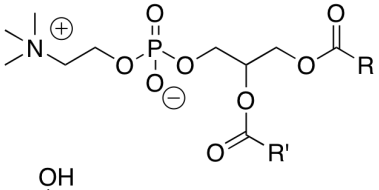

Phosphatidylcholine ~25 mol%

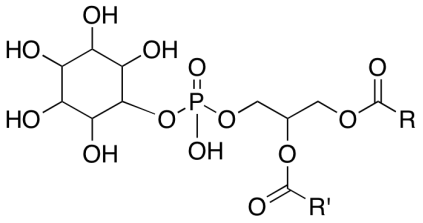

Phosphatidylinositol ~20 mol%

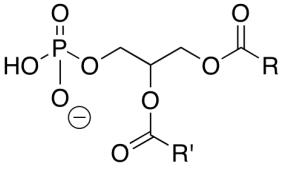

Phosphatidic Acid ~15 mol%

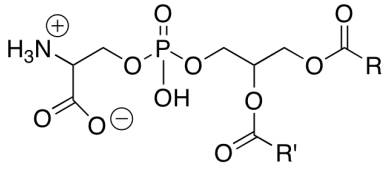

Phosphatidylserine ~1.5 mol%

Scheme 8.2. Representative structures of the phospholipids comprising asolectin. *R* and *R'* refer to fatty acid chains of various lengths. Asolectin also comprises ~3 mol% water. Very minor components are not shown.

Figure 8.7 shows the specific viscosity versus asolectin concentration at n_w = 0, 3, and 6. The addition of water increased the viscosity scaling factor in the semi-dilute unentangled

regime from 2.4 without water to 4.5 and 5.6 at n_w = 3 and 6, respectively. Above c_e, in the semi-dilute entangled regime, the scaling factor changed from 8.4 to 10.5 and 7.4, respectively. The c_e for each series was approximately 35 wt%, with little change observed upon addition of water. The rheological analysis confirmed that the addition of water promoted the growth of the wormlike micelles. At higher n_w, the increased micellar branching led to stronger viscosity scaling relationships at lower concentrations, indicating the micelles were growing rapidly as concentration increased. Above entanglement, the viscosity scaling factor decreased at the highest n_w, since the networked morphology could not entangle to the same extent as the linear worms at lower n_w's.

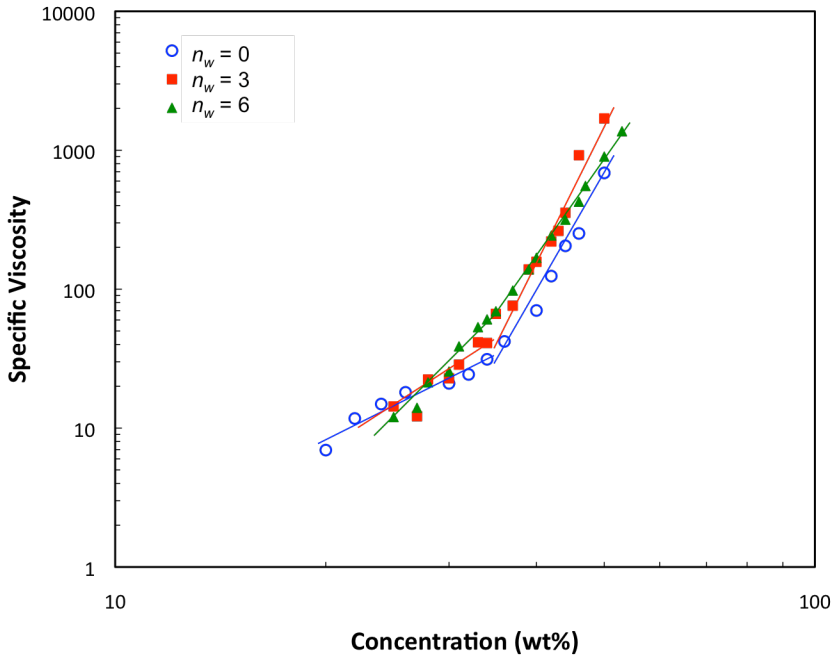

Figure 8.7. Rheology of asolectin in 30/70 $CHCl_3$/DMF with water in the ratios n_w = 0 (circles), n_w = 3 (squares), and n_w = 6 (triangles). The lines represent least-squares fits to the data in the semi-dilute unentangled and semi-dilute entangled regimes.

Solutions of asolectin at n_w = 0, 3, and 6 were electrospun at concentrations from 30 to 50 wt%. Figure 8.8 shows the representative FESEM micrographs of the asolectin fibers at 44 wt% solids. We previously reported that asolectin formed electrospun fibers above 35 wt%.[14] In the

presence of 3 moles of water per mole asolectin, beaded fibers formed above 40 wt% solids. No fiber formation occurred at $n_w = 6$. Although the addition of water promoted micelle elongation and higher viscosities, the existence of branching and a network structure at higher water levels inhibited the asolectin micelles from forming long-range entanglement networks. The micellar network structures could not stabilize the electrospinning jet, resulting in electrospraying rather than fiber formation, even for the highly shear thickening solutions at $n_w = 6$.

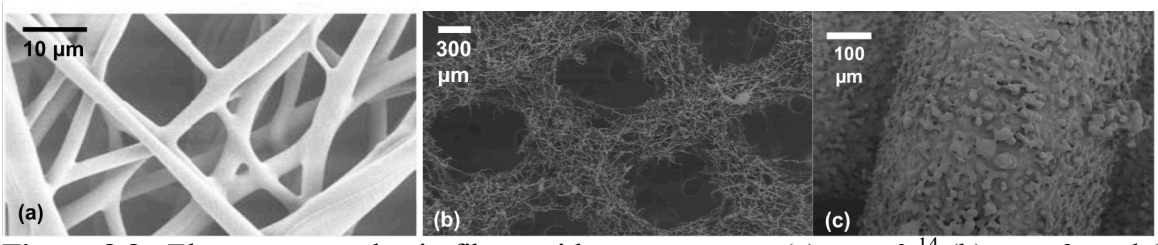

Figure 8.8. Electrospun asolectin fibers with water content (a) $n_w = 0$,[14] (b) $n_w = 3$, and (c) $n_w = 6$. All samples electrospun at an asolectin content of 44 wt%.

8.4.3 Synthesis, Characterization, and Electrospinning of Gelators

Gelators, often classified as either organogelators or hydrogelators, are low molar mass compounds which self-assemble into linear strands to physically gel a solvent.[29-31] Polymeric gelators have also been demonstrated.[32] Often, gelators effectively create a physical gel at very low concentrations (< 15 wt%). Gelators have been designed based on a variety of motifs, including bis-urea groups with bidentate hydrogen-bonding,[31,33,34] L-lysine groups,[35,36] and even phospholipids.[30] Gelators most often self-assembly into long, fibril-type aggregates, which can entangle similar to polymer chains or wormlike micelles.[36]

To investigate the electrospinnability of gelator strands, we synthesized two bis-urea type organogelators. Scheme 8.3 depicts the synthesis of the two gelators. A linear gelator **1** was synthesized by the reaction of 1,6-diisocyanatohexane with 1-aminododecane.[34] A cyclohexane-based gelator **2** was formed by the reaction of 1-isocyanatohexadecane with *trans*-1,2-diaminocyclohexane.[33] The stereochemistry of the cyclohexane center controls the gelation, and

cis-cyclohexane based gelators do not induce gelation.[33] Both gelators were synthesized in toluene at 100 °C with quantitative yields. NMR analysis confirmed the gelator structures.

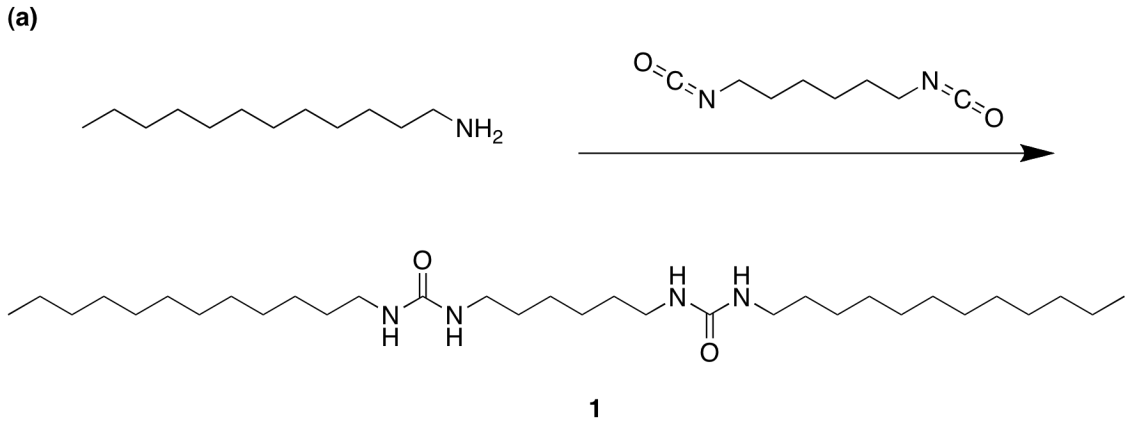

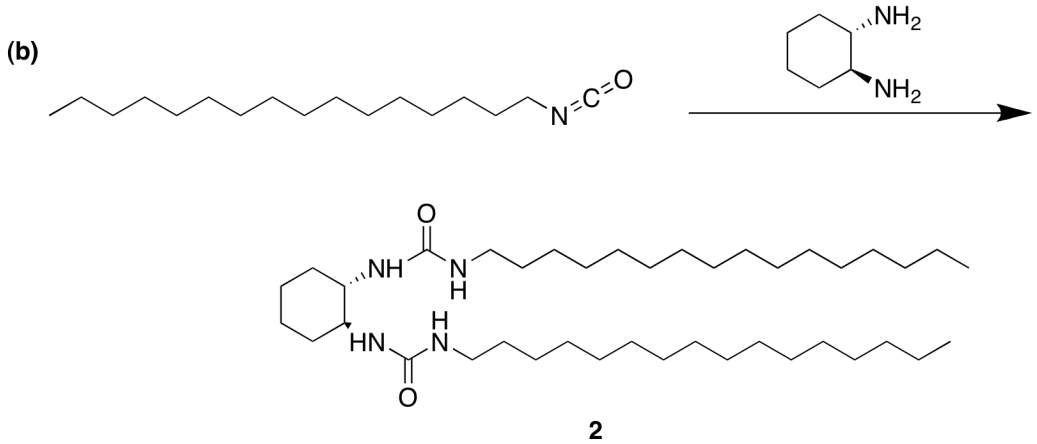

Scheme 8.3. Synthesis of (a) the linear gelator **1** and (b) the cyclohexane-based gelator **2**.

The gelation behavior of the linear and cyclohexane-based gelators differed dramatically. Figure 8.9 shows the dry powder of gelator **1** and a gel formed from 0.5 wt% gelator in chloroform. Although the gelators dissolved and formed gels at room temperature, the solutions were heated above the dissociation temperature and cooled back to room temperature to ensure homogenous gel formation. Table 8.1 lists the solvents gelled by each gelator. The cyclohexane-based gelator (**2**) successfully gelled many polar and nonpolar organic solvents, while the linear gelator (**1**) did not gel many polar organic solvents. In three cases, the addition

of small amounts of chloroform to promote the dissolution of the gelators helped promote the formation of the physical network.

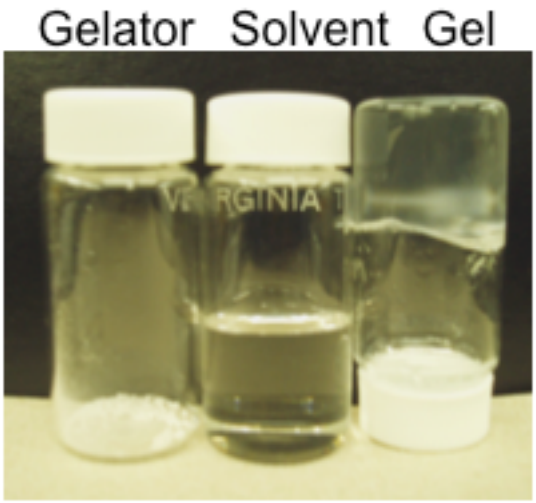

Figure 8.9. Gelation of chloroform by linear gelator **1**. The dried gelator powder is on the right, pure chloroform solvent is in the middle, and a gel formed from 0.5 wt% gelator in chloroform is on the right.

Table 8.1. Gelation of Solvents by Linear and Cyclohexane-Based Gelators

Solvent	Linear Gelator	Cyclohexane Gelator
Chloroform	+	+
DMF	-	+ (with $CHCl_3$)
Toluene	-	+
Acetone	-	-
THF	-	+
Benzene	-	+
2-Butanol	-	+
DMSO	-	+
Isopropanol	-	+
1-Hexanol	+ (with $CHCl_3$)	+
Ethanol	-	+
p-Xylene	+ (with $CHCl_3$)	+

The gels of each gelator were electrospun; gelator **1** was electrospun from a 15 wt% solution in 50/50 1-hexanol/chloroform and gelator **2** from 0.5 wt% in toluene. The solvent systems were optimized so the solvent did not evaporate too quickly during electrospinning. In both cases, no fiber formation occurred and only a film collected on the target. Figure 8.10 shows FESEM micrographs of the two electrospun gelators. In each case, the gel broke into droplets of microgels which deposited as a film during electrospinning. The fibrous structure in the FESEM micrographs respresents the self-assembled gelator strands rather than individual electrospun fibers. The inability of the gels to flow prevented electrospinning. However, the cyclohexane-based gelator formed a viscous dispersion at 4 wt% in 2-butanol. The aggregation was not sufficient to gel the solvent, but the gelator did significantly increase the viscosity. This dispersion successfully electrospun to form large, irregular fibers as depicted in the micrograph in Figure 8.11. The fibers appeared irregular with a surface morphology similar to their solution structure. This is the first example of self-supporting electrospun fibers from gelators.

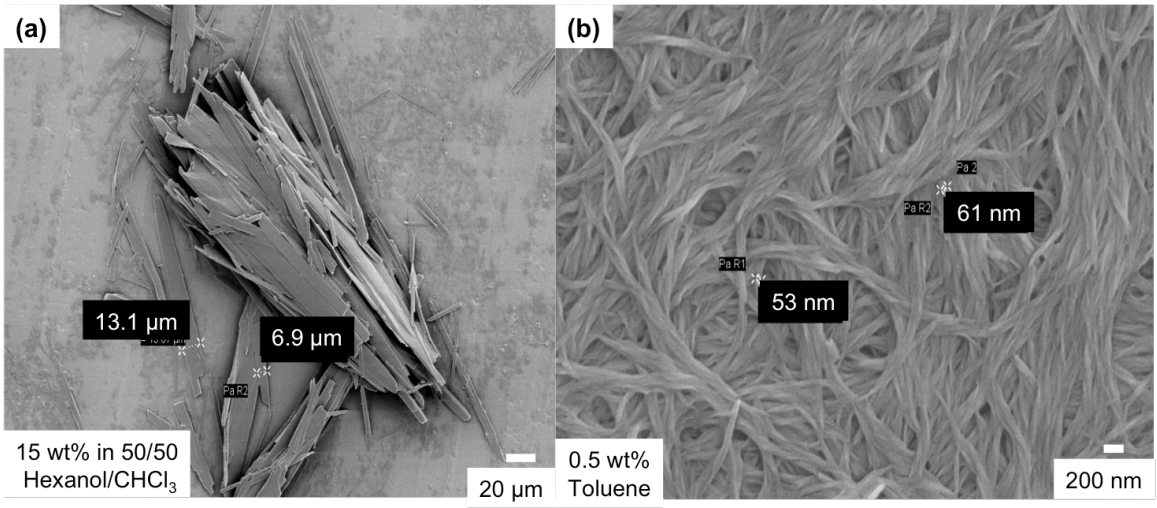

Figure 8.10. FESEM micrographs of (a) gelator **1** electrospun from 1-hexanol/CHCl3 and (b) gelator **2** electrospun from toluene.

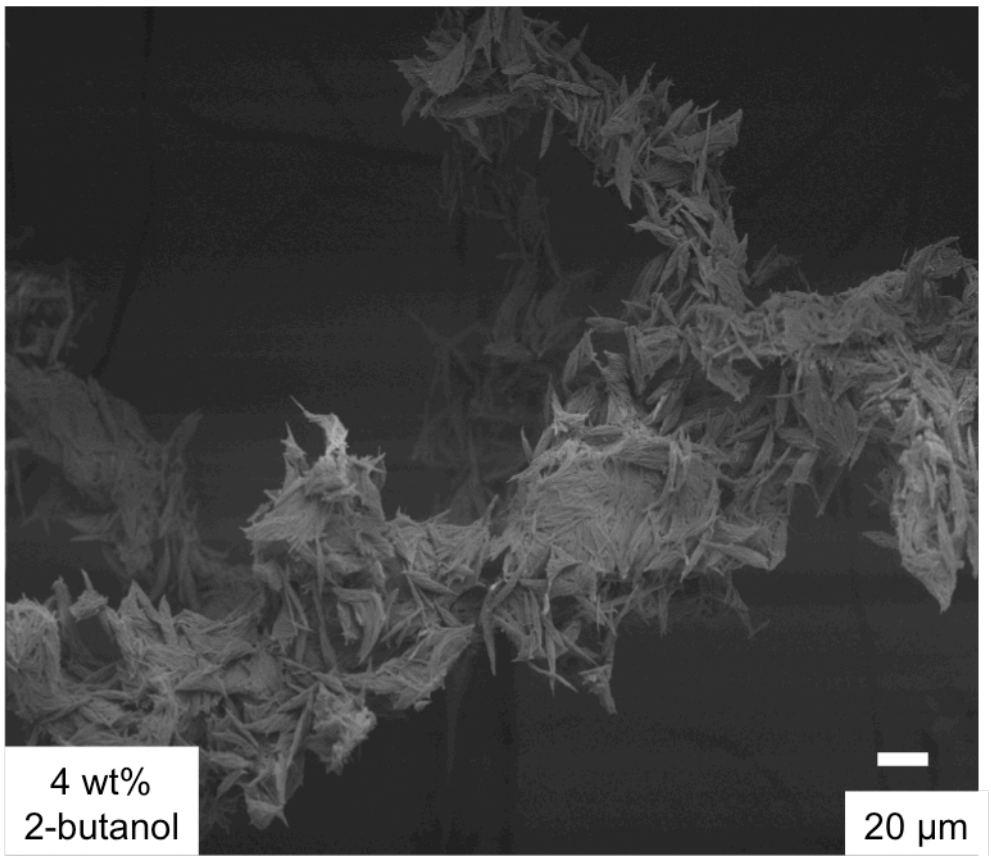

Figure 8.11. FESEM micrographs of the cyclohexane-based gelator **2** electrospun from a dispersion in 2-butanol.

8.4.4 Effect of Added Surfactant on Electrospinning of PMMA

The previous sections presented the electrospinning of fibers composed wholly of low molar mass surfactants. Surface-active additives in low concentrations can also facilitate the electrospinning of neutral polymers. Our laboratories recently reported the electrospinning of PMMA fibers with a perfluorinated surface-migrating additive.[37] The additive reduced the surface tension of the electrospinning solutions, resulting in a suppression of beaded fibers at low concentrations. The additive also selectively migrated to the fiber surface, creating a core-shell type morphology with PMMA as the core and the perfluorinated additive as the shell. Supaphol et al.[38] found the addition of sodium dodecyl sulfate (SDS) to PEO solutions reduced the occurrence of beads during electrospinning and helped form uniform fibers at much lower concentrations. Wnek et al.[18] reported that stable electrospinning requires that electrical forces

exceed the surface forces (primarily the surface tension). Surfactants decrease surface tension, preventing capillary breakup of the electrospinning jet at lower polymer concentrations. In addition, charged surfactants increase solution conductivity, thereby increasing the electrical forces acting on the electrospinning jet. The combination of both effects leads to stable fiber formation at lower polymer concentrations.

To determine the effect of surfactant on poly(methyl methacrylate) (PMMA) flow behavior and electrospinning, we added CTAB (Scheme 8.1) to solutions of PMMA in 4:1 DMF:THF. Two different PMMA samples of 571,000 and 366,000 g/mol were used to examine the influence of molecular weight. Figure 8.12 shows the zero-shear viscosity versus concentration for 571K-PMMA solutions with no added CTAB, 1.0 mM CTAB, and 1:0.01 PMMA:CTAB ratio. The flow behavior for all three series was identical. The critical concentration for entanglements, c_e, was identified at around 6 wt% for 571K-PMMA and 9 wt% for 366K-PMMA.

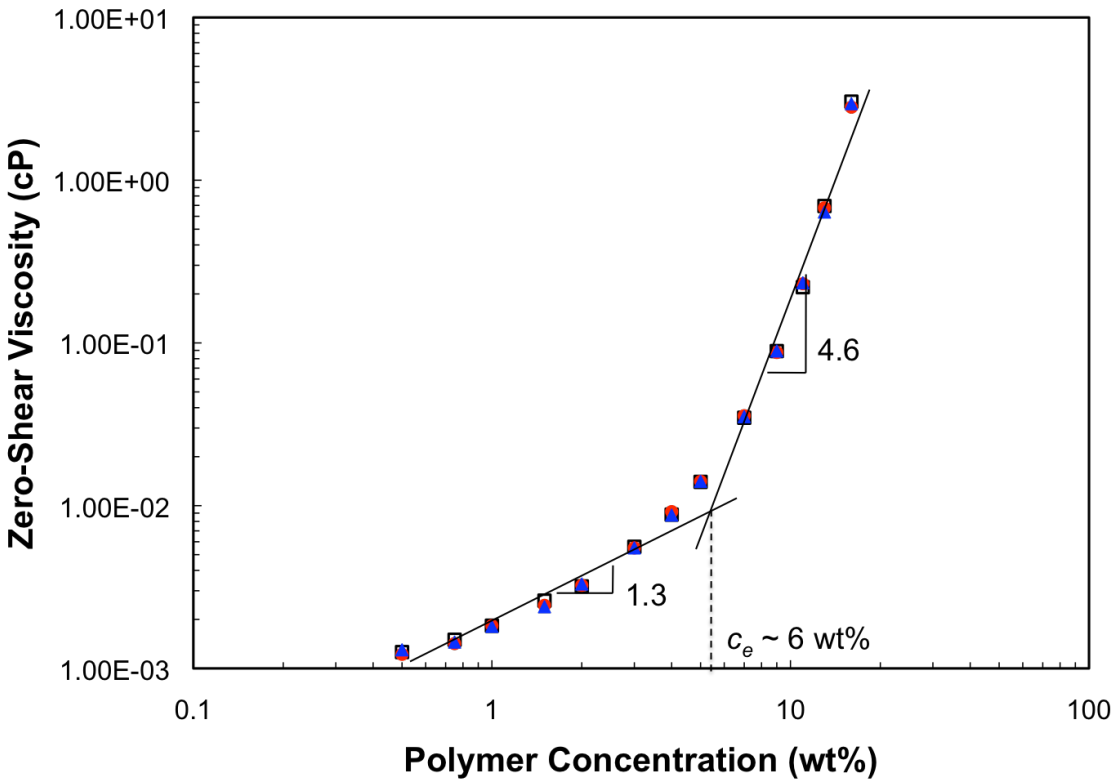

Figure 8.12. Zero-shear viscosity as a function of polymer concentration for 571K-PMMA with (squares) 0 M CTAB, (circles) 1 mM CTAB, and (triangles) 1:0.01 PMMA:CTAB ratio.

Figure 8.13 shows FESEM micrographs of 571K-PMMA electrospun at various concentrations and various CTAB concentrations. Pure PMMA exhibited an onset of fiber formation at 2 wt%, significantly lower than the c_e of 6 wt%. Previous studies reported that polymers of very high molecular weight can electrospin at concentrations below entanglement due to the significantly higher relaxation times.[18,24] The time required for longer polymer chains to disentangle, even at very low levels of solution entanglement, exceeds the electrospinning time scale, resulting in stabilization of the electrospinning jet below the entanglement concentration. The presence of CTAB enabled electrospinning of PMMA at significantly lower polymer concentrations and entanglement numbers. Table 8.2 summarizes the onset of fiber formation and onset of uniform fiber formation for both PMMA molecular weights both with varying amounts of CTAB. The onset of fiber formation for 571K-PMMA corresponded to

number of entanglements per chain (n_e) of 0.64. Theoretical and semi-empirical correlations predict the onset of fiber formation above $n_e = 2.0$ (about $c = c_e$).[17,18] In the presence of CTAB at 0.5 and 1.0 mM, the onset of electrospinning occurred at $n_e < 0.32$. For 366K-PMMA, the onsets of fiber formation in the absence of CTAB and with 1 mM CTAB were 1.4 and 0.45, again suggesting CTAB facilitated electrospinning. In addition, fewer beads were observed in the presence of CTAB, as the surfactant significantly lowers the solution surface tension.

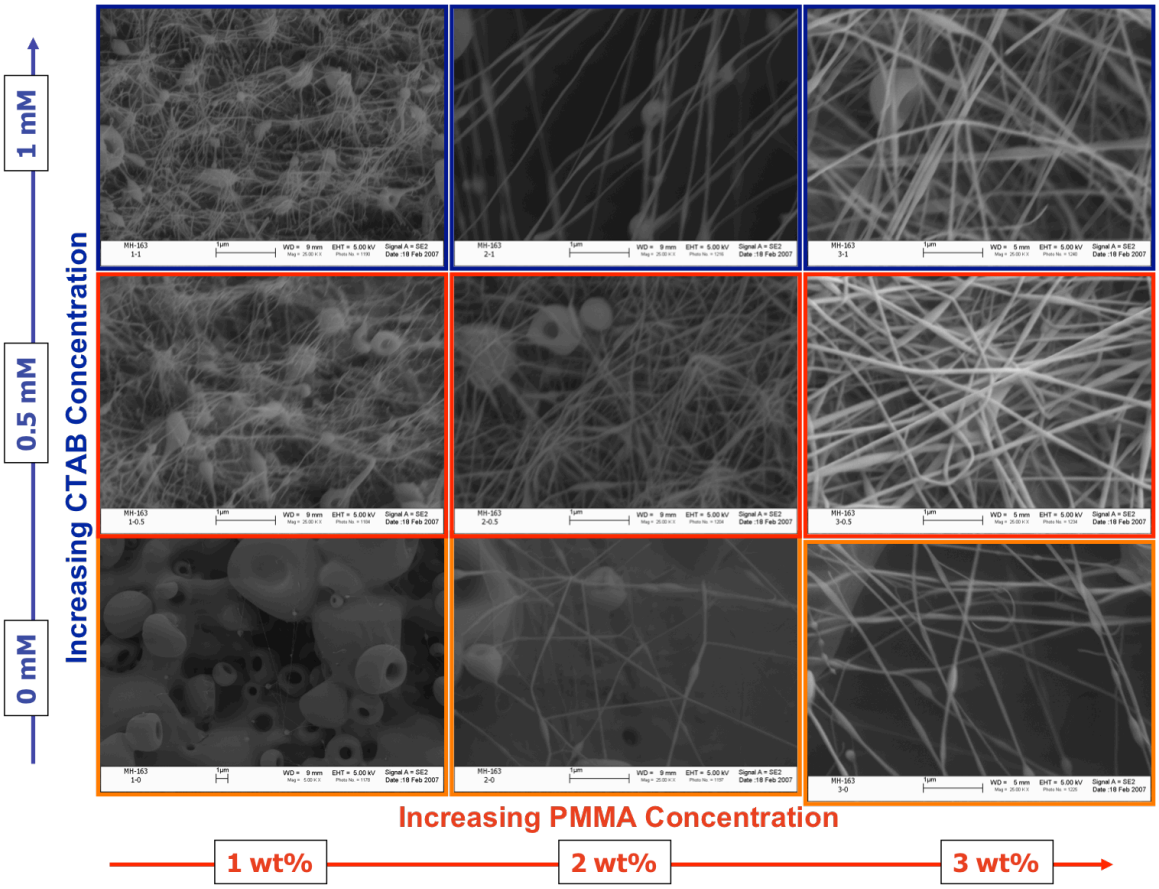

Figure 8.13. FESEM micrographs of electrospun PMMA fibers electrospun from 4:1 DMF:THF with low levels of added CTAB. The scale bar represents 1 μm in all images.

Table 8.2. Electrospinning transitions for PMMA with added CTAB.

PMMA M_w = 366 000 g/mol; M_w/M_n = 2.0			PMMA M_w = 571 000 g/mol; M_w/M_n = 2.3		
CTAB (mM)	n_e (onset)	n_e (uniform)	CTAB (mM)	n_e (onset)	n_e (uniform)
0	< 1.4	> 2.3	0	0.64	> 0.95
1.0	< 0.45	< 0.45	0.5	< 0.32	0.95
			1.0	< 0.32	0.64 – 0.95

8.5 Conclusions

Self-assembled aggregates of CTAB, organogelators, and phospholipids in the presence of water were electrospun. CTAB electrospun from highly viscous solutions below the transition to liquid crystalline phases. A cyclohexane-based gelator successfully electrospun fibers from a dispersion in 2-butanol, but electrospinning of the gels was unsuccessful since they did not flow. The addition of water to asolectin micelles led to branching and network formation, inhibiting electrospinning. In the presence of long flexible wormlike micelles, surfactant solutions could be electrospun. The disruption of those long flexible micelles by adding water to asolectin hindered electrospinning even with similar viscosities. The short, rod-like CTAB micelles cannot entangle to the same extent as the longer and more flexible micelles of asolectin or 12-2-12 gemini surfactant, and uniform fiber formation was difficult. These results suggest the electrospinnability of wormlike micelles can be predicted if one knows the length of the wormlike micelles. This mirrors predictions in the literature correlating the molecular weight of polymers with the concentration for the onset of electrospinning.[17,18,39] Future experiments should focus on directly correlating micelle length and electrospinnability by probing micelle size within entangled solutions, as well as comparing the relaxation times of wormlike micelle solutions with polymer solutions.

In addition, high molecular weight PMMA was electrospun in the presence of CTAB. The surfactant decreased the polymer concentration required for stable fiber formation. Through modification of solution surface tension and conductivity, the concentration window for electrospinning PMMA was increased to very low concentrations. These results demonstrate that the surface-active properties of surfactants can also be harnessed to facilitate the electrospinning of polymer nanofibers well below significant entanglements within solution.

This technique can hopefully be used to electrospin uniform fibers with diameters less than 10 nm.

8.6 Acknowledgements

This material is based upon work supported by the U.S. Army Research Laboratory and the U.S. Army Research Office under grants DAAD19-02-1-0275 Macromolecular Architecture for Performance Multidisciplinary University Research Initiative (MAP MURI) and W911NF-07-1-0452 Ionic Liquids in Electro-Active Devices (ILEAD) MURI.

8.7 References

1. Lagerwall, J. P. F.; McCann, J. T.; Formo, E.; Scalia, G.; Xia, Y. *Chemical Communications* **2008,** *42*, 5420-5422.
2. Ma, M.; Thomas, E. L.; Rutledge, G. C.; Yu, B.; Li, B.; Jin, Q.; Ding, D.; Shi, A.-C. *Macromolecules* **2010,** *43*, 3061-3071.
3. Reddy, C. S.; Arinstein, A.; Avrahami, R.; Zussman, E. *Journal of Materials Chemistry* **2009,** *19*, 7198-7201.
4. Hunley, M. T.; Poetschke, P.; Long, T. E. *Macromolecular Rapid Communications* **2009,** *30*, 2102-2106.
5. Xie, J.; MacEwan, M. R.; Schwartz, A. G.; Xia, Y. *Nanoscale* **2010,** *2*, 35-44.
6. Hunley, M. T.; England, J. P.; Long, T. E. **2010**.
7. McKee, M. G.; Hunley, M. T.; Layman, J. M.; Long, T. E. *Macromolecules* **2006,** *39*, 575-583.
8. Ohkawa, K.; Minato, K.-I.; Kumagai, G.; Hayashi, S.; Yamamoto, H. *Biomacromolecules* **2006,** *7*, 3291-3294.
9. Chronakis, I. S.; Milosevic, B.; Frenot, A.; Ye, L. *Macromolecules* **2006,** *39*, 357-361.
10. Yoshimatsu, K.; Ye, L.; Lindberg, J.; Chronakis, I. S. *Biosensors & Bioelectronics* **2008,** *23*, 1208-1215.
11. Agarwal, S.; Wendorff, J. H.; Greiner, A. *Advanced Materials* **2009,** *21*, 3343-3351.
12. Lee, J. Y.; Bashur, C. A.; Goldstein, A. S.; Schmidt, C. E. *Biomaterials* **2009,** *30*, 4325-4335.
13. Casper, C. L.; Yang, W.; Farach-Carson, M. C.; Rabolt, J. F. *Biomacromolecules* **2007,** *8*, 1116-1123.
14. McKee, M. G.; Layman, J. M.; Cashion, M. P.; Long, T. E. *Science (Washington, DC, U. S.)* **2006,** *311*, 353-355.
15. Cashion, M. P.; Li, X.; Geng, Y.; Hunley, M. T.; Long, T. E. *Langmuir* **2010,** *26*, 678-683.
16. Hunley, M. T.; Karikari, A. S.; McKee, M. G.; Mather, B. D.; Layman, J. M.; Fornof, A. R.; Long, T. E. *Macromolecular Symposia* **2008,** *270*, 1-7.
17. McKee, M. G.; Wilkes, G. L.; Colby, R. H.; Long, T. E. *Macromolecules* **2004,** *37*, 1760-1767.

18. Shenoy, S. L.; Bates, W. D.; Frisch, H. L.; Wnek, G. E. *Polymer* **2005,** *46*, 3372-3384.
19. Dreiss, C. A. *Soft Matter* **2007,** *3*, 956-970.
20. Magid, L. J. *Journal of Physical Chemistry B* **1998,** *102*, 4064-4074.
21. Cappelaere, E.; Cressely, R.; Decruppe, J. P. *Colloids and Surfaces A: Physicochemical and Engineering Aspects* **1995,** *104*, 353-374.
22. Nazir, N.; Ahanger, M. S.; Akbar, A. *Journal of Dispersion Science and Technology* **2009,** *30*, 51-55.
23. Porcar, L.; Hamilton, W. A.; Butler, P. D.; Warr, G. G. *Langmuir* **2003,** *19*, 10779-10794.
24. Yu, J. H.; Fridrikh, S. V.; Rutledge, G. C. *Polymer* **2006,** *47*, 4789-4797.
25. Jerke, G.; Pedersen, J. S.; Egelhaaf, S. U.; Schurtenberger, P. *Phys. Rev. E: Stat. Phys., Plasmas, Fluids, Relat. Interdiscip. Top.* **1997,** *56*, 5772-5788.
26. Kern, F.; Lequeux, F.; Zana, R.; Candau, S. J. *Langmuir* **1994,** *10*, 1714-1723.
27. Hunley, M. T.; McKee, M. G.; Long, T. E. *Journal of Materials Chemistry* **2007,** *17*, 605-608.
28. Shchipunov, Y. A.; Hoffmann, H. *Rheologica Acta* **2000,** *39*, 542-553.
29. de, L. M.; Feringa, B. L.; van, E. J. H. *Eur. J. Org. Chem.* **2005**, 3615-3631.
30. Vintiloiu, A.; Leroux, J.-C. *J. Controlled Release* **2008,** *125*, 179-192.
31. Melendez, R. E.; Carr, A. J.; Sada, K.; Hamilton, A. D. *Mater. Res. Soc. Symp. Proc.* **2000,** *604*, 335-340.
32. Suzuki, M.; Hanabusa, K. *Chem. Soc. Rev.* **2010,** *39*, 455-463.
33. Hanabusa, K.; Shimura, K.; Hirose, K.; Kimura, M.; Shirai, H. *Chemistry Letters* **1996,** *1996*, 885.
34. van Esch, J.; De Feyter, S.; Kellogg, R. M.; De Schryver, F.; Feringa, B. L. *Chemistry - A European Journal* **1997,** *3*, 1238-1243.
35. Suzuki, M.; Hanabusa, K. *Chem. Soc. Rev.* **2009,** *38*, 967-975.
36. Suzuki, M.; Nanbu, M.; Yumoto, M.; Shirai, H.; Hanabusa, K. *New Journal of Chemistry* **2005,** *29*, 1439-1444.
37. Hunley, M. T.; Harber, A.; Orlicki, J. A.; Rawlett, A. M.; Long, T. E. *Langmuir* **2008,** *24*, 654-657.
38. Arayanarakul, K.; Choktaweesap, N.; Aht-ong, D.; Meechaisue, C.; Supaphol, P. *Macromol. Mater. Eng.* **2006,** *291*, 581-591.
39. Gupta, P.; Elkins, C.; Long, T. E.; Wilkes, G. L. *Polymer* **2005,** *46*, 4799-4810.

Chapter 9: Effect of Hyperbranched Surface-Migrating Additives on the Electrospinning Behavior of Poly(methyl methacrylate)

(From: Hunley, M.T.; Harber, A.; Orlicki, J.A.; Rawlett, A.M.; Long, T.E. *Langmuir* **2008**, *24*, 654-657.)

9.1 Abstract

Poly(methyl methacrylate) (PMMA) was electrospun in the presence of a low molecular weight, hyperbranched poly(ethylene imine) additive partially functionalized with perfluorinated and aliphatic end-groups (M_n ~ 1600 g/mol). The additive exhibited surface segregation with an insignificant influence on the rheological behavior of PMMA solutions. A morphological transition from beaded electrospun fibers to uniform fibers was observed upon introduction of additive at low PMMA concentrations. XPS revealed a surface enrichment of fluorine and nitrogen, which are both present in the hyperbranched additive. Surface fluorine content depended primarily on the amount of additive in solution, and a dependency on the PMMA/additive weight ratio was not observed.

9.2 Introduction

Electrospinning has regained popularity as a simple, cost-effective technique to produce nanofibers and fibrous scaffolds.[1-5] Non-woven scaffolds that are produced via electrospinning offer high surface areas and porosities, and have shown applicability for high performance tissue engineering scaffolds,[6-8] drug delivery membranes,[9,10] sensors,[9,11,12] and filters,[13] among many other applications.

In electrospinning, polymer solutions of sufficient viscosity are metered through a capillary and subjected to high electric potential (typically 10-30 kV). The large potential causes droplets of solution to elongate and ultimately accelerate toward a grounded or oppositely charged collector. For viscous, entangled polymer solutions, the droplet stretches into a thin

filament or jet as it approaches the target. During flight, solvent evaporates quickly from the jet, reducing its diameter and increasing the charge density on the surface. At a critical surface charge density, the jet undergoes a "bending instability," resulting in chaotic whipping and stretching of the polymer jet before ultimate deposition on the grounded target. In this simple process, electrospinning typically produces uniform fibers ranging in diameter from tens of nanometers to tens of micrometers.

The large surface area of electrospun nanofibrous membranes enables many biomedical applications, including sensing, tissue scaffolds, and controlled release fabrics. Surface functionalization of nanofibers has also received recent attention.[14-16] For example, Kim et al.[15] modified electrospun poly(lactic acid-*co*-glycolic acid)-*block*-poly(ethylene glycol) scaffolds by covalently attaching lysozyme enzyme. These surface modified scaffolds showed significantly greater affinity for separating lysozyme from complex mixtures than the corresponding cast films, presumably due in part to porosity and higher surface areas. Yang et al.[17] electrospun polyacrylonitrile containing pendant glucose rings.[17] Similarly, these nanofibrous "sugar sticks" demonstrated great affinity for separating concanavalin A protein from binary protein mixtures. Sun et al.[18] demonstrated that polar oligopeptide sequences that were covalently bound to a host polymer migrated to the fiber surface during electrospinning. Similarly, self-complementary hydrogen-bonding groups were observed to migrate to the fiber surface of PMMA copolymers.[16] Deitzel et al.[19] investigated the surface segregation of fluorine in electrospun fibers of random copolymers of methyl methacrylate and tetrahydroperfluoroctyl acrylate. Atomic fluorine contents at the beaded fiber surface were two to three times higher than bulk fluorine content, and were comparable to surface fluorine content in solution cast films of the same copolymers. Electrospun fibers have also demonstrated unexpected hydrophobicity and superhydrophobicity,

even for hydrophilic polymers,[20-22] with water contact angles greater than 150°.[21]

Hyperbranched polymers (HBPs) represent a facile method to functionalize polymer surfaces due to their intrinsic ability for surface migration. In addition, the HBPs can also be modified with surface active end-groups to promote further surface migration. Previously, a poly(ethylene imine) additive functionalized with perfluorinated and aliphatic end-groups was shown to coordinate with polyoxometalates and migrate the complex to the surface of a polymer film.[23] Earlier research efforts have not investigated the surface migration of hyperbranched surface-active additives during an electrospinning process. Such additives could lead to single-step formation and surface-modification of electrospun fibers. We report herein on the electrospinning of poly(methyl methacrylate) nanofibers in the presence of the same additive, and investigations on the self-stratifying abilities of this additive during the rapid electrospinning process.

9.3 Experimental Section

9.3.1 Materials

Poly(methyl methacrylate) was obtained from Sigma-Aldrich. GPC analysis with polystyrene standards revealed M_w = 366 kg/mol and M_w/M_n = 2.0. Tetrahydrofuran (THF) and *N*,*N*-dimethylformamide (DMF) were used as solvents without further purification. The low molecular weight, hyperbranched, end-perfluorinated and alkylated polyethyleneimine additive (PFA) was synthesized as previously reported[23] at the Army Research Laboratory, Aberdeen Proving Ground, MD, and used as received.

9.3.2 Electrospinning and Fiber Characterization

Electrospinning solutions were prepared at the desired concentrations in glass scintillation vials and mixed for 24 h prior to electrospinning. The electrospinning apparatus

consisted of a high-voltage power supply (Spellman CZE-1000R), a syringe pump (KD Scientific), a grounded target (stainless steel mesh), and an acrylic housing to reduce the effect of outside air currents. Electrospinning was conducted at ambient conditions. The solution was transferred to a syringe equipped with a stainless steel, 18-gauge needle. The syringe was placed in the syringe pump and solution metered at 3 mL/h. The positive lead of the high-voltage power supply was connected to the syringe needle and potential increased to 25 kV. Fibers collected on the grounded target 15 cm away. For microscopy, a LEO 1550 field emission scanning electron microscope (FESEM) was used with an accelerating voltage of 5 kV. At least 20 individual fibers were measured using the SEM software to determine average fiber diameters and standard deviations. X-ray photoelectron spectroscopy (XPS) was conducted on a Perkin-Elmer 5300 with a Mg anode at 13 kV accelerating voltage. For conservative estimates, the atomic compositions calculated from XPS measurements were assumed to have (5% error, which is reflected in the error bars on plots of atomic fluorine to carbon ratios.

9.3.3 Silver Nanoparticle Complexation

Silver nanoparticles were prepared according to a literature procedure.[24] Swatches of electrospun fibers were secured between steel mesh and submersed into nanoparticle dispersions (0.59 mg/mL) in hexanes for 10 min. The fibers were dried at room temperature for 15 min, then washed five times with 15 mL of hexanes (5 min incubation in each wash solution). After the final wash, the fibers were dried at room temperature for 90 min.

9.4 Results and Discussion

Solution properties, such as concentration, rheology, conductivity, surface tension, and solvent volatility, play an important role in determining electrospun fiber morphology and diameter.[25-27] The critical concentration for entanglements, c_e, is regarded as an estimate for the

onset of fiber formation for non-associating polymers, above which beaded fibers form, and uniform fibers form at concentrations approaching $2c_e$. PMMA has been shown to undergo electrospinning over a wide range of concentrations depending on molecular weight and solvent.[28,29] Solutions of PMMA with M_w = 366 kg/mol were prepared from 6 to 16 wt% polymer in a 3:1 DMF:THF solvent mixture. Figure 9.1 shows FESEM images of the electrospun PMMA fibers (in the absence of additive). At 6 wt % PMMA, (below c_e) fibers with many polymer droplets were observed. Beaded fibers were obtained at 8 wt % (C = c_e), which became uniform fibers at higher concentrations. It was observed that fibers (albeit fibers with many droplets and beads) formed at concentrations below c_e, possibly due to the exceptionally high molecular weight of the PMMA. It has been proposed that the increased relaxation times of longer polymer chains stabilize the electrospinning jet at reduced levels of entanglement, allowing fiber formation at lower concentrations.[26] In other words, longer polymer chains require more time to disentangle, and because electrospinning occurs over such a short time scale, even slightly entangled high molecular weight polymers could remain entangled long enough to form fibers. Similar behavior has been observed with high molecular weight poly(L-lactide).[30]

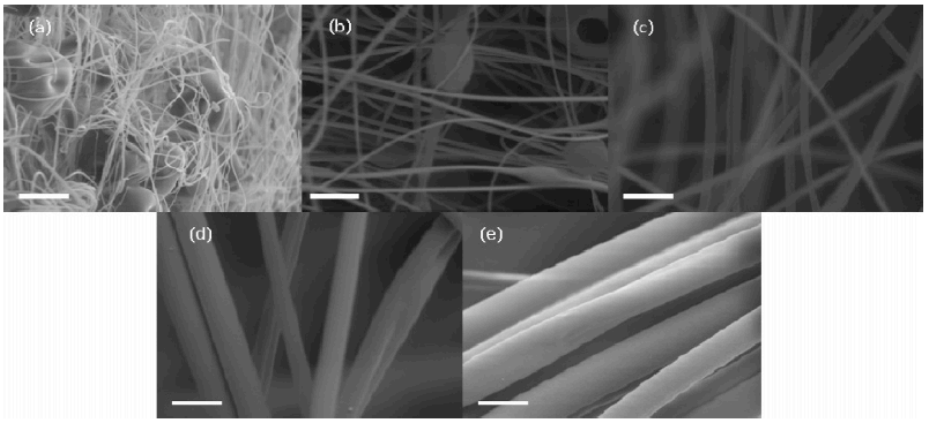

Figure 9.1. SEM images of PMMA fibers electrospun from solutions at concentrations of (a) 6 wt%, (b) 8 wt%, (c) 10 wt%, (d) 13 wt%, and (e) 16 wt%. Fiber and droplets are observed at 6 wt%, leading to beaded fibers at 8 wt%. Uniform fibers are observed at concentrations above 8 wt%. Scale bar equal to 10 μm.

In order to investigate the effects of PFA additive on the electrospinning process and surface fluorine enrichment, PMMA-PFA fibers were electrospun from solutions of 13 wt % PMMA with varying amounts of additive. PFA content ranged from 0 to 10 wt % with respect to PMMA. Droplets of PMMA-PFA solution on Teflon tape were analyzed for contact angles, shown in Figure 9.2. This qualitative measurement of surface tension showed a steady decrease in contact angle up to 6 wt% additive, after which a plateau value was reached. The results indicated that the PFA fully saturates the surface at approximately 6 wt% additive, and solution surface properties should remain constant above this concentration.

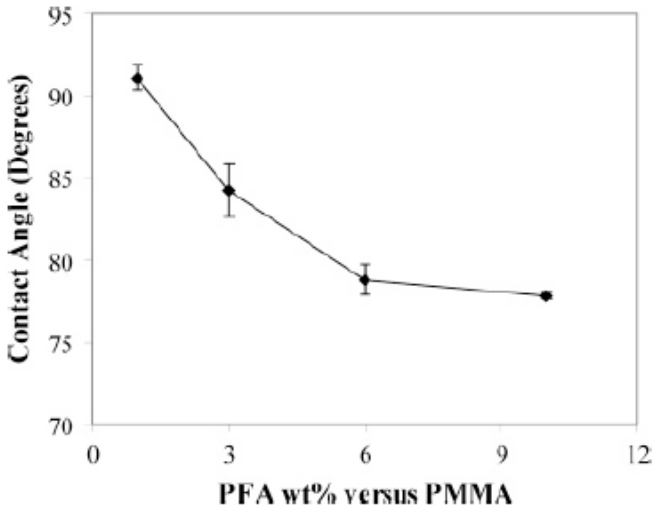

Figure 9.2. Contact angles for droplets of PMMA-PFA solution on Teflon surface. PMMA concentration in solution remained constant at 13 wt %, while PFA concentration varied with respect to PMMA.

XPS analysis of the electrospun PMMA-PFA fibers indicated similar surface saturation of fluorine above 3 wt % additive, as shown in Figure 9.3. An initial steady increase in surface fluorine was observed at lower concentrations of additive, which plateaued and decreased slightly at higher additive concentrations. The observed fluorine levels were approximately 2 orders of magnitude greater than expected if PFA distributed uniformly through the bulk of the

fibers. Elemental analysis of pure PFA yielded a fluorine-to-carbon (F/C) ratio of 0.27, which indicated that the fiber surfaces were primarily composed of PFA. Nitrogen levels at the surface also increased consistently with surface fluorine levels, which suggested that the entire additive molecules migrated to the fiber surface rather than the end groups alone. Figure 9.4 shows fiber diameter versus PFA wt%, and no significant influence of additive concentration on fiber diameter was observed.

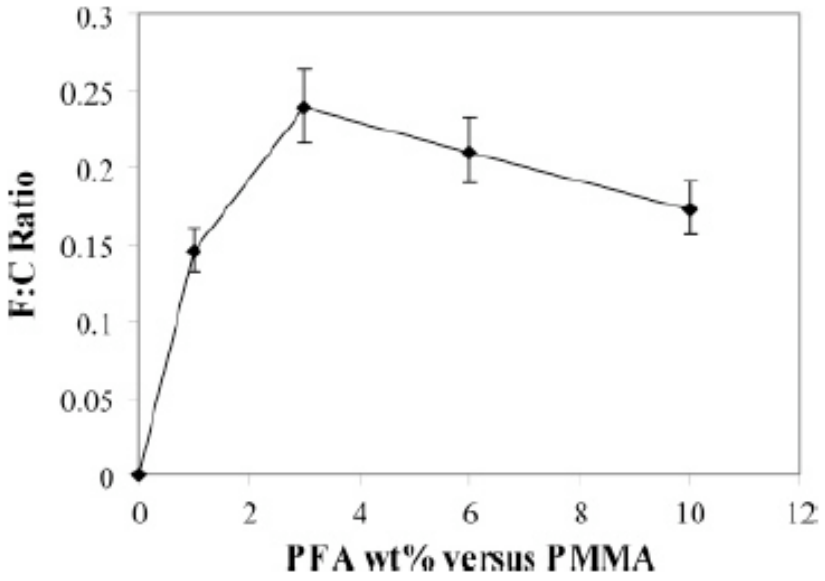

Figure 9.3. Fluorine to carbon ratio for PMMA-PFA fibers with varying PFA content. PMMA concentration in solution remained constant at 13 wt %, while PFA concentration varied with respect to PMMA.

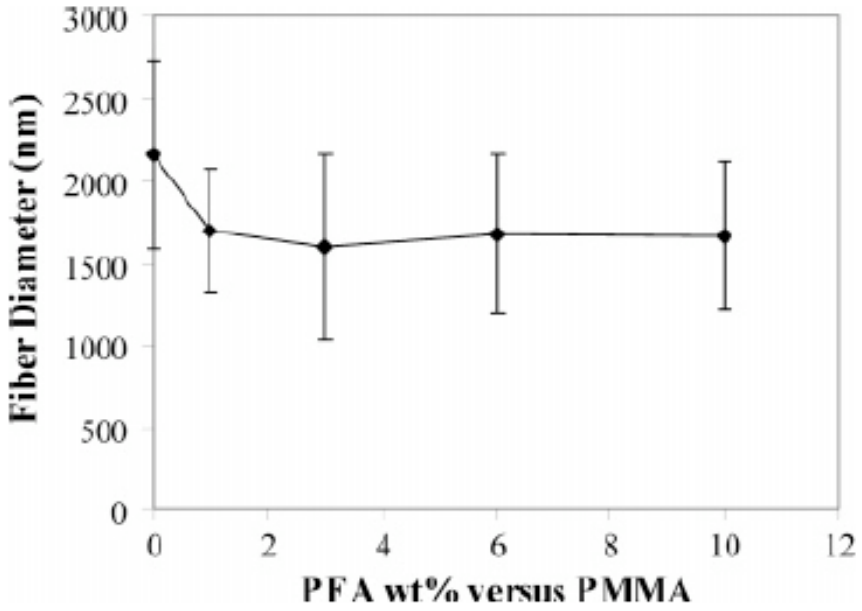

Figure 9.4. Fiber diameter versus PFA concentration for PMMA-PFA fibers. PMMA concentration in solution remained constant at 13 wt%, while PFA concentration varied with respect to PMMA.

Solutions of PMMA and PFA were prepared with varying PMMA concentrations and a constant PMMA-to-PFA ratio to investigate the effect of PFA on fiber morphology. The additive level in each solution remained constant at 1 wt% with respect to PMMA, while PMMA concentration was varied from 6 to 16 wt%. SEM images of the electrospun PMMA-PFA fibers are shown in Figure 9.5. At all PMMA concentrations, even below c_e, uniform fibers formed with no observed droplets or beaded fibers. Other researchers have observed similar bead suppression upon addition of ionic and nonionic surfactants.[31,32] It is believed that reduced surface tension decreases the forces counteracting electrostatic repulsions in the electrospinning jet, generating less tendency to contract into beads or droplets and leading to more uniform fibers. Fiber diameters for the PMMA-PFA fibers at varying PMMA concentrations are compared in Figure 9.6 to fibers containing no additive. No difference was observed in diameter between the PMMA and PMMA-PFA fibers, within one standard deviation.

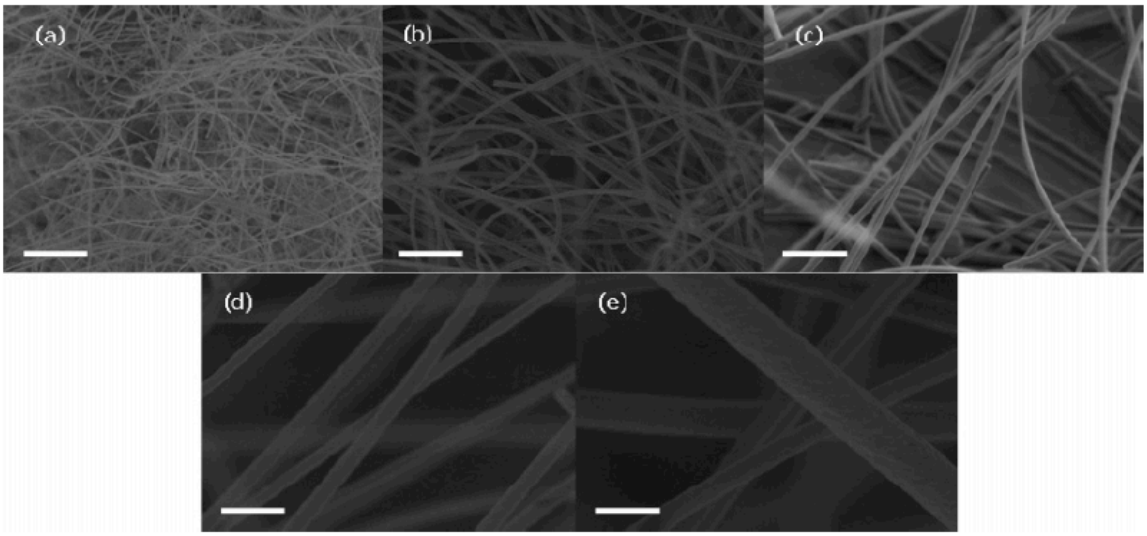

Figure 9.5. SEM images of PMMA-PFA fibers electrospun from solutions at PMMA concentrations of (a) 6 wt%, (b) 8 wt%, (c) 10 wt%, (d) 13 wt%, and (e) 16 wt%. PFA concentration remained constant at 1 wt % with respect to PMMA. Uniform fibers are observed at all concentrations. Scale bar equal to 10 μm.

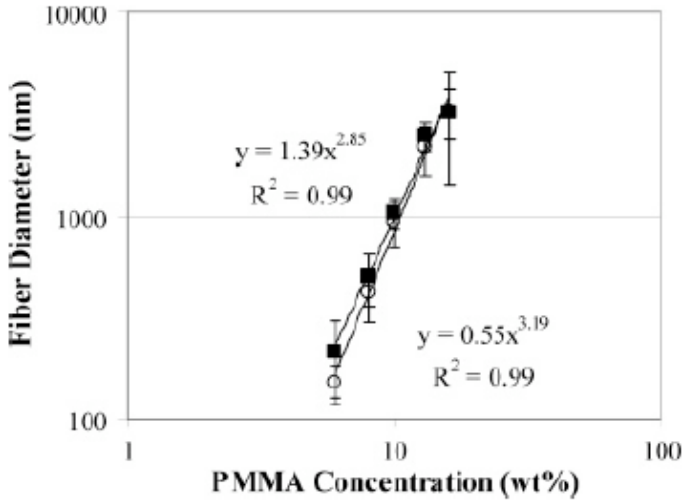

Figure 9.6. Fiber diameter versus PMMA solution concentration for PMMA (circles) and PMMA-PFA (squares) fibers. A power-law fit with the scaling exponent is also shown for each data series.

XPS analysis of the PMMA-PFA fibers further demonstrated the surface segregation of the additive. Figure 9.7 shows F/C ratios versus solution PMMA concentration, determined from XPS analysis. The overall ratio of PMMA to PFA remained constant at all PMMA

concentrations in solution. For a homogeneously distributed additive, the expected surface concentration would also remain constant. However, a sharp dependence of surface fluorine levels on solution concentration was observed for PMMA concentrations below 13 wt%. The plateau in surface F/C ratio above 13 wt% PMMA indicated surface saturation to thicknesses greater than the XPS penetration depth. Regardless of concentration, fluorine levels at the surface were again orders of magnitude above those estimated for uniform distributions of PFA within the fibers. Nitrogen concentrations at the surface were also observed at increasing levels that were consistent with surface fluorine.

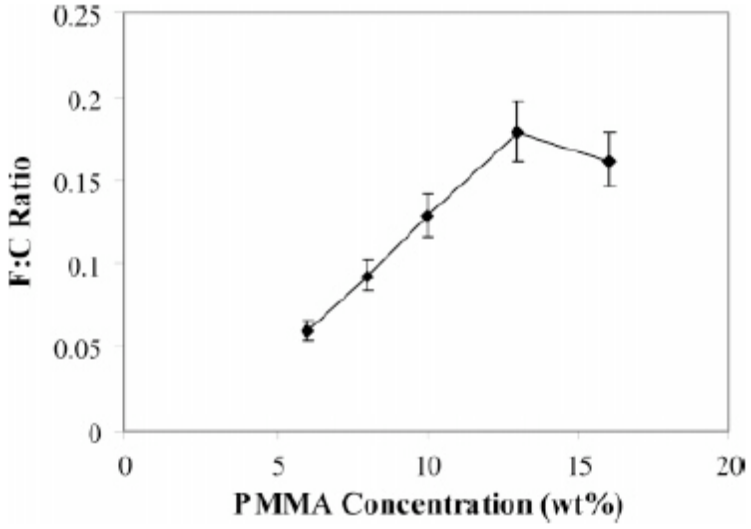

Figure 9.7. Fluorine to carbon ratio for PMMA-PFA fiber surfaces. F/C values are plotted versus PMMA solution concentration. PFA concentration remained constant at 1 wt% with respect to PMMA.

Electrospun PMMA-PFA fibers were exposed to silver nanoparticles dispersed in hexanes to test the adsorption ability of the incorporated hyperbranched additives. Previous work has demonstrated that these additives adsorb silver nanoparticles onto the surface of polyurethane films.[33] Fibers with 0 wt%, 1 wt%, and 5 wt% additive were prepared and submersed in the nanoparticle dispersion. Elemental compositions determined from XPS analysis

of the fibers before and after exposure to silver are tabulated in Table 9.1. After exposure and five washes with hexanes, silver was observed on the fiber surface, depending on the level of PFA present. The presence of silver for additive-free fibers indicated that some nanoparticles might become physically trapped in the porous fiber mats. The significantly larger levels of silver when the PFA was present indicated that the silver preferentially adsorbed to the additive on the fiber surface. XPS also indicated an increase in carbon levels after Ag exposure for fibers with PFA. Since a similar increase was not observed in the oxygen levels, this carbon enrichment could have resulted from residual hexane solvent or oleylamine ligands that were functionalized to the Ag nanoparticles surface.

Table 9.1. Elemental Compositions from XPS of PMMA-PFA Fibers Before and After Exposure to Silver Nanoparticles

Additive	Before					After				
Level (wt%)	C	O	N	F	Ag	C	O	N	F	Ag
0	79.8	20.2				77.4	22.1			0.5
1	71.4	15.5	5.7	7.4		78.2	14.8	2.3	3.1	1.6
3	53.3	14.2	15.6	16.9		70.3	11.2	8.1	8.4	2.0

9.5 Conclusions

The partially perfluorinated hyperbranched polyethyleneimine additive (PFA) was observed to selectively segregate to the surface of electrospun PMMA nanofibers. PMMA fibers ranging from approximately 150 nm to 3 μm, depending on PMMA concentration, were electrospun with and without PFA. The amount of fluorine at the surface depended primarily on additive concentration. Surface F/C elemental ratios increased quickly with the amount of PFA in solution, and reached a plateau value between 0.2 and 0.25. The presence of PFA in solution suppressed beaded fiber formation at low PMMA concentrations. No additional change in fiber spinning behavior was observed upon addition of PFA. The presence of additive on the fiber surface allowed surface functionalization with silver nanoparticles. The ability to tailor surface

migration in electrospun nanofibers allows quick, one-step formation of surface-functionalized nanostructures. By tethering specific chemical functionalities to perfluorinated chains or other surface active additives, nanoscaffolds can be created with the mechanical properties of engineering plastics and high levels of surface functionality and molecular recognition.

9.6 Acknowledgements

We acknowledge Frank Cromer at VT and Wendy Kosik at ARL for their help in performing XPS analysis. This material is based upon work supported by, or in part by, the U.S. Army Research Laboratory and the U.S. Army Research Office under grant number DAAD19-02-1-0275 Macromolecular Architecture for Performance (MAP) MURI.

9.7 References

(1) Li, D.; Xia, Y. AdV. Mater. (Weinheim, Ger.) 2004, 16, 1151-1170.
(2) Reneker, D. H.; Fong, H. ACS Symp. Ser. 2006, 918, 1-6.
(3) McKee, M. G.; Layman, J. M.; Cashion, M. P.; Long, T. E. Science (Washington, DC) 2006, 311, 353-355.
(4) Hunley, M. T.; Long, T. E. Polym. Int., in press.
(5) Hunley, M. T.; McKee, M. G.; Long, T. E. J. Mater. Chem. 2007, 17, 605-608.
(6) Boudriot, U.; Dersch, R.; Greiner, A.; Wendorff, J. H. Artif. Organs 2006, 30, 785-792.
(7) Boland, E. D.; Pawlowski, K. J.; Barnes, C. P.; Simpson, D. G.; Wnek, G. E.; Bowlin, G. L. ACS Symp. Ser. 2006, 918, 188-204.
(8) Teo, W.-E.; He, W.; Ramakrishna, S. Biotechnol. J. 2006, 1, 918-929.
(9) Casper, C. L.; Yamaguchi, N.; Kiick, K. L.; Rabolt, J. F. Biomacromolecules 2005, 6, 1998-2007.
(10) Venugopal, J.; Ramakrishna, S. Appl. Biochem. Biotechnol. 2005, 125, 147-157.
(11) Dersch, R.; Steinhart, M.; Boudriot, U.; Greiner, A.; Wendorff, J. H. Polym. AdV. Technol. 2005, 16, 276-282.
(12) Greiner, A.; Wendorff, J. H.; Yarin, A. L.; Zussman, E. Appl. Microbiol. Biotechnol. 2006, 71, 387-393.
(13) Schreuder-Gibson, H. L.; Gibson, P. ACS Symp. Ser. 2006, 918, 121-136.
(14) Li, D.; McCann, J. T.; Xia, Y. Small 2005, 1, 83-86.
(15) Kim, T. G.; Park, T. G. Biotechnol. Prog. 2006, 22, 1108-1113.
(16) McKee, M. G.; Elkins, C. L.; Long, T. E. Polymer 2004, 45, 8705-8715.
(17) Yang, Q.; Wu, J.; Li, J.-J.; Hu, M.-X.; Xu, Z.-K. Macromol. Rapid Commun. 2006, 27, 1942-1948.
(18) Sun, X.-Y.; Shankar, R.; Borner, H. G.; Ghosh, T. K.; Spontak, R. J. AdV. Mater. (Weinheim, Ger.) 2007, 19, 87-91.

(19) Deitzel, J. M.; Kosik, W.; McKnight, S. H.; Beck Tan, N. C.; DeSimone, J. M.; Crette, S. Polymer 2002, 43, 1025-1029.
(20) Agarwal, S.; Horst, S.; Bognitzki, M. Macromol. Mater. Eng. 2006, 291, 592-601.
(21) Singh, A.; Steely, L.; Allcock, H. R. Langmuir 2005, 21, 11604-11607.
(22) Ma, M.; Hill, R. M.; Lowery, J. L.; Fridrikh, S. V.; Rutledge, G. C. Langmuir 2005, 21, 5549-5554.
(23) Orlicki, J. A.; Kosik, W. E.; Demaree, J. D.; Bratcher, M. S.; Jensen, R. E.; McKnight, S. H. Polymer 2007, 48, 2818-2826.
(24) Hiramatsu, H.; Osterloh, F. E. Chem. Mater. 2004, 16, 2509-2511.
(25) McKee, M. G.; Wilkes, G. L.; Colby, R. H.; Long, T. E. Macromolecules 2004, 37, 1760-1767.
(26) Shenoy, S. L.; Bates, W. D.; Frisch, H. L.; Wnek, G. E. Polymer 2005, 46, 3372-3384.
(27) McKee, M. G.; Hunley, M. T.; Layman, J. M.; Long, T. E. Macromolecules 2006, 39, 575-583.
(28) Gupta, P.; Elkins, C.; Long, T. E.; Wilkes, G. L. Polymer 2005, 46, 4799-4810.
(29) Piperno, S.; Lozzi, L.; Rastelli, R.; Passacantando, M.; Santucci, S. Appl. Surf. Sci. 2006, 252, 5583-5586.
(30) Jun, Z.; Hou, H.; Schaper, A.; Wendorff, J. H.; Greiner, A. e-Polymers 2003, paper no. 9.
(31) Lin, T.; Wang, H.; Wang, H.; Wang, X. Nanotechnology 2004, 15, 1375-1381.
(32) Arayanarakul, K.; Choktaweesap, N.; Aht-ong, D.; Meechaisue, C.; Supaphol, P. Macromol. Mater. Eng. 2006, 291, 581-591.
(33) Orlicki, J. A.; Rawlett, A. M.; Demaree, J. D.; Kosik, W. E.; McKnight, S. H. PMSE Prepr. 2005, 93, 1010-1011.

Chapter 10: Taking Advantage of Tailored Electrostatics and Complementary Hydrogen Bonding in the Design for Nanostructures of Biomedical Applications

(From: Hunley, M.T.; Karikari, A.S.; McKee, M.G.; Mather, B.D.; Layman, J.M.; Fornof, A.R.; Long, T.E. *Macrmol. Symp.* **2008**, *270*, 1-7.)

10.1 Summary

Four-armed, star-shaped poly(D,L-lactide) (PDLLA) was synthesized and terminally-functionalized with either adenine or thymine complementary hydrogen bonding groups (PDLLA-A and PDLLA-T, respectively). The strong hydrogen bonding led to increased viscosity below the dissociation temperature of the hydrogen bonds. Rheology confirmed that these bonds were thermally reversible, with a sharp reduction in viscosity near 100 °C. PDLLA, PDLLA-A, and PDLLA-T were melt electrospun with no significant change in fiber diameter (all between 3.6 and 4.0 μm). However, a blend of PDLLA-A and PDLLA-T formed fibers with an average diameter of 9.8 ± 2.0 μm, resulting from the hydrogen bond associations. Also, the phospholipid 1-palmitoyl-2-oleoyl-sn-glycero-3-phosphoethanolamine (POPE) was melt electrospun at 200 °C and formed uniform fibers with average fiber diameter of 6.5 ± 2.0 μm.

10.2 Introduction

Biology provides great inspiration for polymer scientists in terms of the exquisite structure and function of biological molecules. The hydrogen bond is ubiquitous in biological systems, particularly in the construction of proteins,[1] DNA[2] and RNA. In all cases, hydrogen bonding performs the role of establishing a reversible structure, which allows such processes as replication and transcription in DNA and a myriad of enzymatic reactions. Hydrogen bonding is central to many molecular recognition events in living organisms, notably the biotin-streptavidin interaction.[3] In DNA, hydrogen bonding performs in concert with numerous other non-

covalent interactions such as electrostatic interactions and π-stacking to yield the double helix structure and to impart dynamic properties into DNA.[4] One goal of modern polymer science is to incorporate such functionality and dynamics into synthetic macromolecules.

In our laboratories, we have investigated the effects of regiospecific hydrogen bonding sites,[5] topology, and the use of hydrogen bonding to influence rheological and mechanical performance.[6] The strength of these interactions is a strong function of temperature, solvent, humidity and pH, thus allowing control of properties through a number of environmental parameters. The strength of hydrogen bonding associations is further tunable via structural parameters and molecular design of the hydrogen bonding sites. Nucleobases possess association strengths near 100 M^{-1},[7] which lead to highly dynamic interactions.

Electrospinning provides a means to create tailored nanostructures from polymer solutions and melts.[8–11] The application of a large electric potential to polymeric fluid results in the deformation of the solution towards a grounded or oppositely charged electrode. For dilute solutions or melts of low molecular weight, the fluid will contract into droplets and deposit on the opposite electrode target (electrospraying). In the presence of sufficient entanglements, viscosity, or molecular weight, the fluid will elongate into a continuous filament and deposit on the target as a continuous, electrospun fiber.[12,13] In its simplest form, electrospinning generates a nonwoven mat of randomly oriented fibers with diameters on the order of 10 nm to 1 mm. Previous reports have demonstrated that electrospun mats can be successfully used in biomedical applications as drug-delivery scaffolds, cell growth scaffolds, and tissue and organ engineering scaffolds.[9,10,14] Our group has recently developed semi-empirical relationships relating solution rheology to electrospun fiber diameter for neutral, nonassociating polymers.[12] Random copolymers with self-complementary multiple hydrogen bonding groups showed

positive deviations from this relationship due to aggregation in solution.[15] Polyelectrolytes electrospun from water showed negative deviations from this relationship.[16] The addition of salt to the polyelectrolyte solutions was demonstrated to reduce this deviation.

We have previously reported the synthesis of a series of star-shaped poly(D,L-lactide) (PDLLA) polymers end-functionalized with adenine and thymine complementary base pairs.[17] These polymers demonstrated significant aggregation in solution based on complementary base-pair hydrogen bonding between the adenine and thymine groups. We report herein an investigation of the aggregation of these PDLLA stars in the melt state, as well as melt electrospinning to generate biocompatible and biodegradable fibers. We have also reported recently that the intermolecular attractions and aggregation of phospholipids in solution can be harnessed to electrospin amphiphilic fibers from asolectin.[18] The electrostatic (hydrophilic) and hydrophobic interactions of these low molar mass amphiphiles promote aggregation into cylindrical or wormlike micelles that entangle much like polymer solutions and can be electrospun. We demonstrate in this report that a well-defined phospholipid, 1-palmitoyl-2-oleoyl-sn-glycero-3-phosphoethanolamine, can also be electrospun from the melt state.

10.3 Experimental Part

10.3.1 Synthesis of PDLLA

Adenine- and thymine-terminated, four-arm star-shaped PDLLAs were synthesized as reported previously.[17] In short, acrylate terminated star-shaped polymers were derivatized with adenine and thymine using a Michael addition reaction. ^{1}H NMR spectroscopy confirmed the quantitative addition of terminal adenine and thymine end groups, and size exclusion chromatography (SEC) confirmed the absence of side reactions during functionalization.

10.3.2 Melt Electrospinning

The melt electrospinning apparatus consisted of a glass pipette wrapped in an electrical heating band and grounded. The positive lead of a high voltage power supply (Spellman CZE1000R, Spellman High Voltage Electronics Corp.) was connected to a piece of aluminum foil wrapped around the target and placed approximately 10 cm below the pipette. Polymer or phospholipid powder was placed in the pipette, and the pipette was purged with nitrogen gas to inhibit oxidative degradation and promote fluid flow. The pipette was heated above the melting temperature of the sample and flow began, the target was charged with 30 kV and electrospun fibers were collected.

10.3.3 Characterization

Molar mass and molar mass distribution for PDLLA were determined by SEC using a Wyatt 717 Autosampler at 40 °C in THF. The SEC was equipped with a Waters 2410 refractive index detector, a Wyatt Technology MiniDAWN MALLS detector, and a Viscotek 270 viscosity detector. Melt rheological data were collected using a TA Instruments AR 1000 stress-controlled rheometer with a 25 mm parallel plate geometry. Strain amplitudes were limited to the linear viscoelastic regime over a frequency range of 0.1 to 100 Hz. The temperature was varied from 60 to 180 °C. The fiber diameter and morphology of melt electrospun fibers were analyzed using a LEO 1550 field emission scanning electron microscope (FESEM). Fibers for FESEM analysis were collected on a ¼'' by ¼'' stainless steel mesh, mounted on an SEM disc, and sputter-coated with a 10 nm Pt/Au layer to reduce electron charging. Thermogravimetric analysis (TGA) was performed under N_2 atmosphere at a heating rate of 10 °C/min using a TA Instruments Hi-Res TGA 2950.

10.4 Results and Discussion

10.4.1 PDLLA Synthesis and Characterization

The synthesis and characterization of the adenine- and thymine-functionalized, four-arm PDLLA (PDLLA-A and PDLLA-T, respectively) was described in our recent report.[17] In the previous report, a significant increase in the solution viscosity of a hydrogen-bonded complex consisting of a 1:1 wt:wt mixture of the PDLLA-A and PDLLA-T was observed. In addition, the thermoreversibility of the PDLLA adenine and thymine hydrogen-bonded complexes (PDLLA-(A-T)) in toluene was demonstrated. In this report, we focus on the melt properties of PDLLA-A and PDLLA-T polymers and their melt electrospinning behavior. The structures of PDLLA-A and PDLLA-T are illustrated in Scheme 10.1 below, along with an illustration of the PDLLA-(A-T) complex.

TGA was performed on the A- and T-modified, star-shaped PDLLAs and their hydrogen-bonded complex (M_n = 45600 g/mol, M_w/M_n = 1.37) to determine weight loss as a function of temperature. The onset of weight loss for PDLLA is known to occur at temperatures above 200 °C.[19,20] Dynamic TGA experiments revealed that all PDLLA precursors and complexes did not exhibit appreciably weight loss below 200 °C. In fact, the onset of degradation occurred at 200 °C with a minimal weight loss of 0.7%. Isothermal degradation experiments were also performed at 180 °C for 1 h under nitrogen. The A- and T-terminated, star-shaped PDLLAs, and the hydrogen-bonded complex remained relatively stable under these conditions with approximately 5.5% weight loss observed for the blended samples.

Scheme 10.1. Schematic representation of PDLLA-A, PDLLA-T, and PDLLA-(A-T) (1/1 wt/wt PDLLA-A/PDLLA-T).

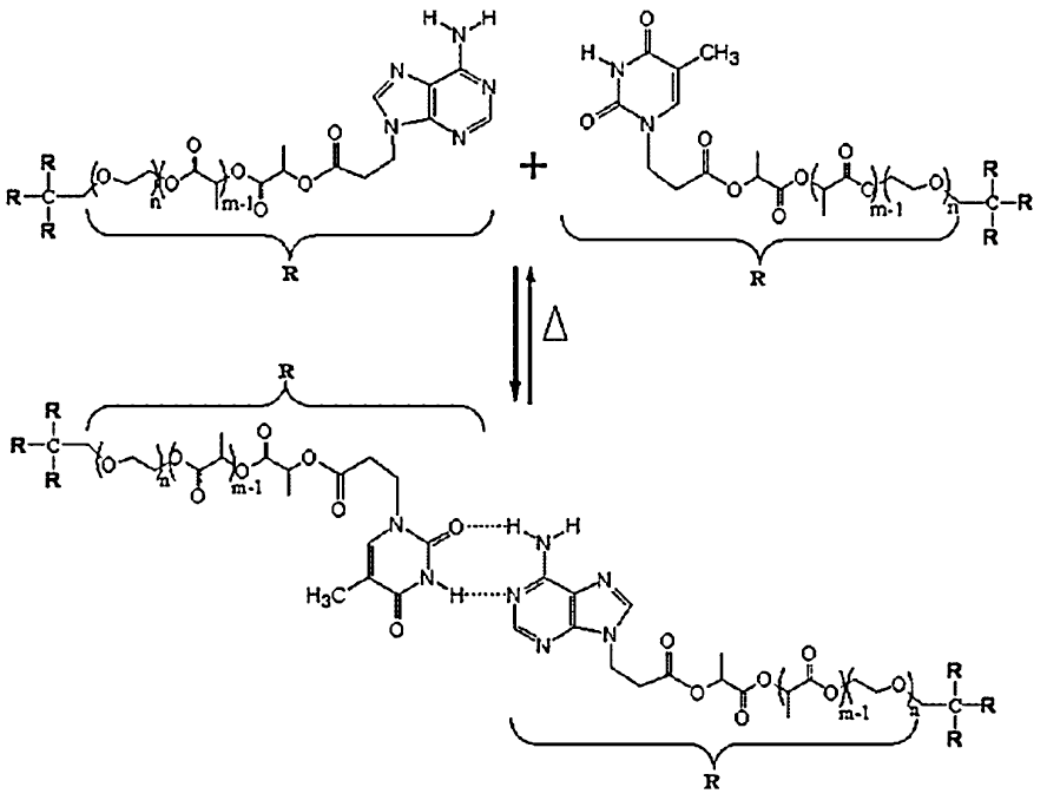

Melt rheological characterization was performed on the four-arm, star-shaped PDLLA-(A-T) complex and a non-functionalized PDLLA of identical molar mass distribution. Figure 10.1 shows the complex viscosity (η^*) as a function of frequency (ω) at 70 and 120 °C (above and below the dissociation temperature of the adenine-thymine base pair). At 70 °C, different viscosity profiles were observed for the non-functionalized PDLLA and the PDLLA-(A-T) complex, even though both samples were of the same molar mass. The complex viscosity of the complex was consistently higher than that of the unfunctionalized PDLLA precursor, reflecting the formation of physical crosslinks through complementary hydrogen bonding. An increase in viscosity and an increase in apparent molar mass was observed at 70 °C. However, the two PDLLA samples exhibited similar η^* profiles at 120 °C, suggesting complete dissociation of the

hydrogen-bonding interactions in the PDLLA-(A-T) complex. Furthermore, the PDLLA-(A-T) hydrogen-bonded complex displayed relatively higher η^* and a greater dependence of viscosity on temperature than the non-functionalized PDLLA precursor (Figure 10.2). The significant decrease in viscosity with temperature was consistent with dissociation of the hydrogen bonding interactions at higher temperatures and suggested the continuous disengagement of the associated hydrogen-bonded chains as the temperature was increased from 70 to 130 °C.

Melt electrospinning was used to prepare micron-sized fibers from the thermoreversible star-shaped PDLLA. The four-arm PDLLA, PDLLA-A, PDLLA-T, and PDLLA-(A-T) complex were melt electrospun at 180 °C and 30 kV with a working distance of 6 cm. The electrospinning temperature was chosen to allow complete dissociation of both the complementary hydrogen bonding interactions between the adenine and thymine units as well as any self-association of the nucleobases. As the polymer sample was heated above the dissociation temperature and the intensity of the electric field was increased, the polymer melt flowed and elongated from the tip of the pipette to form a conical shape known as the Taylor cone prior to jet initiation. As the discharged polymer jet traveled through the ambient air, the polymer cooled and reassociation of the adenine and thymine units was expected before fiber solidification.

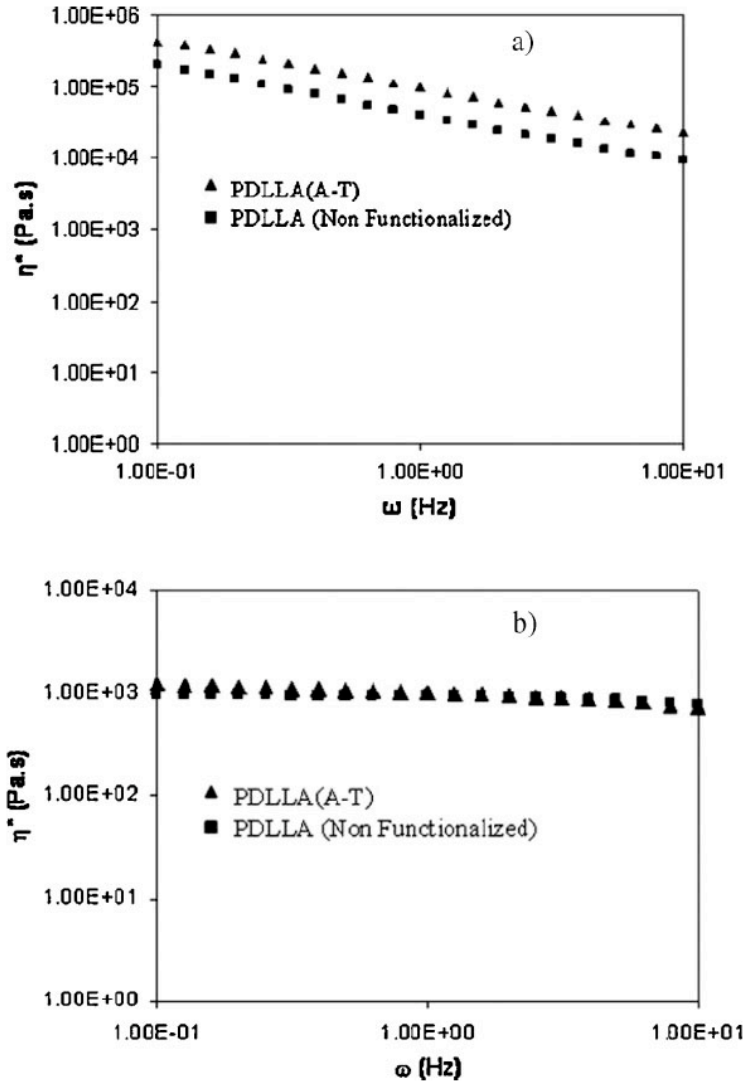

Figure 10.1. Comparison of the complex viscosity (η^*) master curves of PDLLA-(A-T) hydrogen-bonded complex and PDLLA (non functionalized) at (a) 70 °C and (b) 120 °C.

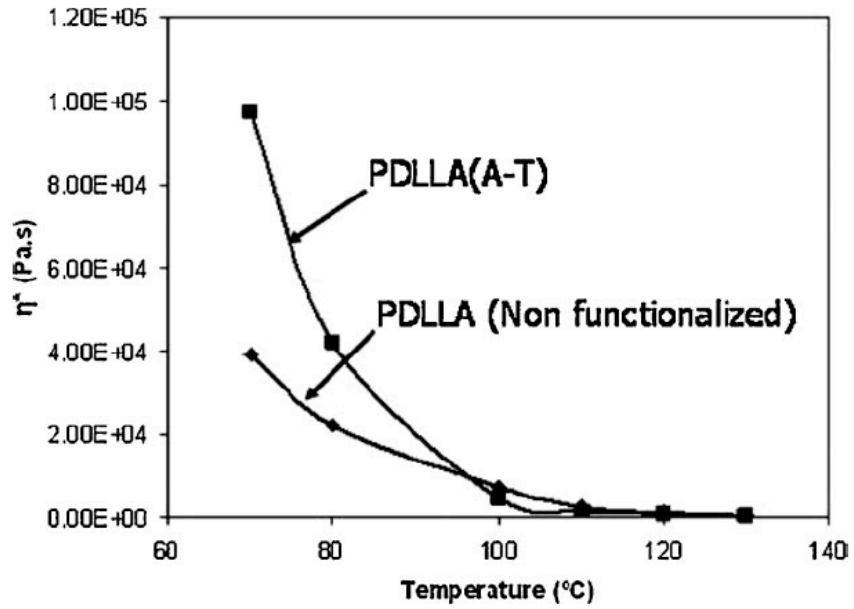

Figure 10.2. Comparison of the complex viscosity (η^*) of PDLLA-(A-T) hydrogen-bonded complex and PDLLA (non functionalized) as a function of temperature.

Electrospun fibers with an average fiber diameter of 3.6 ± 1.0 μm were obtained from the non-functionalized PDLLA precursor (Figure 10.3a). Upon functionalization with adenine and thymine end-groups, the average fiber diameter remained statistically unchanged at 4.0 ± 0.6 μm and 4.4 ± 1.0 μm, respectively (Figures 10.3b and 10.3c). The slight increase in the electrospun fiber diameter after functionalization with the nucleobases suggested minimal self-association of the adenine and thymine groups. In addition, the slightly higher fiber diameter of the PDLLA-T relative to PDLLA-A was consistent with the stronger self-association of the thymine groups ($K_{a(A-A)}$ = 2.4 M^{-1}, $K_{a(T-T)}$ = 3.5 M^{-1} in CDCl3).[21,22] A significant increase of the average fiber diameter to 9.8 ± 2.0 μm was observed for the PDLLA-(A-T) hydrogen-bonded complex (Figure 10.3d). The higher average fiber diameter was consistent with the increased η^* of the complex relative to the non-functionalized PDLLA at an identical temperature. Furthermore, the formation of intermolecular hydrogen-bonding interactions between complementary adenine and

thymine units in the electrospinning jet is proposed to occur based on melt rheological data. These results suggest that thermoreversibility, as well as the strength of the hydrogen-bonding interactions between the end groups of the tailored star PDLLA-based supramolecular polymers, control the fiber diameter in the melt electrospinning process.

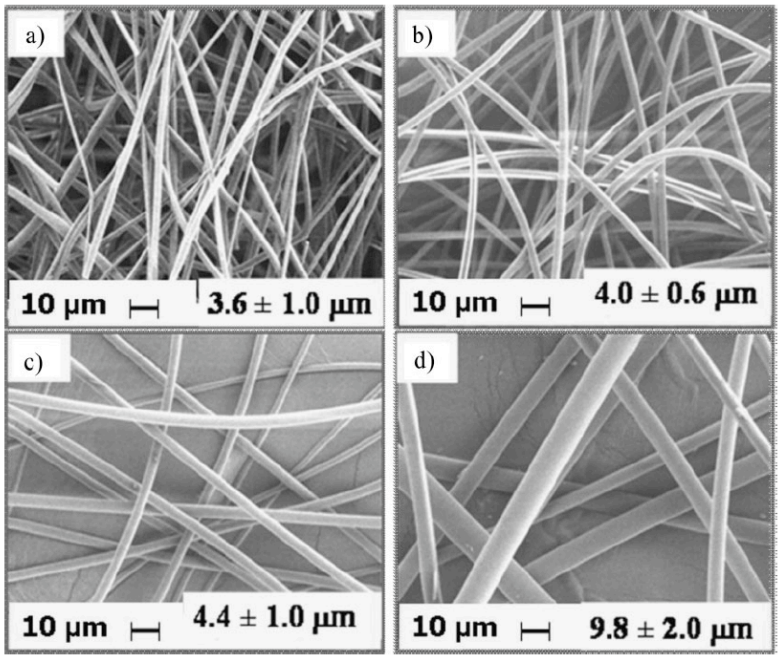

Figure 10.3. FESEM images of electrospun fibers produced from four-arm star-shaped PDLLA (M_w = 45 600 g/mol, M_w/M_n = 1.37). (a) Non-functionalized PDLLA (b) PDLLA-A (c) PDLLA-T (d) (1/1 wt/wt PDLLA-A/PDLLA-T).

10.4.2 Melt Electrospun Phospholipids

Amphiphilic molecules are known to aggregate into specific structures in solution and melt states based on hydrophobic and hydrophilic interactions. The shape of the structure is dominated primarily by the chemical structure of the amphiphile, and the most common aggregate is the spherical micelle. Certain molecules will form cylindrical aggregates or micelles under some conditions. These aggregates in solution have been studied in depth, and their dynamic and rheological properties are analogous to those of polymers. Recently, we demonstrated that reverse cylindrical micelles of phospholipid in solution can be

electrospun.[18,23] These solutions demonstrated rheology similar to polymer solutions, and a critical concentration for entanglements was identified. Above this concentration, uniform fibers could be electrospun.

We have found that a well-defined phospholipid, 1-palmitoyl-2-oleoyl-sn-glycero-3-phosphoethanolamine (POPE), forms long range aggregates in the melt state. When heated to 200 °C in the electrospinning apparatus, the POPE began to flow. The electrospinning jet solidified during flight and solid, amphiphilic fibers were deposited. FESEM images of the electrospun POPE, as well as the chemical structure, are shown in Figure 10.4. Using this electrospinning technique, fibrous scaffolds of biologically-derived phospholipid can be formed.

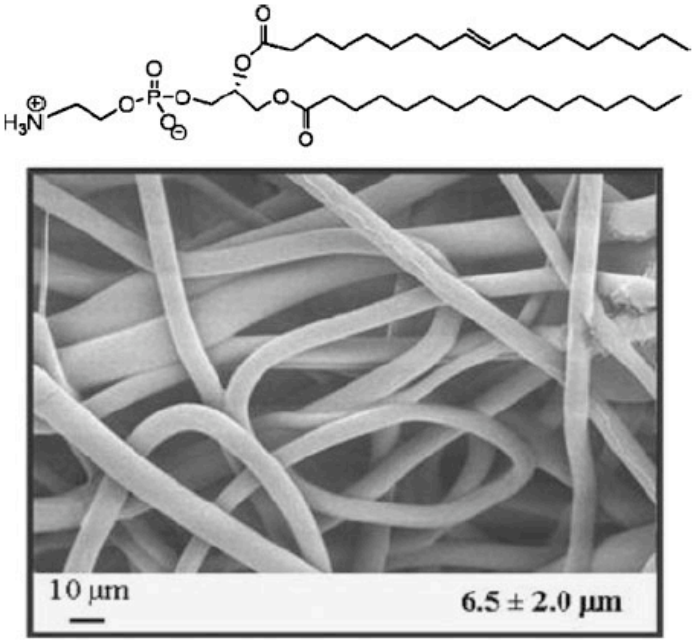

Figure 10.4. Chemical structure and melt electrospun fibers of POPE phospholipid.

10.5 Conclusions

A new family of electrospun biodegradable membranes were prepared from thermoreversible, four-arm, star-shaped PDLLA with terminal complementary hydrogen bonding units or phospholipids. The influence of intermolecular hydrogen bonding on the melt

electrospinning process was investigated. Adenine- and thymine-functionalized, star-shaped PDLLA were blended to obtain PDLLA-based supramolecular polymers through hydrogen bonding interactions. Linear viscoelastic measurements confirmed the formation of a hydrogen-bonded complex with significantly higher melt viscosity compared to the non-functionalized PDLLA precursor and a strong dependence of melt viscosity on temperature. Thermoreversibility of the adenine and thymine complexation controlled the fiber size in the melt electrospinning process. As a consequence, the star-shaped, PDLLA-based supramolecular polymers produced fibers with significantly larger diameters compared to the single component fibers due to the intermolecular hydrogen bonding of the PDLLA-A and PDLLA-T in the molten electrospinning jet. Melt electrospinning of low molar mass amphiphiles was also demonstrated for the first time. This technique can be applied to prepare a wide range of structured, biologically-compatible membranes for biomedical applications.

10.6 Acknowledgements

The authors acknowledge the financial support of the Petroleum Research Fund (ACS-PRF 35190-AC7), which is administered by the American Chemical Society.

10.7 References

[1] A. Aggeli, M. Bell, N. Boden, J. N. Keen, P. F. Knowles, T. C. B. McLeish, M. Pitkeathly, S. E. Radford, Nature 1997, 386, 259.
[2] D. Voet, J. G. Voet, ‘‘Biochemistry’’, John Wiley and Sons. New York: 1995, p. 361.
[3] P. C. Weber, D. H. Ohlendorf, J. J. Wendoloski, F. R. Salemme, Science 1989, 243, 85.
[4] J. Barciszewski, Biotechnologia 1993, 3, 138.
[5] B. D. Mather, J. R. Lizotte, T. E. Long, Macromolecules 2004, 37, 9331.
[6] K. Yamauchi, J. R. Lizotte, D. M. Hercules, M. J. Vergne, T. E. Long, J. Am. Chem. Soc. 2002, 124, 8599.
[7] Y. Kyogoku, R. C. Lord, A. Rich, Proc. Natl. Acad. Sci. USA 1967, 57, 250.
[8] D. H. Reneker, I. Chun, Nanotechnology 1996, 7, 216.
[9] R. Vasita, D. S. Katti, Intl. J. Nanomedicine 2006, 1, 15.
[10] W.-E. Teo, W. He, S. Ramakrishna, Biotechnol. J. 2006, 1, 918.
[11] D. Li, Y. Xia, Adv. Mater. 2004, 16, 1151.
[12] M. G. McKee, G. L. Wilkes, R. H. Colby, T. E. Long, Macromolecules 2004, 37, 1760.

[13] S. L. Shenoy, W. D. Bates, H. L. Frisch, G. E. Wnek, Polymer 2005, 46, 3372.
[14] J. Venugopal, S. Ramakrishna, Appl. Biochem. Biotechnol. 2005, 125, 147.
[15] M. G. McKee, C. L. Elkins, T. E. Long, Polymer 2004, 45, 8705.
[16] M. G. McKee, M. T. Hunley, J. M. Layman, T. E. Long, Macromolecules 2006, 39, 575.
[17] A. S. Karikari, T. E. Long, Biomacromolecules 2007, 8, 302.
[18] M. G. McKee, J. M. Layman, M. P. Cashion, T. E. Long, Science 2006, 311, 353.
[19] C. C. Chien, Y. C. Ju, H. Tseng, M. H. Haw, Y. L. Sheng, Biomaterials 2003, 24, 1167.
[20] H. Abe, N. Takahashi, J. K. Kang, M. Mochizuki, Y. Doi, Biomacromolecules 2004, 5, 1606.
[21] J. Sartorius, H.-J. Schneider, Chem. Eur. J. 1996, 2, 1446.
[22] S. Sivakova, D. A. Bohnsack, M. E. Mackay, P. Suwanmala, S. J. Rowan, J. Am. Chem. Soc. 2005, 127, 18202.
[23] M. T. Hunley, M. G. McKee, T. E. Long, J. Mater. Chem. 2007, 17, 605.

Chapter 11: Melt Dispersion and Electrospinning of Nonfunctionalized Multiwall Carbon Nanotubes in Thermoplastic Polyurethane

(From: Hunley, M.T.; Pötschke, P.; Long, T.E. *Macromol. Rapid Commun.* **2009**, *30*, 2102-2106.)

11.1 Abstract

Nanoscale fibers with embedded, aligned, and percolated non-functionalized multiwalled carbon nanotubes (MWCNTs) were fabricated through electrospinning dispersions based on melt-compounded thermoplastic polyurethane/MWCNT nanocomposite, with up to 10 wt.-% MWCNTs. Transmission electron microscopy indicated that the nanotubes were highly oriented and percolated throughout the fibers, even at high MWCNT concentrations. The coupling of efficient melt compounding with electrospinning eliminated the need for intensive surface functionalization or sonication of the MWCNTs, and the high aspect ratio as well as the electrical and mechanical properties of the nanotubes were retained. This method provides a more efficient technique to generate one-dimensional nanofibers with aligned MWCNTs.

11.2 Introduction

Carbon nanotubes have received significant attention recently as nanoscale fillers to anisotropically enhance the mechanical performance, thermal behavior, and electrical conductivity of polymer nanocomposites at very low concentrations (typically a few weight percent compared to the matrix polymer).[1] These tailored nanocomposites enable anti-static coatings,[2] sensing devices,[3] photovoltaic cells,[4] and drug-delivery agents,[5] among many other uses. Multiwalled carbon nanotubes have diameters ranging from 5–20nm and lengths exceeding hundreds of micrometers, and this exceptionally high aspect ratio leads to highly anisotropic properties.

A major obstacle to large-scale, homogenous, nanocomposite preparation including MWCNTs is the difficulty to homogeneously disperse the nanotubes into the polymer matrix.[1] Physical entanglements of the ‘‘rope-like’’ carbon nanotubes as well as strong van der Waal interactions lead to a thermodynamic driving force for aggregation. Many harsh dispersion strategies to achieve adequate dispersion have emerged such as extended sonication times or enhanced dispersion with the addition of surfactants,[6] chemical functionalization of the nanotube surface (commonly with carboxylic acid sites and other diverse organic functionalities),[7] and in situ polymerization in thepresence of dispersed nanotubes.[8] These well-established processes result in high levels of nanotube dispersion, but require additional processing steps and complex synthetic strategies including strong acids for oxidation, which are not desirable on commercial scales. Moreover, these surface modification strategies lead to reductions in the carbon nanotube conductivity and shortening of the nanotubes.[9] Melt compounding was shown to be a viable strategy to effectively disperse carbon nanotubes into different thermoplastic matrices.[10] Recently, a micro-compounder with an efficient feedback loop for mixing, as well as extrusion on the kilogram scale, were shown in our laboratories to readily disperse non-functionalized carbon nanotubes into polycarbonates and thermoplastic polyurethanes (as used in this study).[10a,11] Short mixing times of approximately 5 min were required for adequate dispersion of the MWCNTs.

Electrospinning processing of dispersions or melts has gained significant research interest in the past decade as a simple laboratory method to produce polymeric and polymeric composite nanofibers.[12] Polymer/carbon nanotube dispersions were also successfully electrospun into nanocomposite fibrous membranes with random and oriented fiber orientations.[13] The high extensional shear that occurs during electrospinning orients the nanotubes along the fiber

axis.[14] Melt-mixed polycarbonate/nonfunctionalized MWCNT nanocomposite dispersions were electrospun into nanofibers and surprising increases in stress and strain at break were reported.[11] However, most studies employed chemically-modified MWCNTs and lengthy solution dispersion (involving sonication) to adequately disperse the nanotubes in the electrospinning solution. Electrospun polyurethane/nanotube composite fibers were reported, however earlier studies have not examined in depth the orientation of MWCNTs in these elastomeric nanofibers.[15] Few reports have discussed the electrospinning of non-functionalized carbon nanotubes,[16] partly due to the difficulty in dispersing these tubes into organic polymers. In this communication, we report the electrospinning of a thermoplastic nanocomposite comprising a nanoscale polyurethane fibrous membrane with dispersed and aligned non-functionalized MWCNTs. Compared to previous reports, this method required significantly less destructive melt mixing and resulted in well-aligned, percolated carbon nanotubes, which are aligned within the polyurethane nanofibers at relatively high concentrations of tubes.

11.3 Experimental Part

11.3.1 Materials

The polyether-based thermoplastic polyurethane, TPU Elastollan 1185 A10, was obtained from Elastogran GmbH (Lemförde, Germany), in pellet form. The polymer is composed of 1,4-butanediol and 4,40-MDI hard segment and PTMO soft segment, with a measured T_g at 36 °C and T_m at 82 °C. The MWCNTs were obtained as a powder from Nanocyl S.A. (Sambreville, Belgium), and are named ‘‘very thin straight and coiled nanotubes.’’ The nanotubes have a purity of greater than 95%, with inner diameters ranging from 2 to 7 nm (mean 4 nm inner diameter) and outer diameters ranging from 3 to 15 nm(mean value 10 nm). The length is up to

50mm. All materials were dried immediately prior to use in an oven at 100 °C for at least 3 h. Solvents were obtained from commercial sources and used without further purification.

11.4 Results and Discussion

The DACA microcompounder successfully dispersed the non-functionalized carbon nanotubes within the thermoplastic polyurethane matrix under mild conditions and short mixing times (210 °C for 5 min). TEM analysis of the extruded nanocomposites indicated thorough mixing of the nanotube agglomerates within the polyurethane composite and the dispersion of many agglomerates into singular nanotubes or small nanotube bundles (Figure 11.1). The polyurethane demonstrated good compatibility with the carbon nanotubes, and easily stabilized the dispersion of the nanotubes. This agreed with previous reports indicating that polyether- and polyester-based polyurethanes readily disperse non-functionalized carbon nanotubes.[15]

Nanocomposites were fabricated with nanotube contents ranging from 0 to 10 wt.-%. The conductivity of the extruded polyurethane/MWCNT strands increased with nanotube content, as shown in Figure 11.2. At lower concentrations, the conductivity was on the order of 10^{-10} S cm^{-1}, and showed a slight increase with increasing nanotube concentration. However, at approximately 3 wt.-%, the conductivity increased approximately six orders of magnitude with only approximately a 1 wt.-% increase in MWCNT incorporation, indicating nanotube percolation. The large conductivity increase indicated that the nanotubes were adequately dispersed in the composite, which formed a charged pathway of low resistance. Percolation at such low MWCNT loadings suggested that the larger aggregates were sufficiently dispersed into smaller and more separated singular tubes and bundles, and TEM analysis verified this observation. Approaching 10 wt.-% MWCNT loading, the nanocomposite conductivity appeared to reach a relatively constant value at approximately 10^{-1} S cm^{-1}.

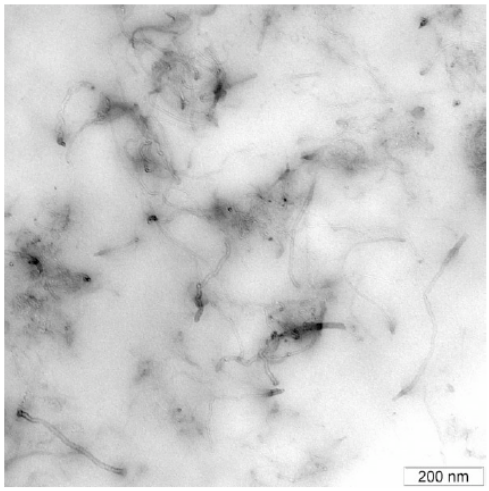

Figure 11.1. Transmission electron micrograph of a cryomicrotomed composite containing 5 wt.-% MWNT after melt mixing.

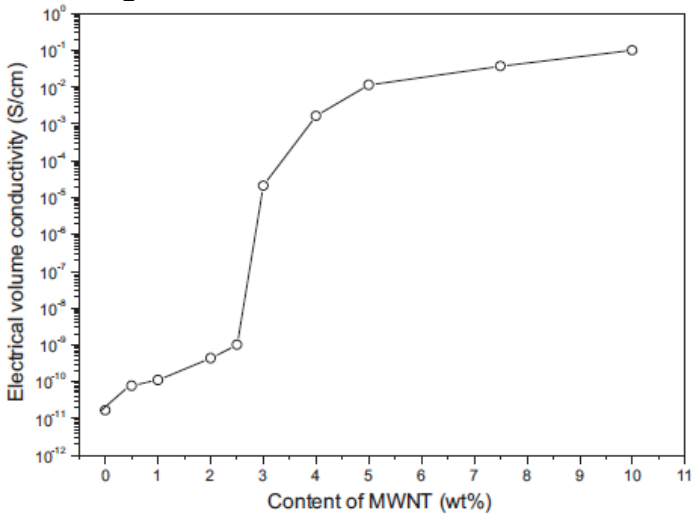

Figure 11.2. Volume conductivity of the polyurethane/MWNT composite after melt mixing.

Electrospinning of dispersions based on these polyurethane/MWCNT nanocomposites was performed to investigate the influence of melt mixing and improved dispersion of the nanotubes on the formation of nanoscale fibers. All samples for electrospinning were above the percolation threshold as determined using conductivity measurements. Increasing nanotube content also significantly increased the solution viscosity for electrospinning samples, and at high nanotube concentrations, the viscosity actually impeded stable electrospinning. Many literature reports investigate the dramatic viscosity increase in dispersions and composites of

well-dispersed carbon nanotubes.[17] In order to electrospin nanotube concentrations of 10 wt.-% (versus polyurethane), the overall polymer concentration was reduced for each successively higher nanotube concentration. Polymer concentrations in the solvent were 15, 14, 13, and 12 wt.-% for the nanocomposites containing 4, 5, 7.5, and 10 wt.-% nanotubes, respectively. Overall solids content for these four mixtures were 15.5, 14.6, 13.9, and 13.2 wt.-%, respectively. Figure 11.3 shows FESEM images for electrospun polyurethane/nanotube nanocomposite fibers at increasing nanotube content. Increasing nanotube concentration led to the presence of undulating surface features on the fibers. These fluctuations were likely due to small fluctuations in solution conductivity and viscosity (due to the nonhomogeneous nature of nanotube dispersions) affecting the electrospinning process. The electrospun composite fibers, however, did not show large defects (such as droplets or beading) upon addition of the nanotubes, even at concentrations as high as 10 wt.-% MWCNTs.

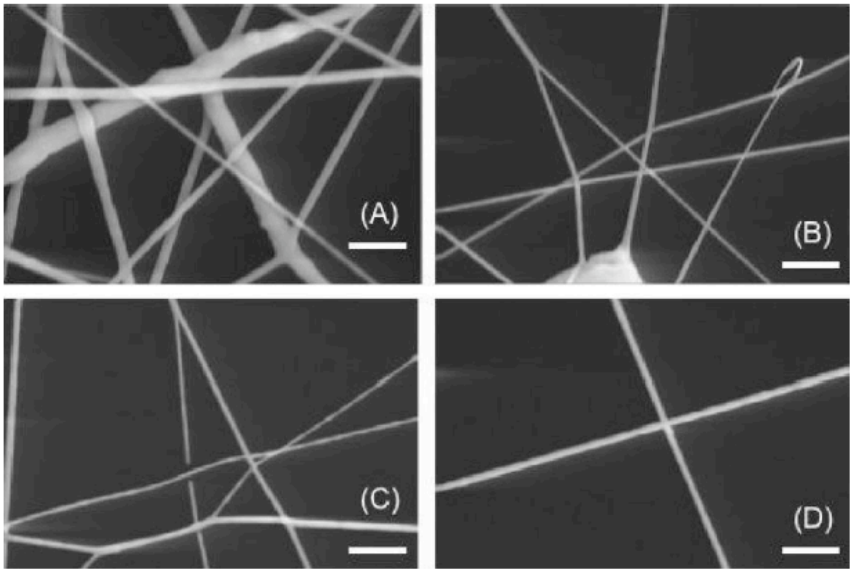

Figure 11.3. Scanning electron micrographs of the electrospun composite nanofibers at MWNT concentrations of (A) 4 wt.-%, (B) 5 wt.-%, (C) 7.5 wt.-%, and (D) 10 wt.-%. These fibers were electrospun from solutions at polyurethane concentrations of (A) 15 wt.-%, (B) 14 wt.-%, (C) 13 wt.-%, and (D) 12 wt.-%. The scale bars represent 1 μm.

TEM analysis of the electrospun fibers was essential to demonstrate the nanotube dispersion and alignment. Figure 11.4 depicts micrographs of the composite fibers at four nanotube concentrations. At the lower concentration, carbon nanotubes appeared highly aligned along the fiber axis with some curving of the nanotubes. As MWCNT concentration increased, a significant degree of orientation was observed. In addition, the nanotubes appeared to exhibit less curling and bending, most likely due to the density of nanotubes within the composite fibers. The higher concentration composite nanofibers visually demonstrated the percolated structure of the nanocomposites. Some aggregates were visible at the highest concentrations of nanotubes, due to the difficulties in fully dispersing theMWCNTs. Figure 11.4(E) shows a ‘‘nanowire,’’ or a singular, isolated, nanotube with a high degree of orientation along the fiber axis. These structures occurred more frequently at high nanotube loadings. At all MWCNT concentrations, the nanotubes were long, which confirmed that the short processing times did not significantly degrade the nanotubes.

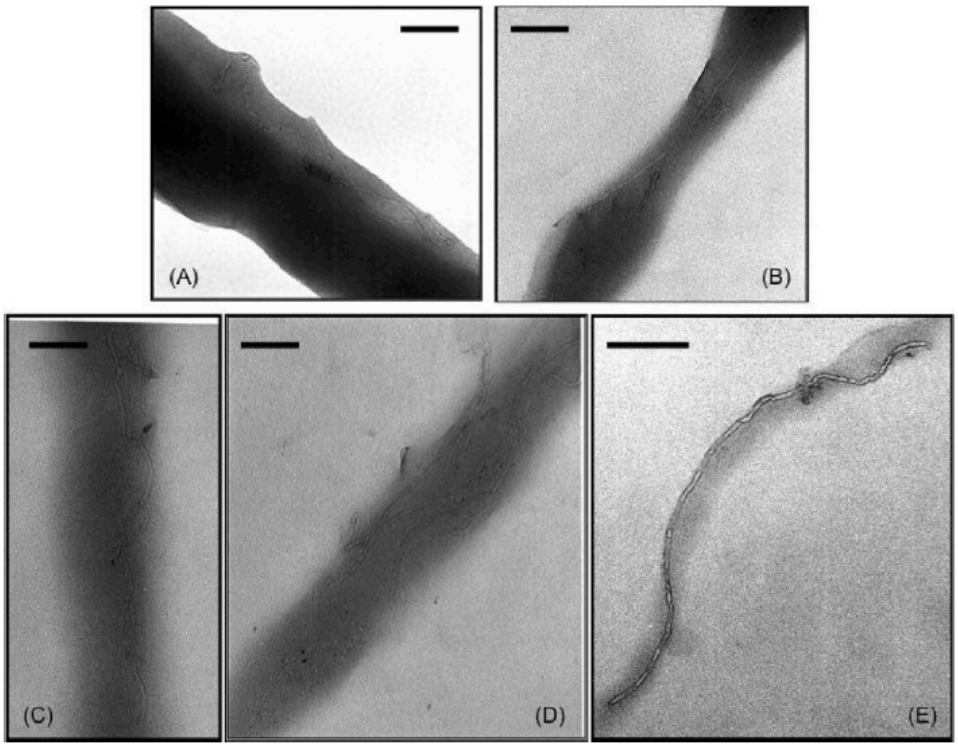

Figure 11.4. Transmission electron micrographs of the electrospun composite nanofibers at MWNT concentrations of (A) 4 wt.-%, (B) 5 wt.-%, (C) 7.5 wt.-%, and (D) 10 wt.-%. (E) A detail of a "nanowire," showing a signle nanotube highly aligned along the nanofiber. The scale bars represent 100 nm.

11.5 Conclusion

We have demonstrated for the first time the role of melt compounding to efficiently disperse non-functionalized MWCNTs in a polyurethane matrix for efficient fiber formation through electrospinning. TEM analysis and electrical conductivity measurements indicated that the short melt mixing adequately dispersed the nanotubes to form percolated composite, non-woven fabrics. It may be assumed that based on the good interactions between the nanotubes and the thermoplastic polyurethane some polymer wrapping occurs during melt mixing which stabilizes the nanotubes in the spinning dispersion. Due to the elimination of intense processing steps such as chemical functionalization of the nanotubes and lengthy sonication treatments for dispersion, the native length and properties of the MWCNTs could be retained. The

electrospinning process also oriented the nanotubes along the fiber axis, creating percolated elastomeric nanofibers. These results reveal that polymer/nanotube composites are attainable in a more efficient manner to produce one-dimensional nanofibers. Ongoing work concentrates on the mechanical and electrical properties of the electrospun composite nanofibers.

11.6 References

[1] [1a] M. Moniruzzaman, K. I. Winey, Macromolecules 2006, 39, 5194; [1b] S. V. Ahir, Y. Y. Huang, E. M. Terentjev, Polymer 2008, 49, 3841.

[2] [2a] M. Sangermano, S. Pegel, P. Pötschke, B. Voit, Macromol. Rapid Commun. 2008, 29, 396; [2b] J. K. W. Sandler, J. E. Kirk, I. A. Kinloch, M. S. P. Shaffer, A. H. Windle, Polymer, 2003, 44, 5893.

[3] [3a] E. Bekyarova, I. Kalinina, M. E. Itkis, L. Beer, N. Cabrera, R. C. Haddon, J. Am. Chem. Soc. 2007, 129, 10700; [3b] C. Li, E. T. Thostenson, T.-W. Chou, Compos. Sci. Technol. 2008, 68, 1227.

[4] J. Geng, T. Zeng, J. Am. Chem. Soc. 2006, 128, 16827.

[5] R. P. Feazell, N. Nakayama-Ratchford, H. Dai, S. J. Lippard, J. Am. Chem. Soc. 2007, 129, 8438.

[6] [6a] M. F. Islam, E. Rojas, D. M. Bergey, A. T. Johnson, A. G. Yodh, Nano Lett. 2003, 3, 269; [6b] J. Hilding, E. A. Grulke, Z. G. Zhang, F. Lockwood, J. Dispersion Sci. Technol. 2003, 24, 1.

[7] [7a] D. Tasis, N. Tagmatarchis, A. Bianco, M. Prato, Chem. Rev. 2006, 106, 1105; [7b] C. M. Homenick, G. Lawson, A. Adronov, Polym. Rev. 2007, 47, 265.

[8] [8a] S. J. Park, M. S. Cho, S. T. Lim, H. J. Choi, M. S. Jhon, Macromol. Rapid Commun. 2003, 24, 1070; [8b] M. Moniruzzamann, F. Du, N. Romero, K. I. Winey, Polymer 2006, 47, 293.

[9] [9a] P. C. Ma, J.-K. Kim, B. Z. Tang, Compos. Sci. Technol. 2007, 67, 2965; [9b] M. B. Bryning, D. E. Milkie, M. F. Islam, J. M. Kikkawa, A. G. Yodh, Appl. Phys. Lett. 2005, 87, 161909/1; [9c] S. Badaire, P. Poulin, M. Maugey, C. Zakri, Langmuir 2004, 20, 10367.

[10] [10a] P. Pötschke, L. Häußler, S. Pegel, R. Steinberger, G. Scholz, KGK Kautschuk Gummi Kunststoffe 2007, 60, 432; [10b] F. Jiang, S. Wu, Y. Wei, L. Zhang, G. Hu, Polym. Polym. Compos. 2008, 16, 509; [10c] A. R. Bhattacharyya, T. V. Sreekumar, T. Liu, S. Kumar, L. M. Ericson, R. H. Hauge, R. E. Smalley, Polymer 2003, 44, 2373; [10d] W. D. Zhang, L. Shen, I. Y. Phang, T. Liu, Macromolecules 2004, 37, 256.

[11] [11a] G.-M. Kim, G. H. Michler, P. Pötschke, Polymer 2005, 46, 7346; [11b] G.-M. Kim, R. Lach, G. H. Michler, P. Pötschke, K. Albrecht, Nanotechnology 2006, 17, 963.

[12] [12a] A. Greiner, J. H. Wendorff, Angew. Chem. Int. Ed. 2006, 46, 5670; [12b] I. S. Chronakis, J. Mater. Process. Technol. 2005, 167, 283.

[13] J. Gao, A. Yu, M. E. Itkis, E. Bekyarova, B. Zhao, S. Niyogi, R. C. Haddon, J. Am. Chem. Soc. 2004, 126, 16698.

[14] Y. Dror, W. Salalha, R. L. Khalfin, Y. Cohen, A. L. Yarin, E. Zussman, Langmuir 2003, 19, 7012.

[15] [15a] R. Sen, B. Zhao, D. Perea, M. E. Itkis, H. Hu, J. Love, E. Bekyarova, R. C. Haddon, Nano Lett. 2004, 4, 459; [15b] D. Kimmer, P. Slobodian, D. Petra´sˇ M. Zatloukal, R. Olejnı´k, P. Sa´ha, J. Appl. Polym. Sci. 2009, 111, 2711; [15c] J. Meng, H. Kong, Z. Han, C. Wang, G. Zhu, S. Xie, H. Xu, J. Biomed. Mater. Res. Part A 2009, 88A, 105.
[16] M. K. Shin, Y. J. Kim, S. I. Kim, S.-K. Kim, H. Lee, G. M. Spinks, S. J. Kim, Sens. Actuators B 2008, 134, 122.
[17] [17a] A. N. G. Parra-Vasquez, I. Stepanek, V. A. Davis, V. C. Moore, E. H. Haroz, J. Shaver, R. H. Hauge, R. E. Smalley, M. Pasquali, Macromolecules 2007, 40, 4043; [17b] P. Po¨tschke, T. D. Fornes, D. R. Paul, Polymer 2002, 43, 3247.

Chapter 12: Electrospinning of Polyurethane Nanofibers Containing Dispersed Acid-Functionalized Multiwall Carbon Nanotubes

12.1 Abstract

The incorporation of nanoscale filler (including carbon nanotubes) within polymer fibers leads to significant improvements in mechanical and electric properties. Acid-functionalized multiwall carbon nanotubes (MWCNT-COOH) were dispersed within polyurethane solutions and electrospun in composite nanofibers. The incorporation of MWCNT-COOH led to slight increases in fiber diameter due to increased viscosity. At 0.1, 0.5, and 1.0 wt% MWCNT-COOH incorporation (with respect to polyurethane), no change in fiber appearance was observed. However, at 5.0 and 10 wt% nanotubes, the fiber surface appeared undulating. Transmission electron microscopy (TEM) revealed that the nanotubes were highly oriented along the carbon nanotube axis. At 5.0 wt% nanotubes, the nanocomposite fibers appeared to reach a percolation threshold. Applications for these nanocomposites include porous conductive membranes and nanowires.

12.2 Introduction

Electrospun nanofibrous membranes have received significant attention in recent years due to their high porosity, high surface areas, and ease of processing.[1-3] The process utilizes a strong electric potential to draw fibers from a polymer solution or melt. The repulsion of surface charges on the fluid jet during electrospinning leads to significant stretching and the formation of nanoscale fibers. These fibers and fibrous membranes are ideally suited for applications including high-flux filters,[4,5] ultrasensitive sensors,[6,7] and biomimetic tissue scaffolds.[8,9]

The incorporation of carbon nanotubes within electrospun fibers leads to increases in electrical and thermal conductivity as well as improved mechanical properties.[10-13] Dubois et al.[14]

investigated the electrospinning of polystyrene (PS)/multiwall carbon nanotubes (MWCNT) and found that the conductivity of the fibrous membranes increased sharply at 4 wt% nanotube incorporation. This concentration corresponded with the percolation threshold, where the distance between nanotubes in the matrix became small enough that there was little resistance to electron flow. The use of styrene-butadiene-styrene copolymer as a compatibilizer to disperse the nanotubes within the polystyrene solutions led to better dispersion of the nanotubes and improved mechanical properties of the fibers. The compatibilizer also improved conductivity below percolation, presumably due to more efficient dispersion of the nanotubes.

Haddon et al.[15] incorporated nanotubes within thermoplastic polyurethane fibers and measured enhancements in conductivity as well as mechanical properties of these robust fibers. Both unfunctionalized and ester-containing nanotubes increased the fiber modulus, but the incorporation of the ester-functionalized nanotubes led to an increase in ultimate elongation for the elastomeric fibers. Similarly, electrospun polyurethane fibers with incorporated nanotubes showed improved cellular adhesion and growth.[16,17] However, most studies of PU/MWCNT composite nanofibers have not directly observed the dispersion of nanotubes within the fibers. Our laboratories recently reported a melt-mixing technique to successfully disperse non-functionalized MWCNTs into a PU matrix and subsequently electrospin the composite into fibers with well-aligned MWCNTs.[18] However, the melt-mixing required high temperatures and high shear rates to adequately disperse the MWCNTs. In this study, we report the electrospinning of PU dispersions with carboxylic-acid functionalized MWCNTs. The carboxylic acid functionalities on the nanotube surface provide enough intermolecular interactions to disperse the nanotubes within polyurethane solutions and electrospin into uniform fibers with aligned nanotubes.

12.3 Experimental

12.3.1 Materials

The poly(tetramethylene oxide)-based polyurethane was synthesized as reported previously.[19] Bayer MaterialScience kindly provided the carbon nanotubes (Baytubes® C 150 P), which were functionalized with acid groups in our labs according to the following procedure. MWNTs (5 g) were dispersed in HNO_3 (aq) (200 mL, 8 M) by sonication and reacted at reflux for 24 h. After reaction, the nanotubes were passed through a 0.45 μm PTFE membrane (Millipore) and washed with deionized water to pH 7. The nanotubes were collected and refluxed in HCl (aq) (200 mL, 1 M) for 24 h, then subsequently washed with deionized water to neutral pH. These functionalized nanotubes were then dried *in vacuo* at 100 °C for 24 h to yield MWCNT-COOH (3.28 g). XPS: C 90.8%, O 9.2%. Solvents *N*,*N*-dimethylformamide (DMF) and tetrahydrofuran (THF) for electrospinning were obtained from commercial sources and used without further purification.

12.3.2 Electrospinning and Nanofiber Characterization

Electrospinning was performed using a homemade setup. The polyurethane solutions or dispersions were placed in a syringe with an 18-gauge, blunt-tipped needle. The syringe was placed in a syringe pump and solution metered at 3 mL/h. The positive lead of a Spellman CZE1200R high voltage power supply was connected to the syringe needle and the voltage increased to 25 kV. Fibers collected on a grounded stainless steel mesh target. Field-emission scanning electron microscopy (FESEM) was performed using a LEO 1550 FESEM operating at 5 kV accelerating voltage. Transmission electron microscopy (TEM) was performed on a Philips EM420 TEM operating at 100 kV accelerating voltage. Samples for FESEM were collected on a ¼" x ¼" stainless steel mesh and sputter coated with 15 nm of 60/40 Au/Pd to prevent charging.

Samples for TEM were collected directly on a 300 mesh copper grid and directly imaged in the TEM.

12.4 Results and Discussion

Scheme 12.1 depicts the synthetic route and the structure of the thermoplastic polyurethane. Our previous report details the mechanical properties of the polyurethane,[19] which exhibited typical thermoplastic elastomeric behavior. Electrospinning the polyurethane from pure DMF led to a film instead of fibers due to the very slow evaporation of the solvent. Conversely, electrospinning from THF resulted in plugging of the syringe needle due to rapid solvent evaporation and no fiber formation. However, the polyurethane electrospun from solvent mixtures of DMF and THF. To investigate the effect of solvent composition, the DMF:THF ratio was varied from 1:1 to 2:1 to 3:1 (all ratios are wt:wt). Fibers became thinner as the DMF ratio increased due to the increased dielectric constant and decreased volatility of the solvent. However, at high levels of DMF (3:1 solvent), the DMF did not evaporate sufficiently during electrospinning and a high degree of fiber fusing occurred. At high concentrations of THF (1:1), the solvent evaporated too quickly, leading to very thick fibers and even clogging of the needle and interruption of the electrospinning. The 2:1 DMF:THF mixture led to consistent electrospinning of uniform fibers with little fusing of the fibers.

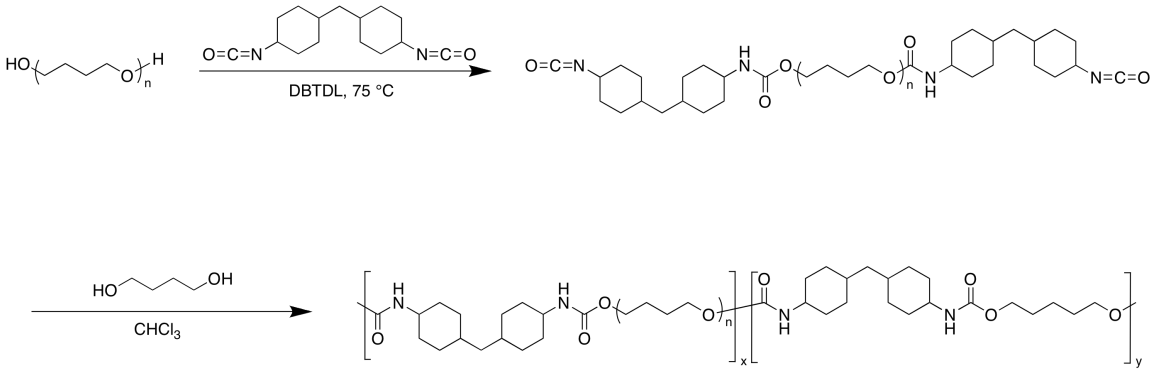

Scheme 12.1. Synthesis of segmented polyurethane based on poly(tetramethylene glycol) soft segment and butanediol chain extender.

The polyurethane concentration in the 2:1 DMF:THF solvent mixture was varied to determine the optimum electrospinning concentration. Figure 12.1 shows the FESEM micrographs of polyurethane fibers electrospun at concentrations from 8 to 15 wt%. At 8 wt%, droplets formed with short interconnecting fibers, indicating insufficient entanglements in solution to form electrospun fibers. Beaded nanofibers formed at concentrations of 10 and 12 wt%, and uniform fibers were electrospun at 15 wt% polyurethane. The average fiber diameters varied from less than 50 nm at 8 wt% to 150 nm at 15 wt%. Solutions of 15 wt% polyurethane were used for all subsequent experiments to ensure the electrospinning of uniform, thin fibers.

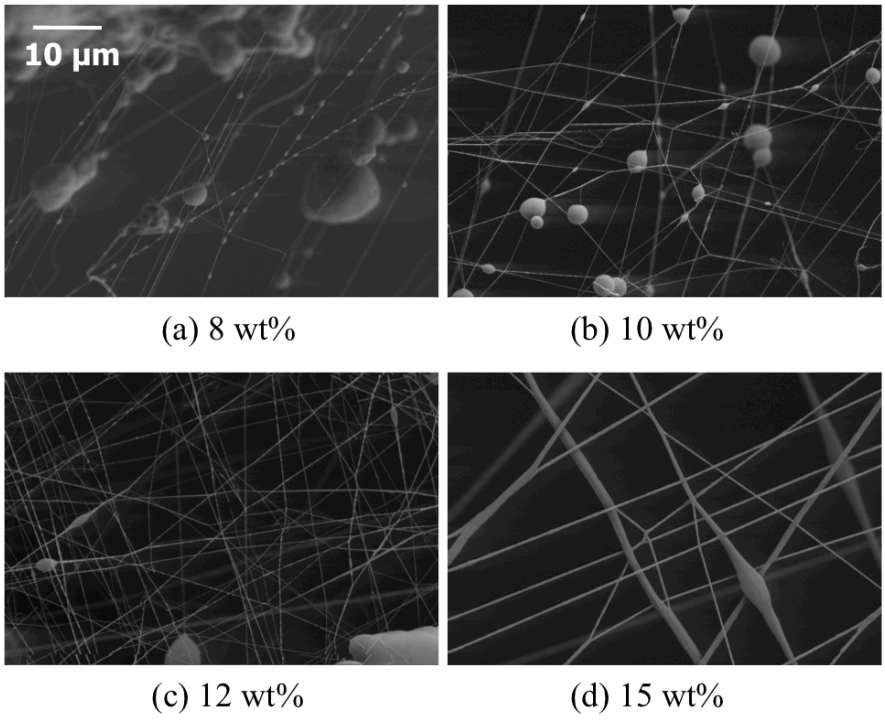

Figure 12.1. FESEM micrographs of polyurethane fibers at (a) 8 wt%, (b) 10 wt%, (c) 12 wt%, and (d) 15 wt%.

Acid-functionalized MWCNTs were dispersed into the polyurethane solutions at 0.1, 0.5, 1.0, 5.0, and 10 wt% carbon nanotubes (with respect to the polyurethane). The carboxylic acid groups on the nanotubes interacted with the PTMO-based polyurethane sufficiently that 30 min

in an ultrasonic bath adequately dispersed the MWCNTs. Although the electrospinning was performed quickly after sonication, the dispersions remained stable for over a week. Figure 12.2 shows the FESEM micrographs of PU/MWCNT nanocomposite fibers. Below 5 wt% MWCNT incorporation, no difference in fiber surface morphology was observed. At 5 and 10 wt% MWCNTs, an undulating surface morphology was observed. The fiber diameter increased slightly upon increasing nanotube loadings, as shown in Figure 12.3. The increase in fiber diameter resulted from the increase in viscosity with increasing concentrations of nanotubes.

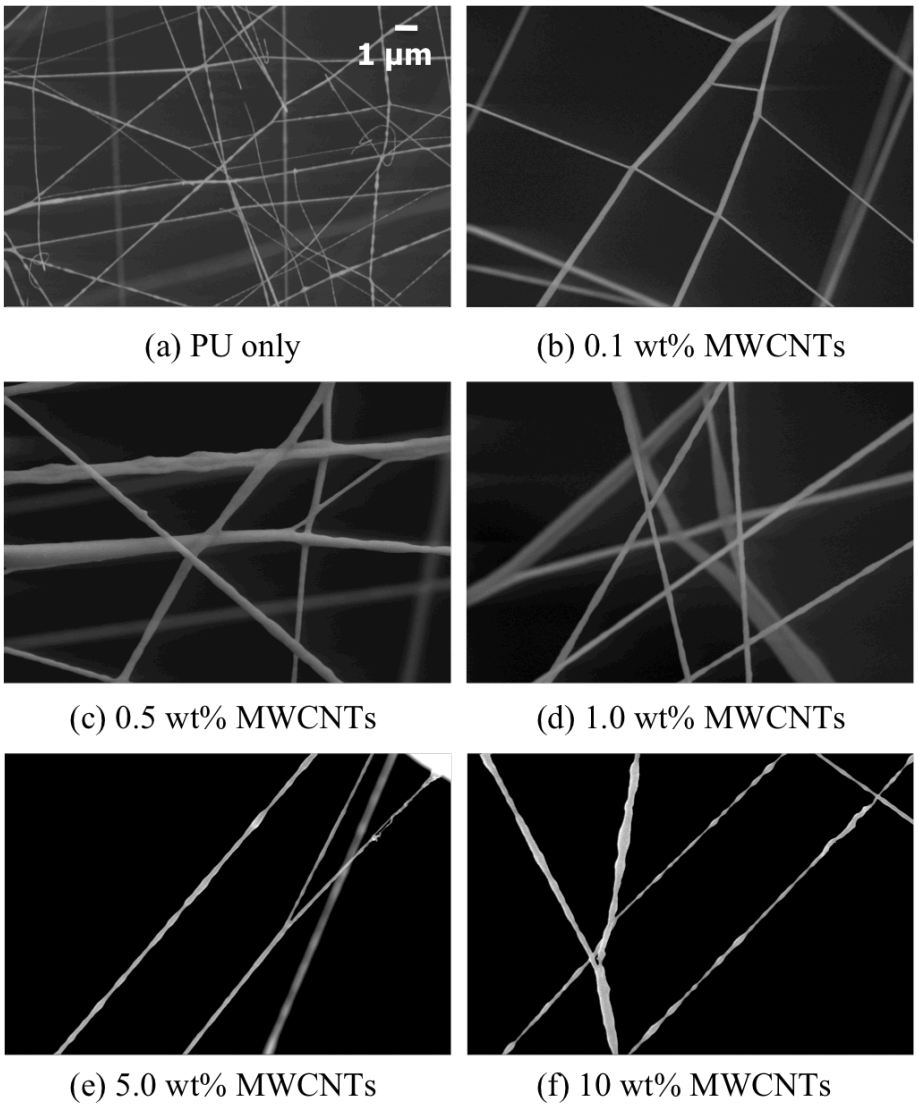

Figure 12.2. FESEM micrographs of PU/MWCNT composite fibers with MWCNT loadings of (a) 0 wt%, (b) 0.1 wt%, (c) 0.5 wt%, (d) 1.0 wt%, (e) 5.0 wt%, and (f) 10 wt%. The scale bar represents 1 micrometer.

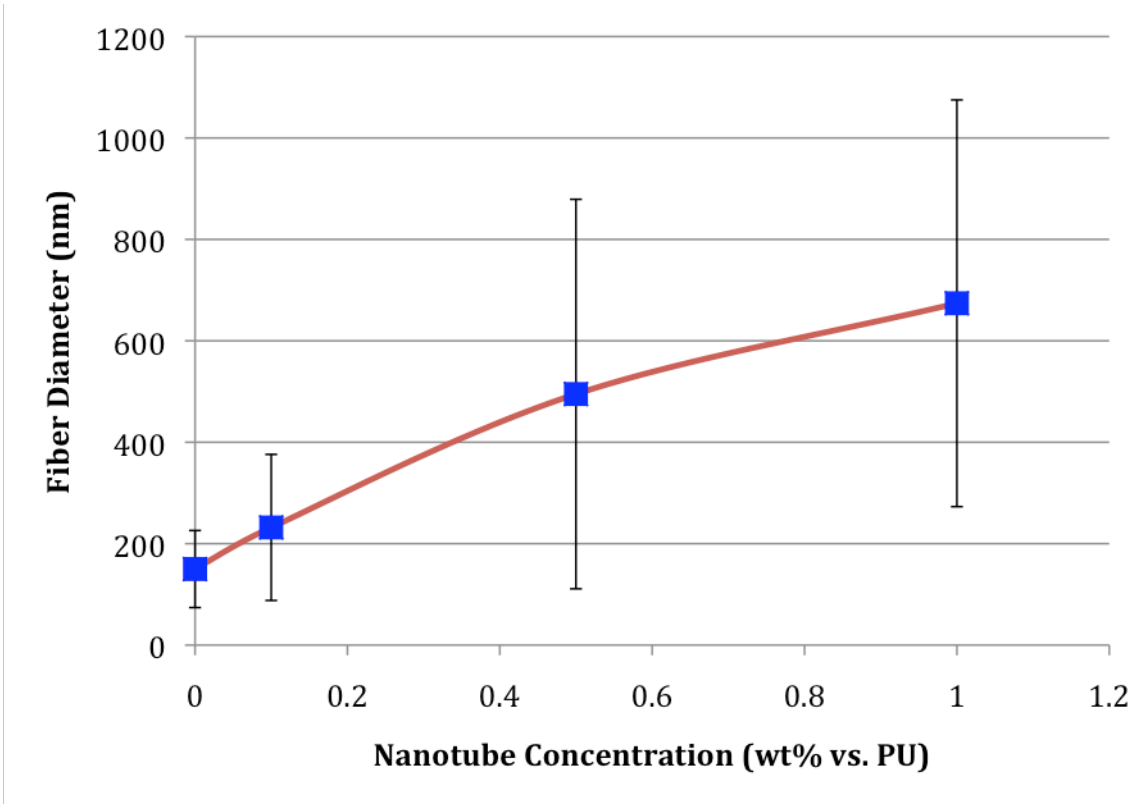

Figure 12.3. Fiber diameter versus nanotube concentration for electrospun polyurethane fibers. Nanotube concentration is versus polyurethane, and polyurethane concentration was held constant at 15 wt% in 2:1 DMF:THF.

TEM analysis revealed the distribution of MWCNTs within the nanocomposite fibers, as shown in Figure 12.4. The nanotubes clearly stretched along the axis of the fiber, as reported previously.[20] Both the electric field and the strong uniaxial flow during electrospinning oriented the nanotubes within the fibers. At nanotube concentrations of 0.1, 0.5, and 1.0 wt%, the MWCNTs remained isolated within the fibers. These tubes retained some of their coiled structure, but oriented highly along the fiber axis. At 5.0 and 10 wt% nanotubes, some small aggregates and clusters of nanotubes occurred, but the nanotubes again oriented predominantly along the fiber axis. Through these TEM observations, the nanotube percolation threshold appeared to be at 5.0 wt% MWCNTs.

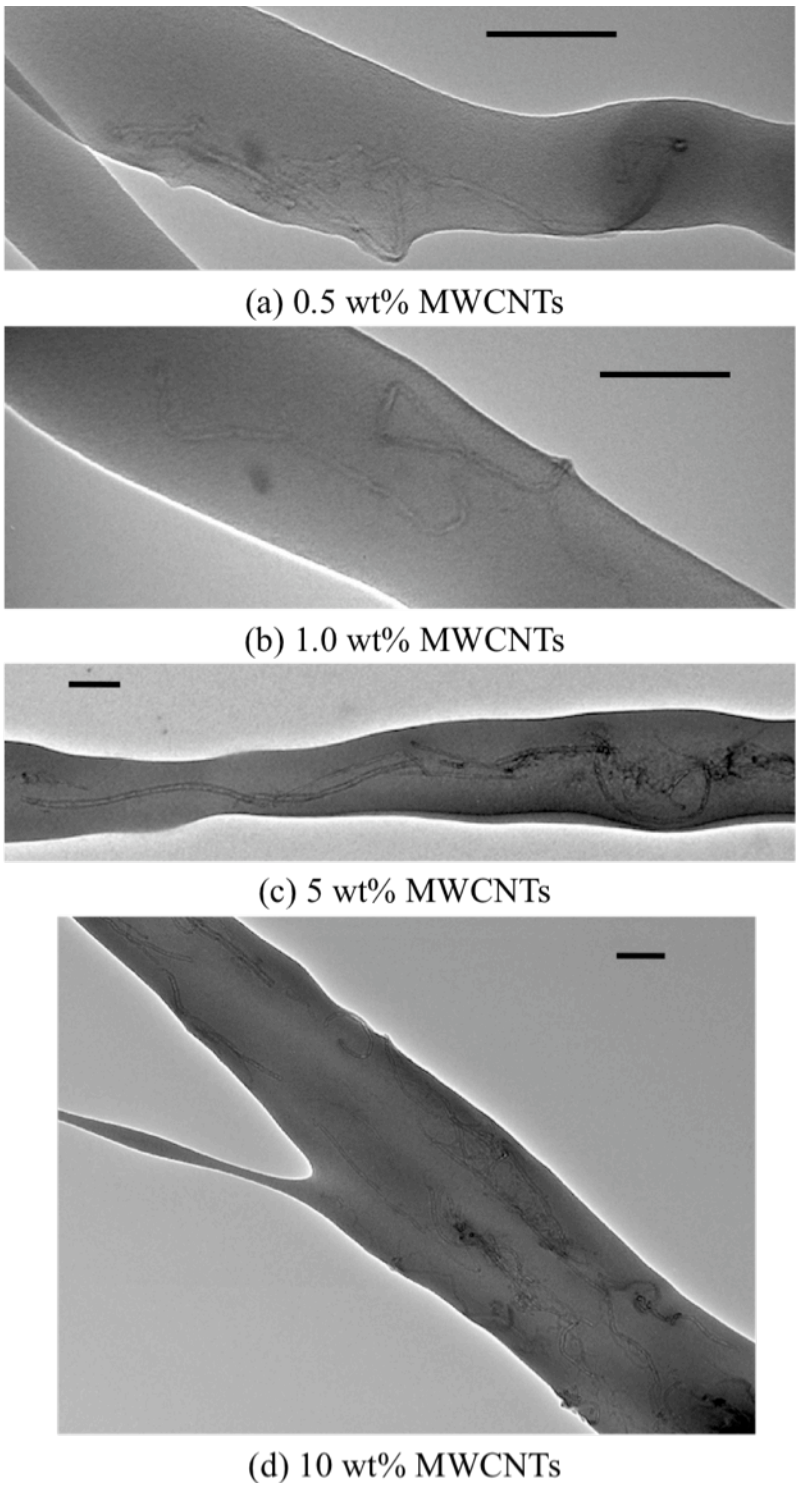

Figure 12.4. TEM micrographs of electrospun PU/MWCNT nanocomposite fibers containing (a) 0.5 wt% MWCNT, (b) 1.0 wt% MWCNT, (c) 5.0 wt% MWCNT, and (d) 10 wt% MWCNT. The scale bar represents 10 μm.

12.5 Conclusions

Acid-functionalized multiwall carbon nanotubes were prepared and dispersed into polyurethane solutions. These dispersions were electrospun into composite nanofibers membranes. The nanofibers showed a slight increase in fiber diameter upon nanotube incorporation and, at high MWCNT content, the surface of the composite nanofibers appeared undulating. In addition, the electrospinning process oriented the nanotubes along the fiber axis. By incorporating the carboxylic acid groups on the nanotube surface, the dispersion of the nanotubes within the polymer solutions was enhanced enough to facilitate their incorporation into nanofibers. These results indicate that surface functionalization can improve the dispersion and alignment of carbon nanotubes within electrospun polymer fibers. These nanocomposite fibers are ideally suited for applications including porous conducting membranes and nanowires.

12.6 Acknowledgements

We acknowledge Bayer MaterialScience for carbon nanotube samples and insightful discussions. Parts of this work were carried out using instruments in the Nanoscale Characterization and Fabrication Laboratory, a Virginia Tech facility operated by the Institute for Critical Technology and Applied Science.

12.7 References

1. Reneker, D. H.; Yarin, A. L. *Polymer* **2008,** *49*, 2387-2425.
2. Greiner, A.; Wendorff, J. H. *Angew. Chem., Int. Ed. Engl.* **2007,** *46*, 5670-5703.
3. Hunley, M. T.; Long, T. E. *Polym. Int.* **2008,** *57*, 385-389.
4. Ramakrishna, S.; Jose, R.; Archana, P. S.; Nair, A. S.; Balamurugan, R.; Venugopal, J.; Teo, W. E. *J. Mater. Sci.*, No pp. yet given.
5. Wang, X.; Zhang, K.; Yang, Y.; Wang, L.; Zhou, Z.; Zhu, M.; Hsiao, B. S.; Chu, B. *J. Membr. Sci.* **2010,** *356*, 110-116.
6. Li, Z.; Zhang, H.; Zheng, W.; Wang, W.; Huang, H.; Wang, C.; MacDiarmid, A. G.; Wei, Y. *Journal of the American Chemical Society* **2008,** *130*, 5036-5037.
7. Zhang, Y.; Dong, H.; Norris, I. D.; MacDiarmid, A. G.; Jones, W. E., Jr. *Polym. Mater. Sci. Eng.* **2001,** *85*, 622-623.

8. Barnes, C. P.; Sell, S. A.; Boland, E. D.; Simpson, D. G.; Bowlin, G. L. *Adv. Drug Delivery Rev.* **2007,** *59*, 1413-1433.
9. Xie, J.; MacEwan, M. R.; Schwartz, A. G.; Xia, Y. *Nanoscale* **2010,** *2*, 35-44.
10. Yeo, L. Y.; Friend, J. R. *Journal of Experimental Nanoscience* **2006,** *1*, 177-209.
11. Xie, X.-L.; Mai, Y.-W.; Zhou, X.-P. *Materials Science & Engineering, R: Reports* **2005,** *R49*, 89-112.
12. Kim, G. M.; et al. *Nanotechnology* **2006,** *17*, 963.
13. Kim, G. M.; Michler, G. H.; P^tschke, P. *Polymer* **2005,** *46*, 7346-7351.
14. Mazinani, S.; Ajji, A.; Dubois, C. *Polymer* **2009,** *50*, 3329-3342.
15. Sen, R.; Zhao, B.; Perea, D.; Itkis, M. E.; Hu, H.; Love, J.; Bekyarova, E.; Haddon, R. C. *Nano Letters* **2004,** *4*, 459-464.
16. Han, Z.; Kong, H.; Meng, J.; Wang, C.; Xie, S.; Xu, H. *Journal of Nanoscience and Nanotechnology* **2009,** *9*, 1400-1402.
17. Meng, J.; Kong, H.; Han, Z.; Wang, C.; Zhu, G.; Xie, S.; Xu, H. *Journal of Biomedical Materials Research, Part A* **2008,** *88A*, 105-116.
18. Hunley, M. T.; Poetschke, P.; Long, T. E. *Macromolecular Rapid Communications* **2009,** *30*, 2102-2106.
19. Williams, S. R.; Wang, W.; Winey, K. I.; Long, T. E. *Macromolecules* **2008,** *41*, 9072-9079.
20. Dror, Y.; Salalha, W.; Khalfin, R. L.; Cohen, Y.; Yarin, A. L.; Zussman, E. *Langmuir* **2003,** *19*, 7012.

Chapter 13: Overall Conclusions

The influence of electrostatic charges and intermolecular interactions on the solution rheological and electrospinning behavior of a series of polymer systems was explored. First, 2-(*N*,*N*-dimethylamino)ethyl methacrylate (DMAEMA) was used to create several polymer series of tailored charge and topology. Linear homopolymer polyelectrolytes were prepared by neutralizing PDMAEMA with various acids or by anion exchange. The investigated counteranions included Cl^-, NO_3^-, BF_4^-, $N(CN)_2^-$, PF_6^-, triflate (TfO^-), and bis(trifluoromethanesulfonyl)imide (Tf_2N^-). Thermal analysis revealed that the polyelectrolytes with more basic anions degraded at lower temperatures ($T_{d,5\%}$ for PDMAEMA-HCl was 230 °C, which increased to 320 °C for PDMAEMA-$HNTf_2$) through the Hofmann elimination mechanism. The counteranion selection also controlled the glass transition temperature, ranging from 164 °C for PDMAEMA-HCl to 38 °C for PDMAEMA-$HNTf_2$. In dilute solution, the conductivity of the polyelectrolytes followed trends of counteranion mobility. Solution conductivity in the semi-dilute concentration regimes followed the same trends, and all conductivities followed power law relationships with concentration. Solution rheology indicated all polyelectrolytes behaved as strong polyelectrolytes in aqueous solution, independent of anion.

Electrospinning of the polyelectrolytes with Cl^-, BF_4^-, and TfO^- counteranions revealed significant differences in electrospinning behavior compared to neutral polymers. Several previous reports demonstrated that neutral polymers begin to form stable electrospun fibers just above the critical concentration for entanglements, when solution elasticity suppresses capillary breakup of the electrospinning jet. The PDMAEMA-based polyelectrolytes required much higher viscosities and solution concentrations for stable electrospinning at comparable molecular weights. The PDMAEMA-based polyelectrolytes were electrospun from many concentrations in

the semi-dilute entangled regimes, but the onset of fiber formation did not occur until 3.1c_e, 1.8c_e, and 1.2c_e for the polyelectrolytes with Cl^-, BF_4^-, and TfO^- counteranions, respectively. The zero-shear viscosities at the onset of electrospinning also systematic decreased from 330 to 30 cP, respectively. Independent of concentration and viscosity, the polyelectrolytes formed fibers with diameters 1-2 orders of magnitude lower than those expected for neutral, non-associating polymers. Many reports in the literature similarly indicated that polyelectrolytes require significantly higher viscosities for stable electrospinning. These results suggest that the polyelectrolyte instabilities during electrospinning can be suppressed through the selection of hydrophobic and charge-delocalized ionic structures.

The copolymerization of DMAEMA with di(ethylene glycol) methyl ether methacrylate (MEO_2MA) yielded low-T_g random copolymers with amine content ranging from 0 to 100 mol%. Thermal analysis indicated that the MEO_2MA repeating units did not microphase separate, even after neutralization of the amine groups to form charged copolymers. The T_g's of the uncharged copolymers agreed well with Fox Equation predictions. However, the T_g's of the charged copolymers with either Cl^- or BF_4^- counteranions deviated from the Fox Equation predictions. The positive deviations arose from associative interactions between the MEO_2MA repeating units and the cationic ammonium groups, restricting polymer mobility. The Gordon-Taylor Equation successfully described the copolymer polyelectrolyte glass transition behavior when the *K*-parameter was significantly higher than ideal. The experimentally estimated *K*-values for poly(DMAEMA-HCl-*co*-MEO_2MA) and poly(DMAEMA-HBF_4-*co*-MEO_2MA) were 0.9 and 1.3, respectively. Solution shear viscosity analysis of the copolymer polyelectrolytes in the semi-dilute concentration regimes indicated that polyelectrolyte behavior developed at low ionic contents (~10 mol%) as the ionic groups led to extended chain conformations even at low

charge density. Solution conductivity analysis revealed considerable counteranion condensation at higher charge densities. The copolymers with 5 and 10 mol% ionic content behaved as if all counterions were dissociated, while the PDMAEMA-HCl homopolymer polyelectrolyte demonstrated approximately 57 mol% ionic dissociation. These copolymers indicated that low-T_g comonomers can be included within charged copolymers to lower the glass transition without significantly affecting the number of charged monomers participating in conduction. Control over glass transition can ultimately lead to the development of ionomer membranes for electro-active devices with enhanced conductivity performance.

The control of topology opens a new facet of macromolecular architectures for high performance polymers. PDMAEMA star polymers were synthesized using atom-transfer radical polymerization (ATRP) with control over the number and length of arms. Saccharide-based initiators with 5 and 8 initiation sites were used. The star-shaped polymers were neutralized using HCl and HBF_4 similar to linear PDMAEMA polymers discussed above, and measured thermal properties in the solid state (glass transition temperature and decomposition temperature) matched those of the linear polyelectrolyte analogues. The star-shaped polymers were alkylated using methyl iodide and anion exchanged to generate star-shaped PDMAEMA-HCl polyelectrolytes. In solution, the rheological and conductivity behavior of the star polyelectrolytes deviated significantly from that of linear polyelectrolytes. The polyelectrolyte specific viscosity scaling factors increased for the star polyelectrolytes (0.5 and 2.1 in the semi-dilute unentangled and semi-dilute entangled regimes, respectively) compared to linear polyelectrolytes (0.5 and 1.5, respectively). Also, solution conductivity for the linear polyelectrolytes was twice that of the star polyelectrolytes. The changes in solution behavior arose from increased counteranion condensation at the core of the star and significantly

compacted conformations compared to linear polyelectrolytes of the same molecular weight. Electrospinning of the uncharged PDMAEMA stars followed previously observed trends for neutral branched polymers. The onset of fiber formation occurred around the c_e, similar to linear polymers. However, the star polyelectrolytes required extremely high viscosities (> 4500 cP, ~5c_e) before fiber formation occurred, compared to more moderate values of 350 cP and 3c_e for linear polyelectrolytes.

The electrostatic and hydrophobic interactions of low molar mass surfactants facilitate self-assembly into a wide variety of conformations and structures in solution and the melt. Our group recently demonstrated that cylindrical or "wormlike" micellar aggregates can be electrospun to form uniform fibers. Rheological investigations of the model surfactant cetyltrimethylammonium bromide (CTAB), which is known to form wormlike micelles in aqueous solution, provided more insight into the electrospinning of low molar mass surfactants. The solution rheology of CTAB indicated strong aggregation occurred as the surfactant worms grow and begin to entangle. However, CTAB did not electrospin as well as other surfactants (phospholipids as well as 12-2-12 ammonium gemini surfactants), even at high viscosities. The ability of the wormlike micelles to entangle was proposed as a hypothesis for the difficulty electrospinning CTAB. This model surfactant forms much shorter and rigid cylindrical micelles as compared to phospholipids and gemini surfactants, suggesting that the CTAB micelles cannot entangle enough to provide elasticity to stabilize the electrospinning jet. Further experiments with asolectin confirmed that the ability of wormlike micelles to entangle is paramount for electrospinning. By adding water in a stoichiometric ratio to asolectin (0:1, 3:1, and 6:1 water:asolectin ratios), the worms can be lengthened and branched. However, the densely branched or networked solution structures do not electrospin as well as the linear asolectin

worms, even though the zero-shear viscosities are very similar. The highly branched structures cannot entangle as readily and the electrospinning jet is not stabilized. These results provide a stronger basis to predict the electrospinnability of wormlike micelles of low molar mass surfactants based upon knowledge of the solution structure and rheological behavior.

Low molar mass gelators based on a bis-urea bidentate hydrogen-bonding functionality were synthesized. The 1,2-*trans*-cyclohexane-based gelator with two hexadecyl pendant arms successfully gelled most organic solvents at low concentrations (<5 wt%). Gelled solutions of the gelator did not electrospin due to their inability to flow. However, a coating of gelator strands on the target was still achieved. A dispersion of the gelator in 2-butanol successfully electrospun to form stable but highly-irregular fibers. This is the first example of electrospun fibers generated from low molar mass gelator.

The addition of surfactant to polymer electrospinning solutions decreases the surface tension and increases solution conductivity, two factors which both increase electrospinnability. The addition of CTAB in low concentrations (0.5 and 1.0 mM) to PMMA electrospinning solutions resulted in uniform fiber formation at concentrations well below entanglement. PMMA with M_w = 571 kg/mol electrospun form 4:1 DMF:THF at 2 wt%, corresponding to $(n_e)_{soln}$ = 0.64. The electrospinning at $(n_e)_{soln}$ < 2 resulted from the very high molecular weight. However, upon addition of CTAB at concentrations of 0.5 and 1.0 mM, the onset of electrospinning occurred at $(n_e)_{soln}$ < 0.32. Similarly, PMMA with M_w = 366 kg/mol electrospun at $(n_e)_{soln}$ values of 1.4 and < 0.45 for CTAB concentrations of 0 and 1.0 mM, respectively. The addition of CTAB also led to reduction of fiber diameters at constant polymer concentrations. Based on these results, CTAB or other surfactants can be used to facilitate electrospinning of ultrafine, nanoscale fibers with extremely high specific surface areas.

Oligomeric, hyperbranched, end-perfluorinated poly(ethylene imine) (PEI)-based additives similarly facilitated the electrospinning of PMMA fibers. The addition of low levels of the additive reduced the surface tension of the solutions and led to suppression of beads during electrospinning at low PMMA concentrations. Due to its low surface energy, the additive selectively migrated to the fiber surface during electrospinning, as indicated by XPS analysis. The resulting fibers had a core-shell structure, with perfluorinated shell and PMMA core. The use of self-migrating additives allows the formation of specific functional nanofiber architectures without the need for elaborate coaxial electrospinning equipment.

End-functionalized star-shaped poly(D,L-lactide)s (PDLLAs) were synthesized with either adenine or thymine end groups. The hydrogen-bonding interactions between adenine and thymine base pairs led to significantly increased intermolecular interactions below the hydrogen-bond dissociation temperature. Melt rheological analysis indicated this dissociation occurred around 90 °C. A blend of the PDLLA-Adenine and PDLLA-Thymine had a complex viscosity almost twice as high as the separate star polymers at 70 °C. However, the complex viscosities for the unfunctionalized PDLLA and PDLLA(A-T) mixture were almost identical at 120 °C. Melt electrospinning of the star PDLLAs showed very little difference in fiber diameter for unfunctionalized PDLLA, PDLLA-A, and PDLLA-T (3.6 ± 1.0, 4.0 ±0.6, and 4.4 ± 1.0 μm, respectively). However, a mixture of PDLLA-A and PDLLA-T showed fibers diameters twice as large (9.8 ± 2.0 μm). The melt electrospinning behavior suggests polymers can be designed with low molecular weights for easy processing, but complementary hydrogen-bonding groups can help lead to more durable properties in the solid state.

Multiwalled carbon nanotubes (MWCNTs) have emerged as a relatively simple means to enhance the mechanical and electrical properties of polymer composites and polymer fiber

composites. However, carbon nanotubes are difficult to disperse uniformly through the polymer matrix without aggregation. Using a microextruder melt-mixer, nonfunctionalized MWCNTs were mixed into a thermoplastic polyurethane with very good dispersion. The extruded composites were electrospun from 4:1 DMF:THF solvent mixture to form nanofibers with well-dispersed, highly-aligned nanotubes. TEM analysis indicated the nanotubes preferentially aligned along the fiber axis, forming nanowires. The effect of MWCNT surface functionalization of fiber dispersion was investigated. Carboxylic acid-functionalized MWCNTs were dispersed into polyurethane solutions and electrospun. Without elaborate melt-mixing, the MWCNTs also dispersed very well and aligned along the fiber axis. At lower MWCNT loadings (<5 wt% with respect to polymer), the MWCNTs were well separated and few nanotubes aggregates were observed by TEM. The addition of MWCNTs can increase the mechanical properties and electrical conductivities of electrospun nanofibrous membranes, enhancing their performance in electro-active devices.

Chapter 14: Suggested Future Work

14.1. Comparison of Phosphonium- and Ammonium-Based Polyelectrolytes

The polyelectrolytes presented in this work all contain the ammonium cation. While synthetically accessible, this cation readily degrades at moderate temperatures and often leads to significant associations between cations and anions. However, the phosphonium cation offers significantly improved thermal stability. Phosphonium-based ionic liquids often show very low T_g's or T_m's due to weaker ionic associations with the larger phosphonium cation. An interesting study would investigate the solution rheological and electrospinning behavior of phosphonium-based polyelectrolytes compared to the ammonium polyelectrolytes discussed in the previous chapters. However, phosphorus-containing compounds are not readily commercially available and not easily prepared as the phosphonium cation is not as synthetically feasible. Many tertiary phosphorous compounds are highly pyrophoric due to the easy oxidation of the phosphorous.

Preliminary results indicated that the commercially-available monomer diphenyl vinyl phosphine (DPVP) readily copolymerizes with *n*-butyl acrylate (*n*BA) using AIBN in toluene (Scheme 14.1). ^{31}P NMR revealed that no oxidation occurred during the copolymerizations. *In situ* FTIR determined the reactivity ratios were $r_{n\mathrm{BA}} = 0.13$ and $r_{\mathrm{DPVP}} = 0.45$. The subsequent alkylation of DPVP with alkyl halides yields a phosphonium-containing monomer. Studies of the solution rheological behavior of phosphonium-containing polymers are limited throughout the literature, but there are no reports to date of electrospun phosphonium-containing polymers. Future efforts should concentrate on studying the solution rheological, conductivity, and electrospinning behavior of these phosphonium-containing polymers to elucidate the differences between ammonium and phosphonium polyelectrolytes.

Scheme 14.1. Copolymerization of DPVP and *n*BA.

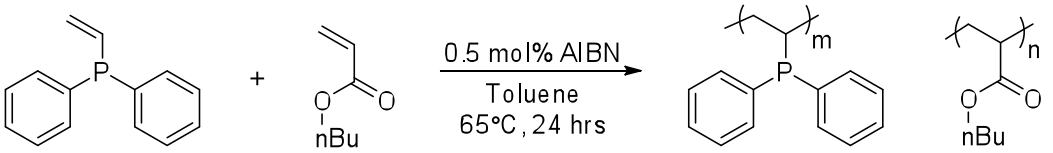

Similarly, phosphorous-containing anionic polyelectrolytes can be synthesized by alkaline hydrolysis of the polymers of diethylvinyl phosphonate (DEVP). Weiss et al. reported that these anionic ionomers display extremely different solid-state behavior depending on the specific countercation. These ionomers present a novel, thermally stable platform to investigate the behavior of phosphorous-containing anionic polyelectrolytes.

Scheme 14.2. Copolymerization of DEVP with *n*BA and subsequent alkaline hydrolysis to form the anionic phosphonate polyelectrolyte.

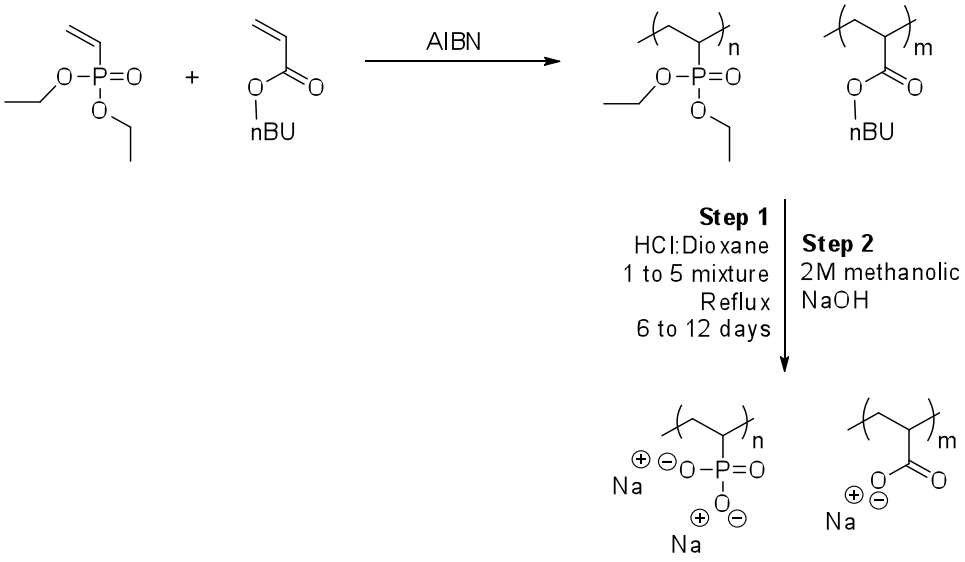

14.2. Electrospun Polyelectrolytes with Varying Ionic Content

The charged copolymers presented in Chapter 6 present a thorough investigation into the solution behavior and conductivity of charge-containing copolymers. Starting at very low ionic content, the rheological behavior followed that expected for polyelectrolytes of high charge density. The different reports studying the electrospinning behavior of chitosan at different

levels of deacetylation imply that lower charge densities will result in increased electrospinnability. However, no systematic studies have investigated the behavior of ionomers of varying ionic content.

The PDMAEMA-based copolymers should be electrospun at varying ionic contents to investigate the effect of charge density on electrospinnability. The poly(DMAEMA-HCl-*co*-MEO_2MA) copolymers are fully soluble in aqueous solvents, eliminating solubility problems associated with most ionomers. The solution rheological and solution conductivity data in Chapter 6 indicated that polyelectrolyte behavior occurred at low ionic contents (~10 mol% DMAEMA-HCl) and conductivity began to plateau near 50 mol% DMAEMA-HCl content. The electrospinning experiments could determine if controlling the charge density can help control electrospinnability.

14.3. Tailored Charge-Containing Polymers for Specific Fiber Geometries

Polyelectrolyte fibers offer a wide range of chemical functionalities for high performance fibrous membranes. However, highly-functional monomers are often expensive and do not provide the same mechanical properties as other commercial polymers. Chapter 9 illustrates how a surface-migrating additive can be used to add specific functionality to the surface of fibers. Even at very low concentrations (5 wt% vs. PMMA), the perfluorinated additive formed a surface layer on the electrospun fibers. Similarly, Long et al. reported that random copolymers of PMMA with self-complementary hydrogen bonding groups showed a surface enrichment of the polar hydrogen bonding group in electrospun fibers. The authors hypothesized that the strong electric field brought the polar hydrogen bonding groups to the surface of the electrospinning jet.

Future experiments should utilize the self-organizing effects of electrospinning to develop high-performance, functional membranes. Block copolymers with one charged block and one neutral block should self-assemble during electrospinning, possibly producing core-shell fibers with charged shells. The presence of small charged blocks relative to the uncharged blocks could reduce the electrospinning instabilities of polyelectrolytes while providing surface-functionalized polymers. The use of high-T_g neutral blocks and polymerized ionic liquid charged blocks could also yield fibrous membranes with fluid-like ion-conducting domains and rigid, neutral domains providing structural support. Poly(ethylene glycol) chains and zwitterionic groups are known as "stealth" coatings as they resist cellular adhesion and protein fouling. The specific incorporation of these functionalities onto the surface of polymer fibers can help create anti-fouling and anti-cell adhesion fibrous membranes.

14.4. Ionic conductivity of Poly(DMAEMA-HCl-co-MEO$_2$MA) Ionomers

As demonstrated in Chapter 6, charge-containing polymers with controllable T_g's and varied ionic content were synthesized. The solid state ionic conductivity behavior of these copolymers should be studied as a function of ionic content and counteranion. The decreased T_g's should dramatically increase the ionic conductivity, even as the ionic content is reduced. The ionic conductivity in the presence of added ionic liquid and the retardation of ion mobility by the crown ether-like MEO_2MA repeating units should be investigated thoroughly. The solid-state conductivity performance of these polymers is critical for application in electro-active devices.

14.5. Influence of Carbon Nanotube Surface Chemistry of Dispersion in Electrospun Fibers

Surface-functionalization of carbon nanotubes improves their dispersibility in organic and aqueous solvents, as well as their dispersibility within polymer matrices. The influence of

surface chemistry (e.g. carboxylic acid groups, amine groups, hydrogen-bonding groups, and grafted polymers) on the dispersion and alignment during electrospinning should be investigated.